

IRE

PERIODICAL
UNIVERSITY OF HAWAII
LIBRARY



Transactions

on Microwave Theory and Techniques

Volume MTT-8

JULY, 1960

Number 4

In This Issue

**Advances in Microwave Theory and Techniques in Great Britain,
Western Europe, and Japan—1959**

Design and Measurement of Two Broad-Band Coaxial Phase Shifters

Method of Measuring Inductive Capacities in the Millimeter Range

**Measurement Techniques of Parametric Amplifier and
Mixer Noise Figure**

Duplexing Systems at Microwave Frequencies

Impedances of an Elliptic Waveguide for the H_1 Mode

Analysis of a Transmission Cavity Wavemeter

Scattering of a Plane Wave on a Ferrite Cylinder at Normal Incidence

Phase Adjustment Effect on Cascaded Reflex Klystron Amplifiers

TE Modes of the Dielectric Loaded Trough Line

Coupling of Modes in Uniform, Composite Waveguides

7800
3

PUBLISHED BY THE

Professional Group on Microwave Theory and Techniques

Report of Advances in Microwave Theory and Techniques in Great Britain—1959*

JOHN BROWN†, SENIOR MEMBER, IRE

INTRODUCTION

THE continued research effort in the microwave field is reflected by the number of papers, which is as great as in any previous year. The single topic attracting the largest number of contributions has been that of waveguides for long-distance communication. This is partly the result of a very successful International Convention organized by the Institution of Electrical Engineers in London during January, 1959. To some extent it also indicates the amount of work which has been proceeding during the last few years and which now suggests that operational waveguide communication links may be in service within the foreseeable future.

Waveguides of the more conventional type have not been neglected, and the papers listed indicate a steady improvement in component design, methods of manufacture, and techniques of measurement. A somewhat surprising impression is given by the relatively small number of papers on solid-state microwave devices: this is certainly not representative of the effort devoted to this topic at present, and it is likely that there will be a marked increase in this number during the next year. Progress in microwave tube design and in microwave measurement techniques also continues.

1. TRANSMISSION LINES AND WAVEGUIDES

In this section the properties of structures capable of transmitting electromagnetic waves are considered. During the period under review, papers have appeared on strip lines, waveguides operating with only one propagating mode, multimode waveguides, and artificial dielectrics.

1.1 TEM Lines

No original material has been published, but a useful survey of the properties of strip lines has appeared. This contains information on the basic properties of strip lines and on the design and manufacture of strip-line components and of transducers to waveguides or coaxial lines.

- [1] A. F. Harvey, "Parallel plate transmission systems for microwave frequencies," *Proc. IEE*, vol. 106, pt. B, pp. 129–140; March, 1959.

1.2 Waveguides

The efforts made during the last few years to develop multimode waveguides for long-distance communication

have been widely publicized as a result of the Convention referred to in the Introduction. The papers presented at this Convention have been published in Supplement No. 13 of volume 106, part B of the *Proceedings of the Institution of Electrical Engineers* and will be discussed in appropriate sections of this article. (This issue will be referred to throughout as IEE suppl. no. 13 B.) An authoritative review of this topic has been given by Prof. H. M. Barlow in this supplement, and other review articles have also appeared.

- [2] H. M. Barlow, "Introductory survey," IEE suppl. no. 13 B, pp. 1–8.
 [3] H. M. Barlow, "Long-distance transmission by waveguide," *Brit. Commun. & Electronics*, vol. 6, pp. 92–95; February, 1959.
 [4] F. J. D. Taylor, "GPO interest in long distance transmission by waveguide," *ibid.*, p. 96.
 [5] L. Lewin, "A long distance waveguide telecommunication system," *ibid.*, pp. 97–100.
 [6] A. E. Karbowski, "Assessment of waveguide performance as a long-distance transmission medium," *ibid.*, pp. 168–186. See also *Electronic Engrg.*, vol. 31, pp. 520–525; September, 1959.
 [7] F. J. D. Taylor, "Some views on system application," IEE suppl. no. 13 B, pp. 186–187.

Propagation in overmoded waveguides is complicated by mode conversion, which can lead to the distortion of information, and experimental and theoretical results are reported for several types of low-loss guide.

- [8] A. E. Karbowski, "Distortion of information in non-uniform multimode waveguide," IEE suppl. no. 13 B, pp. 9–16.
 [9] A. E. Karbowski and V. H. Knight, "An experimental investigation of waveguide for long distance communication," *ibid.*, pp. 17–29.
 [10] H. E. Rowe and W. D. Warters, "Transmission deviations in waveguide due to mode conversion: theory and experiment," *ibid.*, pp. 30–36.
 [11] H. Larsen, "Delay distortion and equalization in H_0 waveguides for long range communication," *ibid.*, pp. 188–194.

A general analysis of the behavior of waveguides of arbitrary cross section has been carried out.

- [12] G. Reiter, "Generalised telegraphist's equation for waveguides of varying cross-section," *ibid.*, pp. 54–57.

Further results on the H guide and new improved forms of this guide were reported.

- [13] F. J. Tischer, "Properties of the H -guide at microwave and millimetre-wave regions," *ibid.*, pp. 47–53.

The properties of a waveguide consisting of spaced conducting disks with circular holes are claimed to compare favorably with those of solid guides.

- [14] A. W. Gent, "The attention and propagation factor of spaced-disc circular waveguide," *ibid.*, pp. 37–46.

There is now general agreement that the most promising available waveguide for long-distance communication is that formed from a helical conductor covered by

* Received by the PGMTT, April 21, 1960.

† Elec. Engrg. Dept., University College, London, Eng.

a suitable insulating jacket. Detailed information on the design theory, properties, and methods of manufacture of such a guide has been given.

- [15] H. G. Unger, "Helix waveguide design," *ibid.*, pp. 151–155.
- [16] G. Piefke, "The influence of helix wire diameter on the modes in helix waveguide," *ibid.*, pp. 110–118.
- [17] L. Lewin, "Winding and jointing helical wound waveguide," *ibid.*, pp. 156–158.
- [18] A. C. Beck and C. F. P. Rose, "Waveguide for circular electric mode transmission," *ibid.*, pp. 159–162.

1.3 Surface Waves

Surface waves offer an alternative method of long-distance communication, and the experience gained from an operational system has been reviewed.

- [19] G. Goubau, "Some characteristics of surface wave transmission lines for long distance transmission," *ibid.*, pp. 166–167.

Theoretical and experimental results are given for several types of reactive surface.

- [20] K. P. Sharma, "The estimation of the reactance of a loss free surface supporting surface waves," *Proc. IEE*, vol. 106, pt. B, pp. 427–430; July, 1959.

A disadvantage of surface waves is the possible conversion of power to radiation, this being the equivalent of the excitation of unwanted modes in overmoded guide. Two aspects of this have been investigated, the first dealing with discontinuities such as changes in reactance or the presence of conductors in the path of the wave, and the second with the effect of curvature in the reactive surface supporting the wave.

- [21] K. P. Sharma, "An investigation of the excitation of radiation by surface waves," *Proc. IEE*, vol. 106, pt. B, pp. 116–122; March, 1959.
- [22] H. M. Barlow, "The power radiated by a surface wave circulating around a cylindrical surface," *ibid.*, pp. 180–185.

Interest in methods of launching surface waves continues and studies of slot launchers for both radial surface waves and single wire lines have been made. It is pointed out that although slot launchers can have a high launching efficiency, there is an inevitable restriction on the bandwidth of operation. A comparison is made with supergain antennas.

- [23] J. Brown and K. P. Sharma, "The launching of radial cylindrical surface waves by a circumferential slot," *ibid.*, pp. 123–128.
- [24] J. Brown and H. S. Stachera, "Annular slot launchers for single-conductor transmission lines," *IEE suppl. no. 13 B*, pp. 143–145.

An instructive comparison of problems involving surface waves, Čerenkov radiation, diffraction, and neutron scattering draws attention to the essential unity of the theoretical treatments.

- [25] J. D. Lawson, "Electromagnetic wave problems," *Electronic and Radio Engr.*, vol. 36, pp. 332–338; September, 1959.

1.4. Artificial Dielectrics

Further results on the properties of artificial dielectrics have been presented and the possible use of these materials in dispersive prisms for frequency scanning and in radomes as low reflection materials is discussed.

- [26] J. S. Seeley and J. Brown, "The use of dispersive artificial dielectrics in a beam scanning prism," *Proc. IEE*, vol. 106, pt. B, pp. 93–102; March, 1959.

- [27] J. S. Seeley, "The quarter wave matching of dispersive materials," *ibid.*, pp. 103–106.
- [28] A. Carne and J. Brown, "Theory of reflections for the rod-type artificial dielectric," *ibid.*, pp. 107–115.

2. WAVEGUIDE COMPONENTS

Work in components is largely directed to increasing the bandwidth over which satisfactory operation can be achieved, and to improving methods of manufacture. Tchebycheff functions have been used in the design of several waveguide components such as directional couplers and filters, and a guide to the use of such functions has been prepared. A useful bandwidth improvement can be obtained.

- [29] R. Levy, "A guide to the practical application of Chebyshev functions to the design of microwave components," *Proc. IEE*, vol. 106, pt. C, pp. 193–199; September, 1959.

A stepped-waveguide transition between two rectangular waveguides of different cross section has been designed with steps in both guide height and width. The design and performance of such a transition connecting no. 11 and no. 12 waveguides is discussed, satisfactory results being achieved over the frequency range 3.7–4.3 gigacycles (gc).

- [30] D. Wray, "Frequency compensation for simple stepped waveguide transforming sections," *Electronic Engr.*, vol. 31, pp. 76–79; February, 1959.

The position of the short circuits on the arms of a hybrid junction used as a duplexer has been examined with a view to optimizing the bandwidth of operation.

- [31] R. Levy, "Hybrid junctions," *Electronic & Radio Engr.*, vol. 36, pp. 308–312; August, 1959.

An interference-type two-hole directional coupler can be tuned by dielectric phase shifters between the coupling holes to give perfect directivity at any wavelength within a wide frequency range. Design details have been given.

- [32] W. G. Voss, "Modified two-hole directional coupler," *Electronic & Radio Engr.*, vol. 36, p. 28; January, 1959.

The properties of waveguide switches of mechanical types have been compared with those using discharge tubes and ferrites.

- [33] J. W. Sutherland, "Waveguide switches and branching networks," *Electronic Engr.*, vol. 31, pp. 64–65; February, 1959.

Improvements in the design of cavity resonators which have been reported include the reduction of the effects of spurious modes in TE_{01n} resonators and an increase in the tuning range of TE_{11n} wavemeters for use in J and K bands.

- [34] A. Cunliffe and R. N. Gould, "High Q echo boxes," *Electronic & Radio Engr.*, vol. 36, pp. 29–33; January, 1959.
- [35] P. Andrews, "The design of broadband circular wavemeters," *Brit. Commun. & Electronics*, vol. 6, pp. 354–357; May, 1959.

The tuning range of X -band cavities designed for use with plug in klystrons has been increased to 30 per cent.

- [36] R. Mather and J. Sharpe, "Wide range tuning cavities for reflex klystrons," *Electronic Engr.*, vol. 31, pp. 390–393; July, 1959.

A simple acid-copper electroforming process suitable for laboratory use has been developed. Investment casting from frozen mercury patterns has proved to be suitable for the manufacture of components of normal commercial performance at frequencies around 10 gc.

- [37] P. Andrews, "The electroforming of waveguide components," *Electronic Engrg.*, vol. 31, pp. 150-153; March, 1959.
- [38] H. H. Scholfield, H. H. H. Green, and R. E. Gossett, "Manufacture of waveguide parts by investment casting from frozen mercury patterns," *Proc. IEE*, vol. 106, pt. B, pp. 431-434; July, 1959.

The development of the TE_{01} mode for long-distance communication has created the need for components designed for circular guides operating in this mode. Two new types of transducers which couple from rectangular guide to the TE_{01} mode in circular guide have been developed for operation at frequencies around 30 gc. The first uses slot coupling from a rectangular guide inserted along the axis of the circular guide and a bandwidth of 2 gc has been achieved. The second, which is designed specifically for narrow-band use, has the rectangular guide wrapped around the circumference of the circular guide, slot coupling again being used: the bandwidth obtained using 46 slots is of the order of 50 mc.

- [39] B. Oguchi and K. Yamaguchi, "Centre-excited type of rectangular TE_{01} to circular TE_{01} mode transducer," *IEE Suppl.* no. 13 B, pp. 132-137.
- [40] Y. Klinger and L. Lewin, "Channel insertion feed," *ibid.*, pp. 138-142.

Attention has also been given to transducers coupling circular guides of different radii, when both guides support the TE_{01} mode. The problem is to avoid conversion to other modes, and solutions involving either tapers or steps have been proposed.

- [41] L. Solymar, "Design of a two-section conical taper in circular waveguide system supporting the H_{01} mode," *ibid.*, pp. 119-120.
- [42] L. Solymar, "Monotonic multi-section tapers for overmoded circular waveguides," *ibid.*, pp. 121-128.
- [43] L. Solymar, "Step transducers between over-moded circular waveguides," *ibid.*, pp. 129-131.

Estimates have been made of the transmitted mode amplitudes when a circular waveguide with an incident TE_{01} mode is connected to a guide whose cross section differs slightly from circular.

- [44] L. Solymar, "Over-moded waveguides," *Electronic & Radio Eng.*, vol. 36, pp. 426-428; November, 1959.

It has been suggested that overmoded rectangular waveguides may be useful at millimetric wavelengths, and the problem of mode conversion again arises. Results have been derived for a pyramidal taper connecting two rectangular waveguides of different cross sections.

- [45] L. Solymar, "Mode conversion in pyramidal-tapered waveguides," *Electronic & Radio Engr.*, vol. 36, pp. 461-463; December, 1959.

The possible excitation of unwanted modes at bends in a low-loss waveguide is one of the most difficult problems to be overcome, and several ingenious suggestions have been made. Two main lines of attack are being used. The first relies on modifying the surface reactance

of the guide wall to inhibit the excitation of the unwanted modes and a general discussion of this possibility has been given. Results have been given for one particular configuration. The helix guide can also be considered from this point of view, and experimental values for the performance of a bend have been provided. Further information on bends will be found in several of the papers listed in Section 1.2.

- [46] H. M. Barlow, "A method of changing the dominant mode in a hollow metal waveguide and its application to bends," *IEE suppl.* no. 13 B, pp. 100-105.
- [47] P. Marie, "A bend for TE_{01} mode propagated in circular waveguide," *ibid.*, pp. 108-109.
- [48] M. Thue, J. Bendayan, and G. Comte, "Researches on transmission of TE_{01} waves in circular waveguides in the vicinity of 25 and 35 gc/s," *ibid.*, pp. 94-97.

The second line of attack is to introduce an inhomogeneous dielectric into the waveguide with the object of preserving the field pattern of the wanted mode as it propagates around the bend.

- [49] H. M. Barlow and D. C. Rickard, "Experiments on circular H_{01} wave propagation in a curved waveguide filled with an inhomogeneous dielectric," *ibid.*, pp. 106-107.

3. SOLID-STATE DEVICES

The only papers published during 1959 on maser and mavar devices have been theoretical. The first gives a unified treatment of the noise properties of maser and mavar amplifiers by using the concepts of negative temperature and negative quality factor.

- [50] E. D. Farmer, "The noise and gain properties of molecular and parametric amplifiers," *J. Electronics & Control*, vol. 7, pp. 214-232; September, 1959.

The effect of the series resistance of a variable capacity semiconductor diode on the performance of a variable reactance amplifier has been analyzed.

- [51] P. Bobish and C. Sondhauss, "Einfluss des zeitabhängigen Serien-Wirkwiderstandes einer Kapazitätsdiode beim Mavar-Aufwärts mischer," *J. Electronics & Control*, vol. 7, pp. 344-366; October 1959.

Ferrite devices continue to attract considerable attention and progress has been reported in several directions. Further theoretical contributions on the properties of circular waveguides containing ferrites have appeared and the behavior at the interface between an empty rectangular waveguide and one completely filled with a ferrite has been analyzed.

- [52] P. J. B. Clarricoats, "A perturbation method for circular waveguides containing ferrites," *Proc. IEE*, vol. 106, pt. B, pp. 335-340; May, 1959.
- [53] R. A. Waldron, "Theory of mode spectra of cylindrical waveguides containing gyromagnetic media," *J. Brit. IRE*, vol. 19, pp. 347-356; June, 1959.
- [54] L. Lewin, "A ferrite boundary value problem in a rectangular waveguide," *Proc. IEE*, vol. 106, pt. B, pp. 559-563; November, 1959.

A ferrite modulator, using Faraday rotation, has been designed to operate at high modulation frequencies. When used as a single-sideband modulator at X band, this device gives an output which is not more than 20

db below the input signal for modulation frequencies up to 10 mc.

- [55] A. L. Morris, "Microwave ferrite modulator for high modulation frequencies," *J. Brit. IRE*, vol. 19, pp. 117–129; February, 1959.

The performance of a ferrite mixer has been analyzed and the conversion efficiency is shown to be 14 db worse than a conventional crystal mixer.

- [56] L. Lewin, "The efficiency of ferrite as a microwave mixer," *Proc. IEE*, vol. 106, pt. C, pp. 153–157; September, 1959.

The possibility of using a ferrite rod in a circular waveguide as the basis of a traveling-wave amplifier has been examined theoretically. It is concluded that pulsed operation is necessary and that gains of up to 3 db/inch may then be obtained at X band, the bandwidth being of the order of 100 mc.

- [57] P. J. B. Clarricoats, "The gain of travelling wave ferromagnetic amplifiers," *Proc. IEE*, vol. 106, pt. C, pp. 165–173; September, 1959.

4. MICROWAVE ELECTRONICS

The emphasis has been on theoretical work designed to facilitate the construction of oscillators with higher power outputs and amplifiers with improved noise performance.

Expressions for the plasma frequency reduction factors in space charge waves have been obtained.

- [58] D. H. Trevena, "On space charge waves," *J. Electronics & Control*, vol. 6, pp. 50–64; January, 1959. See also comments by R. H. C. Newton, *ibid.*, pp. 321–324; April, 1959.

An analysis of the effects of collisions on space charge waves has been made and leads to suggestions for reducing the noise in beam-type tubes and for measuring the collision frequency in a plasma.

- [59] S. V. Yadavalli, "Collision damping of space charge waves in a plasma," *J. Electronics & Control*, vol. 7, pp. 261–267; September, 1959.

Further theoretical studies of coupling systems have been made.

- [60] T. S. Chen, "Design and performance of coupled-helix transducers for travelling wave tubes," *J. Electronics & Control*, vol. 6, pp. 289–306; April, 1959.
- [61] A. Ashkin, W. H. Louisell, and C. F. Quate, "Fast wave couplers for longitudinal beam parametric amplifiers," *J. Electronics & Control*, vol. 7, pp. 1–32; July, 1959.

A comparison of theoretical and experimental results on multistart helices intended for use in high-power traveling-wave tubes has been made.

- [62] G. W. Buckley and J. Gunson, "Theory and behavior of helix structures for a high power pulsed travelling wave tube," *Proc. IEE*, vol. 106, pt. 5, pp. 478–486; September, 1959.

A method of focusing sheet beams by a periodic arrangement of magnetic fields has been suggested. This has possible applications in fast-wave traveling-wave tubes.

- [63] P. A. Sturrock, "Magnetic deflection focussing," *J. Electronics & Control*, vol. 7, pp. 162–168; August, 1959.

A traveling-wave tube using a clover-leaf slow wave structure and a ferrite isolator has been shown to give an

output power of 1 kw at X band. The gain is 22 db and the tube can be tuned over a 6 per cent range of frequency.

- [64] M. O. Bryant, J. F. Gittens, and F. Wray, "An experimental C.W. power travelling wave tube," *J. Electronics & Control*, vol. 6, pp. 113–129; February, 1959.

The advantages of using a double tuned output circuit on a multicavity klystron have been demonstrated on an S-band tube. A power output of 2 Mw, for an input power of 25 watts and a beam power of 10 Mw, has been achieved over a 5.5 per cent frequency range.

- [65] H. J. Curnow and L. E. S. Mathias, "A multi-cavity klystron with double tuned output circuit," *Proc. IEE*, vol. 106, pt. B, pp. 487–488; September, 1959.

The performance of a magnetron tuned by a waveguide has been examined. An equivalent circuit for the magnetron has been deduced from the form of the input admittance characteristic and has been used to predict the operating frequency as a function of the length of the tuning waveguide. Good agreement with measured values is reported.

- [66] T. S. Chen, "Tuning and the equivalent circuit of multi-resonator magnetrons," *J. Electronics & Control*, vol. 7, pp. 33–51; July, 1959.

The cross-modulation which can arise in a frequency-modulated klystron as a result of frequency pulling has been examined theoretically. An idealized Rieke diagram is assumed and numerical results are given for the second and third harmonics produced.

- [67] D. T. Gjessing, "A simple investigation of the cross-modulation distortion arising from the pulling effect in a frequency modulated klystron," *Proc. IEE*, vol. 106, pt. B, pp. 473–477; September, 1959.

A theoretical study of an electron beam parametric amplifier shows that the Manley-Rowe relations are satisfied.

- [68] W. H. Louisell, "A three-frequency electron beam parametric amplifier and frequency converter," *J. Electronics & Control*, vol. 6, pp. 1–25; January, 1959.

A survey of particle accelerators has been prepared.

- [69] A. F. Harvey, "Radio-frequency aspects of electronuclear accelerators," *Proc. IEE*, vol. 106, pt. B, pp. 43–57; January, 1959.

5. MEASUREMENTS

Progress continues in improving measurement techniques for conventional waveguide systems and in developing methods for the rapid assessment of component performance. The interest in low-loss waveguides has shown the need for measurement techniques which are suitable for use in multimode guides and are capable of measuring very low attenuation.

5.1. Standing-Wave Measurements

Two new automatic standing-wave plotters have been developed. The first is based on a rotary standing-wave indicator, the need for mechanical rotation of the crystal detector being eliminated by the use of a ferrite polarization rotator. The VSWR is displayed directly on a

meter. The second uses directional couplers, the signal being provided by a backward-wave oscillator which can be swept over the frequency range 7.5–11.0 gc. A cathode-ray tube presentation gives a plot of reflection coefficient against frequency.

- [70] E. Laverick and J. Welsh, "An automatic standing wave indicator for the 3 cm band," *J. Brit. IRE*, vol. 19, pp. 253–262; April, 1959.
- [71] J. C. Dix and M. Sherry, "A microwave reflectometer display system," *Electronic Engrg.*, vol. 31, pp. 24–29; January, 1959.

A reflectometer has been designed for use with strip lines in the frequency range 40–100 mc.

- [72] G. H. Millard, "Triple V.H.F., reflectometer," *Electronic and Radio Engrg.*, vol. 36, pp. 11–13; January, 1959.

The reciprocity theorem has been applied to the problem of standing wave measurements and it is shown that there may be advantages in interchanging the oscillator and detector.

- [73] G. D. Monteath, "Reciprocity in R.F. measurements," *Electronic & Radio Engrg.*, vol. 36, pp. 18–20; January, 1959.

Waveguide circuits which are made in integral form cannot be tested by using conventional standing-wave indicators. A specially designed plug-in reflectometer overcomes this difficulty.

- [74] G. Craven and V. H. Knight, "The design and testing of integrally constructed waveguide assemblies," *Proc. IEE*, vol. 106, pt. B, pp. 321–334; May, 1959.

Various problems related to standing-wave measurements have been discussed.

- [75] J. R. G. Twistleton, "The transformation of admittance through a matching section and lossless waveguide junction," *Proc. IEE*, vol. 106, pt. B, pp. 175–179; March, 1959.
- [76] L. Lewin, "Phase measurements through tapered junctions," *Proc. IEE*, vol. 106, pt. B, pp. 495–496; September, 1959.

5.2. Measurements of Low-Loss Waveguides

The attenuation in low-loss guide can be measured accurately by using a convenient length to form a resonant cavity. The Q values involved are of the order of 10^6 and special techniques have been developed to facilitate accurate measurements.

- [77] J. A. Young, "Resonant-cavity measurements of circular electric waveguide characteristics," *IEE suppl. no. 13 B*, pp. 62–65.
- [78] A. E. Karbowski and R. F. Skedd, "Testing of circular waveguides using a resonant cavity method," *ibid.*, pp. 66–70.
- [79] D. G. Keith-Wqlker, "An equipment for measuring the attenuation of low-loss waveguide transmission lines," *ibid.*, pp. 71–74.

Special methods have been developed to detect the presence of unwanted modes, and a survey of these has been given. A spinning dipole has been used to obtain a complete field pattern in a cross section of the waveguide.

- [80] H. G. Effemey, "A survey of methods used to identify microwave fields or wave modes in cylindrical waveguides," *ibid.*, pp. 75–83.
- [81] H. M. Barlow & M. G. F. Wilson, "The spinning dipole technique applied to the measurement of waveguide modes," *ibid.*, pp. 84–88.

The magnitudes of the spurious modes excited by a transducer from a single-mode to a multimode guide have been deduced from impedance measurements in the single-mode guide when the multimode guide is terminated by an adjustable short circuit.

- [82] Y. Klinger, "The measurement of spurious modes in overmoded waveguides," *ibid.*, pp. 89–93.

5.3. Miscellaneous Measurements

A Hall effect wattmeter has been constructed to operate at a frequency of 4 gc for input powers in the range 30 mw to 20 watts. The semiconductor is mounted in a resonant cavity, less than 3.4 per cent of the incident power being absorbed. The accuracy is ± 3 per cent and is unaffected by the standing-wave ratio of the load, provided it exceeds 0.1.

- [83] L. M. Stephenson and H. M. Barlow, "Power measurement at 4 gc by the application of Hall effect in a semiconductor," *Proc. IEE*, vol. 106, pt. B, pp. 27–30; January, 1959.

An incandescent filament lamp has been used as a noise source and is shown to have a higher noise temperature than a discharge tube but the bandwidth of operation is less.

- [84] E. W. Collings, "A filament noise source for 3 gc," *Proc. IEE*, vol. 106, pt. B, pp. 97–101; March, 1959.

Phase differences between the side bands of an amplitude-modulated signal are used as the basis of a method for measuring high Q factors (see also [77]–[79]).

- [85] F. H. James, "A method for the measurement of very high Q -factors of electromagnetic resonators," *Proc. IEE*, vol. 106, pt. B, pp. 489–491; September, 1959.

Details have been given of the frequency standard which is based on the cesium resonance in X band.

- [86] L. Essen, E. G. Hope, and J. V. L. Parry, "Circuits employed in the N.P.L. caesium standard," *Proc. IEE*, vol. 106, pt. B, pp. 240–244; March, 1959.

A frequency standard covering the range 7–20 gc with a short-term stability better than 1 in 10^7 has been provided by multiplication from a 100-kc crystal.

- [87] B. H. L. James and M. T. Stockford, "A microwave frequency standard," *Electronic Engrg.*, vol. 31, pp. 2–7, 82–87; January–February, 1959.

Optical techniques of measurement suitable for use at millimeter wavelengths have been surveyed.

- [88] A. F. Harvey, "Optical techniques at microwave frequencies," *Proc. IEE*, vol. 106, pt. B, pp. 141–157; March, 1959.

Report of Advances in Microwave Theory and Techniques in Western Europe—1959*

GEORGES GOUDET†

DURING 1959, the main progress in Western Europe was concerning further development of types "O" and "M" carcinotrons and studies about quantum devices. Nevertheless, other subjects have not been neglected.

1. VACUUM AND GAS TUBES

1.1 Vacuum Tubes

1.1.1 Conventional tubes: Some new conventional tubes for decimetric waves have been introduced, especially in Germany. The PC 86 type, intended for use as grounded grid amplifier, has been developed by Telefunken.

A water cooled disk triode, the EC 59, has been designed on the basis of the previous EC 57 type, and has an output power of 10 w CW at 4000 mc with a bandwidth of 100 mc and a gain of about 10 db.

H. Buenger, "PC 86, Eine neue entwickelte Gitterbasistriode für dezimeterwellen," *Telefunken Z.*, no. 122, pp. 262–265; December, 1958. (In German.)

V. V. Schwab and J. G. van Wijnngaarden (Valvo GmbH Radio-röhrenfabrik, Hamburg), "Le tube EC 59, une triode d'émission d'une puissance de 100 W à 4000 MHz," *Philips Tech. Rev.*, no. 9, pp. 253–262; May, 1959. (In French.)

A planar measuring diode, the distance between electrodes of which can vary from 40 μ to 1 mm, has been constructed at the University of Berlin, to enable study of the space charge and transient phenomena at the frequencies between 1.6 and 4 kmc, the current density being able to reach 200 ma/cm² and anode voltage up to 30 volts.

K. Hennings (Tech. Univ., Berlin), "Leitwerte—Messungen an einer plan parallelen diode im Laufzeitgebiet," *Nachrichtentech. Z.*, no. 9, pp. 459–461; September, 1959. (In German.)

The Centre National d'Etude des Télécommunications uses analogical means for the study of electron guns: an automatic rheographic curve with automatic curve tracer and a device intended for testing electron guns, including facilities of electrical supply, vacuum, magnetic fields and travelling of electrodes. This installation has proved very useful for solving problems involved in the design of microwave tubes.

J. Henaff (C.N.E.T., Paris), "Les moyens d'étude d'optique électronique du CNET," *Echo des Recherches*, no. 34, pp. 16–31; August, 1959. (In French.)

The use of vacuum diodes for the detection of microwaves has been studied in Spain by the Instituto Nacional de Electronica.

E. Meyer and F. Wächter, "Deteccion de microondas en valvulas de vacio," *Revista "INE,"* vol. 2, pp. 165–178; July, 1959. (In Spanish.)

1.1.2 Magnetrons: The French company Lignes Télégraphiques et Téléphoniques have developed a whole set of components for the Q-band. In this way, a pulsed magnetron operating at 35,000 mc and delivering a peak power of 200 kw has been realized. The mean power is 80 w. The anode structure is of the "rising sun" type and includes 26 cavities. The development of this tube has been conducted under a contract of the French Government.

R. Zwobada, "A 200 kw 80 w Q-band magnetron," *Proc. IEE*, pt. B., vol. 105, suppl. no. 10, pp. 426–428, 443, 445; May, 1958.

A line of CW magnetrons operating in the frequency band 2425–2475 mc has been developed for industrial use, delivering RF power from 100 w to 1 kw. They are characterized by a high efficiency and a long life expectancy.

Mlle Cagnac (C.S.F.), "Les magnétrons industriels," *Onde électrique*, no. 390, pp. 723–725; September, 1959. (In French.)

Experimental magnetrons operating on the wavelengths of 32, 12, 8 and 4 mm have been realized by the Philips Laboratories at Eindhoven, The Netherlands. They can deliver peak powers of, respectively 1100, 70, 80 and 40 kw.

J. Verweel and G. H. Plantinga, "Une série de magnétrons à impulsions, à cathode L, pour ondes centimétriques et millimétriques," *Philips Tech. Rev.*, vol. 21, pp. 1–10; December, 1959. (In French.)

In order to obtain CW power of a few kilowatts, magnetrons are available; but for higher powers, it is necessary to use several tubes in parallel. It has been shown that the use of separated injection devices permits, by overlying suitable modes of oscillation, a nearly constant repartition of the density of energy to be obtained in the useful space.

W. Schmidt (Entwicklungslab, Valvo GmbH Radio röhrenfabrik, Hamburg), "Parallelbetrieb von mehreren Einkopplungssystemen in Mikrowellen generator mit abgeschlossenen Arbeitsräumen," *Elektron. Rundschau*, no. 8, pp. 280–282; August, 1959. (In German.)

1.1.3 Klystrons: Electronic-hysteresis phenomena occurring at the build-up of oscillations in reflex klystrons have been explained by taking a careful survey of the variation of beam admittance as a function of repeller

* Received by the PGMTT, April 29, 1960.

† Laboratoire Centrale de Telecommunications, Paris, France.

voltage and RF voltage in the gap between the grids. The conclusion is that these phenomena are essentially due to secondary emission in the space comprised between the grids of the klystron cavity.

R. P. Musson-Genon and C. Audouin, "A new analysis of electronic hysteresis and secondary-emission phenomena in local-oscillator reflex klystrons," *Proc. IEE*, pt. B, vol. 105, suppl. no. 12, pp. 1006-1007; May, 1958. (In English.)

An electron gun suitable for the production of a small-diameter beam has been studied for high-power broadband klystrons. The beam is produced by a convergent gun, the cathode being placed in a magnetic field of suitable shape.

C. Zlotykamin, "High density electron gun with magnetic field," *Proc. IEE*, pt. B, vol. 105, suppl. no. 12, pp. 939-940; 1958. (In English.)

Theoretical considerations show that the efficiency of high-power pulsed klystrons is little impaired by the use of high perveances. The correlative lowering of the applied voltage is advantageous for the realization of the power supplies and for certain characteristics of the tube.

P. Palluel and G. Kantorowicz (C.S.F., Paris), "Klystrons de puissance élevée en impulsions utilisant une grande pervéance," *Onde électrique*, no. 383, pp. 109-115; February, 1959. (In French.)

The problem of the improvement of linearity of frequency-modulated reflex-klystron has been studied. A solution using a special load, the impedance of which, correcting the modulation characteristic of the klystron, has been developed, and the possibilities of practical realization investigated. Such a circuit has been successfully tested with different types of klystrons.

G. Cicconi (Div. Ponti Radio, Fabbr. ital. Magnet. Marelli, Milano), "Sul miglioramento della linearità di clistron reflex come generatori modulati in frequenza," *Alta frequenza*, no. 6, pp. 634-682; December, 1958. (In Italian.)

A determination of the phase aberration coefficient in a reflex klystron has been made by studying the beam admittance and the variation of amplitude as a function of the position of departure from the cathode.

J. Bonnerot, "Détermination du coefficient d'aberration de phase dans un klystron reflex," *Compt. Rend. Acad. Sci., Paris*, no. 20, pp. 2023-2025; November 16, 1959. (In French.)

1.1.4 Travelling-wave tubes: The most important parameters of travelling-wave tubes influencing the gain have been investigated, including the different means for focusing the electron beam. The possible upper limits for the gain have been evaluated, as far as noise and oscillation by internal reflections are concerned.

A calculation of the reflections of a non-uniform active helix line with a localized attenuation has shown the influence of these reflections on gain, delay and impedance fluctuations. Some characteristic measurements have confirmed the validity of the theoretical investigations.

W. Klein (Standard Elektrik Lorenz, Stuttgart), "Die Grenzen der Verstärkung von Wanderfeldröhren für Richtfunkstrecken," *Arch. elektr. Übertragung*, no. 7, pp. 273-286; July, 1959. (In German.)

It has been shown that the calculation of the minimum noise figure of electron-beam amplifiers can be performed in a manner similar to the calculation of the minimum noise figure of network fourpoles.

M. T. Vlaardingerbroek "Noise in electron beams and in four-terminal networks," *Phillips Res. Repts.*, vol. 14, no. 4, pp. 327-336; August, 1959. (In English.)

At the Institut für Hochfrequenztechnik, of Zürich, a study of rectangular electron beams has been conducted.

R. A. Aeschlimann, "Untersuchungen über Elektronenstrahlen mit rechteckigen Querschnitt," Juris-Verlag, Zürich, dissertation at Eidgenössische Technische Hochschule, no. 2866; 1959. (In German.)

An analysis has been made of the interaction between an electron beam and an electromagnetic wave propagating along a helix wound around the beam. The conditions of operation of a traveling-wave tube have been calculated, and the characteristic curves established. Numerical applications have been made, using an electronic computer.

A. Martorell, "Análisis de un tubo de onda progresiva," *Rev. Telecommunic.*, no. 54, pp. 2-14; December, 1958. (In Spanish.)

Problems involved in the design of low-noise traveling-wave tubes have been studied in order to improve their noise figure.

P. H. J. A. Kleijnen, "Traveling wave buizen," *Tijdschr. Nederl. Radiogenootsch.*, vol. 24, nos. 2/3, pp. 71-88; 1959. (In Dutch.)

A. Versnel, "Lopende golfbuizen met laag ruisgetal," *Tijdschr. Nederl. Radiogenootsch.*, vol. 24, nos. 2/3, pp. 101-112; 1959. (In Dutch.)

A traveling-wave tube with helical conductor with an output power of 10 w at 4000 mc has been realized.

C. T. de Wit (Natuurk Lab., N. V. Philips Gloeilampenfabr., Eindhoven), "Een 10 watt lopende golfbuis voor de 7.5 cm band," *Tijdschr. Nederl. Radiogenootsch.*, no. 2-3, pp. 89-100; 1959. (In Dutch.)

A traveling-wave amplifier operating at 4 kmc has been developed for use in transmitters of multi-channel microwave links.

W. Klein (Telefunken, Ulm/Donau), "Die Wanderfeldröhre TL 6 als Endverstärker in 4 GHz-Richtfunkanlagen," *Fernmelde Frax*, no. 21, pp. 810-820; November, 1959. (In German.)

Considerable work has been done at the French firm Compagnie Générale de Télégraphie sans Fil (C.S.F.) concerning *M*-type tubes. Theoretical and experimental approaches have been used simultaneously in order to determine precisely the phenomena involved. The results of an experimental study made on an electron gun for traveling-wave tube have been analyzed as concerns the variation of the cathode current vs the applied voltage in the presence of a magnetic field.

A. F. Leblond (C.S.F., Paris), "Study of the electron trajectories in guns for *M*-type tubes," *Proc. IEE*, pt. B, vol. 105, suppl. no. 12, pp. 1021-1023; May, 1958.

A new analogous method has been used for studying the grouping of electrons in a beam in interaction with a slow wave in the presence of crossed electrical and

magnetic fields. Interesting experimental results have been obtained this way.

B. Epsztajn (C.S.F., Paris), "An experimental study of large signal behaviour in *M*-type valves in the presence of space charge by the use of an analogous method," *Proc. IEE*, pt. B, vol. 105, suppl. no. 10, pp. 598–604; May, 1958.

Two kinds of anomalous phenomena have appeared during the development of *M*-type carcinotron: concerning the static behavior of the tube, independent of 1) RF phenomena and 2) dynamical phenomena. The latter are: anomalous power/current characteristics, parasitic oscillations, hysteresis and discontinuities.

J. Nalot and R. Visocekas (C.S.F., Paris), "Anomalous behaviour in the *M*-type carcinotron," *Proc. IEE*, pt. B, vol. 105, suppl. no. 10, pp. 538–542; May, 1958.

An experimental tube analogous to the *M*-type carcinotron, the carmatron, has been realized and its characteristics compared with that of *M*-type carcinotron and variable voltage magnetron.

O. Doehler, B. Epsztajn, and J. Arnaud (C.S.F., Paris), "Operational characteristics of the carmatron tube," *Proc. IEE*, pt. B, vol. 105, suppl. no. 10, pp. 529–533; May, 1958.

It has been shown that the advantages of the *M*-type tubes, namely their high efficiency (45 per cent) and their high-power capabilities (1 kw at 3000 mc), can be preserved in pulsed operation, and the problems arising from this mode of operation have been discussed. Tubes of this type operating in the *S* and *X* bands have been constructed.

M. Favre (C.S.F., Paris), "Results obtained on cross-field carcinotrons under pulsed operation," *Proc. IEE*, pt. B, vol. 105, suppl. no. 10, pp. 533–537; May, 1958.

A pulsed magnetron amplifier delivering a peak output power of several megawatts, with an efficiency of 50 per cent and a relative bandwidth of 15 per cent, has been developed by Compagnie Française de Télégraphie sans Fil. This tube operates by interaction between an electron beam simultaneously perpendicular to the electrical and magnetic fields. The tube is of coaxial shape, the beam being bent by a magnetic field produced by an intense direct current circulating in the circular sole.

O. Doehler, A. Dubois, and D. Maillart (C.S.F., Paris), "An *M*-type pulsed amplifier," *Proc. IEE*, pt. B, vol. 105, suppl. no. 10, pp. 454–457; May, 1958.

The Compagnie Générale de Télégraphie sans Fil continues the development of type-*O* carcinotron, directed towards higher operating frequencies. In this way, furthering the previous development of tubes operating up to 100 kmc, laboratory samples of type-*O* carcinotrons oscillating up to 170 kmc have been constructed. These tubes involve a convergent gun delivering a concentrated beam, the density of which is 40 to 50 a/cm². The output power is about 1 mw, but it appears possible to design tubes delivering up to 50 mw at 150 kmc. Improvements on hand will probably permit operation at a frequency of 200 to 250 kmc rather near the limit of this kind of tube, estimated to be in the vicinity of 300 kmc.

Yeou Ta (C.S.F., Paris), "Carcinotrons de type *O* fonctionnant à 2 mm," *Onde électrique*, no. 391, pp. 789–794; October, 1959. (In French.)

The manufacture of *M*-type carcinotrons necessitates a high mechanical accuracy. Technological processes have been developed in order to meet the requirements of production of very small electrodes, especially for the millimetric-wave tubes.

G. Boucher (C.S.F., Paris), "Technology of carcinotrons for short and long wavelengths," *Proc. IEE*, pt. B, vol. 105, suppl. no. 12, pp. 897–900; May, 1958.

A backward-wave oscillator has been developed by Siemens und Halske A.G., using a circular beam of 0.3 mm to 0.35 mm diameter and a current density of 15 to 20 a/cm². The beam is guided in the space of interaction with the delay line, by means of a permanent magnet. This tube oscillates from 26.5 to 48 kmc and delivers a power greater than 40 mw.

F. Gross (Siemens und Halske, München), "Ein Rückwärtswellenoszillator mit periodischer Verzögerungsleitung für den Frequenzbereich von 25 bis 48 GHz," *Arch. elekt. Übertragung* no. 8, pp. 356–362; August, 1959. (In German.)

The Gundlach theory has been applied to the *O*-type carcinotron using an interdigital line poorly matched. The effects of the reflections on the frequency characteristic of the tube have been studied, as well as the case of transients. The results fit well with experimental results.

K. H. Loecherer (Inst. Hochfrequenztech., Univ. Berlin), "Bemerkungen zur Theorie der Rückwärtswellenröhre," *Nachrichtentech. Z.*, no. 4, pp. 187–192; April, 1959. (In German.)

At the University of Berlin, carcinotron-type tubes using interdigital lines have been constructed. The influence of reflections on the frequency stability has been studied in detail, and a tube operating in the 4–8 cm band realized, giving an output power of 50–800 mw.

G. Bolz (Tech. Univ., Berlin), "Aufbau und Eigenschaften von Rückwärtswellenröhren," *Nachrichtentech. Z.*, no. 3, pp. 120–127; March, 1959. (In German.)

1.2 Gas Tubes

1.2.1 *Duplexer tubes*: The difficulties encountered in the realization of high-power twin TR tubes for the 23-cm band have led to another solution, using a total coupling junction. This leads to a very simple construction, and the gas tube is easy to replace.

P. Tchéditch (C.S.F., Paris), "Duplexeur pour grande puissance dans la bande 23 cm," *Onde électrique*, vol. 38 (August, 1958), special suppl. no. 376 ter, pp. 478–480; March, 1959. (In French.) This special supplement of *Onde électrique*, published in March, 1959, will hereafter be referred to as simply "special suppl. no. 376 ter; March, 1959."

For powers higher than 15 mw in the *S* band, a screen duplexer has been realized. It utilizes a totally coupled junction, the window of which contains small quartz tubes with argon. Such devices have been tested with peak powers up to 30 mw.

R. Vauthey (C.F.T.H.), "Duplexeur à rideau et son utilisation en très grande puissance," *Onde électrique*, special suppl. no. 376 ter, pp. 488-493; March, 1959. (In French.)

The problem of high-power duplexing in millimetric waves has been solved by the use of a 3-db hybrid junction containing gas tubes, and acting as a switch. This solution appears to be reliable and much better than the one using conventional TR and ATR tubes, which are too difficult to manufacture and unable to withstand high power.

H. Weill (S.N.E. Radio-Industrie, Paris), "Duplexeur haut niveau à large bande réalisable en ondes millimétriques," *Onde électrique*, special suppl. no. 376 ter, pp. 473-477; March, 1959. (In French.)

1.2.2 *Gas masers*: The effects of the multiple diffusion of the optical resonance light upon the lifetime of the excited atomic level are studied. The theory allows to find again the case of one atom (single diffusion); for two atoms, the equations of evolution of the excited state probabilities are coupled by coefficients that physically correspond to the passage of the excitation from one atom to another. This is then applied to the case of N atoms in a gas. Some experiments confirm the prevision of the theory.

J. P. Barrat, "Etude de la diffusion multiple cohérente de la lumière de résonance optique. Application au niveau 6^3P_1 du mercure," *J. Phys. Radium*, vol. 20, pp. 541-548; May, 1959; pp. 633-646, June, 1959; p. 657; July, 1959. (In French.)

A realization of a beam cesium atomic clock is going on in Italy at Torino, where the study was begun in 1957. The report is concerned with the first eighteen months work.

M. Boeala, "Costruzione di un campione di frequenza al cesio presso l'Istituto Elettrotecnico Nazionale 'Galileo Ferraris'," *Ricerca sci.*, vol. 29, pp. 267-271; February, 1959. (In Italian.)

1.2.3 *Plasmas*: A theoretical analysis of the plasma-field coupling has been conducted with a careful study of the hypothesis. The fundamental equations thus established have been applied to the study of the main types of electromagnetic and magnetohydrodynamic waves capable of propagating through a thoroughly ionized plasma.

J. M. Dolique (C.S.F., Paris), "Propagation des ondes électromagnétiques dans les plasmas complètement ionisés résistifs," *Ann. Radioélect.*, no. 56, pp. 107-141; April, 1959. (In French.)

A study has been made of the propagation constant of the TE_{10} modes in a rectangular waveguide containing a thin film of gyroelectric plasma.

L. Gabarre and L. Cairo (Inst. Henri-Poincaré, Paris), "Méthode variationnelle pour la propagation des ondes électromagnétiques dans un plasma," *Compt. Rend. Acad. Sci., Paris*, no. 18, pp. 1750-1752; November 2, 1959. (In French.)

A study has been conducted of the electronic distribution in an inhomogeneous and anisotropic Lorentzian plasma by means of statistical mechanics, and the results have been extended to the case of an applied alternative field.

R. Jancel and T. Kahan (Inst. Henri-Poincaré, CNRS, Paris), "Mécanique statistique d'un plasma lorentzien inhomogène et anisotrope: étude de la distribution électronique," *J. Phys. Radium*, no. 10, pp. 804-811; October, 1959. (In French.)

Stable RF plasmoids have been obtained, at the resonance frequency of the plasma, with a density of about 10^7 electrons/cm³ and a temperature in the vicinity of 10^5 °K.

R. Geller, "Production de plasmoides de haute fréquence stables à la fréquence de résonance du plasma," *Compt. Rend. Acad. Sci., Paris*, no. 25, pp. 2749-2751; December 21, 1959. (In French.)

A plasma torch operating in the 2400-mc band has been realized. It consists of a coaxial blow-pipe and a microwave generator using a CW magnetron. It is thus possible to create, in an oxygen-free zone, a temperature higher than 3000°C with a power less than 1 kw. In the useful zone, the active molecules are dissociated by free electrons. At the output of the waveguide, the plasma forms a glowing zone where ions recombine at the contact of the material to be heated and transmit their bonding energy under heat form.

W. Schmidt (Entwicklungsab., Valvo GmbH), "Der mikrowellen-Plasmabrenner," *Elektron. Rundschau*, no. 11, pp. 404-406; November, 1959. (In German.)

1.2.4 *Miscellaneous*: In order to produce harmonics of an RF field, an oscillating beam of secondary electron has been directed, through holes in the cavity, towards a resonator tuned on harmonics. With the oscillating multiplication producing a high proportion of harmonics, resonators are excited.

K. Krebs and H. von Villiez (Phys. Inst. tech., Univ. Berlin), "Die Anregung von Hohlraumresonatoren durch Pendelvervielfachung von Sekundärelektronen," *Z. Phys.*, vol. 154, no. 1, pp. 27-33; 1959. (In German.)

2. PASSIVE CIRCUITS AND SOLID-STATE DEVICES

2.1 *Transmission Lines*

Silver-plated microwave elements of very high precision (better than 1/100 mm) were obtained by the Laboratoire de Radioélectricité de la Faculté des Sciences de Clermont-Ferrand by evaporating silver in vacuum on "Plexiglass" and after depositing copper by electroforming.

G. Raoult and R. Fauguin, "Galvanoplastie sur plexiglass argenté. Son application à diverses réalisations hyperfréquences," *J. Phys. Radium*, vol. 20, pp. 29A-31A; April, 1959. (In French.)

The principal causes of perturbations in microwave guides have been studied; it is shown that generally the differences in aperture dimensions produce more mismatch than assembling defects such as off-settings, rotation or misaligning. Siemens und Halske A.G. has realized a universal measuring line for the 1-13 gc band, the realization of the junctions is described in detail, concurrently with that of the isolating supports.

- U. V. Kienlin and A. Kuerlz (Siemens und Halske A.G., München), "Reflexionen an Hohlleiter—Flanschverbindungen Entwicklungs," *Ber. S. und H. Akt. Ges. Dtsch.*, vol. 22, pp. 85–88; April, 1959. (In German.)
- W. Krauss (Berlin), "Spezielle probleme der Höchfrequenz—Mess-technik mit Hohlleitern," *Nachrichtentech. Z.*, pp. 351–359; August, 1959. (In German.)
- M. Ebisch (Siemens und Halske A. G., München), "Koaxiale Mess-leitung—Einsätze Hoher Genauigkeit für den Frequenzbereich 1 bis 13 GHz," *Frequenz Deutsch.*, no. 2, pp. 52–56; February, 1959. (In German.)

Researches on transmission of TE_{01} waves in circular waveguides are pursued.

- P. Marie (C.N.E.T., Issy-les-Moulineaux), "Transition créant le mode TE_{01} circulaire à partir du mode TE_{01} rectangulaire," *Onde électrique*, special suppl. no. 376 ter, pp. 471–472; March, 1959. (In French.)
- A. Jauman (Zentral Lab. Siemens und Halske A.G., München), "Ueber Richtungkoppler zur Erzeugung des H_{01} —Welle in runden Hohlleiter—Entwicklung," *Ber. S. und H. Akt. Ges.*, vol. 22, pp. 12–18; April, 1959. (In German.)
- J. Bendayan, G. Comte and M. Thue (C.N.E.T., and Les Câbles de Lyon), "Research on transmission of TE_{01} waves in circular waveguides in the vicinity of 25 and 35 Gc/sec," *Proc. IEE*, pt. B, vol. 106, suppl. no. 13, pp. 94–99; January, 1959. (In English.)
- H. Schnitger, "Die Hohlkabeltechnik," *Jahrb. elekt. Fernmeldewes.*, vol. 10, pp. 109–147, 1958 (In German.)

2.2 Linear Circuits

2.2.1 Dipoles: A calorimeter for the measurement of high power was studied. The dissipative device is not mounted in the main waveguide but is coupled to it by means of a grating. The precision is better than two per cent.

- T. Jaeger and M. V. Schneider (Inst. Hochfrequenztech., Eidgenoss. tech. Hochsch., Zürich), "Ein Breitbandiges Mikrowellenkalorimeter für Hohe Leistungen," *Arch. elektr. Übertragung.*, vol. 13, pp. 21–25; January, 1959 (In German.)

The impedance presented by a reflex-klystron to its output guide out of an oscillating lobe varies rapidly with reflex electrode voltage. This impedance variation can be utilized to amplitude modulate the energy flowing through a waveguide. The modulation obtained is linear.

- R. Metivier and P. Audoin (C.F.T.H., Paris), "Modulation en amplitude à l'aide d'un klystron-reflex de l'énergie hyperfréquence transmise sur un guide d'ondes," *Onde électrique*, special suppl. no. 376ter, pp. 509–512; March, 1959. (In French.)

2.2.2 Reciprocal multipoles: In view of the study of octopoles and of lossless directional couplers, a graphical method is described for the determination of the reflection coefficient based on the positions of short-circuiting slugs.

- H. Lueg (Telefunken Ulm/Donau), "Méthode de mesure pour l'examen des octopoles et coupleurs directs sans pertes entre les lignes homogènes utilisant des pistons de court-circuits," *Onde électrique*, special suppl. no. 376 ter, pp. 380–387; March, 1959. (In French.)

A theoretical and experimental study was conducted on the necessary conditions for the convenient measurement of a symmetrical impedance. The measurement is easy, provided a symmetrical measuring line is available.

- H. Fricke (Tech. Hochsch., Aachen), "Messung symmetrischer Scheinwiderstände im Meter und Dezimeterwellengebiet," *Nachrichtentech. Z.*, vol. 12, pp. 233–238; May, 1959. (In German.)

A certain number of microwave filter studies were published in the special supplementary issue of *Onde électrique*, vol. 38.

- L. Milosevic (C.F.T.H., Paris), "Blocs d'aiguillage sélectif en hyperfréquence," *Onde électrique*, special suppl. no. 376 ter, pp. 341–369; March, 1959. (In French.)
- S. Drabovitch (C.F.T.H., Paris), "Un filtre U.H.F. à faibles pertes pour liaisons hertziennes 'transhorizon'," *Onde électrique*, special suppl. no. 376, pp. 412–418; March, 1959. (In French.)
- M. Clement (Cie gén. télégr. sans fil, Paris), "Etude et réalisation d'aiguillage par filtres en anneaux pour faisceaux hertziens," *Onde électrique*, special suppl. no. 376 ter, pp. 419–423; March, 1959. (In French.)
- R. Havot (Lab. électron. Phys. appl., Paris), "Filtres de branchement pour faisceaux hertziens à 4000 MHz," *Onde électrique*, special suppl. no. 376 ter, pp. 441–446; March 1959 (In French.)
- P. Marie (C.N.E.T., Issy-les-Moulineaux), "Filtres d'aiguillage hyperfréquence," *Onde électrique*, special suppl. no. 376 ter, pp. 424–429; March, 1959. (In French.)

A paper dealing with the computation of microwave filters was published by Societa Magneti Marelli, Milano. It recalls the most important papers already published and presents an abacus for the quick computation of a filter and the rules to be applied to obtain a particular response. It also describes some filters realized in the 800–2000 MHz band.

- L. Caroli and U. Cucina, "Progetto e attuazione di filtri per micro-onde," *Alta frequenza*, vol. 28, pp. 211–232; July–August, 1959. (In Italian.)

Siemens und Halske A.G. have published a study of filters considering only those networks which have attenuation poles. These networks can be utilized in filters which must present a very high attenuation on only one side of the pass-band.

- F. Kuenemund (Siemens und Halske A.G., München), "Hohlleiter-filter mit verteilter Dämpfungscharakteristik," *Frequenz Deutsch.*, vol. 13, pp. 97–102; April, 1959. (In German.)

A coaxial three-path rotary joint and a multiple-path rotary joint realized by means of annular waveguides was described in the special supplementary issue of *Onde électrique*. A very small dead angle is left in multiple-path rotary joint.

- A. Depauw and J. Danis (SNE Radio-Industrie, Paris), "Joint tournant à trois voies hyperfréquences," *Onde électrique*, special suppl. no. 376 ter, pp. 460–462; March, 1959 (In French.)
- M. Sirel (SNE Radio-Industrie, Paris), "Joint tournant à nombre de voies multiples," *Onde électrique*, special suppl. no. 376 ter, pp. 463–470; March, 1959. (In French.)

Some directional couplers were studied in 1959. Perturbation calculus allows the computation of a directional coupler having a longitudinal slot of any section. For a particular attenuation, the width of the slot increases when the guide wavelength decreases, or when the intensity near the slot decreases, or else when the length of the coupling decreases. Some experimental results confirm these theoretical data.

H. Pascher (Siemens und Halske A.G., München), "Langschlitz—Richtungskoppler für H. Wellen," *Arch. elekt. Übertragung*, vol. 13, pp. 76–82; February, 1959. (In German.)

A skin coupler may be obtained by reducing the wall thickness between two cylindrical waveguides so that transmission of microwave power through the wall is possible. The "top wall coupler" has promising properties as a broad-band system. The loss of the system cannot be avoided. Application for *K*-band, *J*-band frequencies and above seems to be promising. The thin metallic layers can also be used as detector-devices.

V. M. Schneider (Ecole polytechnique fédérale, Zürich), "The skin coupler, a method of directional coupling," *Onde électrique*, special suppl. no. 376 ter, pp. 375–377; March, 1959. (In English.)

M. Schneider, "Eigenschaften und Anwendungen dünner metallischer Schichten im Mikrowellenbereich," *Tech. Mitt. P.T.T.*, vol. 37, pp. 465–495; November, 1959. (In German.)

A coaxial directional coupler has been studied in Italy. They consider the two lines coupled by an octopole, and demonstrate that directional coupling is obtained for certain internal structures of the octopole and certain values of the impedances which constitute it. They deduct the directional condition, the coupling expressions, and the input impedance.

I. Bucci (Fabbr. Ital. Magneti Marelli, Milano), "Accoppiatori diretti in linea coassiale," *Alta Frequenza* vol. 28, pp. 260–276; July–August, 1959. (In Italian.)

A few circuits which allow stabilization of the klystron frequency by means of a cavity have been described:

J. Fagot and J. Queva (Cie gén. Télégr. sans Fil, Paris)—"Stabilisation d'un klystron-reflex par une cavité extérieure à haute surtension," *Onde électrique*, special suppl. no. 376 ter, pp. 395–402; March, 1959. (In French.)

L. Milosevic (C.F.T.H. Paris)—"Oscillateur stabilisé," *Onde électrique*, special suppl. no. 376 ter, pp. 403–411; March, 1959. (In French.)

Circuits which allow automatic frequency control are also described:

L. del Bello (Fabr. Apparech. Communic. electr. Standard, Milano), "Commando di Frequenza per clistron con cavità di riferimento," *Alta Frequenza*, vol. 27, pp. 629–633; December, 1958. (In Italian.)

C. Levallant (C.F.T.H., Paris), "Discriminateur hyperfréquence à large bande; application aux têtes HF monobouton," *Onde électrique*, special suppl. no. 376 ter, pp. 513–528; March, 1959. (In French.)

B. Basini (Fabbr. Ital. Magneti Marelli, Milano), "Cavità di riferimento per comando automatico di frequenza," *Alta frequenza*, pp. 277–284; July–August, 1959. (In Italian.)

At the end the preceding paper, the author describes a particular cavity with ferrite giving a modulable resonant frequency. Its utilization is described.

Wide-band ferrite attenuators, with low insertion losses, may eventually dissipate important UHF powers and allow the control and the adjustment of the UHF power.

P. Sermet and J. Murier (Lab. HF, Fac. Sci., Grenoble), "Asservissement et régulation de puissance dans les bandes *X* et *S* par des atténuateurs à ferrites," *Onde électrique*, special suppl. no. 376 ter, pp. 529–534; March, 1959. (In French.)

A simple network, comprising klystron, absorption wavemeter, detection crystals, and magic *Te*, allows one to measure *Q* factors from 2000 to 8000 as well as much lower values (about 200) in the *X* band. The measuring method and its precision are given.

A. Strub (Lab. HF, Fac. Sci., Univ. Grenoble), "Appareillage simple pour la mesure de facteurs de surtension dans la bande *X*," *J. Phys. Radium*, vol. 20, pp. 42A–43A; April, 1959. (In French.)

A spectrometer using the cavity and pulse techniques has been studied; the output response signals from a reference cavity and the measuring cavity are not directly compared. They are sent through two pulse generators whose networks trigger pulses of a microsecond on determined points of each response curve. The measure is obtained by comparison of the relative position of these pulses on the screen of a synchroscope.

A. Gozzini, A. Battaglia (Ist. Fis., Univ. Piza), G. Boudouris, D. Ilias (Lab. Phys. Atmosph., Paris), and F. Bruin (Naturr. Lab., Univ. Amsterdam), "Un spectromètre en microonde utilisant la technique des cavités et des impulsions," *Onde électrique*, special suppl. no. 376 ter, pp. 430–440; March, 1959. (In French.)

2.2.3 Nonreciprocal multipoles: A number of studies on ferrites and their behavior in UHF have been published in 1959.

A. Vassiliev (Cie gén. Télégr. sans Fil, Paris), "Contribution à l'étude des ferrites pour leur emploi en UHF," *Onde électrique*, spec. suppl. no. 376, pp. 574–581; March, 1959. (In French.)

F. Picherit, "Effet Faraday de divers bâtonnets de ferrites," *Compt. Rend. Acad. Sci., Paris*, vol. 249, pp. 69–70; July 6, 1959. (In French.)

Equimolecular substitution of Cr_2O_3 or Al_2O_3 in Ni-Zn ferrites allows the absorption of UHF waves crossing the material to diminish considerably.

W. Kagan and R. Vautier (C.N.R.S., Paris), "Ferrites à faibles pertes en hyperfréquence," *Onde électrique*, special suppl. no. 376 ter, pp. 560–564; March, 1959. (In French.)

R. Vautier and W. Kagan (Lab. Magnétisme, C.N.R.S., Bellevue), "Propriétés aux hyperfréquences de ferrites chromites de Ni-Zn," rept. of Colloque National de Magnétisme, Strasbourg, July 8–10, 1957, pp. 326–336; 1959. (In French.)

The variations with the temperature of the resonant frequency and of the nonreciprocal phase delay or the Faraday rotation nearly disappear for certain dimension of ferrite element.

W. Haken and C. von Haza-Radlitz (Siemens und Halske A.G., München), "Ferrit-Körper mit Temperaturunabhängigen gyromagnetischen Eigenschaften," *Arch. elektr. Übertragung*, vol. 13, pp. 157–160; April, 1959. (In German.)

The propagation in circular waveguide filled up with a gyromagnetic substance was studied in the particular case where the low value of susceptibilities allows the definition of two modes: one quasi TE and one quasi TM. The expressions of the different emergent-wave characteristics were obtained: wavelength, absorption, polarization-plan rotation and ellipticity.

J. Soutif (Lab. Electrostatique Phys. du métal, Grenoble), "Propagation dans un guide d'onde circulaire rempli d'une substance gyromagnétique," *Onde électrique*, special suppl. no. 376 ter, pp. 599–601; March, 1959. (In French.)

The report of the Colloque National de Magnétisme, Strasbourg (July 8–10, 1957) was published in 1959. An experimental study to check the theoretical results shortly recalled was described. Metals salts in state *S* were used where the ship-orbit coupling did not interfere and where the powder isotropy was obtained, not by mean, but by an intrinsic quality of each grain.

J. Soutif-Guicherd, "Effet Faraday paramagnétique," rept. of the Colloque National de Magnétisme, Strasbourg, July 8–10, 1957, pp. 301–303; 1959. (In French.)

The measurements of ferrite complex permeability show anomalies incompatible with the classical theory of the gyromagnetic effect. The resonant points found at very high frequencies are attributed to the spin waves. The anomalies that exist at lower frequencies may be explained in considering the ferromagnetic material as formed by little magnets with mutual induction.

P. M. Prache (Soc. Lignes Télégr. Téléph., Paris), "Les anomalies de la perméabilité des ferrites aux fréquences élevées," *Bull. Soc. franç. électriciens*, vol. 9, pp. 329–340; June, 1959. (In French.)

The propagation modes in a waveguide with parallel walls filled up with ferrite magnetized in a parallel to walls direction were calculated. They determine a relatively simple form of the characteristic equation.

G. Barzilai and G. Gerosa (Ist. Elettrotec., Univ. Roma), "Modes in rectangular guides filled with magnetized ferrite," *Onde électrique*, special suppl. no. 376, pp. 612–617; March 1959. (In English.)

G. Barzilai and G. Gerosa, "Modes in rectangular guides partially filled with transversely magnetized ferrite" IRE TRANS. ON ANTENNAS AND PROPAGATION, vol. AP-7, special suppl., pp. S471–S474; December, 1959.

The propagation of electromagnetic waves in a circular waveguide containing a gyromagnetic material was studied. The gyromagnetic axis of the material is parallel to the waveguide. The material has the shape of a cylindrical envelope of thickness δ adjacent to the waveguide wall.

A. P. van Gelder, A. M. de Graaf, and R. Kronig (Tech. Hogeschool, Delft), "New calculations on the Faraday effect in wave guides," *Appl. Sci. Res.*, vol. 7, pp. 441–448; 1959. (In English.)

A relatively large number of papers have been published on the realization of nonreciprocal circuit elements "Uniline" and "circulators."

R. Taupin and M. Hai Thai (Cie Gén. Télégr. sans Fil, Paris), "Emploi des ferrites dans les circuits hyperfréquences," *Onde électrique*, special suppl. no. 376 ter, pp. 582–587; March, 1959. (In French.)

H. G. Beljers (N.V. Philips, Eindhoven), "Ferrite isolators in the 8–9 mm waveband," *Onde électrique*, special suppl. no. 376 ter, pp. 617–648; March, 1959. (In English.)

R. Dessert (L.E.P., Paris) "Eléments de circuits hyperfréquence non réciproques utilisant des ferrites," *Onde électrique*, suppl. no. 376 ter, pp. 653–659; March, 1959. (In French.)

M. Vadjjal and A. Fiorini (Univ. Padoue), "Sfasatore con ferrite per circolatori a larga banda," *Note Recens., Notiz.*, vol. 8, pp. 305–312; May–June, 1959. (In Italian.)

E. Schanda (Wien), "Einwegschwächer in Rechteck—Hohlleitern," *Elektrotech. u. Maschinenbau*, vol. 76, pp. 174–177; April, 1959. (In German.)

Milano has studied more particularly the influence of the dielectric support and the geometrical dimensions of the ferrite plate.

U. Milano (Ist. sup. Poste e Telecommunic., Roma), "Isolateurs de résonance à plaques diélectriques dans la bande X," *Onde électrique*, special suppl. no. 376 ter, pp. 569–573; March, 1959. (In French.)

U. Milano, "Sul comportamento di ferriti di Ni-Zn e di Mg-Mn in attenuatori non reciproci a risonanza ferromagnetica nella gamma dei 900 MHz," *Note Recens., Not. Ital.*, vol. 8, pp. 611–633, November–December, 1958; pp. 3–20, January–February, 1959. (In Italian.)

Siemens und Halske A.G. pursued the study of ferrites and of their UHF applications. They particularly studied the demagnetization factors of the ferrite element set in waveguides.

W. Haken (Siemens und Halske A.G., München), "Ueber den Einfluss leitender Flächen auf die gyromagnetische Resonanz von Ferritkörpern, Entwicklung," *Berl. S. und H. Akt. Ges.*, vol. 22, pp. 28–32; April, 1959. (In German.)

J. Deutsch (Siemens und Halske A.G., München), "Einige Ferrit-Bauelemente für die Mikrowellentechnik," *Nachrichtentech. Fachber.*, vol. 12, pp. 9–14; 1958. (In German.)

J. Deutsch, N. Haken, and C. V. Hazaradlitz (Siemens und Halske A.G., München), "Neue Richtungsleitungen für Richtfunksysteme," *Nachrichtentech. Z.*, vol. 12, pp. 367–370; July, 1959. (In German.)

High-frequency modulation in waveguides is possible by Faraday effect. An example is given of realization allowed to reach a frequency modulation up to 10 mc.

F. Dachert, J. Robieux and P. Trevoux (Cie gén. Télégr. sans Fil, Paris), "Nouvelles applications des ferrites en hyperfréquence," *Ann. Radioélectr.*, vol. 14, pp. 17–30; January, 1959. (In French.)

2.3 Nonlinear Circuits and Quantic Networks

2.3.1 *Semi-conductor devices:* Improvements were brought up to classical mixers for radio links in the 4000-mc band.

R. Bergere (LMT Boulogne-Billancourt), "Mélangeurs haut et bas niveaux pour faisceaux hertziens," *Onde électrique*, special suppl. no. 376 ter, pp. 494–498; March, 1959. (In French.)

The Eidgenössische Technische Hochschule, Zürich, has published a paper on frequency mixing in the UHF band.

F. Furrer, "Ueber Frequenzumsetzung im Mikrowellenbereich," *Juris-Verlag, Zürich*, dissertation ETH No. 2864; 1959. (In German.)

Some new theoretical and experimental studies have been made concerning the possibility of developing a maser for submillimetric or infrared waves, at the Institute of Physics of the University of Cologne.

D. Geist, "Sind die Landaus niveaus der freien Träger für einen Submillimeterwellen Halbleitermaser ausmiltzbar?" *Z. Naturforschg.*, pt. a, vol. 14, p. 752; August, 1959. (In German.)

At the Atomic Energy Center, in Saclay (France), Combrisson and Solomon study the silicon at the temperature of liquid helium:

J. Combrisson and I. Solomon, "Polarisation dynamique du silicium 29 à basse température," *J. Phys. Radium*, vol. 20, p. 683; July, 1959. (In French.)

Several writers give equivalent schemes for the parametric amplifiers using variable-capacitance silicon diodes; these theoretical studies end in an evaluation of the gain-bandwidth product, stability and noise figure.

J. C. Simon, "Action d'une perturbation progressive sur une onde électromagnétique guidée," *Ann. radioélectricité*, vol. 14, pp. 3-16; January, 1959. (In French.)

W. Dahlke, R. Maurer, and J. Schubert, "Theorie des Dioden-Reaktanzverstärkers mit Parallelkreisen," *Arch. elekt. Übertragung*, vol. 13, pp. 321-340; August, 1959. (In German.)

A. P. Speiser, "Parametrische Resonanz und Parametrische Verstärker," *Sci. électr.*, vol. 5, pp. 61-75; June, 1959. (In German.)

2.3.2 Devices using magnetic resonances: An approach is made by several workers in France (especially at the University of Grenoble), with the object of having a better knowledge of the solid-state phenomena involved in the ferromagnetic materials.

R. Pauthenet, "Résultats expérimentaux sur le blocage du moment magnétique de l'ion terre rare dans les grenats," *J. Phys. Radium*, vol. 20, p. 388; February-March, 1959. (In French.)

J. Pauleve, B. Dreyfus, and M. Soutif, "Résonance ferrimagnétique des ferrites et grenats à température de compensation," *J. Phys. Radium*, vol. 20, p. 355; February-March, 1959. (In French.)

R. Aleonard and J. C. Barbier, "Etude paramagnétique à haute température des ferrites grenats de terres rares," *J. Phys. Radium*, vol. 20, p. 378; February-March, 1959. (In French.)

G. Villers, R. Pauthenet, and J. Loriers, "Propriétés magnétiques des ferrites du type grenat substitués par Al, Ga et Cr," *J. Phys. Radium*, vol. 20, p. 382; February-March, 1959. (In French.)

G. Asch, "Résonance magnétique du cobalt polycristallin à 35,500 MHz en fonction de la température," *Compt. Rend. Acad. Sci. (Paris)*, vol. 248, no. 6, pp. 781-784; February 9, 1949. (In French.)

Some experimental studies are made that end in the realizations of ferromagnetic parametric amplifiers.

G. A. Boutry, "Amplificateurs paramétriques et annihilation de l'hystérésis ferromagnétique par polarisation orthogonale," *Compt. Rend. Acad. Sci. (Paris)*, vol. 248, no. 3, pp. 384-386; January 19, 1959. (In French.)

2.3.3 Solid-state masers: Theoretical studies concerning the possibilities of the several quanta transitions between Zeeman Sublevels, and the shapes of the lines, have led to an experimental work.

J. M. Winter, "Etude théorique et expérimentale des transitions à plusieurs quanta entre les sous-niveaux Zeeman d'un atome," *Ann. Phys.*, vol. 4, pp. 746-811; July-August, 1959. (In French.)

Groschwitz studied the probabilities of transition in the electromagnetic perturbation energy, taking into account the phases of the waves.

E. Groschwitz, "Zur theorie des Masers," *Z. Naturforsch.*, pt. a, vol. 14, pp. 305-307; March, 1959. (In German.)

A special microwave circuitry is developed with the aim of measuring physical constants of the matter, especially relaxation times, life time of the levels. The radio-frequency spectroscopy has made much progress improving the maser techniques.

M. Bruma, "Circuits hyperfréquences utilisables en spectroscopie paramagnétique électronique," *Onde électrique*, special suppl. no. 376 ter, pp. 547-549; March, 1959. (In French.)

M. Jacobowicz and J. Uebersfeld, "Effet Overhauser et double effet dans les fluides adsorbés sur le charbon," *Compt. Rend. Acad. Sci.*, vol. 249, no. 25, pp. 2743-2745; December 21, 1959. (In French.)

R. Kronig, "Fysisch onderzoek met microgolven," *Tijdschr. Nederl. Radiogenootsch.*, vol. 24, no. 2-3, pp. 113-117; 1959. (In Dutch.)

A. Landesman, "Etude de la relaxation d'une voie paramagnétique par observation de signaux de résonance nucléaire," *J. Phys. Radium*, vol. 20, p. 937; December, 1959. (In French.)

G. Raoult, R. Fanguin, and A. Chabrier, "Polarisation rotatoire magnétique de sels paramagnétiques Fe, Cr à 10,000 MHz," *Arch. Sci. (Geneva)*, vol. 12, fasc. spécial, pp. 215-225; 1959. (In French.)

G. Berthet, F. Blanc, J. Grangeon et G. Raoult, "Spectre de résonance paramagnétique électrique du chromicyanure de potassium," *Arch. Sci. (Geneva)*, vol. 12, fasc. spécial, pp. 226-233; 1959. (In French.)

Report of Advances in Microwave Theory and Techniques in Japan—1959*

KIYOSHI MORITA†, SENIOR MEMBER, IRE

INTRODUCTION

THIS report on advances in theory, experiments, and applications of the microwave field is based on papers appearing in the *Journal of the Institute of Electrical Communication Engineers of Japan*, which is the most widespread and well-esteemed journal in the communication and electronics field in Japan. Advances in the realms of microwave sources, detectors, transmission lines, measurements, radiation, and propagation are mentioned.

SOURCES AND DETECTORS

The traveling-wave-type parametric amplifier consisting of a periodically loaded transmission line with variable capacitance diodes was analyzed theoretically by using a T matrix of each stage which was reduced into a diagonal form [1]. Gain and noise figure characteristics were studied in this analysis. This theory was extended to another one [2], in which a new operator was introduced for the analysis. The operator is a product of a diagonal matrix expressing the pump phase relation and a T matrix of a basic section of a periodically distributed parametric amplifier. Power gain of the amplifier was determined by the use of the characteristic vectors which are derived from the characteristic roots of this operator in the case of the synchronous pumping.¹

[1] S. Saito, "Transmission line involving parametric elements, especially on periodically distributed parametric amplifier," *J. Inst. Elec. Commun. Engrs. Japan*, vol. 42, pp. 573–579; June, 1959.

[2] K. Kurokawa and J. Hamasaki, "An analysis of periodically distributed parametric amplifier," *ibid.*, vol. 42, pp. 579–585; June, 1959.

The nonlinear barrier capacitance of a silver bonded diode, which is composed of a silver whisker including gallium and an N-type germanium, was studied experimentally. The ratio of the variable capacitance to the constant one of the diode was very large in comparison with that of the usual variable capacitance diode. Cutoff frequency of the diode was as large as more than 400 kmc. The electrical forming was the most important process for the good characteristics of the diode, and the best condition of this process was determined.

* Received by the PGMTT, April 29, 1960.

† Tokyo Inst. Tech., Tokyo, Japan.

¹ The contents of this paper were also published in K. Kurokawa and J. Hamasaki, "Mode theory of lossless periodically distributed parametric amplifiers," *IRE TRANS. ON MICROWAVE THEORY AND TECHNIQUES*, vol. MTT-7, pp. 360–365; July, 1959.

[3] S. Kita and K. Sugiyama, "The nonlinear capacitance of silver bonded diode," *ibid.*, vol. 42, pp. 1186–1192; December, 1959.

The available output power of a ferrite parametric oscillator was discussed theoretically. In an ideal case in which RF fields of the signal and idler are uniform in a spherical ferrite sample, a magnitude of a uniform precession increases as the pump power becomes large. However, the magnitude cannot exceed a certain value after the generation of oscillation, even though the pump power increases. Power loss in the sample, except that due to the excitation of the uniform precession, may be neglected. If the RF fields in the sample are not uniform, further loss due to the nonuniformity increases with the pump power. Therefore, actual available power is limited by the loss in the sample.

[4] T. Hashimoto, "Theoretical consideration on the output power of Mavar," *ibid.*, vol. 42, pp. 1193–1199; December, 1959.

A disk-on-rod circuit, which is composed of a disk-loaded inner conductor and an outer shield, was studied as a slow wave circuit of a traveling-wave tube. The coupling between a higher order mode of the circuit and an electron beam, which flowed axially, was analyzed. Formulas for the phase constants and coupling impedances of the lowest and higher modes were derived. For the convenience of designing the circuit, cutoff frequencies, phase constants, and coupling impedances for the specified frequencies were given in figures. The measured values of the guided wavelength were in good agreement with the theoretical ones.

[5] K. Ura, M. Terada, and E. Sugata, "Analysis of higher mode operation of disk-on-rod type traveling wave tubes," *ibid.*, vol. 42, pp. 145–150; February, 1959.

A traveling-wave tube with a cavity as an input buncher was proposed for an efficient frequency multiplier. The effect of a drift space between input buncher cavity and output helix of the traveling-wave tube on the harmonic generation was studied theoretically, and the efficiency could be remarkably increased by choosing the length of the drift space properly. The experimental results on the determination of the optimum length of the drift space agreed substantially with the theoretical ones. The fifth harmonic power of –25 db below the input power of 4160 mc was obtained experimentally.

[6] K. Morita and M. Kawamura, "Effect of drift space on the harmonic power by cavity type traveling wave tube," *ibid.*, vol. 42, pp. 159–164; February, 1959.

The space charge effect in a reflex klystron was studied analytically by the successive approximation

method. Formulas of correction factors due to space charge for a bunching angle and a phase angle were derived. In case of rather large transit cycle, the bunching efficiency was expressed approximately in the form of a simple equation. The results were proved to be applicable to the usual reflex klystron, and also may be useful in evaluating the space charge effect of the reflex klystron.

- [7] M. Terada, H. Hamada, and E. Sugata, "Space charge effects in reflex klystron," *ibid.*, vol. 42, pp. 591-597; June, 1959.

A transfer function of an *O*-type backward-wave oscillator was obtained assuming that the tube acts as a linear device and that steady-state frequency response may be expressed approximately by power series expansion of a pair of poles [8]. Build-up time of the oscillator output and frequency pushing characteristics may be derived from this function. The output signal for the pulsed backward-wave amplifier may be calculated through the use of the Laplace transformation. Furthermore, the frequency pushing characteristics of an *O*-type backward-wave oscillator were analyzed in detail, taking the effects of space charge and circuit loss into account [9]. The results were confirmed experimentally by a helix-type backward-wave oscillator, and were in good agreement with measured values.

- [8] I. Sakuraba, "Transfer function of the *O*-type backward-wave oscillator," *ibid.*, vol. 42, pp. 750-754; August, 1959.
 [9] I. Sakuraba, "Analysis of the *O*-type backward-wave oscillator frequency pushing," *ibid.*, vol. 42, pp. 810-815; September, 1959.

Reduction of the beam noise was studied with respect to the power theorem. It is impossible to remove the beam noise in the slow wave, but the beam noise in the fast wave may be reduced because of the fact that the slow wave carries the negative power, whereas the fast wave has the positive one. Cavity coupler and helix coupler for a fast wave amplifier such as a parametric amplifier were proposed for the removal of the beam noise. The optimum noise figures were given theoretically in both cases.

- [10] S. Saito, "Some consideration of beam noise reduction from the point of power theorem, especially on fast wave amplifier," *ibid.*, vol. 42, pp. 221-225; March, 1959.

A novel theory on the minimum noise figure of a traveling-wave tube was derived. This is based on the Haus-Robinson theory concerning the minimum noise figure and the earlier theory on the noise reduction at the potential minimum plane proposed by Watkins. Higher current density at the potential minimum plane is more desirable and extreme low-noise figure, for example 2.2 db for 1000 mc, may be obtained, if current density as high as 300 ma/cm² at the potential minimum plane could be realized near the temperature-limited region. A divergent electron gun with a very small cathode area should be used for a low-noise traveling-wave tube, because large beam current is undesirable for that type of tube.

- [11] T. Ohkoshi, "On the minimum noise figure of traveling wave tubes—a theory considering the noise of the potential minimum plane," *ibid.*, vol. 42, pp. 833-838; September, 1959.

TRANSMISSION LINES

Advanced surface waveguides composed of thin dielectric sheets were proposed as a low-loss transmission line. The electric field is parallel to the dielectric sheet in the field configuration of the propagation mode. Two examples of *O* guide, which consists of a hollow cylindrical thin dielectric, and *X* guide, having an *X*-shaped dielectric structure in cross section, were described. The TE fundamental mode for the *O* guide was analyzed and its theoretical characteristics as a transmission line were discussed. A practical guide, such as thin polyethylene tube, is suitable for the SHF region, where the attenuation constant is lower than that of the coaxial line, *G*-line, and rectangular waveguide.²

- [12] M. Sugi and T. Nakahara, "Surface wave transmission line composed of dielectric sheet," *ibid.*, vol. 42, pp. 731-737; August, 1959.

A new variational principle was proved for the determination of the propagation constant of waveguide with wall impedance. The effect of the small wall impedance on the propagation constant and the separation of a degeneracy was discussed in detail. These results were compared with that from the perturbation method, which was improved to be applicable to a waveguide with inhomogeneous media. In this analysis, not only the TE and TM modes but also the TEM and hybrid modes may be treated simultaneously.

- [13] K. Kurokawa, "Propagation constants of waveguides with wall impedances," *ibid.*, vol. 42, pp. 60-61; January, 1959.

In a taper-type circular electric mode transducer, unwanted modes were analyzed in the excitation of the TE₀₁ mode. Telegraphist's equations of the transducer were derived in an oblique coordinate of a helix system by introducing the expanded transverse fields in terms of normal mode functions of sector waveguides into Maxwell's equations. From these telegraphist's equations inhomogeneous second-order linear differential equations were obtained. Magnitudes of the unwanted modes were determined by integrating these equations numerically. The theoretical values of the unwanted TE₁₁, TE₂₁, TE₃₁, and TM₁₁ modes were in good agreement with measured values.

- [14] S. Iiguchi, "Mode conversion in excitation of TE₀₁ wave through TE₀₁ mode transducer," *ibid.*, vol. 42, pp. 1213-1219; December, 1959.

An adjustable phase shifter for the circular electric mode was proposed. A movable dielectric rod is located coaxially inside a concentric dielectric layer in a circular waveguide. There is an optimum ratio between the radii of the rod and the circular waveguide.

- [15] S. Kumagai and N. Kumagai, "An adjustable phase shifter for circular electric mode," *ibid.*, vol. 42, p. 61; January, 1959.

² The contents of this paper also appeared in M. Sugi and T. Nakahara, "*O*-guide and *X*-guide: an advanced surface wave transmission concept," IRE TRANS. ON MICROWAVE THEORY AND TECHNIQUES, vol. MTT-7, pp. 366-369; July, 1959.

MEASUREMENTS

Tensor permeability and dielectric constant of ferrite were measured by the use of a rectangular cavity of the TE_{101} or TM_{120} degenerate mode at 7 kmc. In this method all components of the permeability and dielectric constant can be measured by changing the position of a thin disk ferrite sample in the cavity. Errors due to slight unsymmetry of the sample or cavity were evaluated by the perturbation method. The measured values were compared with that from the resonant theory.

[16] F. Okada, "Measurement of ferrite constants by rectangular cavity resonators," *ibid.*, vol. 42, pp. 758–764; August, 1959.

Microwave measurements employing spark waves as a microwave source were proposed. Because of the wide-band frequency spectrum characteristics of the spark waves, circuit constant cannot be measured directly. In a case of VSWR measurement, a measured value may be transformed into a real value by known frequency characteristics of band-pass filter connected at the output of the source.

[17] T. Kawano, "Measurements of microwave circuit elements employing spark waves," *ibid.*, vol. 42, pp. 62–63; January, 1959.

RADIATION AND PROPAGATION

Radiators of an Echelette grating spectrometer for millimeter waves were studied in order to obtain a general understanding about the operating principle using an analogy for an optical instrument. To avoid the near-zone effect, electromagnetic horns with small apertures were employed. It was shown both theoretically and experimentally that an inevitable phase error due to spherical phase fronts of horns was allowable up to about 120° . Although a large parabolic mirror has a complicated radiation pattern in the near-zone region, the phase front deviation from a plane wave is no more than a few tens of degrees. Therefore, the performance of the spectrometer is satisfactory even for a short distance between the antenna and the grating.

[18] T. Sueta, "A study on antenna for millimeter wave grating spectrometer," *ibid.*, vol. 42, pp. 677–683; July, 1959.

To transmit microwaves over a mountain, two large flat conducting plates located close to each other are often used as reflectors for a passive repeater, which is called the passive repeater of the second kind. Since this system may be considered as a special application of a microwave periscope, the propagation loss may be calculated through an analysis of a receiving antenna in

the Fresnel zone. The results were compared with that determined through the scattered field by the Huygens principle, and they agreed with each other.

[19] T. Soejima, "Passive repeater of the second kind using double flat reflectors," *ibid.*, vol. 42, pp. 502–507; May, 1959.

In a case where the plane wave was incident to a thin dielectric spherical shell, an internal electromagnetic field was calculated approximately from Maxwell's equations by a direct integral method. From this analysis a simple formula for a back-scattering cross section was derived which may be applicable for the whole range of ka ($k = 2\pi/\lambda$, and a is a radius of the shell) and the refraction coefficient of the shell.

[20] A. Yokoyama, "Back-scattering of a thin dielectric spherical shell," *ibid.*, vol. 42, pp. 36–39; February, 1959.

Effective reflection coefficients of snow surfaces were measured over a snow-covered terrain of 100 meters distance in the X band, and were compared with that of the 4-kmc band. Dependence of the effective reflection coefficient on the complex dielectric constant of snow was studied, and a new parameter, derived from Fresnel's reflection equation, was introduced. The dielectric properties of snow had a fairly large influence on the variation of the effective reflection coefficients, which was considerably greater than that given in the 4-kmc band. If the snow surface was rough, larger scattering of the incident wave was obtained at 9 kmc than at 4 kmc.

[21] M. Suzuki, "Equivalent reflection coefficient in 9-kmc band propagation over snow covered terrain," *ibid.*, vol. 42, pp. 490–495; May, 1959.

Microwave fading and fluctuation of communication quality in microwave relay links were studied statistically in order to find a communication transmission standard. Many fundamental propagation tests and measurements of fading and thermal noise at actual microwave links were carried out. Analysis was made from numerous measured values, and important factors for the design of the microwave radio links were clarified.

[22] K. Morita, "Fading of microwave relay links," *ibid.*, vol. 42, pp. 923–929; October, 1959.

ACKNOWLEDGMENT

The assistance of Prof. H. Iwakata, Chairman of the Technical Committee on Microwave Transmission, in the preparation of this manuscript is gratefully acknowledged.

The Design and Measurement of Two Broad-Band Coaxial Phase Shifters*

C. F. AUGUSTINE AND J. CHEAL,† MEMBER, IRE

Summary—Two mechanical (servo-driven) phase shifters were developed in response to systems requirements of low torque, compactness, octave bandwidth, and linear relation between mechanical motion and phase shift. One phase shifter relies upon the axial motion of a dielectric slug through a helix wound from modified miniature rigid coaxial cable. The second design consists of a 3-db coupler with ganged movable shorts on two ports. The helix design displayed phase shift of 720 degrees at 3 kmc and linearity to within ± 3 degrees. The coupler design is capable of achieving 720 degrees phase shift at 3 kmc and linearity within ± 2 degrees. A precision measuring facility (phase bridge) was developed for the purpose of determining the electrical performance of the phase shifters. A brief analysis is included to illustrate the prediction of maximum possible errors in the phase bridge and the phase shifters, in terms of transmission line parameters.

INTRODUCTION

TWO phase shifters were developed to meet systems requirements that were unusually demanding both electrically and mechanically. The requirements were essentially as follows:

Electrical:

- 1) Operation in the TEM mode from 2 to 4 kmc.
- 2) Phase shift vs mechanical motion linear to within ± 3 degrees.
- 3) Total phase shift of at least 400 degrees at 3 kmc.
- 4) Insertion loss of less than 3 db.

Mechanical:

- 1) Low torque.
- 2) Small size.
- 3) Rugged construction.
- 4) Simple mechanical motion.

The two designs meet these requirements through novel techniques employed to obtain both the electrical accuracy and the small size.

At the outset of the development program, it was recognized that an accurate test facility would be necessary to determine electrical performance. An S-band phase bridge was designed for this purpose. At the conclusion of this paper, a brief explanation of this phase bridge and an analysis of maximum possible measurement errors are given.

HELICAL PHASE SHIFTER

In this device phase shift is the result of axial motion of a cylindrical slug through a helical transmission line. The slug and transmission line are shown in Fig. 1.

* Received by the PGMTT, July 31, 1959; revised manuscript received, February 8, 1960. Presented at IRE-PGTT Nat'l. Symp., Harvard University, Cambridge, Mass., June 1-3, 1959.

† Research Div., Bendix Aviation Corp., Detroit, Mich.

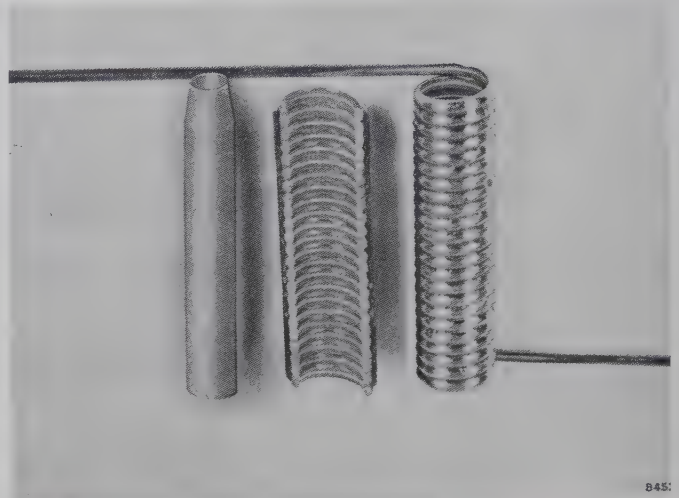


Fig. 1—Helix and dielectric slug.

The slug is comprised of low loss material having a high dielectric constant, and is available under the trade name of Stycast. It has a dielectric constant and loss tangent of about 15 and 0.001, respectively, from 2 to 4 kmc.

The helix is 2.25 inches long with an inner diameter of 0.450 inch. It is fabricated from miniature 50-ohm coaxial cable which has an outside diameter of 0.085 inch. The outer shield is solid copper and the center conductor is supported by a solid dielectric of teflon. A portion of this cable is machined away until the center conductor is exposed but still firmly supported by the dielectric. The helix is formed by wrapping the machined coax on a removable cylindrical mandrel and soldering the outer shield of successive turns together.

The cylindrical coax is tapered into the machined coax at both ends of the helix to effect a smooth wide-band electrical transition. The dielectric slug is also tapered to provide a better impedance match. The clearance between the outside diameter of the dielectric slug and the inside diameter of the helix is about 0.002 inch. This clearance must be kept small so that the high dielectric constant material will have maximum effect on the rather weak fringing fields around the exposed center conductors.

Fig. 2 shows how helix and slug are assembled. The helix is potted into the barrel assembly. It is supported during the potting process with a mandrel, which assures that the ID of the helix will remain concentric with the lead-screw bearings. The slug is mounted on the lead screw, which is in turn driven by the servo motor through a gear train.

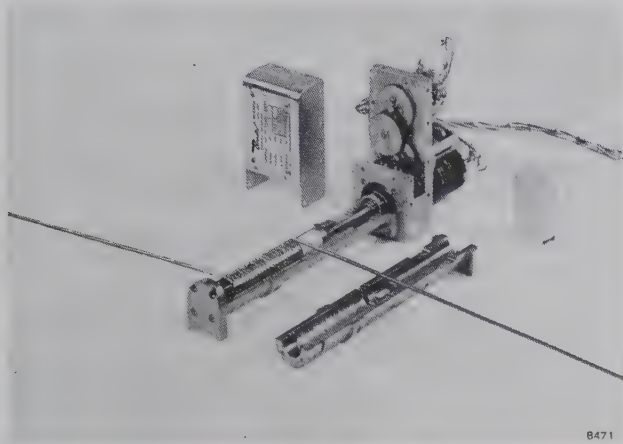


Fig. 2—Partially assembled helical shifter.

A typical curve of the relation between slug penetration into the helix and phase shift is shown in Fig. 3. Total phase shift for 1.8 inches of slug penetration is 490 degrees at 2.97 kmc and is linear to within ± 3 degrees. Maximum insertion loss at 3 kmc is less than 2 db. If lower loss is desired, a slug formed of Alite or an aluminum oxide of equivalent properties would give some improvement over the Stycast. From 2 to 4 kmc, the loss tangent and dielectric constant of this material are about 0.0007 and 8.5, respectively.

The maximum VSWR measured as a function of slug position was 1.5; however, a large portion of this mismatch can be attributed to the input and output connectors. Although the unit was designed to operate primarily over the frequency range of 2 to 4 kmc, the phase shift characteristics were checked at both higher and lower frequencies. Fig. 4 shows a plot of phase shift vs slug travel at 500, 1000, 2000, 4000, and 8000 mc. These curves indicate that the device is usable over this entire range, with total phase shift linearly related to frequency.

Aside from the phase-shifter applications, this helical transmission line has been used for testing ferrites and absorbing material. A compact variable attenuator can be fabricated by inserting a slug of high loss material into the helix.

PHASE SHIFTER USING 3-DB COUPLER

The second type of phase shifter utilizes an operating principle based on the variation of line lengths. Fig. 5 is a schematic representation of this operating principle, which is well-known in connection with waveguide hybrids. Opposite ports of the 3-db coupler are terminated with movable shorts. The terminated line lengths are kept equal by a suitable ganging technique. With equal power split between the two terminated ports, the reflected power is added at the fourth port and cancelled at the input. Phase difference between input and output is then a function of l . In this phase shifter, a change in the short positions by one-half wavelength corresponds to 360 degrees of phase shift.

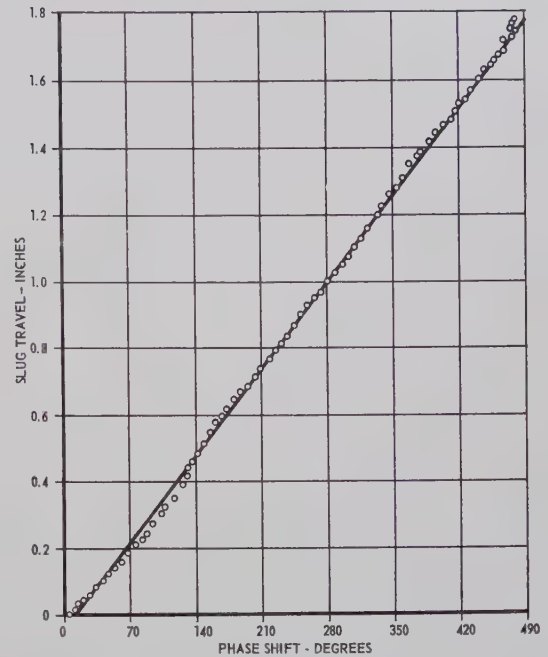


Fig. 3—Phase shift vs slug penetration at 2.97 kmc.

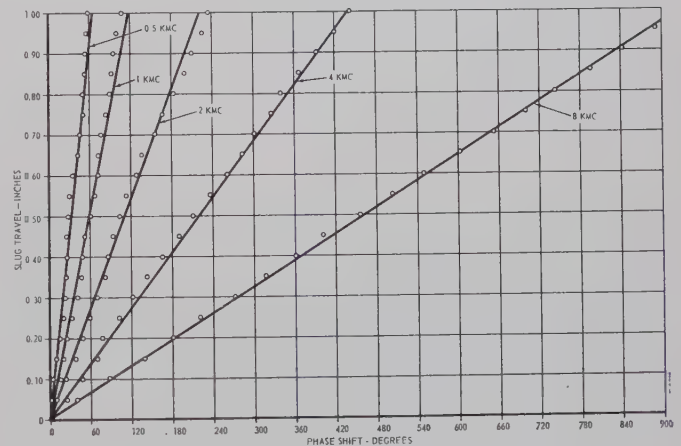


Fig. 4—Phase shift vs slug penetration at various frequencies.

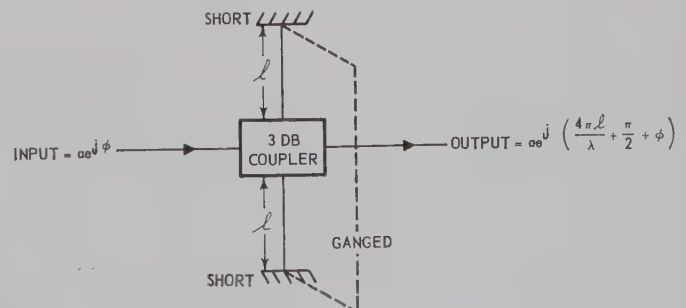


Fig. 5—Relation between input and output

Fig. 6 shows the 3-db coupler with input and output connections. The coaxial leads are brought in through the sides of the housing cylinder. The flat strips in the center of the cylinder form the broadband coupling section and are one-quarter wavelength long at the center of the frequency band. The two ports that are terminated with the movable shorts are brought around on the front side of the cylinder and curved around the outer periphery.

In Fig. 7, the coaxial line is shown with a portion of the cable machined away to expose the inner conductor. A coaxial line having an outside diameter of 0.141 inch is used for this purpose. Sliding contacts short the center conductor to the outer shield, and phase shift is accomplished by a rotary motion of the arm.

The 3-db coupler characteristics are shown in Fig. 8. The coupling is almost exactly 3 db from 2.7 to 3.3

kmc, and less than 0.5 db deviation was measured from 2 to 3.9 kmc. The slight departure from equal power division will contribute to an impedance mismatch at the input port. The reflected power resulting from this mismatch will not affect the phase linearity if multiple reflections are suppressed with a matched line looking back from the input port. However, any discontinuities in the input line will contribute to phase nonlinearity. For example, if the connector on the input port has a VSWR of 1.2 and the coupling is 3.5 db rather than 3 db, it can be shown that this combination can lead to a maximum deviation from linearity of 2.5 degrees.

The curve relating radial displacement of the ganged shorts to phase shift at 3 kmc is given in Fig. 9. The maximum departure from the linear curve is less than ± 2 degrees.

A complete assembly with speed-reduction gears and servo drive is shown in Fig. 10. The unit is less than 3 inches high, including the servo motor, and is 3.25 inches in diameter.

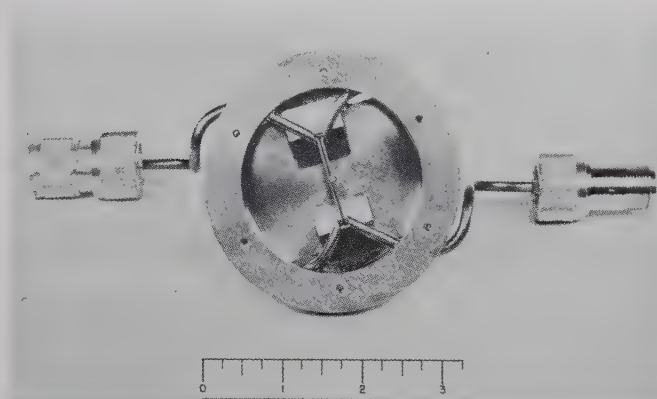


Fig. 6—Rear view showing 3-db coupler.



Fig. 7—Front view showing ganged shorts.

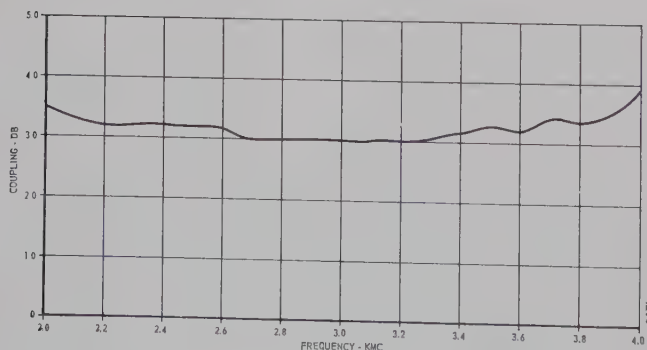


Fig. 8—Characteristics of 3-db coupler.

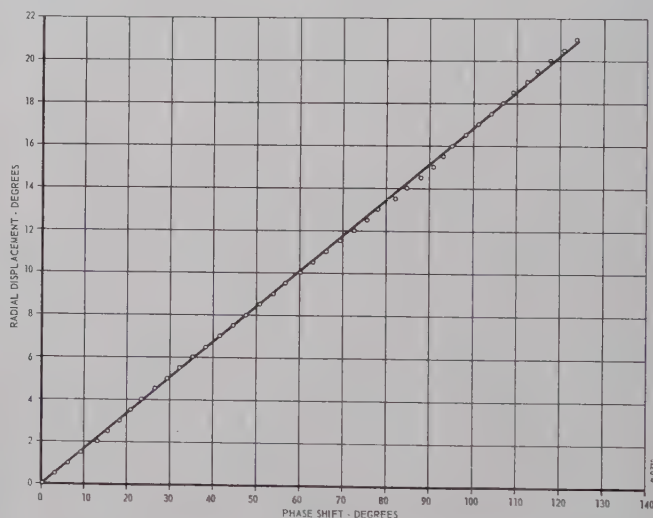


Fig. 9—Phase shift vs radial displacement.

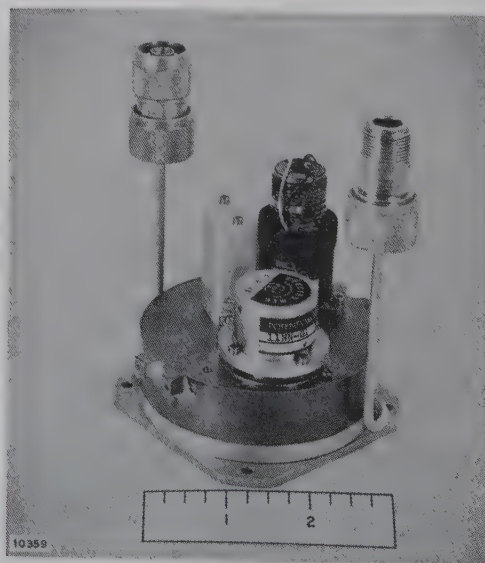


Fig. 10—Complete assembly.

MEASUREMENT TECHNIQUES

As mentioned previously, an S-band phase bridge was developed for the measurement of the phase-shifter performance. A block diagram of the bridge is shown in Fig. 11. Bridges of this type are preferred over slotted lines in phase measurement because greater accuracy and resolution can be obtained.

Power division and recombination is accomplished by two 3-db stripline couplers. The standards are commercially-available coaxial line stretchers that have been equipped with a precision mechanical movement. Fixed coaxial attenuators are placed at the inputs and outputs of the line stretchers to guarantee good impedance match at these ports.

There are two principal sources of error in the phase bridge. The first results from the fact that the line-stretcher standards do not face perfect impedances. The other comes about because the device to be measured is inserted between terminals that deviate slightly from the nominal impedance. A simple method of determining maximum possible errors of the first type is illustrated in Fig. 12. The line stretcher is assumed perfect, but there are impedance discontinuities at the input and output terminals resulting in reflection coefficients q_1 and q_2 . These reflection coefficients will cause a departure from linearity in the mechanical displacement vs phase-shift characteristic. The exact magnitude of the departure can be found by adding up all the terms resulting from multiple reflections just to the left of q_2 , dividing by the voltage that would be obtained at this point if q_1 and q_2 were zero, and taking the argument of

the complete expression, i.e.,

$$\text{angular departure} = \text{ARG} \frac{\sum_{l=0}^N (q_1 q_2)^N e^{j\beta(2N+1)l}}{e^{j\beta}} \quad (1)$$

For small reflection coefficients, the maximum departure is found with sufficient accuracy as,

$$\text{maximum departure} \simeq \arctan |q_1| |q_2|. \quad (2)$$

For example, in the line stretchers used in the phase bridge,

$$|q_1| \simeq |q_2| = 0.09,$$

which results in a maximum departure or possible error of ± 0.5 degrees.

If the discontinuities represented by q_1 and q_2 are part of the phase shifter under consideration (they may, for example, be connectors at the input and outputs), then the deviation just described is not an error but is a part of the performance characteristics. If the device is measured between perfect impedances, there is no question but that a true insertion phase measurement is made. In practice, however, this cannot be the case and confusion may arise since deviation from the expected characteristic is partially due to impedance irregularities at the terminals of the device and partially due to deviations at the terminals of the testing facility. For example, the situation may be as shown in Fig. 13. Reflection coefficients q_3 and q_4 may be due to connectors at the ports of a phase shifter to be tested, and q_1 and q_2 may be reflection coefficients at the ports of the measurement facility. It is possible to have a line length between q_1 and q_3 such that the reflection coefficient q_i looking back from the phase shifter has a maximum value given by

$$|q_i|_{\max} = |q_1| + \frac{|q_3| (1 + |q_1|^2)}{1 + |q_1| |q_3|}. \quad (3)$$

A similar expression relates q_0 with q_2 and q_4 . When all reflection coefficients are small, the maximum possible error is very nearly given by

maximum possible error

$$\simeq \arctan |q_i| |q_0| - \arctan |q_3| |q_4|. \quad (4)$$

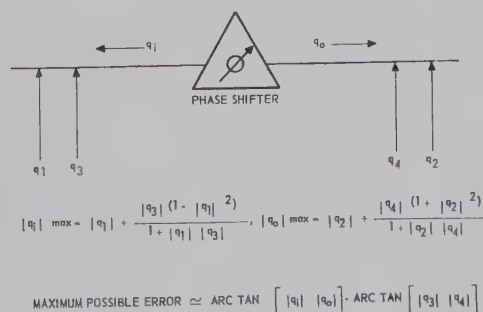


Fig. 13—Maximum possible error caused by impedance deviations at the bridge terminals.

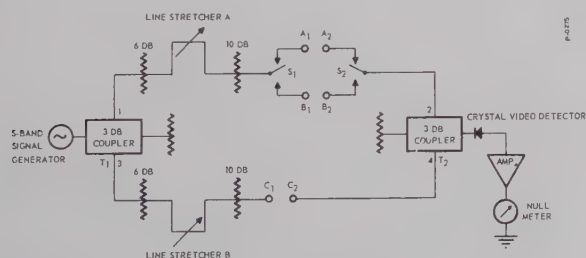


Fig. 11—S-band bridge.

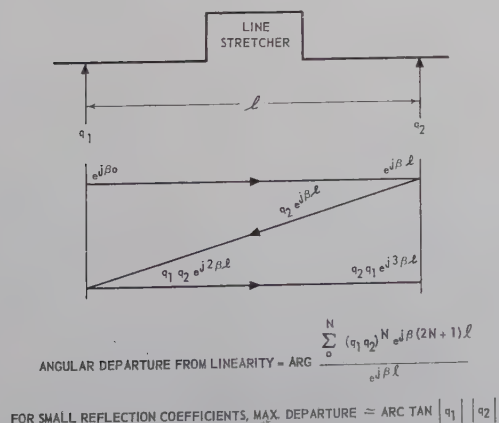


Fig. 12—Maximum departure from linearity as a function of two impedance discontinuities.

The maximum possible error that can occur during a measurement on a phase bridge is therefore equal to the sum of (2) and (4), and is always a function of the deviation from nominal impedance at the terminals of the device under test. However, it is very unlikely that the line lengths between discontinuities would be arranged so that the error would achieve the maximum possible value during any measurement.

Unequal power division between the two bridge arms will introduce no direct error. However, if the inequality is large enough to decrease appreciably the sharpness of the output null, error may be introduced because of increased uncertainty in the exact setting of the line stretchers.

CONCLUSION

Both phase shifters have the advantage of small physical size, potential rugged construction and linear relation between phase shift and mechanical motion. The low driving torque necessary to accomplish phase

shift is an attractive feature for servo-control applications.

The helical phase shifter has a bandwidth advantage over the coupler type but has a greater insertion loss. The bandwidth of the helix phase shifter extends from UHF up through *C* band, whereas the bandwidth of the coupler type is limited to less than an octave. However, the linearity of the coupler type is somewhat greater than in the helical phase shifter. Both designs are intended for low-power receiver types of applications, and maximum power-handling capacity has not been determined.

For precise phase measurements, bridge methods are recommended rather than slotted-line techniques. The chief source of measurement error is caused by interactions between impedance deviations at the terminals of the phase shifter and deviations at the terminals of the testing facility. The maximum possible phase errors that can occur as a result of the deviations can be calculated by the methods that have been given.

A Dielectric Resonator Method of Measuring Inductive Capacities in the Millimeter Range*

B. W. HAKKI† AND P. D. COLEMAN†, MEMBER, IRE

Summary—A novel technique for the measurement of dielectric and magnetic properties of a homogeneous isotropic medium in the range of approximately 3 to 100 kmc is described. An accuracy of ± 0.1 per cent is possible in the determination of permittivity or permeability in those cases where the loss tangent is sufficiently small. The measuring structure is a resonator made up of a right circular cylindrical dielectric rod placed between two parallel conducting plates. For measurement of permittivity two or more resonant TE_{0n1} mode frequencies are determined whereas for the measurement of permeability two or more resonant TM_{0n1} mode frequencies are determined. The dielectric or magnetic properties are computed from the resonance frequencies, structure dimensions, and unloaded Q . Since the loss tangent is inversely proportional to the unloaded Q of the structure, the precision to which Q is measured determines the accuracy of the loss tangent.

I. INTRODUCTION

MOST of the methods for the measurement of dielectric and magnetic properties of materials at microwave frequencies fall into the following

categories: perturbation techniques, optical methods, transmission line methods, or exact resonance methods. The perturbation techniques have notably been used in ferrite measurements where a small piece of the material to be measured, either in the form of a disk or a sphere, is placed in a metallic resonant cavity operating in a known mode and the shift in resonant frequency and the Q of the structure is noted.¹⁻⁴ Optical techniques at microwave frequencies⁵ are inherently suited for measurements below a wavelength of one centimeter, but

¹ W. Von Aulock and J. H. Rowen, "Measurement of dielectric and magnetic properties of ferromagnetic materials at microwave frequencies," *Bell Sys. Tech. J.*, vol. 36, pp. 427-448; March, 1957.

² E. G. Spencer, R. C. LeCraw, and F. Reggia, "Measurement of microwave dielectric constants and tensor permeabilities of ferrite spheres," *PROC. IRE*, vol. 44, pp. 790-800; June, 1956.

³ J. O. Artman and P. E. Tannenwald, "Measurement of permeability tensor in ferrites," *Phys. Rev.*, vol. 91, pp. 1014-1015; August 15, 1953.

⁴ J. O. Artman and P. E. Tannenwald, "Microwave susceptibility measurements in ferrites," *J. Appl. Phys.*, vol. 26, pp. 1124-0000; September, 1955.

⁵ T. E. Talpey, "Optical methods for the measurement of complex dielectric and magnetic constants at centimeter and millimeter wavelengths," *IRE TRANS. ON MICROWAVE THEORY AND TECHNIQUES*, vol. MTT-2, pp. 1-13; September, 1954.

* Received by the PGMTT, December 24, 1959; revised manuscript received, February 15, 1960. This work was sponsored by the U. S. Atomic Energy Commission under Contract No. AT(11-1)-392.

† Elec. Engrg. Res. Lab., University of Illinois, Urbana, Ill.

their only drawback is that a relatively large amount of the material is needed. Finally, transmission line techniques have been applied widely^{6,7} but they have the very serious disadvantage of the very small waveguide size used below 4 mm, which gives rise to practical difficulties. All the above methods have a rather limited accuracy of the order of ± 1 per cent in the values of permittivity and permeability obtained. On the other hand an exact resonance method has recently been proposed by Karpova⁸ which gives an accuracy of ± 0.1 per cent. In this method a circular disk of the material to be measured is inserted in the gap of a reentrant cavity of known dimensions, Fig. 1, and the resonant frequency and Q of the structure are measured from which the dielectric constant and loss tangent are obtained. This is a high accuracy method but the physical size of the resonant structure for the low millimeter range might pose a problem unless a high order mode cavity is used.⁹

In order to circumvent the problem of physical size and still maintain a high accuracy, an open boundary resonant structure was used in the form of a dielectric rod, of the material to be measured, placed between two mathematically infinite conducting plates.¹⁰

II. GENERAL ANALYSIS

A. Measurement of Permittivity

Let it be assumed for the present that the permeability of the material of interest is equal to that of free space, and it is required to measure the permittivity. Consider now a circular cylindrical rod of relative dielectric constant κ , permeability μ_0 , length L , and radius a placed between two large perfectly conducting plates (Fig. 2). If the dielectric material is isotropic then the characteristic equation for this resonant structure operating in the TE_{0nl} mode is (see Appendix I)

$$\alpha \frac{J_0(\alpha)}{J_1(\alpha)} = -\beta \frac{K_0(\beta)}{K_1(\beta)} \quad (1)$$

where $J_0(\alpha)$ and $J_1(\alpha)$ are the Bessel functions of the first kind of orders zero and one, respectively, $K_0(\beta)$

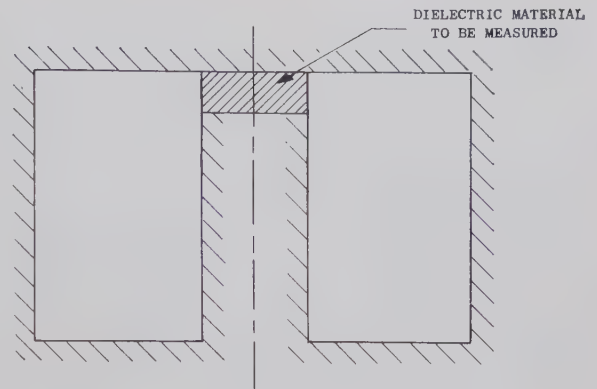


Fig. 1—A reentrant cavity structure used by Karpova⁸ to measure dielectric properties.

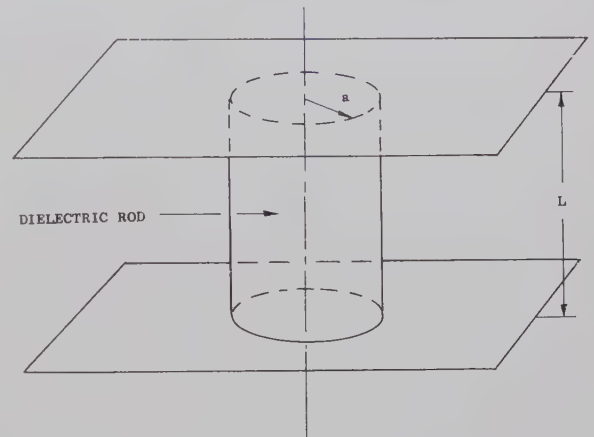


Fig. 2—Dielectric rod placed between two infinite parallel perfectly conducting plates.

and $K_1(\beta)$ are the modified Bessel functions of the second kind of orders zero and one, respectively. The parameters α and β depend on the geometry, the resonant wavelength, and dielectric properties; thus

$$\alpha = \frac{2\pi a}{\lambda_0} \left[\kappa_1 - \left(\frac{c}{v_p} \right)^2 \right]^{1/2} \quad (2)$$

$$\beta = \frac{2\pi a}{\lambda_0} \left[\left(\frac{c}{v_p} \right)^2 - 1 \right]^{1/2} \quad (3)$$

c being the velocity of light and v_p the phase velocity in the structure so that

$$\frac{c}{v_p} = \left(\frac{l\lambda_0}{2L} \right) \quad (4)$$

where l is the number of longitudinal variations of the field along the axis, and λ_0 is the free space resonant wavelength.

It is seen that the characteristic equation is a transcendental equation and hence a graphical solution is necessary. The resulting mode charts are given in Figs. 3 and 4 where to each value of β there corresponds an infinite sequence $\{\alpha_n\}$ which solves (1); the definition of the subscript n is now self-evident.

⁶ C. Montgomery, "Technique of Microwave Measurements," M.I.T. Rad. Lab. Ser., McGraw-Hill Book Co., Inc., New York, N. Y., vol. 11; 1947.

⁷ A. R. Von Hippel, "Dielectric Materials and Applications," John Wiley & Sons, Inc., New York, N. Y.; 1956.

⁸ O. V. Karpova, "On the absolute measurement of solid dielectric parameters by means of a π resonator," *Soviet Phys.*, vol. 1 (Solid-State), pp. 220-228; February, 1959.

⁹ H. E. Bussey and L. A. Steinert, "Exact solution for a gyromagnetic sample and measurements on a ferrite," *IRE TRANS. ON MICROWAVE THEORY AND TECHNIQUES*, vol. MTT-6, pp. 72-76; January, 1958.

¹⁰ This work has similar aspects to the exhaustive and excellent work done at Northwestern University by R. E. Beam, *et al.*, whose results are included in the final report, "Investigations on Multi-Mode Propagation in Waveguides and Microwave Optics"; November, 1950. Also, a similar idea for a slow-wave resonant structure was independently proposed by Prof. R. Pantell and the details carried out by Dr. R. Becker in his Doctoral dissertation, "The Dielectric Tube Resonator." See also, R. H. Pantell, P. D. Coleman, and R. C. Becker, "Dielectric slow-wave structures for the generation of power at millimeter and submillimeter wavelengths," *IRE TRANS. ON ELECTRON DEVICES*, vol. ED-5, pp. 167-173; July, 1958.

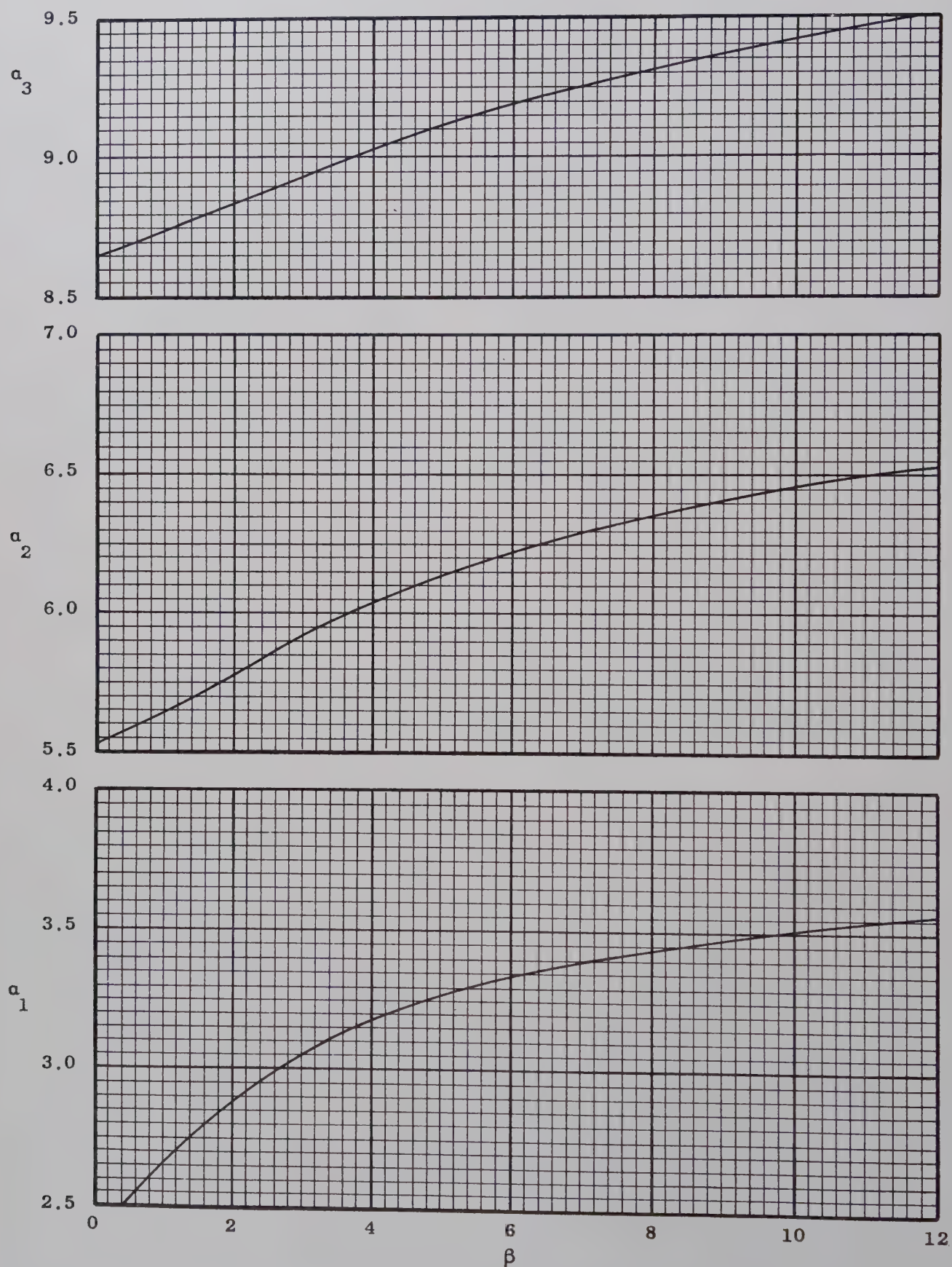


Fig. 3—The solution of the characteristic equation for TE_{onl} modes for $n=1$ up to 3.

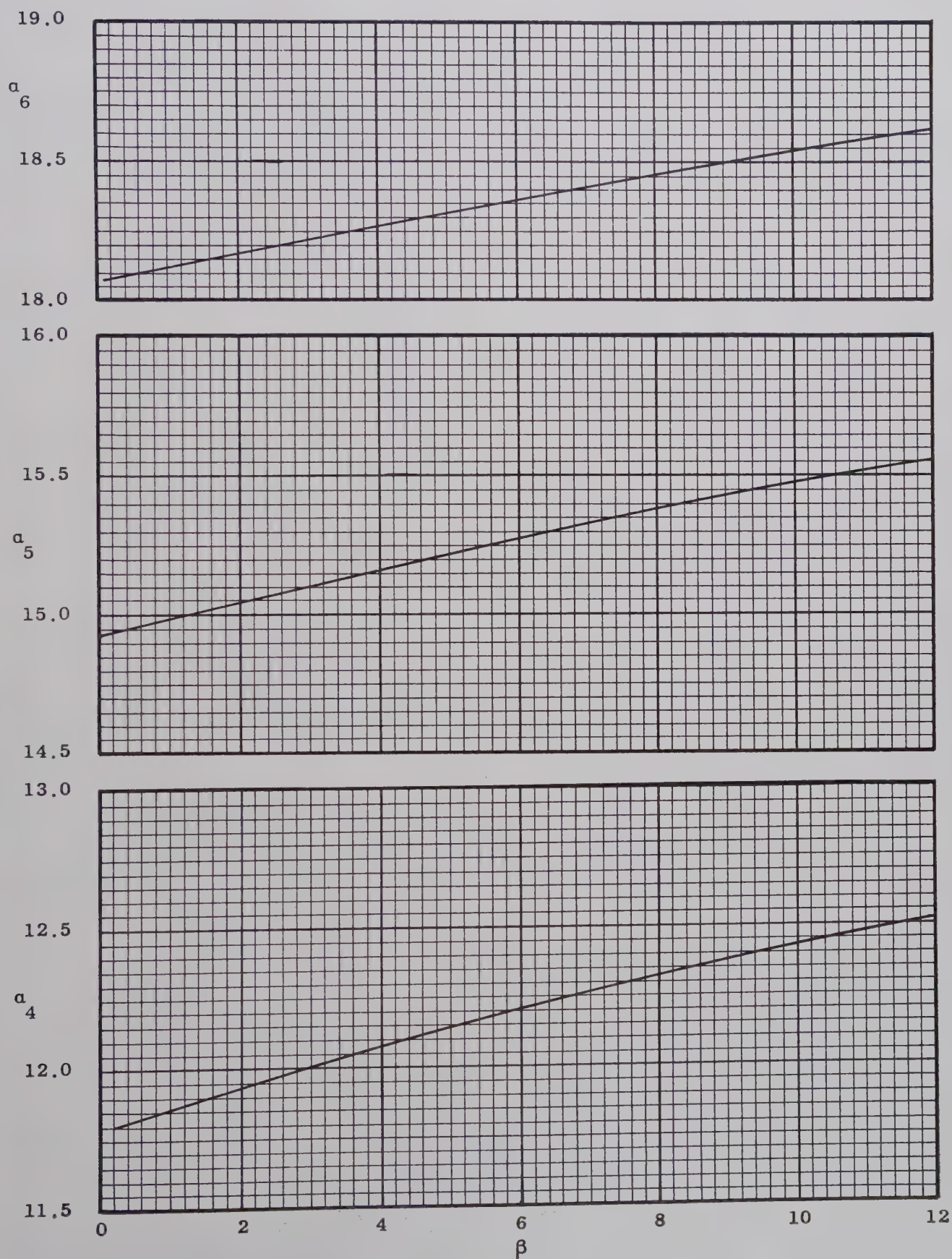


Fig. 4—The solution of the characteristic equation for TE_{onl} modes for $n=4$ up to 6.

Noteworthy in (1) is the fact that the characteristic equation and the resulting mode charts are "universal" as far as the permittivity is concerned. This makes possible the use of the mode charts for practically all values of relative dielectric constants conceivable. Consider now the problem of determining the relative dielectric constant of a structure of known dimensions resonating in a TE_{onl} mode with a resonant wavelength λ_0 . Eq. (4) is substituted in (3) which gives

$$\beta_l = \frac{2\pi a}{\lambda_0} \left[\left(\frac{l\lambda_0}{2L} \right)^2 - 1 \right]^{1/2}. \quad (3a)$$

But to β_l there corresponds an α_n which can be obtained from the mode chart of the characteristic equation. Once the appropriate value of α_n is obtained the relative dielectric constant can be immediately calculated from (2), assuming that the mode indexes n and l are known,

$$\kappa_1 = \left(\frac{\alpha_n \lambda_0}{2\pi a} \right)^2 + \left(\frac{l\lambda_0}{2L} \right)^2. \quad (5)$$

However, in practice the most difficult aspect of the problem is the determination of the mode indexes. In the first place the modes of interest are restricted to the TE_{onl} which form a small portion of all the possible modes of operation, hence the method of excitation has to be such as to excite TE_{onl} modes exclusively. Unfortunately, such a highly selective method of excitation is rather difficult to obtain, thus it should be expected that spurious resonances other than the TE_{onl} modes will be present. In the second place, even after the excitation of the TE_{onl} mode is accomplished there remains the determination of n and l . The most obvious method of determining l would be by actually counting the longitudinal variations of the field by a perturbation technique. However, at wavelengths below 8 mm and for high relative dielectric constants, say about 1000, the spacing of the nulls along the cavity is of the order of 0.1 mm which is not all too easy to measure by a perturbation method; another method seems to be necessary.

If the dielectric constant and cavity dimensions give rise to an α_n and a β_l which fall in a region of the mode chart where there is enough discrimination then a very simple procedure is possible. Suppose that a structure with certain dimensions has a resonant frequency λ_0 ; since the particular integral value of l is not known, a table of β_l , obtainable from (3), is arranged for all values of l ranging from one up to any reasonable value. Now for each value of β_l several values of α_n are obtained from the mode chart; next, for each pair of values (α_n, β_l) a dielectric constant is obtained from (5). Another resonant cavity with different dimensions is designed and the same procedure is repeated; the value of dielectric constant common to both sets of values is the correct value. To eliminate any ambiguity a third cavity is designed so as to resonate at a certain frequency by using the obtained value of κ , and it is observed whether

the actual resonant frequency is close to the designed value to within certain tolerances. If the signal source has a wide enough frequency range and if the dielectric properties remain nearly constant throughout this range then it might be possible to use the same cavity and excite two different TE_{onl} modes. An illustrative example is given for teflon in Table I, which gives a value of 2.044 for the relative dielectric constant at room temperature and a frequency of 35 kmc.

TABLE I
PROCEDURE FOLLOWED IN OBTAINING THE RELATIVE DIELECTRIC
CONSTANT OF TEFLON AT 25°C. CAVITY DIMENSIONS ARE
 $L = 18.81$ MM, $a = 14.44$ MM; $\kappa = 2.044$.

	κ			λ_0 mm
	$l=5$	$l=6$	$l=7$	
$n=1$	1.393	1.979	2.654	8.564
$=2$	1.638	2.237	2.925	
$=3$	2.044	2.656	3.353	
$=4$	2.621	3.248		
$=5$	3.371			
$n=1$	1.443	2.044	2.746	8.713
$=2$	1.698	2.314	3.026	
$=3$	2.120	2.749		
$=4$	2.718	3.355		
$=5$	3.493			

B. Measurement of the Loss Tangent

Once the mode of operation and the dielectric constant are determined, it is a simple matter to derive the loss tangent of the dielectric material from a measured value of the unloaded Q of the structure. The unloaded Q of the cavity is defined as 2π times the ratio of the maximum energy stored to the energy lost in one cycle. The energy stored consists of energy within and outside the dielectric rod whereas energy losses consist of copper losses in the end walls and dielectric losses in the rod itself. An expression for the loss tangent of the material used can be derived and gives (see Appendix II)

$$\tan \delta = \frac{A}{Q_0} - B \quad (6)$$

where

$$A = 1 + \frac{J_1^2(\alpha_n)}{\kappa K_1^2(\beta_l)} \left[\frac{K_0(\beta_l) K_2(\beta_l) - K_1^2(\beta_l)}{J_1^2(\alpha_n) - J_0(\alpha_n) J_2(\alpha_n)} \right] \quad (7)$$

and

$$B = \frac{l^2 R_s}{2\pi f^3 \mu^2 \kappa \epsilon_0 L^3} \left\{ 1 + \frac{J_1^2(\alpha_n)}{K_1^2(\beta_l)} \left[\frac{K_0(\beta_l) K_2(\beta_l) - K_1^2(\beta_l)}{J_1^2(\alpha_n) - J_0(\alpha_n) J_2(\alpha_n)} \right] \right\} \quad (8)$$

where the terms have the usual definition, α_n and β_l being the solutions of the characteristic equation (1) for the particular mode for which the Q_0 of the structure has been determined, and R_s is the surface resistance of the end walls, equal to $(\pi f \mu / \sigma)^{1/2}$, σ being the conductivity. It is seen from (6) that when $\kappa \gg 1$, as for ferroelectric materials, and end-wall losses are neglected,

then the loss tangent is approximately

$$\tan \delta \approx \frac{1}{Q_0}.$$

In order to facilitate computations a graphical plot of the factors involved in (7) and (8) has been prepared. Thus A and B can be written as

$$A = 1 + \frac{1}{\kappa} F(\alpha) G(\beta) \quad (7a)$$

$$B = \frac{l^2 R_s}{2\pi f^3 \mu^2 \kappa \epsilon_0 L^3} [1 + F(\alpha) G(\beta)] \quad (8a)$$

where the definitions of $F(\alpha)$ and $G(\beta)$ are self-evident. Plots of $F(\alpha)$ vs α and $G(\beta)$ vs β are given in Figs. 5 and 6.

Finally, since this is an inherently high accuracy method it would be of interest to study the effect of losses on the resonant frequency. For this purpose the expressions derived by Slater¹¹ for the effect of losses can be used. If ω_0 is the resonant frequency of the lossless structure, and $\tan \delta$ is the dielectric loss coefficient of the medium, then the resonant frequency of the structure when dielectric losses are accounted for is¹²

$$\omega = \omega_0 \left[1 - \left(\frac{\tan \delta}{2} \right)^2 \right]^{1/2}. \quad (9)$$

Now, for $(\frac{1}{2} \tan \delta)^2 \ll 1$, (9) can be expanded and gives

$$\omega_0 \approx \omega \left[1 + \frac{1}{8} (\tan \delta)^2 \right]. \quad (9a)$$

It is seen that even for a $\tan \delta = 0.1$ the resulting shift in the resonant frequency is about 0.1 per cent. In addition, effects of copper losses on the resonant frequency can be safely neglected.

C. Measurement of Permeability

The same technique can be applied for the measurement of permeability as that indicated above except for one difference: in order to get a characteristic equation which is "universal" for all permeabilities it would be necessary to use the TM_{onl} modes which give rise to a characteristic equation of the form

$$\frac{\alpha J_0(\alpha)}{J_1(\alpha)} = -\kappa \beta \frac{K_0(\beta)}{K_1(\beta)} \quad (10)$$

where the relative dielectric constant κ has been retained in case the magnetic material has a permittivity different from that of free space, and the independent variables α and β are now given by

$$\alpha = \frac{2\pi a}{\lambda_0} \left[\mu_r \kappa - \left(\frac{l\lambda_0}{2L} \right)^2 \right]^{1/2} \quad (11)$$

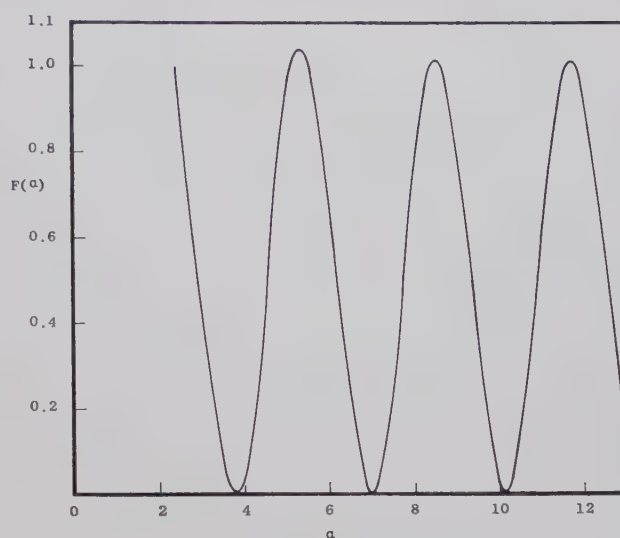


Fig. 5— $F(\alpha)$ vs α .

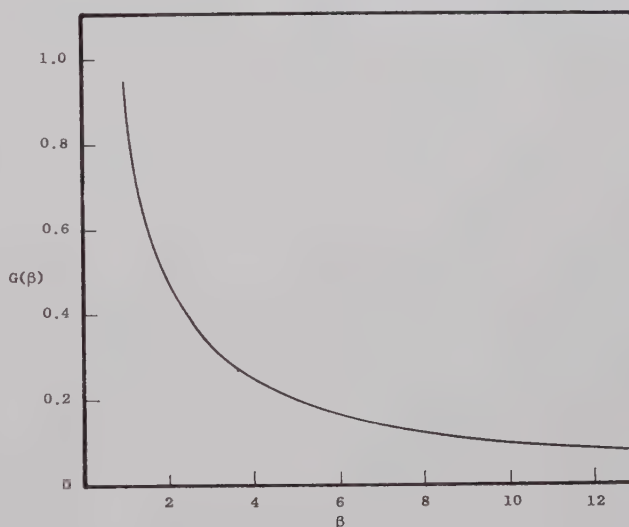


Fig. 6— $G(\beta)$ vs β .

$$\beta = \frac{2\pi a}{\lambda_0} \left[\left(\frac{l\lambda_0}{2L} \right)^2 - 1 \right]^{1/2}, \quad (12)$$

μ_r being the relative permeability of the material. It is obvious from (10) that should the magnetic material have a relative dielectric constant equal to one then (10) becomes identical to (1), and the mode charts already obtained would be applicable; otherwise a new set of mode charts must be derived for each value of relative dielectric constant κ . Once this is accomplished the procedure follows through in an identical fashion to that for the determination of permittivity, and further exposition is not warranted.

D. Experimental Details

Consider next experimental aspects of the measurement of permittivity. It has already been pointed out that the modes relevant to permittivity measurements are the TE_{onl} modes. In practice it has been found that

¹¹ J. Slater, "Microwave Electronics," D. Van Nostrand Co., Inc., New York, N. Y.; 1950.

¹² The results obtained by Slater are still valid in this case in spite of the lack of orthogonality of the eigenfunctions in the finite interval $0 < r < a$.

an iris coupling in the narrow side of a guide operating in the dominant TE_{01} mode gives satisfactory results. The resonant structure in this case behaves as a reaction type cavity; details of the structure are shown in Fig. 7. It was found to be almost imperative to incorporate some tuning mechanism in the resonant structure, *e.g.*, moving one end wall, in order to detect the structure resonance on, for example, the saw-tooth modulated output of the klystron. This is due to the fact that most dielectric materials have rather large losses at microwave frequencies and hence give rise to low Q structures. In addition, the coupling may not be strong enough to give a noticeable depression on the bell-shaped output of the klystron as seen on an oscilloscope. Thus tuning the structure by moving one end wall was found to be helpful in locating the resonances.¹³ The cavity can be placed in the microwave circuit in any of the conventional ways, *e.g.*, either on line or by the use of a magic- T bridge.

The Q of the resonant cavity is measured by any of several possible ways, the VSWR method¹⁴ being used

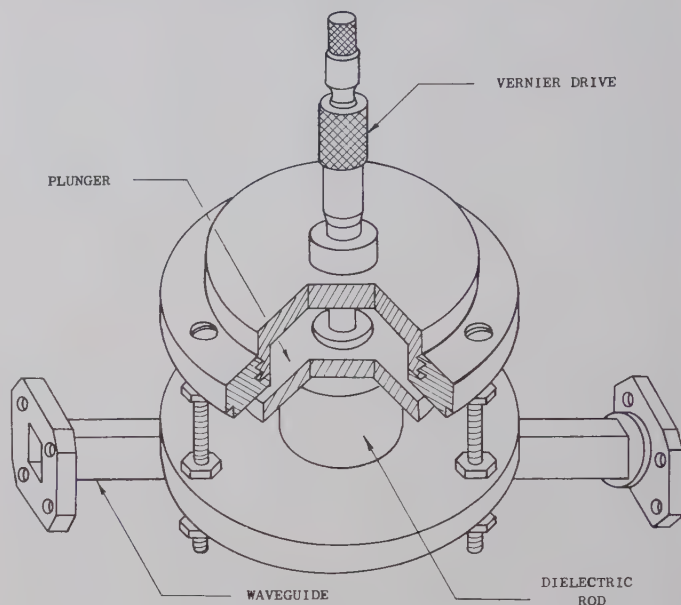


Fig. 7—The dielectric rod cavity arrangement. A section of one end wall is driven by a vernier for tuning purposes.

TABLE II

DIELECTRIC CONSTANT AND LOSS TANGENT OF SEVERAL MATERIALS AT ROOM TEMPERATURE AT A FREQUENCY OF 35 KMC

Material	κ	$\tan \delta$	Values Quoted by Other Authors			
			Author	κ	$\tan \delta$	Frequency (Kmc)
Teflon	2.044	10×10^{-4}	Von Hippel ⁷	2.08	6×10^{-4}	25
	± 0.2 per cent	± 10 per cent	Handbook ¹⁵	2.08	6×10^{-4}	25
Polystyrene	2.543	33×10^{-4}	Von Hippel ⁷	2.54	12×10^{-4}	25
	± 0.2 per cent		Karpova ⁸	2.495	4.9×10^{-4}	2
			Talpey ⁵	2.52	92×10^{-4}	36
Lucite	2.580	50×10^{-4}	Von Hippel ⁷	2.57	32×10^{-4}	25
	± 0.2 per cent		Handbook ¹⁵	2.57	32×10^{-4}	25

in this particular case. The results for several materials have been included in Table II.

III. CONCLUSION

By measuring the resonant frequency of a dielectric rod between two large parallel conducting plates it was possible to measure the dielectric constant of teflon, polystyrene, and lucite to an accuracy better than ± 0.2 per cent. The accuracy was limited by the probable error in the wave meter and errors in taking the dimensions of the samples. The error is much less for low loss materials, *i.e.*, high Q resonant structures, since the absorption curve of the resonant structure is more sharply displayed on the bell-shaped output of a saw-tooth modulated klystron. Errors in the mode chart

can be theoretically reduced to an arbitrarily small value through more accurate numerical computations. The loss tangent has errors in it which are inherent in those involved in measurement of Q . It is quite possible to use a frequency stabilized circuit such as that used by Von Aulock¹ to improve on the accuracy of Q measurements. It should be pointed out, however, that this method would lose its main advantage—accuracy—in those cases where both the dielectric and magnetic properties are simultaneously unknown and an auxiliary technique is used to determine one or the other.

One of the interesting features of this scheme is its possibility in measurement of dielectric constant and loss tangent of nonlinear dielectric materials, *e.g.*, ferroelectrics. If a dielectric rod resonant structure is made of such a material and its resonance absorption curve

¹³ Needless to say, when data are taken the end walls should be in direct contact with the cylindrical rod.

¹⁴ E. L. Ginzton, "Microwave Measurements," McGraw-Hill Book Co., Inc., New York, N. Y.; 1957.

¹⁵ "Reference Data for Radio Engineers," Federal Telephone and Radio Co., New York, N. Y., 3rd ed.; 1949.

displayed on the bell-shaped output of a klystron, then it would be possible to study the effect of the strength of excitation on the dielectric properties of the nonlinear material by noting the frequency shift and distortion of the resonance curve. This, added to the fact that this scheme is inherently suited to the study of the effect of dc electric bias on the dielectric properties since dc voltage can easily be applied between the two end walls, yielding information concerning the incremental permittivity of the material. Naturally, this is not without its own share of problems; for instance, for ferroelectric materials the size of the cavity has to be small if it is to operate in a reasonably low order mode. Also, with the high dielectric constant of ferroelectric materials there is the problem of impedance matching, where a low impedance matching device is needed. Nevertheless, it is believed that such difficulties can be overcome.

APPENDIX I

THE CHARACTERISTIC EQUATION FOR TE_{onl} MODES

The characteristic equation for the TE_{onl} modes in a dielectric rod resonant structure will be obtained. The usual vector \mathbf{L} , \mathbf{M} , and \mathbf{N} solutions of the vector Helmholtz equation are convenient and hence will be used. Since TE modes are of interest let

$$\mathbf{E}(\mathbf{r}) = \mathbf{M}(\mathbf{r}) = \nabla \times [\chi\psi(\mathbf{r})] \quad (13)$$

which in cylindrical coordinates gives

$$\mathbf{E}(\mathbf{r}) = \nabla\psi(\mathbf{r}) \times \mathbf{i}_z \quad (14)$$

where the scalar function $\psi(\mathbf{r})$ satisfies the scalar Helmholtz equation

$$\nabla^2\psi(\mathbf{r}) + \omega^2\mu\epsilon\psi(\mathbf{r}) = 0. \quad (15)$$

Eq. (15) is to be solved in the two regions I and II, *i.e.*, inside the rod and outside the rod, respectively, such as to satisfy the appropriate boundary conditions.

Region I

If there is no ϕ variation then a solution of the above equation will be

$$\psi_1(\mathbf{r}) = A_1 J_0(k_1 r) \sin \gamma z \quad (16)$$

where

$$k_1^2 = \omega^2\mu\epsilon_1 - \gamma^2, \quad (17)$$

and

$$\begin{aligned} \mathbf{E}_1(\mathbf{r}) &= A_1 \nabla [J_0(k_1 r) \sin \gamma z] \times \mathbf{i}_z \\ \therefore \mathbf{E}_1(\mathbf{r}) &= \mathbf{i}_\phi A_{1k} J_1(k_1 r) \sin \gamma z. \end{aligned} \quad (18)$$

It is seen that $\mathbf{E}_1(\mathbf{r})$ satisfies the boundary conditions at $z=0$ and L if

$$\gamma = \frac{l\pi}{L} \quad l = 1, 2, 3, \dots \quad (19)$$

Next, from Maxwell's first equation we have

$$\begin{aligned} \mathbf{H}_1(\mathbf{r}) &= \frac{j}{\omega\mu} \nabla \times \mathbf{E}_1(\mathbf{r}) \\ \mathbf{H}_1(\mathbf{r}) &= \frac{jA_{1k_1}}{\omega\mu} [-i\gamma J_1(k_1 r) \cos \gamma r + \mathbf{i}_z k_1 J_0(k_1 r) \sin \gamma z]. \end{aligned} \quad (20)$$

Region II

The scalar potential $\psi_2(\mathbf{r})$ is a solution of

$$\nabla^2\psi_2(\mathbf{r}) + \omega^2\mu\epsilon_0\psi_2(\mathbf{r}) = 0 \quad (21)$$

hence

$$\psi_2(\mathbf{r}) = A_2 K_0(k_2 r) \sin \gamma z$$

where

$$k_2^2 = \gamma^2 - \omega^2\mu\epsilon_0. \quad (22)$$

It is necessary here to use the modified Bessel functions since the modes are nonradiating. Thus from (14) and (22) we obtain

$$\mathbf{E}_2(\mathbf{r}) = \mathbf{i}_\phi A_2 k_2 K_1(k_2 r) \sin \gamma z \quad (23)$$

and finally

$$\begin{aligned} \mathbf{H}_2(\mathbf{r}) &= \frac{-jA_2 k_2}{\omega\mu} [\mathbf{i}_r \gamma K_1(k_2 r) \cos \gamma z \\ &\quad + \mathbf{i}_z k_2 K_0(k_2 r) \sin \gamma z]. \end{aligned} \quad (24)$$

The boundary condition of continuity of the tangential components of the fields at $r=a$ gives rise to the characteristic equation

$$\alpha \frac{J_0(\alpha)}{J_1(\alpha)} = -\beta \frac{K_0(\beta)}{K_1(\beta)} \quad (25)$$

where

$$\alpha = ak_1 \quad \text{and} \quad \beta = ak_2.$$

APPENDIX II

THE Q OF THE STRUCTURE FOR TE_{onl} MODES

The unloaded Q of any resonant structure is defined as 2π times the ratio of the maximum stored energy to the energy lost in one cycle. The energy storage takes place partly in the dielectric rod and partly outside the rod, similarly the energy losses are due to losses in the end walls and dielectric losses in the cavity. Thus

$$Q_0 = \frac{\omega(U_{\text{cav}} + U_{\text{sp}})}{W_{\text{walls}} + W_{\text{cav}}}. \quad (26)$$

Now, the stored energy is

$$U_{\text{cav}} = \int_{\text{cav}} \frac{\epsilon_1}{2} |\mathbf{E}_1(\mathbf{r})|^2 d\mathbf{r} \quad (27)$$

$$U_{\text{sp}} = \int_{\text{sp}} \frac{\epsilon_0}{2} |\mathbf{E}_2(\mathbf{r})|^2 d\mathbf{r} \quad (28)$$

whereas the energy losses are

$$W_{\text{walls}} = R_s \int_{\text{walls}} |H(r) \times i_z|^2 dS \quad (29)$$

where R_s is the surface resistance of the walls and is equal to $R_s = (\pi f \mu / \sigma)^{1/2}$, f being the frequency, μ the permeability, and σ the conductivity. The energy losses in the cavity are

$$W_{\text{cav}} = \frac{\omega \epsilon_1 \tan \delta}{2} \int_{\text{cav}} |E_1(r)|^2 dr. \quad (30)$$

Eqs. (27)–(30) can be evaluated for the TE_{onl} mode field components given in Appendix I and the result manipulated to give $\tan \delta$, the dielectric loss tangent, in

terms of known parameters. The result is

$$\tan \delta = \frac{1}{Q_0} \left[1 + \frac{1}{\kappa} F(\alpha) G(\beta) \right] - \frac{l^2 R_s}{2\pi f^3 \mu^2 \kappa \epsilon_0 L^3} \left[1 + F(\alpha) G(\beta) \right] \quad (31)$$

where

$$F(\alpha) = J_1^2(\alpha_n) / [J_1^2(\alpha_n) - J_0(\alpha_n) J_2(\alpha_n)], \quad (32)$$

and

$$G(\beta) = [K_0(\beta_l) K_2(\beta_l) - K_1^2(\beta_l)] / K_1^2(\beta_l). \quad (33)$$

Graphical plots of $F(\alpha)$ vs α and $G(\beta)$ vs β are given in Figs. 5 and 6, respectively.

Summary of Measurement Techniques of Parametric Amplifier and Mixer Noise Figure*

R. D. HAUN, JR.†, MEMBER, IRE

Summary—Expressions are derived for the noise factor of a frequency mixing circuit under two different operating conditions: 1) single-sideband operation with input only in a band of frequencies at ω_1 ; and 2) double-sideband radiometer operation with incoherent inputs in the bands both at frequency ω_1 and at $\omega_2 = \omega_3 - \omega_1$. In both cases, the output is taken only at ω_1 .

It is shown that the noise figure for radiometer double-sideband operation is not always 3 db less than for single-sideband operation. It is also shown that it is possible to obtain an output signal-to-noise ratio which is greater than the input signal-to-noise ratio for coherent double-sideband operation.

Methods are analyzed for measuring the effective noise temperature of this circuit by using a broad-band noise source.

I. INTRODUCTION

THE AUTHOR of this paper has recently had occasion to attempt measurements of the noise figure of a quasi-degenerate parametric microwave amplifier.¹ During the course of this experiment, it was quite surprising to find that the measured values of noise

figure were less than 3 db, although a simple theory^{2,3} (which was believed to be fairly well understood) predicted that the noise figure of this device should always be greater than 3 db. It was soon realized that this apparent anomaly had come about because the method of measurement (with a broad-band noise tube) gave the radiometer double-sideband rather than the single-sideband figure, whereas the theoretical calculations were for single-sideband operation only.

Further reflection on this problem also revealed that it is possible to obtain an output signal-to-noise ratio which is greater than the input signal-to-noise ratio with the parametric amplifier in double-sideband operation.

Searching the literature on noise figure for analogous situations, one finds that confusion exists on this point of single- vs double-sideband noise figure. Uenohara⁴

* Received by the PGMTT, September 14, 1959; revised manuscript received, February 17, 1960.

† Research Labs, Westinghouse Elec. Corp., Pittsburgh, Pa.

¹ R. D. Haun, Jr. and T. A. Osial, "Measurements on a 4.6 kmcps Diode Parametric Microwave Amplifier," Westinghouse Electric Corp., Pittsburgh, Pa., Scientific Paper No. 6-41003-4-P1, June, 1959; unpublished.

² R. D. Haun, Jr., "Small Signal Theory of Microwave Parametric Amplifiers and Up-Converters Using High-Q-Non-Linear Reactances," Westinghouse Electric Corp., Pittsburgh, Pa., Scientific Paper, No. 8-1047-P2, November 3, 1958; unpublished.

³ H. Heffner and G. Wade, "Gain, bandwidth, and noise characteristics of the variable parameter amplifier," *J. Appl. Phys.*, vol. 29, pp. 1321–1331; September, 1958.

⁴ G. H. Herrman, M. Uenohara, and A. Uhlir, Jr., "Noise figure measurements on two types of variable reactance amplifiers using semiconductor diodes," *Proc. IRE*, vol. 46, pp. 1301–1303; June, 1958.

refers to this problem and simply states that the single-sideband noise figure F_{SSB} is 3 db greater than the double-sideband noise figure F_{DSB} for a quasi-degenerate parametric amplifier. Heffner⁵ states that F_{SSB} is at least 3 db greater than F_{DSB} in a parametric amplifier. Cohn⁶ shows that if the power gain of the device is the same for an input at each of the two sidebands, the double-sideband noise figure is 3 db less than the single-sideband value; however, he does not consider the case where the gain is different for inputs at different sideband frequencies.

It is the purpose of this paper to treat this problem in detail in the hope that it will resolve some of the confusion, so that different workers in the field of parametric amplification can specify unambiguously the noise properties of a given device.

A parametric amplifier or a nonlinear resistance mixer can be used in three ways, each of which will be discussed in the following section:

1) *Single-sideband operation* in which signal power flows into the network only in the frequency band at ω_1 and the output of the network is taken only in the band at ω_1 ;

2) *Double-sideband radiometer operation* in which incoherent signals are fed into the network in the bands both at ω_1 and ω_2 , and the output of the network is taken only in the band at ω_1 ;

3) *Coherent double-sideband operation* where, for each input in the band at ω_1 , there is coherent input (*i.e.*, an image of the input at ω_1) in the band at $\omega_2 = \omega_3 - \omega_1$ and the output of the network is taken only in the band at ω_1 .

II. DEFINITIONS OF NOISE QUANTITIES FOR PARAMETRIC AMPLIFIERS AND MIXERS

The noise factor F of a network is defined as⁶⁻⁸

$$F = \frac{N_{out}}{GN_{in}} \quad (1)$$

where

N_{in} = the available input thermal noise power in a bandwidth B from a room temperature (290°K) resistor connected to the input terminals of the network;

N_{out} = the total noise power in the bandwidth B which flows out of the network toward a load (assuming the input is connected to the room temperature resistor giving rise to N_{in});

G = the power gain of the network for incoherent signals and is defined as

$$G = \frac{N'_{out}}{N_{in}}; \quad (2)$$

N'_{out} = that portion of the total output noise power which results from the input N_{in} .

It will be noted that the definitions of F and G given here contain the somewhat arbitrary condition that N_{in} be the available power from a room temperature source connected to the input of the amplifier. These definitions have a definite convenience in the microwave case because then the available power is simply the power which flows down the input transmission line toward the network, and G is the ratio of the actual power delivered by the network into an output waveguide to the maximum power which could be delivered into this waveguide by the source itself. However, for the purpose of specifying the noise properties of the amplifier, one could have chosen arbitrarily some other definition of N_{in} because, as we shall see below, these definitions are simply aids in computing from measurements the effective temperature of the noise generated inside the amplifier, and the noise figure obtained with a given choice of definitions is simply a convention for expressing this effective temperature in terms of signal-to-noise ratio.

In this paper, we consider a transmission-type network (a parametric amplifier or a mixer) in which an input signal at frequency ω_1 mixes with a local oscillator at frequency ω_3 to give outputs at both ω_1 and $\omega_2 = \omega_3 - \omega_1$ (see Fig. 1). There are four sources of noise in such a network.

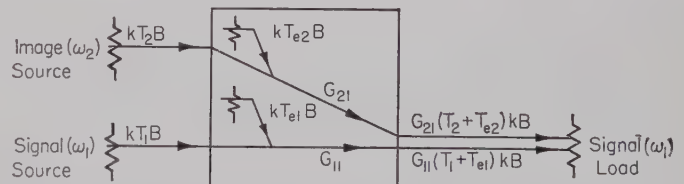


Fig. 1.

- 1) Noise which flows from the external signal source into the network in the band at frequency ω_1 , is amplified, and then flows out at the same frequency;
- 2) Noise which flows from the external source or image load into the network in the ω_2 band, is frequency converted by mixing with the local oscillator (ω_3), and then flows out in the signal band (ω_1);
- 3) Noise which is generated inside the amplifier in the frequency band at ω_1 and then flows out at the same frequency;

⁵ H. Heffner, "Masers and parametric amplifiers," *Microwave J.*, vol. 2, p. 37; March, 1959.

⁶ S. B. Cohn, "The noise figure muddle," *Microwave J.*, vol. 2, pp. 7-11; March, 1959.

⁷ "IRE Standards on electron devices—methods of measuring noise," *Proc. IRE*, vol. 41, pp. 890-893; July, 1953.

⁸ "IRE Standards on measuring noise in linear two ports, 1959," *Proc. IRE*, vol. 48, pp. 60-68; January, 1960.

- 4) Noise which is generated inside the amplifier in the frequency band at ω_2 , is frequency converted, and then flows out in the ω_1 band.

The internally generated noise, 3) and 4), may have its origins in the internal losses of the amplifier, in the local oscillator, in other images of the signal (e.g., $\omega_4 = \omega_3 + \omega_1$), or in other mechanisms internal to the amplifier.^{2,3}

If we define G_{11} as the power gain for input and output at frequency ω_1 , and G_{21} as the power gain for frequency conversion from an input at ω_2 to an output at ω_1 , the total noise power output of the network at frequency ω_1 is

$$N_{out} = kB(G_{11}T_1 + G_{11}T_{e1} + G_{21}T_{e2} + G_{21}T_2) \quad (3)$$

where

k = Boltzmann's constant,

B = bandwidth of output,

T_1 = noise temperature of external signal source in the ω_1 band,

T_2 = noise temperature of external load or source in the ω_2 band,

T_{e1} and T_{e2} = the effective input noise temperatures of the internal ω_1 and ω_2 circuits, respectively. These are the noise temperatures of resistors which when connected to the appropriate input terminals of the network would result in the same noise output as the noise generated internal to the network.

For convenience, let us define a total effective internal noise temperature by

$$T_e = T_{e1} + \frac{G_{21}}{G_{11}} T_{e2}. \quad (4)$$

This is the noise temperature of a resistor which when connected only to the ω_1 input terminals would result in the same output noise power as the noise generated internal to the network.

A. Single-Sideband Operation (Input at ω_1 Only)

As a first example, let us assume that signal power flows into the network only at ω_1 , that only the ω_1 input terminals are connected to a noise source of effective temperature T_1 , and that the ω_2 circuit is connected only to load at temperature T_2 . Then the output noise at frequency ω_1 is

$$N_{out} = kB(G_{11}T_1 + G_{21}T_2 + G_{11}T_e). \quad (5)$$

The noise factor is

$$\begin{aligned} F_{SSB} &= \frac{N_{in}}{N'_{out}} \frac{N_{out}}{N_{in}} \\ &= \frac{N_{in}}{N'_{out}} \frac{kB(G_{11}T_1 + G_{21}T_2 + G_{11}T_e)}{kBT_1} \end{aligned} \quad (6)$$

where T_1 must be taken as $T_0 = 290^\circ\text{K}$. Since

$$\frac{N_{in}}{N'_{out}} = \frac{1}{G_{11}},$$

we have

$$F_{SSB} = 1 + \frac{T_e}{T_0} + \frac{G_{21}}{G_{11}} \frac{T_2}{T_0}. \quad (7)$$

B. Double-Sideband Radiometer Operation (Incoherent Inputs at ω_1 and ω_2)

On the other hand, if a broad-band noise source of temperature T_1 is used to feed equal power in at both ω_1 and ω_2 , the noise out is

$$N_{out} = kB(G_{11}T_1 + G_{21}T_1 + G_{11}T_e), \quad (8)$$

and the noise incident on the amplifier is

$$N_{in} = 2kT_1B \quad (9)$$

where equal amounts of power flow into the signal and image input terminals. The noise factor is, therefore,

$$F_{DSB} = \frac{N_{in}}{N'_{out}} \frac{kB(G_{11}T_1 + G_{21}T_1 + G_{11}T_e)}{2kBT_1} \quad (10)$$

where T_1 must be taken as $T_1 = T_0 = 290^\circ\text{K}$ in (10). In radiometer operation, the incident signal is equivalent to the thermal noise

$$N_{in} = 2kBT_s \quad (11)$$

where equal amounts of power flow into the signal and image input terminals. The output signal is then

$$N'_{out} = kT_sBG_{11} + kT_sBG_{21} \quad (12)$$

so that the noise factor is

$$\begin{aligned} F_{DSB} &= \frac{2}{G_{11} + G_{21}} \frac{G_{11}T_0 + G_{21}T_0 + G_{11}T_e}{2T_0} \\ &= 1 + \frac{G_{11}}{G_{11} + G_{21}} \frac{T_e}{T_0}. \end{aligned} \quad (13)$$

For the special case where $G_{11} = G_{21}$, we have

$$F_{DSB} = \frac{1}{2}F_{SSB}, \quad (14)$$

where it has been assumed that for single-sideband operation the image circuit load is at room temperature (i.e., $T_2 = T_0$). These conditions will be satisfied for a quasi-degenerate parametric amplifier at high gain.

For $G_{11} \neq G_{21}$ or for $T_2 \neq T_0$, the radiometer double-sideband noise figure will not be one half the single-sideband value. Even for quasi-degenerate operation (i.e., where ω_1 and ω_2 are almost equal) G_{21} and G_{11} can differ by factors of 10 so that caution should be exercised in using (14).¹

C. Double-Sideband Coherent Operation (Coherent Inputs at ω_1 and ω_2)

Now suppose that equal amplitude coherent signals flow into the network at frequencies ω_1 and ω_2 . Suppose also, that the time origin has been chosen so that the fields at ω_1 and at the pumping frequency are in phase. Then, for a transmission-type parametric amplifier using a nonlinear capacitor, it is shown in Appendix I that, if ϕ is the phase lead of the input ω_2 relative to the input at ω_1 , the ratio of S_{out} , the total signal power out at frequency ω_1 , to S_{in} , the total available signal power in at frequencies ω_1 and ω_2 , is

$$\frac{S_{out}}{S_{in}} = \frac{1}{2} \left[G_{11} + G_{21} + 2\sqrt{G_{11}G_{21}} \cos\left(\phi + \frac{\pi}{2}\right) \right]. \quad (15)$$

Since the input and output noise will be the same as in double-sideband radiometer operation, (8), (9), and (15) give the relative input and output signal-to-noise ratios for double-sideband coherent operation of the capacitive parametric amplifier

$$\frac{S_{in}/N_{in}}{S_{out}/N_{out}} = \frac{G_{11}T_0 + G_{21}T_0 + G_{11}T_e}{\left[G_{11} + G_{21} + 2\sqrt{G_{11}G_{21}} \cos\left(\phi + \frac{\pi}{2}\right) \right] T_0}. \quad (16)$$

For a mixer using a nonlinear resistance, a similar analysis shows that the power gain for coherent double-sideband operation is

$$\frac{S_{out}}{S_{in}} = \frac{1}{2} [G_{11} + G_{21} + 2\sqrt{G_{11}G_{21}} \cos(\phi + \pi)], \quad (17)$$

and

$$\frac{S_{in}/N_{in}}{S_{out}/N_{out}} = \frac{G_{11}T_0 + G_{21}T_0 + G_{11}T_e}{[G_{11} + G_{21} + 2\sqrt{G_{11}G_{21}} \cos(\phi + \pi)] T_0}. \quad (18)$$

For the special case of optimum phase (*i.e.*, when the cosine is unity) when also $G_{11} = G_{21}$, we have

$$\frac{S_{in}/N_{in}}{S_{out}/N_{out}} = \frac{1}{2} + \frac{1}{4} \frac{T_e}{T_0} \quad (19)$$

$$= \frac{1}{4} F_{SSB} \quad (20)$$

where it has been assumed that $T_2 = T_0$ for operation as a single-sideband amplifier.

From (19), we see that for $T_e < 2T_0$ (a condition which can be achieved in practice) it is possible to obtain a signal-to-noise ratio at the output of the device which is larger than it is at the input. At first thought, this may seem to imply that this device violates the laws of thermodynamics by absorbing thermal noise from the input, but further reflection shows that this is not the case; instead, the device adds noise to the input (because

$T_e > 0$) but the amplitude of the noise is not increased proportionally as much as is the amplitude of the signal. This occurs because the coherence of the two input "signals" at ω_1 and ω_2 and the pump at ω_3 allows the signal to be selectively amplified relative to the noise. In order for this improvement in signal-to-noise ratio to occur, it is necessary for the ω_1 and ω_2 input signals to have a certain phase relationship with respect to the pump at ω_3 . Since on the average the noise at ω_1 and ω_2 will not have the correct phase relative to the pump (ω_3), the noise will not be amplified as much as is the signal.

III. MEASUREMENT OF THE NOISE FACTOR WITH A BROAD-BAND NOISE SOURCE

One of the most convenient methods for measuring the noise factor of a network consists of connecting a noise source to the input of the network, and varying the effective temperature of this source so as to double the output noise power of the amplifier.

Let us assume that a matched variable room temperature attenuator is placed in the transmission line between the noise source (with effective temperature βT_0) and the input of the network. Let the ratio of power transmitted to power incident for this attenuator be α .

A. Single-Sideband Noise Factor Measurement

Assume that the input is filtered so that one need consider only power which flows into the network from the noise source in a frequency band of width B at ω_1 and that the ω_2 circuit is connected only to a load at temperature T_2 . With the noise source off (*i.e.*, with $\alpha \ll 1$), the input noise power will be

$$(N_{in})_1 = kT_0B. \quad (21)$$

The resulting output at ω_1 will be

$$(N_{out})_1 = G_{11}kT_0B + G_{21}kT_2B + G_{11}kT_eB. \quad (22)$$

When the noise source (of temperature βT_0) is turned on, and the attenuator is set at a value α which gives double the noise output, the noise input power is given by

$$(N_{in})_2 = \alpha k(\beta T_0)B + (1 - \alpha)kT_0B. \quad (23)$$

The resulting output power at ω_1 will be

$$(N_{out})_2 = G_{11}[1 + \alpha(\beta - 1)]kT_0B + G_{21}kT_2B + G_{11}kT_eB \quad (24)$$

$$= 2(N_{out})_1. \quad (25)$$

Solving (24), (25), and (22) for T_e , we obtain

$$T_e = [\alpha(\beta - 1) - 1]T_0 - \frac{G_{21}}{G_{11}} T_2. \quad (26)$$

If we consider the image load to be a part of the network, then the total effective noise temperature (*i.e.*, the

temperature of noise generated both internally and in the image load) will be

$$(T_e)_{\text{total}} = T_e + \frac{G_{21}}{G_{11}} T_2 \quad (27)$$

or using (26),

$$(T_e)_{\text{total}} = [\alpha(\beta - 1) - 1]T_0. \quad (28)$$

From (7), the single-sideband noise factor will therefore be

$$F_{\text{SSB}} = \alpha(\beta - 1). \quad (29)$$

B. Radiometer Double-Sideband Noise Factor Measurement

If the input is not filtered, and power flows into the network in a band of width B at frequency ω_1 , and in a band of width B at frequency ω_2 , the total input noise power when the noise source is off will be

$$(N_{\text{in}})_1 = 2kT_0B. \quad (30)$$

The resulting output at ω_1 will be

$$(N_{\text{out}})_1 = G_{11}kT_0B + G_{21}kT_0B + G_{11}kT_eB. \quad (31)$$

When the noise source (of temperature βT_0) is turned on and the attenuator is set at a new value α' to double the output noise power, the input noise is

$$(N_{\text{in}})_2 = 2\alpha'k(\beta T_0)B + 2(1 - \alpha')kT_0B, \quad (32)$$

where half the power flows in at each frequency (ω_1 and ω_2), and the resulting output power at ω_1 is

$$(N_{\text{out}})_2 = G_{11}[\alpha'(\beta - 1) + 1]kT_0B + G_{21}[\alpha'(\beta - 1) + 1]kT_0B + G_{11}kT_eB \quad (33)$$

$$= 2(N_{\text{out}})_1. \quad (34)$$

Solving (31), (33), and (34) for T_e , we obtain

$$T_e = \frac{G_{11} + G_{21}}{G_{11}} [\alpha'(\beta - 1) - 1]T_0. \quad (35)$$

From (13), the radiometer double-sideband noise factor will therefore be

$$F'_{\text{DSB}} = \alpha'(\beta - 1). \quad (36)$$

Comparing (36) with (29), we see how confusion can arise if the experimenter does not take care to note whether or not power flows into the network at both the ω_1 and ω_2 bands.

The single-sideband noise factor can be computed from the wide-band noise source measurements by substituting (35) in (7), and noting that $T_2 = T_0$. Doing this, one obtains

$$F_{\text{SSB}} = \left(1 + \frac{G_{21}}{G_{11}}\right) \alpha'(\beta - 1). \quad (37)$$

For the special case where $G_{21} = G_{11}$ (for example, in a quasi-degenerate parametric amplifier at high gain), the measured radiometer double-sideband noise factor is one half the single-sideband value.

IV. DISCUSSION

From Sections II and III, one sees that the principal difference between single-sideband and double-sideband operation lies in whether the image circuit external load is considered as part of the network or as part of the source. For single-sideband operation, this load is included in the amplifier and contributes a term to the total effective noise temperature of the device. For double-sideband operation, this load is a part of the source, and the device cannot be penalized for noise generated by it.

The difference between radiometer and coherent double-sideband operation depends upon whether or not the inputs in the two sidebands are coherent. If they are coherent, then by properly choosing their phases relative to the pump, it is possible to amplify selectively these coherent inputs and increase the output signal-to-noise ratio relative to the input signal-to-noise ratio. It should be noted that the optimum choice of relative phase depends upon whether a nonlinear capacitance, a nonlinear inductance, or a nonlinear resistance is used as the time varying element in the mixing network.

One further possible point of confusion remains with respect to the single-sideband mixer or parametric amplifier: if the signal field is fed only into the network at frequency ω_1 but both the ω_1 and ω_2 input terminals are connected to the antenna, then the total effective noise temperature of the device $(T_e)_{\text{total}}$ [see (27)] will depend upon T_2 , the temperature of the input circuit at ω_2 . This means that when used with a low temperature source the noise figure of a single-sideband mixer circuit will be lower than the value computed from the measurements of Section III.

From the section on measurements, one sees that the confusion as to what parameter is actually being measured is greatly reduced if it is realized that the noise tube technique is actually a means for determining the total effective internal noise temperature T_e , and, that from this quantity, the noise figure can be computed for each specific type of operation.

APPENDIX I

DERIVATION OF GAIN EXPRESSION FOR COHERENT DOUBLE-SIDEBAND OPERATION

Using the definitions as indicated in Fig. 2, one can derive the expression for the midband gain of an inverting transmission-type parametric amplifier for coherent double-sideband operation as follows.²

Assume a current generator I_1 is connected to the ω_1 input of the amplifier and that a current generator I_2 is connected to the ω_2 input (See Fig. 2). Let V_{11} be the voltage at frequency ω_1 , developed as a result of I_1 , and let V_{21} be the voltage at frequency ω_1 developed as a result of I_2 .

Letting $\alpha = g/g_1$ in Heffner,³ we have

$$V_{11} = \frac{I_1}{g_1(1 - \alpha)}.$$

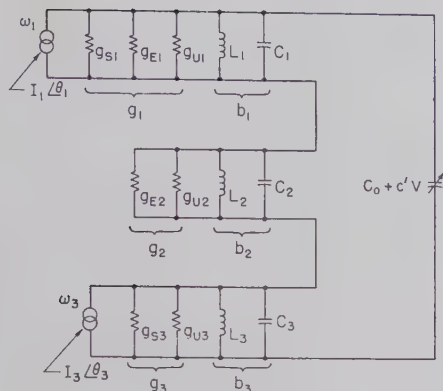


Fig. 2.

From the treatment of Heffner,³ one can show that

$$V_{21} = -\frac{j\omega_1 c' V_3}{g_1 g_2 (1 - \alpha)} I_2^*.$$

The total signal power delivered to g_{E1} , the external load in the ω_1 circuit, will be

$$S_0 = (V_{11} + V_{21})(V_{11}^* + V_{21}^*)G_{E1}.$$

Assuming $I_2 = I e^{j(\omega_2 t + \phi)}$, and $I_1 = I e^{j\omega_1 t}$, and assuming the phase of the pump to be zero, this can be rewritten as

$$S_0 = G_{11}S_1 + G_{21}S_2 + \frac{2g_{E1}\omega_1 c' V_3 I^2}{g_1^2 g_2 (1 - \alpha)^2} \cos\left(\phi + \frac{\pi}{2}\right),$$

where

$$S_1 = \frac{|I_1|^2}{4g_{S1}} = \text{signal power incident at frequency } \omega_1$$

$$S_2 = \frac{|I_2|^2}{4g_{S2}} = \text{signal power incident at frequency } \omega_2$$

$$G_{11} = \frac{4g_{E1}g_{S1}}{g_1^2(1 - \alpha)^2}$$

$$G_{21} = \frac{\omega_1}{\omega_2} \frac{4g_{S2}g_{E1}}{g_1 g_2} \frac{\alpha}{(1 - \alpha)^2}.$$

Since for small signals

$$\alpha \doteq \frac{\omega_1 \omega_2 (c')^2 V_3^2}{g_1 g_2},$$

we obtain

$$S_0 = G_{11}S_1 + G_{21}S_2 + 2\sqrt{G_{11}G_{21}}S_1 S_2 \cos\left(\phi + \frac{\pi}{2}\right).$$

The incident signal power is given by

$$S_i = S_1 + S_2.$$

But, for equal input couplings $S_1 = S_2$, so that the gain for coherent inputs at ω_1 and ω_2 with output at ω_1 is

$$G_{\text{DSB}} = \frac{S_0}{S_i} = \frac{1}{2} \left[G_{11} + G_{21} + 2\sqrt{G_{11}G_{21}} \cos\left(\phi + \frac{\pi}{2}\right) \right].$$

A similar analysis could be carried out for a nonlinear resistance mixer; it would then be found that the factor $\cos(\phi + \pi/2)$ in the preceding should be replaced by the factor $\cos(\phi + \pi)$.

Duplexing Systems at Microwave Frequencies*

A. F. HARVEY†

Summary—The paper reviews the various methods of duplexing at microwave frequencies. General principles, including the use of passive and solid-state devices, are first discussed. The characteristics of gaseous-discharge duplexing tubes of both self- and externally-excited types are examined and data for typical examples given. The various arrangements of discharge tube duplexers and methods of measuring their performance are described. The survey concludes with a bibliography.

* Received by the PGMTT, October 5, 1959; revised manuscript received, February 18, 1960.

† Royal Radar Estab., Malvern, England.

LIST OF PRINCIPAL SYMBOLS

B_0 = applied magnetic flux density, weber/m².

c = speed of light in vacuo = $(\epsilon_0 \mu_0)^{-1/2} = 3 \times 10^8$ m/sec.

D_a = ambipolar diffusion coefficient, m²/sec.

e = charge on electron = 1.60207×10^{-19} coulomb.

h_a = attachment probability.

m = mass of electron = 9.1085×10^{-31} kg.

N = density of electrons, m⁻³.

N_L = Loschmidt's constant = 2.687×10^{25} m⁻³ atm⁻¹.

p = pressure, mm Hg.
 r = radius, meter.
 t = time, second.
 v_d = drift velocity, m/sec.
 Z = impedance, ohms.
 α = attenuation coefficient, nepers/m.
 α_r = recombination coefficient, $m^3/\text{ion-sec}$.
 β = phase-change coefficient, rad/m.
 γ = propagation coefficient = $\alpha + j\beta$.
 ϵ = dielectric constant.
 ϵ_0 = electric space constant = 8.85416×10^{-12} farad/m.
 η_a = attachment cross section, meter².
 λ_0 = wavelength in free space, meter.
 λ_g = guide wavelength, meter.
 μ_0 = magnetic space constant = $4\pi \times 10^{-7}$ henry/m.
 ν_a = attachment frequency, c/s.
 ν_e = electron-ion collision frequency, c/s.
 σ = conductivity, mhos/m.
 τ = time constant, second.
 ω = angular frequency, rad/sec.
 ω_c = cyclotron angular frequency, rad/sec.
 ∇ = Laplacian operator.

Recovery times quoted are for 3 db loss; values for 6 db are somewhat shorter.

I. PRINCIPLES OF DUPLEXING

A. Passive Circuit

Duplex operation of a microwave system permits the passage of signals, having a common frequency, along a transmission line; it should not be confused with duplexing, which depends upon the difference in frequency of the two signals. The particular example considered is the use of a common circuit, such as an antenna, by both a transmitter and a receiver. Desirable qualities of a duplexer include low attenuation and high discrimination over a wide frequency band, freedom from manual adjustments, reliability and long life.

With CW operation, the duplexer is required to keep the transmitter disconnected from the receiver at all times and yet allow maximum coupling between the transmitter and antenna and between the antenna and receiver. With high-power pulsed operation the discrimination required to give adequate protection [111] to the receiver is about 60–80 db. Further practical requirements are that protection should be afforded from occasional random pulses received from nearby equipments and that the duplexer should recover to the receiving state in a time of 1–50 μsec according to the application.

If the first stage of the receiver is a semiconductor point-contact diode then, to avoid burn out, the leakage power of the duplexer must be maintained below about 50 mw. The thermal time constant of the diode contact is around 10^{-7} seconds and any transient effect in the duplexer must have an energy not exceeding 0.01 erg for temporary and 0.1 erg for permanent deterioration.

Some recent low-noise RF amplifiers are even more sensitive [16] to leakage and, moreover, much of their advantage is lost if the duplexer itself adds appreciable noise.

A passive duplexer can, for example, be constructed from lossless four-terminal-pair junctions [114], [115] and Fig. 1 shows a hybrid T so employed. Energy from the transmitter divides between the matched termination on one arm and the antenna on the other while energy received by the antenna divides equally between the transmitter and receiver. The resulting 6-db total loss may be shown to be the minimum for such a simple circuit. The discrimination between transmitter and receiver is reduced by imperfections of the junction or mismatches in the termination and antenna. Such residual leakage can be balanced out, over a small frequency band, to a level of less than -100 db.

Passive duplexers based on circularly-polarized waves have negligible attenuation and, in addition, provide isolation of the transmitter from impedance changes of the antenna. The transmitted wave possesses one hand of polarization and the received wave, due to reflection, possesses the other hand: discrimination can thus be achieved by a suitable circuit. The arrangement shown in Fig. 2(a) contains two-orthogonal transducers from TE_{01} rectangular to TE_{11} circular mode. The circular waveguide contains a quarter-wave plate and Fig. 2(b) gives the phases of the electric field components of the transmitted energy. Fig. 2(c) shows that a reflected

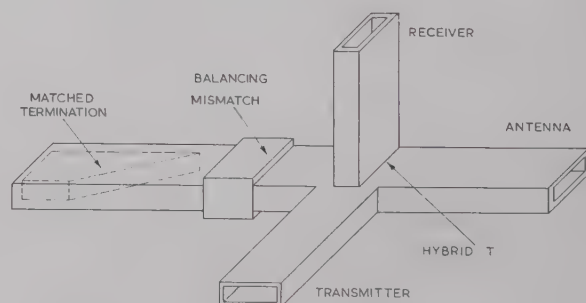


Fig. 1—Simple passive duplexer. This device gives a 3-db loss on both transmission and reception.

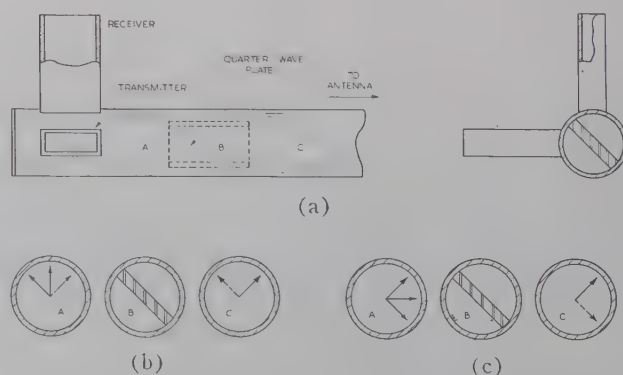


Fig. 2—Passive duplexer using circular polarization. (a) Assembly. (b) Electric vectors during transmission. (c) Electric vectors during reception.

signal is converted, after passage through the plate, to a plane wave, polarized so that it enters the receiver arm.

The conversion from plane- to circular-polarization may be carried out at the antenna [69] by the use of, for example, a polarized mirror [100]. Alternatively, the transmitter and receiver can be connected to opposite rectangular arms of a turnstile six-terminal-pair junction, the remaining pair of arms being terminated in short circuits so that they differ in length by $\frac{1}{4}\lambda_0$. At a frequency of 9 gc (gigacycles), such a duplexer has given [85] an isolation better than 40 db over a band of 100 mc. Another adjustment of the turnstile junction enables duplexing to be achieved with crossed linear polarizations of the transmitted and received signals.

The prefix for mega ($=10^6$) has been changed from m to M. This is to avoid serious confusion later on between milliwatt (mw) and megawatt (now Mw).

The restriction on the polarization is removed by the use of ferrite circulators. In the four port example shown in the inset of Fig. 3, energy from the transmitter *T* proceeds to the antenna *A* while energy from the antenna proceeds to the receiver *R*. A dummy load *L* is connected to the fourth port to absorb any leakage. The discrimination of an experimental Faraday-rotation duplexer [53] for 35 gc is shown by Fig. 3 to be better than 30 db over a 0.7 per cent band around the balanced frequency. Circulators for 9 gc, in which the ferrite is placed in the short-circuited circular guide of a turnstile junction, have shown [20] a similar discrimination with an insertion loss of 0.4 db, a VSWR of 1.25 and an overall length of 1.5 inches. Such duplexers are very satisfactory for CW systems of about 50-watts mean power.

With the duplexer of Fig. 3 and a transmitter giving 19 kw in 0.2- μ sec pulses the finite frequency spectrum led to a leakage of 400 mw: such a high value could be reduced by broadband design. Duplexers for high powers must ensure that the ferrite, which is exposed to the full transmitted power, can withstand high voltages and dissipate, with the aid of air- or water-cooling, the heat generated consequent upon its attenuation.

B. Solid-State Switches

The high degree of protection required by pulsed operation may be obtained by time-division duplexing in which an attenuator or switch is energized in synchronism with the transmitter pulse. Low noise and high operating speed can be achieved by placing suitable solid-state devices in the receiver arm of a passive duplexer. To avoid a leakage transient due to the finite response time it is desirable to pretrigger the switch so that it has full insertion loss before the initiation of the transmitter pulse. Alternatively the transient may be removed by power limiters based, for example, on travelling-wave tubes [29] or ferrites [110].

The point-contact semiconductor diode is suitable [4], [33-35], [87] as a switch since the impedance, including that of its mount, may be varied from a low inductive to a high capacitive value with a bias change

of, say, -0.6 to $+0.6$ volt. Improved performance is obtained [18] by connecting the diode in parallel with the shunt capacitance of a high-pass series *m*-derived filter. Typical parameters of such a switch are: frequency, 500-1000 mc; bandwidth, 20 mc; discrimination, >55 db; insertion loss, 2 db and operating time, $<\frac{1}{2}$ μ sec.

In the duplexer [38] shown in Fig. 4, one of two ferrite circulators is reversed during the reception period: this switched circulator handles only low powers. Ferrite switches [124] operate by change of the magnetic field and some difficulty arises in making the rapidly varying field [21] penetrate the surrounding metal wall of the waveguide. At the lower frequencies sufficient room exists to place [113] the magnetizing coil around the actual ferrite. In Faraday-rotation devices a helical slot may be cut to follow the plane of polarization of the transmitted wave: this design has the disadvantage that in the closed, or reversed, position the cross-polarized components reduce the discrimination unless RF chokes are employed [93].

More usual practice takes advantage of the different penetration depths obtaining at the modulation and microwave frequencies. Films, 0.0001-inch thick, can be made on plastics such as Perspex and include electroplated silver [53] and vacuum-evaporated aluminum [11]. The switching power can be reduced by the use of toroidal-shaped [121] ferrites. Successful ferrite switches have been constructed for 9 gc [5], 55 gc [31] and 70 gc [122]. A typical example for the first frequency would have [72], [73] maximum and minimum attenuation better than 35 db and 1 db, with a switching time of $\frac{1}{4}$ μ sec.

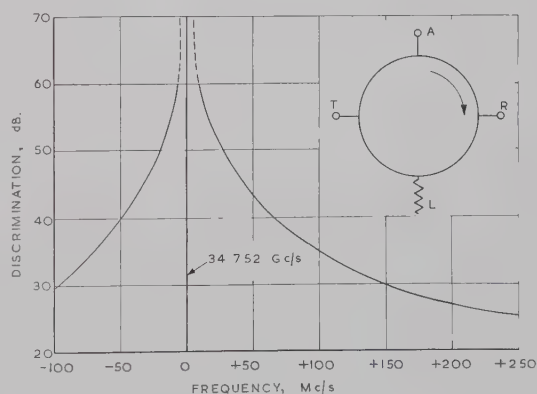


Fig. 3—Discrimination of a ferrite duplexer. The inset shows the arrangement of ports. Input power 40 kw. Ferrite-type B3.

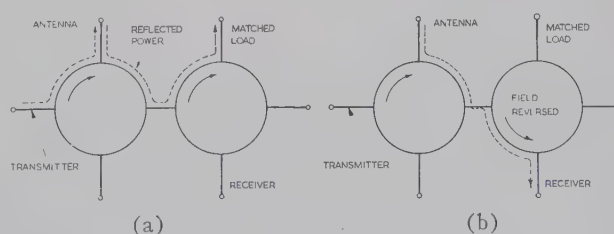


Fig. 4—Duplexer using a switched ferrite circulator. The arrangement uses one switched and one unswitched circulator. (a) Transmission. (b) Reception.

Balanced duplexers incorporate hybrid junctions which provide additional discrimination, thus giving improved protection and greater bandwidth. The power division and standing waves inherent in this duplexer result in the transmission line being exposed to twice the transmitter power and the switching devices to one half. The duplexer of Fig. 5 employs ferrite stubs whose electrical length is normally $\frac{1}{2}\lambda_g$ so that a signal from the antenna proceeds without reflection to the receiver. During the transmission period the stubs are switched to a length of $\frac{3}{4}\lambda_g$. Complete reflection occurs and the $\frac{1}{2}\lambda_g$ relative spacing of the stubs ensures that the transmitter power proceeds to the antenna.

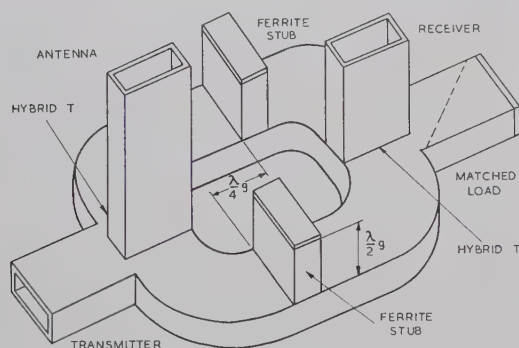


Fig. 5—Balanced duplexer with ferrite switches. The electrical length of the stubs is switched from $\frac{1}{2}\lambda_g$ to $\frac{3}{4}\lambda_g$ during transmission.

There is insufficient experience on the use of solid-state devices in duplexers for pulsed operation to form a reliable estimate of their merits. They appear to be suitable for applications where low noise, very rapid response, light weight and long life are required. With their present state of development, however, the usual duplexer for high-power pulsed operation incorporates, often exclusively, devices based on the phenomena of gaseous electronics.

II. CHARACTERISTICS OF DUPLEXING TUBES

A. Circuit Arrangement

The electrical discharges which provide the basis of duplexing tubes are due to ionization processes taking place at low pressure, at ordinary temperature and usually in rare gases. Their characteristics may be examined under the states of breakdown, the discharge proper and the afterglow. Breakdown of a gas takes place under the influence of an applied field which is sufficiently large to cause cumulative ionization [19], [74], [119]. The typical dc gaseous discharge consists of four main regions: cathode dark space, negative glow, Faraday dark space and positive column. The negative glow is associated [12] with much of the potential drop, high electron density and low electron collision frequency. The positive column is associated [43, 123] with low electron density and high collision frequency. In an HF discharge [2] the electrodes play only a minor role and the discharge presents a smooth appearance. The electron and current densities can reach very high

levels and may exceed 10^{15} electrons/cm³ and 15 a/cm² respectively.

The gaseous discharge in duplexing tubes may be externally excited by dc or HF means or internally excited by electric fields at the operating microwave frequency [15], [59]–[61]. The properties resulting from the interaction between the electrons and the microwave field are well known [41]: they endow the discharge with a conductivity given by [62], [79], [82]

$$\sigma = \frac{Ne^2\nu_c}{m(\omega^2 + \nu_c^2)} \quad (1)$$

and a relative permittivity given by

$$\epsilon = 1 - \frac{Ne^2}{m(\omega^2 + \nu_c^2)\epsilon_0} \quad (2)$$

Differentiation of (1) shows that the conductivity is a maximum when $\omega = \nu_c$, the phase angle being then 45°. The transfer of energy from the RF field to the discharge is then a maximum and corresponds to minimum values of breakdown power, arc loss and leakage through the discharge. Fluctuations in the velocity and collision-rate of the electrons result in noise which may be expressed as an equivalent temperature [17], [95].

Duplexing tubes require a microwave structure, coupled to the transmission line and designed so that optimum interaction takes place between the gaseous discharge and the RF electric field. In tubes with dc or IF excitation, efficient interaction is achieved by working in the negative glow. The arc-leakage power of RF excited tubes tends to be constant over a wide range of incident powers but, as with other parameters, it is dependent upon the nature of the discharge. In general, high electron density and other desirable properties, coupled with long working life, are provided by a basic filling of one of the heavier rare gases to a pressure of 2–20-mm Hg.

A distributed structure contains the discharge in a portion of transmission line, sealed at either end by low Q-factor windows. The design may be in the form of a coaxial line [37], [90], [91], [106], interaction taking place in a gaseous discharge established between the inner and outer conductors. At frequencies above 10 gc, the difficulty in constructing close-tolerance transducers is avoided by employing rectangular or circular [112] waveguides. The interaction distance must usually be several wavelengths and bulkiness at frequencies lower than 10 gc can be avoided by the use of slow-wave structures. One example [103] for 3 gc employs an interdigital line, the discharge taking place at the tips of the fingers. In general, distributed-structure tubes must employ either heated cathodes or very high pulsed voltages to produce a sufficiently intense electron density but, on the other hand, large microwave powers can be controlled.

Resonant structures provide a much increased interaction between the gaseous discharge and the RF field. Practical shapes tend to give nonhomogeneous dis-

charges with rapid variation [96] of electron density so that theory cannot be accurately applied. A typical high Q -factor circuit consists, as shown in Fig. 6(a), of a single cavity, usually resonant in a modified TM_{010} mode. The interaction region is between the tips of the two cones and Q -factors are around 300. Such structures tend to give a leakage due to transmission in modes not possessing voltage maxima at the gap, but since this is about -70 db it shows up only at very high incident powers. Tuning of the cavity is achieved by adjustment of the cone gap.

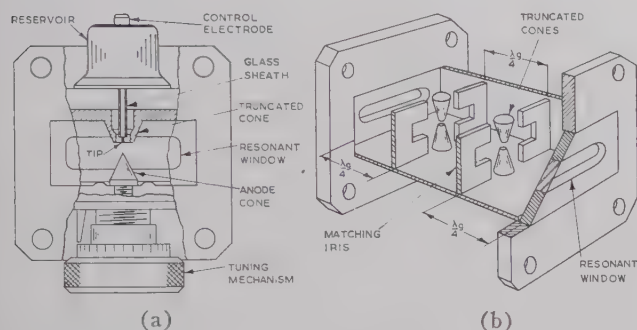


Fig. 6—Resonant structures using gas discharges. (a) High Q -factor tunable. (b) Low Q -factor broadband. The frequency is about 9.5 gc.

Fig. 6(b) shows an alternative low Q -factor structure which contains two cone assemblies, each being tuned by an inductive iris. The Q -factor of each element, loaded by the terminating impedance of the waveguide, is determined by the gap between the cones and the dimensions of the iris and is about 4. At either end of the structure, resonant slots, with a Q -factor half that of the cones, are included: these serve as terminations of a binomial filter and increase the bandwidth. The resonant elements are spaced $\frac{1}{4}\lambda_g$ apart, at which distance some interference due to evanescent modes is present. In such tubes, breakdown first occurs at the cones and this leads rapidly, with high incident powers, to breakdown of the gas in the vicinity of the input window. The combined attenuation of the window and gap discharges is of the order 80–100 db. Broad-band tubes are tending to supplant the high Q -factor types since, in particular, they are capable of operation at very high powers and avoid signal loss associated with incorrect tuning.

At the lower frequencies increased flexibility of design and operation is achieved by separation of the discharge tube and the circuit elements. In the tuneable single-cavity arrangement the discharge takes place in a cell in which the electrodes are brought out via disk seals. An early example [22] was used over the range 2.30–3.75 gc with different external structures. Fine tuning is achieved with moveable plungers and coupling to an external transmission line may be by loop or aperture. More recently, this plug-in feature has been applied [128] to broad-band structures so that, at each stage of the device, an independent choice can be made of the discharge characteristics.

B. Priming the Discharge

The statistical time lag occurring between the application of the exciting field and the complete buildup of the gaseous discharge is undesirable in practical tubes. The delay may be shortened by maintaining a continuous weak ionization in the breakdown region which, in the case of prepulsed externally-excited tubes, can satisfactorily be provided from a radioactive substance. About 10 microcuries of tritium, which is a source of low-energy β -particles with a half-life of 12.26 years, forms a safe and convenient priming agent.

In self-excited tubes, the time lag allows microwave energy to pass unattenuated to give a transient of duration about 5×10^{-9} seconds. The energy in this spike is minimized by correct design of the resonant structure and choice of the nature and pressure of the gas filling but, in addition, a large initial ionization of the order 10^8 electrons/cm³ is necessary. This ionization is generally provided by the glow discharge of a keep-alive or primer. The primer must have negative polarity and may be positioned either inside and coaxial with the suitably hollowed RF electrode or at the side of the interaction space. The electron density must not be so high as to cause undue interaction loss in the low-level condition. Moreover, the discharge allows electrons with random energies to enter the RF field, thus forming a noise source internal to the receiving system. In practice currents around 100 μ a are employed.

Keep-alive circuits are prone to relaxation oscillations and, under certain conditions, wander of the discharge and glow-to-arc transitions. These effects result in periods of low electron density and hence large spike energy. The tendency towards oscillation is reduced by placing one megohm of the total current-limiting resistance close to the primer terminals. A further precaution involves operating the discharge in the abnormal region [109] by covering the electrode with a glass or ceramic sleeve down to the end, which is exposed by grinding off the insulation. Such an electrode of restricted area also has the advantage of reducing wander by localizing the discharge. An arc is characterized by low potential and high current and can thus be maintained only by the stored energy in the distributed capacitance of the electrode: it extinguishes after a time of the order 10^{-4} μ sec. With an electrode capacitance of 10 μ mf and running conditions of 500 volts, 100 μ a the glow discharge will not restart for 50 μ sec. These glow-to-arc transitions can be avoided by ensuring that the electrode surfaces do not become contaminated.

Sputtering of the keep-alive cathode causes slow clean-up of the gas filling with consequent deterioration in the tube properties. This erosion can be reduced [65], [126] by proper design of the electrode shape and choice of the metal constituting the keep-alive tip. Kovar is in general use but rhodium plating or the provision of stainless steel tips reduces the effect. Gas clean-up also occurs under the influence of the RF discharge, especially with high powers. The working life of the tube

can be prolonged by, for example, the inclusion of a gas reservoir. This gas clean-up may be studied [26] in experimental tubes by including a radioactive tracer such as krypton-85 with the usual gas filling.

The interaction loss, noise and shortened life due to the keep-alive discharge may be improved by maintaining the current small and increasing it, by means of a prepulse, just prior to the start of the transmitter pulse. In this way substantial priming can be achieved so that the spike energy is diminished while the small residual discharge protects the receiver by ensuring that occasional random pulses, although large enough to cause temporary deterioration of the diode contact, are not large enough to lead to permanent damage.

C. Quenching the Discharge

In the afterglow of the discharge the electrons, whose average energy is initially high, tend to acquire, at a rate determined by the probability [45] of collision for momentum transfer, a Maxwellian distribution of velocity with an equilibrium temperature that of the gas. The early afterglow, which is of promising interest in the study of duplexing tubes, is thus characterized by a time-varying electron energy distribution function. Moreover, the electron density is reduced by three physical mechanisms, which may operate singly or together, according to the relation

$$dN/dt = D_a \nabla^2 N - \alpha_r N^2 - h_a v_c N. \quad (3)$$

Diffusion [3] involves the motion of the electrons to the discharge boundary and thus depends upon the mobility of the particles and the path length traversed. The decay is exponential with a time constant which, for a spherical container of radius r , is given by

$$\tau = r^2 / \pi^2 D_a. \quad (4)$$

A typical value of D_a , reduced to a gas pressure of 1 mm Hg, is 900 for argon [8]. Recombination between an electron and a positive ion involves [83] the release of energy in another form: one example of such a process is surface recombination which leads to translational kinetic energy of a third particle. The decay leads to a linear relation between $1/N$ and t and experiments [7], [66] on helium ions at 3 gc gave values of α_r about 1.7×10^{-8} cm³/ion-sec. Attachment involves [81] the formation of a negative ion [84] on capture of an electron by a neutral gas molecule. Experimentally, three attachment parameters can be measured: the attachment cross section η_a , the attachment probability h_a and the attachment coefficient η/p . The attachment frequency can be expressed in terms of one of these parameters by

$$v_a = h_a v_c = \frac{p N_L}{760} \eta_a v_d = p \left(\frac{\eta}{p} \right) v_d. \quad (5)$$

In strongly attaching gases, the frequency of attachment is of order 10^6 to 10^8 times the pressure [1], [36], [50], [52].

Recovery of a duplexing tube at the end of the dis-

charge period requires the electron concentration in the interaction space to fall rapidly to a negligible value. The selection of working pressure below 100 mm Hg means that loss of electrons by diffusion to the walls of the container is slow [83]. If, however, short diffusion paths and adequate clearances are provided, surface recombination enables recovery times of 30–50 μ sec to be achieved with pure rare gas fillings. Solid inserts packed around the electrodes or interaction space form a suitable recovery agent, provided the material is of low permittivity and dielectric loss and is capable of withstanding high temperature. Quartz crystals, hard-glass fragments and hollow ceramic beads are easy to handle and pack while permitting the insertion of pretuning plungers. Rapid deionization is also achieved with quartz wool which, consisting of very fine fibres, has a large surface per volume ratio. This material is only convenient for simple shapes since, unless it is carefully packed, voids occur which result in increased diffusion time.

Quenching of the discharge by electron attachment is an efficient process if enhanced by the introduction, in element or compound form, of hydrogen, oxygen, nitrogen and the halogens. Experiments [125] with powers up to 200 kw in the range 3–35 gc have shown, for example, that, with an initial filling of argon at 11 mm Hg, the inclusion of hydrogen at a partial pressure of 1 mm Hg reduced the recovery time from 200 μ sec to 4 μ sec. Although effective as a quenching agent, hydrogen cleans up rather quickly: this disadvantage may be overcome by arranging a continuous supply from, for example, a replenisher such as titanium hydride.

Recovery times as short as one microsecond are achieved by the addition of water vapor which has a very large recombination coefficient but also some attendant disadvantages. The products of dissociation migrate in any dc field present towards the metallic electrodes with which they react chemically [57]. The dominant surface reaction results [13] in the formation of nonconducting oxides. Such a film on the cathode greatly facilitates [68] glow-to-arc transitions which tend to occur [32] in bursts of 10–20 with intervals between bursts of 5–60 minutes. In certain circumstances the chemical reactions lead to the formation of a conducting oxide which continues until short circuiting of the primer gap occurs.

These chemical reactions lead, as may be expected, to a gradual clean-up of water vapor. Long life may be attained by giving the tube a higher partial pressure of water vapor than is initially necessary but this process leads to worsening of other parameters such as arc loss and leakage energy. Water vapor replenishers maintain a sensibly-constant partial pressure and thus increase the working life. A typical replenisher consists [27] of carefully cleaned pure iron filaments on which 0.2 per cent by weight of water vapor has been absorbed. When placed in the tube envelope the partial pressure remains near 0.2 mm Hg over the temperature range -20°C to $+120^\circ\text{C}$ for a long period.

III. EXTERNALLY-EXCITED TUBES

A. Phase Change

If a gaseous discharge completely fills a waveguide the propagation coefficient

$$\gamma = \alpha + j\beta \quad (6)$$

has components given by [92]

$$2\alpha^2 = \left| \frac{\omega^2}{c^2} (\epsilon - 1) - \left(\frac{2\pi}{\lambda_g} \right)^2 + j\omega\mu_0\sigma \right| + \left\{ \frac{\omega^2}{c^2} (\epsilon - 1) - \left(\frac{2\pi}{\lambda_g} \right)^2 \right\} \quad (7)$$

$$2\beta^2 = \left| \frac{\omega^2}{c^2} (\epsilon - 1) - \left(\frac{2\pi}{\lambda_g} \right)^2 + j\omega\mu_0\sigma \right| - \left\{ \frac{\omega^2}{c^2} (\epsilon - 1) - \left(\frac{2\pi}{\lambda_g} \right)^2 \right\}. \quad (8)$$

If $\nu_e \ll \omega$ so that

$$\sigma = 0; \epsilon - 1 = -\omega_p^2/\omega^2 \quad (9)$$

and, further, if

$$\omega_p^2/c^2 < (2\pi/\lambda_g)^2 \quad (10)$$

then

$$\alpha = 0; \beta = \left[\left(\frac{2\pi}{\lambda_g} \right)^2 - \frac{\omega_p^2}{c^2} \right]^{1/2}. \quad (11)$$

The change in phase coefficient due to the discharge is given by

$$\Delta = \frac{2\pi}{\lambda_g} - \left[\left(\frac{2\pi}{\lambda_g} \right)^2 - \frac{\omega_p^2}{c^2} \right]^{1/2} \simeq (\omega_p^2/c^2)(\lambda_g/4\pi). \quad (12)$$

If $\Delta \ll (4\pi/\lambda_g)$ the ratio (Δ/λ_g) should be independent of frequency for constant electron density. If

$$\omega_p^2/c^2 \gg (2\pi/\lambda_g)^2 \quad (13)$$

then $\beta=0$ and the waveguide is cut off.

These effects have been put to practical use [97] in the phase changer shown in Fig. 7(a). Interaction takes place between the RF field and the negative glow surrounding two filamentary cathodes: these are spaced $\frac{1}{4}\lambda_g$ apart axially to improve impedance matching. The device, when filled with krypton to a pressure of 1 mm Hg, gave, at 9.55 gc, the values of potential drop and phase change vs discharge current shown in Fig. 7(b). The phase change was independent of the microwave input level up to 100 mw. For the discharge length of 8.4 cm and a phase change of 180° , (12) requires an electron density about 0.45 the cutoff value. Such calculations are confirmed by the attenuation values shown in Fig. 7(b): these are quite low until the condition of waveguide cutoff is approached. This particular microwave arrangement is broad-band and achieved satisfactory performance over the range 8.9–10.2 gc: the life of the tube was 500 hours with a discharge current of 6 ma.

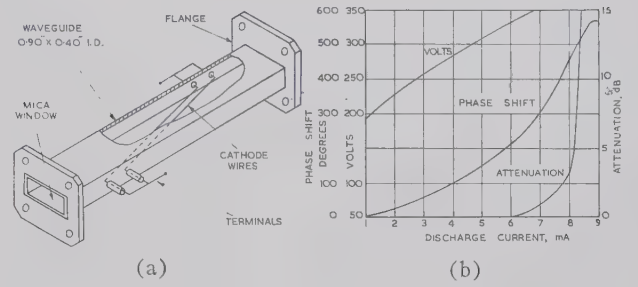


Fig. 7—Gas-discharge phase-change tube. (a) General arrangement. (b) Properties at a frequency of 9.55 gc.

If a magnetic field is applied orthogonal to the RF electric field, the electrons acquire a helical motion with angular frequency

$$\omega_c = eB_0/m. \quad (14)$$

As the magnetic field is varied through this resonance value the breakdown voltage exhibits a sharp dip [14], [30], [70], [71], [89], [120]. As an example of use in duplexers, a switch tube based on this property has shown [116] a discrimination of 60 db with an arc loss of 0.4 db: the input power was 250 kw peak at 2.85 gc and the low-level insertion loss was 0.1 db. Another switch [117] is controlled by the turning on and off of a magnet field set at the resonance value. The breakdown power varies with gas pressure and, for example, at 2.84 gc with argon, the values with and without the applied field are respectively 0.01 kw and 1 kw for 0.3 mm. Hg and 0.03 kw and 60 kw for 0.03 mm Hg. The firing time is of the order of $0.01 \mu\text{sec}$. The non-reciprocal properties [10], [23], [39], [42], [44], [48], [86] of magnetized discharges have, however, not found much application in passive duplexers since they appear [98] to be inferior to ferrites in respect to manufacturing cost, response time, power handling capacity, noise output and life.

B. Attenuators

Gaseous discharges can form the basis of variable attenuators but have the disadvantage of an associated noise power equivalent to a temperature of up to $10,000^\circ\text{K}$. In one distributed structure [56] for 9.5 gc, the central conductor of a coaxial line is a heated oxide cathode. The attenuation, although large, is rather dependent on cathode temperature: for this reason, cold cathode tubes are preferable. A mixture of hydrogen with the rare gas quickens the response and reduces the discharge current for a given attenuation. Another design for the same frequency consists [12] of an oxide cathode, 2 inches long and 0.02-inch diameter, mounted in a 0.9 inch by 0.4-inch waveguide. Krypton at 2-mm Hg is a suitable filling but the attenuation showed a sharp peak at a cathode temperature corresponding to a glow-to-arc transition. In a version for 50 gc, the discharge is made between the two broad walls of the waveguide, these being insulated from the rest of the structure: an attenuation of 30 db can be achieved with a discharge current of 10 ma.

An attenuator [99] employing a resonant structure has already been shown in Fig. 6(a): it has a Q -factor of 295 and is tuneable over the range 8.9–9.5 gc. The control electrode is glass sheathed so that only the 0.028-inch diameter magnesium tip is exposed. With a filling of krypton at 10 mm Hg and about 80 volts between the electrodes, the attenuations at currents of 100 μ a and 200 μ a were 15 db and 30 db respectively for an RF input of 50 μ w. The attenuation is sensitive to the level of incident power, falling by a factor of 4 when the latter was increased from 3 mw to 100 mw. A two-gap broadband structure enables similar attenuations, with an input VSWR of 1.2, to be maintained over a frequency band of 650 mc.

C. Pulsed Switches

When the ionization in an attenuator is so intense that large reflection and loss occur, the device more closely resembles a switch: its use is normally confined to pulse operation with low duty cycles. In one novel switch [40] the positive column of a gaseous discharge formed part of the inner conductor of a coaxial line. In the absence of the discharge, the outer conductor is too small to sustain waveguide propagation and no power passes. This principle has been used [51] to provide a wide-band multiway switch of low insertion loss. The noise inherent in the required dense discharge was kept small by pulse operation, the gas and tube conditions being such that the recovery time is of the order of one millisecond; dc gaseous discharges have also formed the basis of waveguide [118] and cavity [80], [112] switches. For example, the negative-glow CV2379 tube yields [28] more than 20 db attenuation for 0.5-watt excitation power. The recovery time is 12–20 μ sec and passive protection is afforded against unsynchronized pulses by virtue of its steady "simmering" electrode current of 50 μ a. The life exceeds 1500 hours.

The disadvantages of internal electrodes may be avoided by employing HF excitation of the discharge. One such tube, shown in Fig. 8(a), consists [76] of a 5-mm internal-diameter precision quartz tube. An insert, ground to a dumbbell shape, is sealed off to contain air at atmospheric pressure and the intervening space filled by xenon at 60 mm Hg with a small amount of tritium. Ionization is achieved by applying a 30 mc voltage between the waveguide and an excitation electrode shown in Fig. 8(b). Two tubes may be fed from a high-output impedance push-pull oscillator whose output is about 200 watts peak. The complete switch, with each tube forming a low Q -factor resonant element, is shown in Fig. 8(c). It provides a pulsed attenuation of at least 50 db with a recovery time less than 30 μ sec: the VSWR is better than 1.15 over a 10 per cent frequency band and the insertion loss is below 0.1 db. For operation at 10 gc the insert may be omitted while at 35 gc the tube forms a distributed structure along the waveguide, the excitation electrodes being placed at both ends.

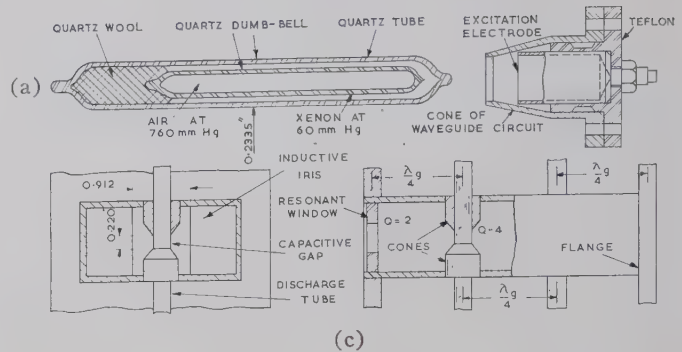


Fig. 8—Pulsed attenuator with HF excited discharge. (a) Discharge tube. (b) Excitation system. (c) Two views of the assembly for 3 gc.

IV. SELF-EXCITED TUBES

A. Single-Function Switches

Self-excited tubes operate by differences in the levels of the incident microwave energy. They require high electric fields which are usually the result of short pulses with fast rise times and thus their design tends to be empirical. Such tubes generally employ resonant structures and may be broadly divided into single- and multiple-function classes.

A simple gas switch consists of a resonant iris in a waveguide. At low power levels, energy is allowed to pass with only small reflection but, at high power levels, the electron density in the discharge results in a large reflection of the incident power with corresponding large attenuation of the transmitted power. Such a discharge element is rarely used by itself but forms the basis of more complicated tubes. For example, in the ATR (or TB) tube shown in Fig. 9(a), the iris is terminated on one side by a short-circuited $\frac{1}{4} \lambda_g$ line. The device thus behaves, at the input window, as an open circuit in the low-level condition and a short circuit under power breakdown. The cavity dimensions and window susceptance are chosen to give the maximum impedance under low-level operation. Technical data on a few typical ATR tubes are given in Table I. The 1B36 and VX8104 tubes are of circular section and are provided with a machined bevel for contact with the main waveguide: these tubes also include a deformable diaphragm as the short circuit, thus permitting a small amount of preset tuning during manufacture. ATR tubes are usually filled with argon to about 10 mm Hg, no recovery or priming agents being found necessary.

The desirable characteristics of a pre-TR tube include large reflection and small arc loss when ionized, short recovery time, low insertion loss and ability to withstand high incident powers. Spike leakage is not important and thus keep-alives are not provided. An early example, the 1B38 for 2.8 gc, consisted [109] of two resonant discharge gaps spaced $\frac{1}{2} \lambda_g$ apart. Recent tubes [105] for 1.2 gc based on this design incorporate window of ceramic sheet or gas filled quartz containers.

Plug-in tubes have advantages of simplicity, bandwidth and long life. They are finding increasing applica-

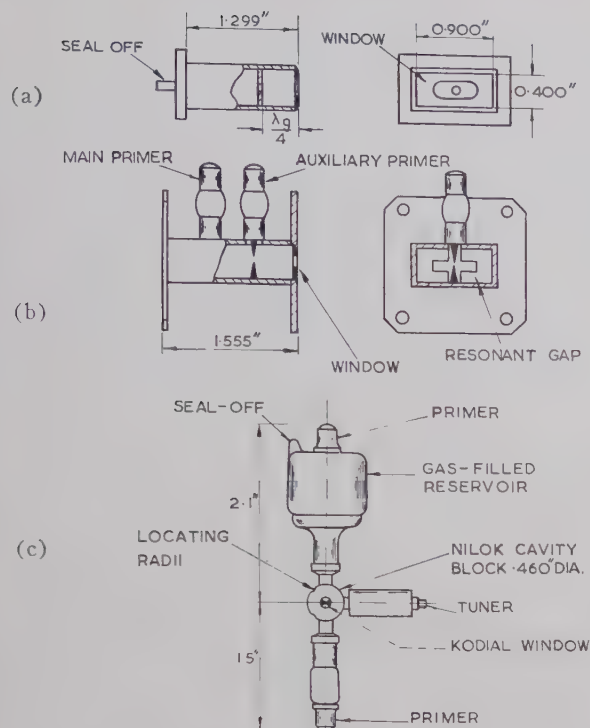


Fig. 9—Typical duplexing tubes. (a) CV2308 ATR tube for 9.5 gc. (b) CV2311 broadband TR tube for 9.5 gc. (c) CV2300 tunable TR tube for 35 gc.

TABLE I
TYPICAL ATR TUBES

Type number	1B44	CV2308	1B36	VX8104
Frequency, gc	2.6–3.1	9.0–9.6	23–25	34–36
Loaded window Q -factor	5.5	6.5	7.5	7.5
Breakdown power, kw	10	4	2	2
Arc loss, db	0.5	0.5	0.5	0.5
Maximum power, kw	—	100	—	50

tion and Table II gives technical data on typical examples. The CV2339 and CV2430 are designed so that the component parts can be assembled by high temperature brazing or cold welding, both methods allowing the tubes to be baked at 450°C during pumping to eliminate gaseous impurities. Choked mounts are required with plug-in tubes since the discharge tends to behave as the inner conductor of a coaxial line with consequent leakage of energy by radiation. The CV2482 is an argon filled quartz tube [94] ground to the correct size to match a 0.9-inch \times 0.4-inch waveguide over the band 8–12 gc: operation down to 3 gc is possible in an iris-matched mount.

Passive-protection tubes are associated with low leakage during the transmitting pulse and, in the receiving period, protection from unsynchronized pulses with low noise generation. The properties of typical tubes are given in Table III, the low leakage values being achieved by fitting keep-alives. In the VX3262 plug-in

TABLE II
TYPICAL PLUG-IN PRE-TR TUBES

Type number	CV2339	CV2430	CV2482	VX1023
Frequency, gc	2.5–4.0	2.5–4.0	8–12	34.36
Loaded gap Q -factor	1.2	1.0	matched	matched
Breakdown power, kw	4	1	15	8
Insertion loss, db	0.05	0.07	0.1	—
Arc loss, db	0.15	0.4	0.2	—
Recovery agent	steatite	water vapor	quartz wool	high pressure
Recovery time, μ sec	30	5	5	4
Spike, ergs/pulse	1500	1000	150	2000
Flat, watts	100	100	180	—
Maximum power, mw	1.5	0.5	0.5	0.1

TABLE III
TYPICAL PASSIVE-PROTECTION TUBES

Type	VX3262	CV2359
Frequency, gc	2.5–3.0	8.9–9.6
Construction	plug-in	two-gap
Loaded gap Q -factor	5.3	4
Breakdown power, mw	70	100
Insertion loss, db	0.10	1.0
Recovery agent	water vapor	none
Recovery time, μ sec	5	40
Interaction loss, db	0.05	0.1
Spike, ergs/pulse	0.15	0.1
Flat, mw	5	5
Maximum power, watts	3	10,000

tube, the depreciation of receiver noise factor is maintained [28] less than 0.02 db by enclosing the keep-alive discharge as much as possible. A two-gap broadband design is used [75] for the CV2359. A weak keep-alive discharge is maintained from a side electrode and the filling is argon at 20 mm Hg. The recovery time varies from 12 μ sec at 10 watts input to 100 μ sec at 100 kw. At low levels the VSWR is better than 1.17 over a 5 per cent bandwidth while the life exceeds 10,000 h.

B. Multiple-Function Switches

1) *Tube Arrangement*: It is possible and has, in fact, long been common practice to combine, in a single unit, the functions performed by several tubes. Such a TR tube [107], [109] must possess, with high incident powers small arc loss, low spike and flat leakages and short recovery time coupled with, in the receiving condition, low insertion loss and protection against unsynchronized pulses.

At frequencies around 3–10 gc fixed tuned broadband structures are in general use. One example, the CV2311, is shown in Fig. 9(b): brief technical data for this and other TR tubes are given in Table IV. Breakdown occurs first at the cone containing the keep-alive electrode with incident powers less than one watt but until the input window breaks down, the equivalent short circuit is $\frac{1}{4}\lambda_g$ from the required position. Short recovery time in the TR tubes is ensured by partial filling with water vapor. Other broadband TR tubes include the CV2312 for 8.5–9.3 gc, the 1B63A for 8.5–9.5 gc and the three-gap 1B58A as listed.

TABLE IV
TYPICAL TR TUBES

Type	1B58A	CV2429	CV2311	1B26	CV2330
Frequency, gc	2.6–3.1	2.5–4.0	9.2–10.0	23.4–24.6	34–36
Construction	3-gap	plug-in	2-gap	tuneable	tuneable
Loaded gap Q -factor	5.5	4	—	220	150
Breakdown power, watts	10,000 (window)	0.15 (gap)	4000 (window)	—	—
Insertion loss, db	0.3	0.15	0.5	0.8	1.0
Recovery time, μ sec	12	7	4	4	2
Keep-alive type	side-arm	co-axial	double	co-axial	double
Spike, ergs/pulse	0.2	0.2	0.2	0.03	0.03
Flat, mw	40	20	30	20	20
Maximum power, kw	—	0.3	250		

Tuneable-cavity tubes, such as the cell type 1B27 for 3 gc and integral-type CV221 and 1B24 for 9 gc, now find only limited application. This design does, however, lend itself to very wideband operation by means of windows of extremely low Q -factor. The troubles attendant upon a large glass area are overcome by using a window consisting of two or three parallel slots. A tube of the latter design, with a window Q -factor of 0.25, possesses [105] a total bandwidth of 40 per cent centered on 1.2 gc. The tuneable TR tube is, moreover, not so critical as regards tolerances on, for example, the position of the keep-alive electrode and hence continues to find use at the higher frequencies. Two examples have been given in Table IV, the CV2330 for 35 gc being illustrated in Fig. 9(c).

The CV2429, illustrated in Fig. 10, is a plug-in TR tube which allows operation, by choice of mount dimensions, at frequencies near 3 gc, in bandwidth steps of 6–10 per cent. In the CV2378 the keep-alive, and hence the water vapor replenisher, is omitted. The breakdown is much higher, with a spike of 10 ergs/pulse and a flat of 20 watts, but the tube is suitable as the first of a pair in a TR combination. The recovery time,

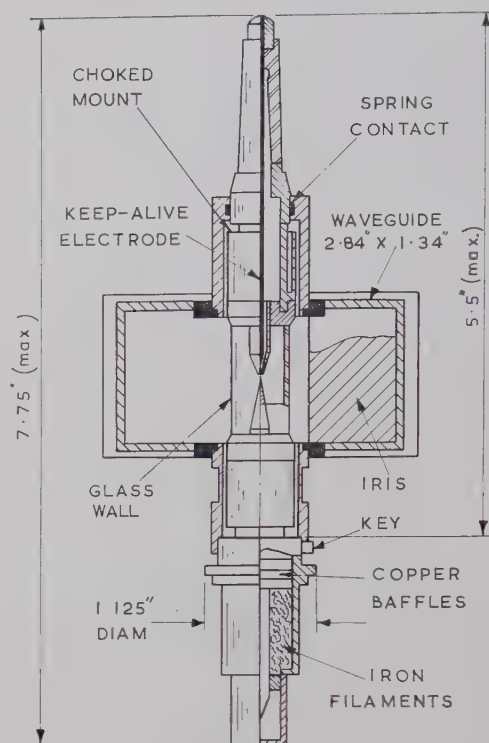


Fig. 10—Plug-in CV2429 TR tube. Frequency 3 gc. A keep-alive and water-vapor replenisher are provided.

being a function of the incident power, is often short enough for the second tube of the pair to fulfill a given requirement when a pure rare gas filling is used.

2) *Performance Control*: It will have been realized that the TR tube, containing both water vapor and a keep-alive, achieves its multiple functions only with a reduction in life. Investigations have thus been made with the view to improving this factor by an understanding of the discharge mechanisms involved. For example, direct observation of the spike by means of a high-speed oscilloscope reveals [24] the dependence of the operation of a tuneable 1B24 tube on various parameters. Fig. 11(a) shows that the spike amplitude is independent of incident power in the range 135 watts to 2.56 kw. The tube was filled with hydrogen and water vapor, both at 15 mm Hg. The spike is also constant as the keep-alive current is reduced from 100 μ a to 9 μ a but, at zero current, it rose to a maximum of 64 watts^{1/2} before switching action was effected. The spike is sensitive to gas pressure and Fig. 11(b) shows that, with xenon, the minimum occurs at 6.2 mm Hg; with argon, it is 14.8 mm Hg and with helium, above 40 mm Hg. The breakdown power is seen from Fig. 11(c) to have a minimum at a pressure characteristic to each gas. In the case of helium the results agree well with theory [101].

Keep-alive characteristics may be studied with the aid of Fig. 12(a) which shows how the spike falls [47] with increase of initial ionization, measured in arbitrary units of light emission. Random fluctuations of electron density after about 100 h operation, due to wander of

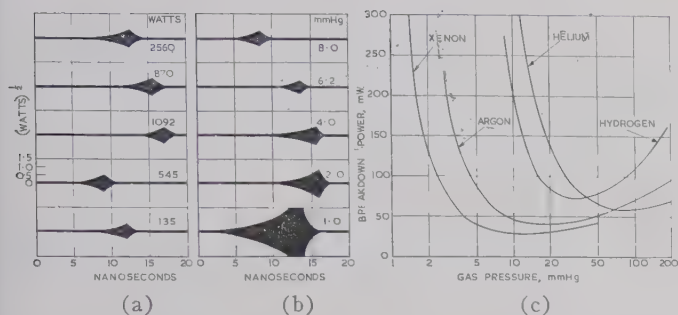


Fig. 11—Breakdown performance of a TR tube. Frequency is 9.375 gc with 1B24 tube. (a) Effect of incident power. (b) Effect of gas pressure. (c) Breakdown power vs gas pressure.

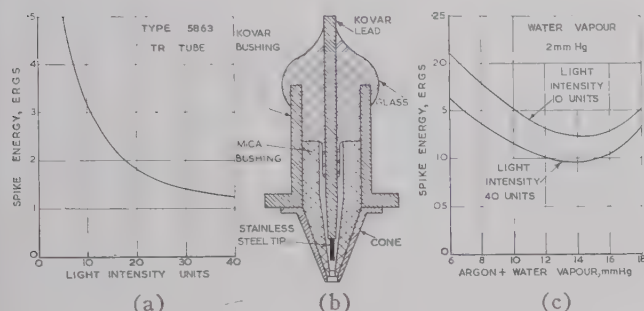


Fig. 12—Performance of TR tube keep-alive. (a) Leakage vs electron density. (b) Improved keep-alive electrode. (c) Leakage vs total pressure.

the discharge, are avoided by fitting, as shown in Fig. 12(b), a bushing made of quartz, sapphire or mica. Fig. 12(c) shows that the spike is now less sensitive to electron density, and, in fact, such tubes can operate at 200 kw peak input for periods exceeding 1000 h. An alternative approach [13] to this problem depends upon the greatly-reduced probability of coincidence between these extinction periods and the arrival of a transmitter pulse by the use of two independent primers. Such TR tubes have been shown in Fig. 9 and experience confirms that the chance of failure, even once in, say, the 10^9 pulses involved in a typical 500-h run is substantially eliminated.

In a broadband TR tube, the arc loss and recovery time are controlled predominantly by the gas characteristics and physical conditions in the vicinity of the input window where the electron density is high. On the other hand, spike and, to a first approximation, flat leakage are determined by the characteristics near the resonant gaps. The conditions for optimizing these two groups of parameters can be independently ensured by isolation of the corresponding regions of the tube. This is confirmed [46] by experiments made on a demountable three-gap TR tube in which the window was encapsulated so that the appropriate gas filling was confined in an envelope separate and distinct from that in the main body. The incident power was at 2.8 gc in 350-kw pulses of one-microsecond duration at 1000 gc. With an argon filling, and a body pressure of 5.8 mm Hg, the spike- and flat-leakage-energies remained constant at 0.3

erg/pulse and 7 mw respectively for window pressures up to at least 40 mm Hg. The recovery time, on the other hand, varied with pressure, being 160 μ sec and 40 μ sec at 6 mm Hg and 40 mm Hg respectively. This independence of characteristics is maintained on inclusion of quartz wool or water vapor recovery agents, making such a technique a practical, if complicated, approach to improved TR tubes performance at the lower frequencies.

V. DISCHARGE-TUBE DUPLEXERS

A. Branched Guide

A conventional branched-guide discharge-tube duplexer is shown in Fig. 13, two gas switches being connected in *E*-plane stubs from the main transmission line. The window of the ATR tube is nearly flush with the inner wall while that of the TR tube is about $\frac{1}{4}\lambda_g$ away. On transmission, both windows break down, and the power proceeds to the antenna. In the low level condition the quiescent ATR tube presents a high admittance across the main line at a plane *A* such that antenna power proceeds through the TR tube and into the receiver. At powers exceeding 50 kw at 10 gc and 100 kw at 3 gc the life of the TR tube can be prolonged by the use of a pre-TR tube suitably positioned in the stub. Branched duplexers can have any combination of series or shunt stubs and may be designed [109] for two-channel working.

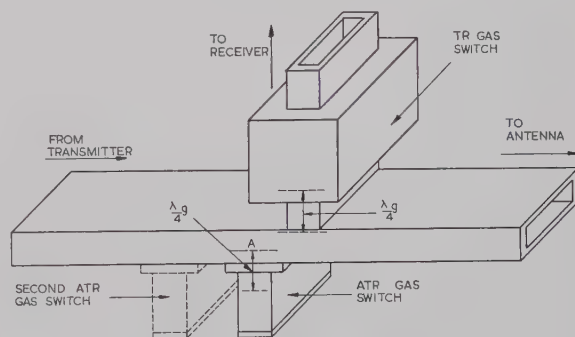


Fig. 13—Branched gaseous-discharge duplexer.

For efficient operation of, for example, a series-junction duplexer, Z_t , the impedance of the cold transmitting tube transformed along the line and combined with that of the ATR tube, should be zero. For any other value, there is a branching loss factor given by

$$L = 1 + \frac{1}{2}Z_t. \quad (15)$$

If, over the working frequency band, the impedance of the cold transmitting tube, or of the ATR tube during its recovery period, causes Z_t to fall outside acceptable limits then two or more ATR tubes may be employed. The exact distance between the ATR tubes depends [109] on the bandwidth required, the position of the TR tube and on whether or not the ATR tubes are stagger tuned.

The power handling capacity of the normal branched duplexer is limited by available tubes to about 300 kw at 9.5 gc and 1 mw at 3 gc. Higher capacity may be achieved in duplexers based on full transfer directional couplers. Energy flowing along the main line from the antenna is H -coupled to the auxiliary guide, and thence to the receiver, by a window aperture. Under high power conditions, the window breaks down and energy proceeds from the transmitter along the main line to the antenna. For the frequency band, 8.6–9.5 gc, the low-pressure gas filling may be [64] in the auxiliary guide or, alternatively, in the intervening space of a double walled window. The latter gave an insertion loss of 0.5 db, spike of 0.1 erg/pulse, flat of 20 mw and a recovery time of 6 μ sec. In the "curtain" full-transfer duplexer [88] about 20 quartz gas tubes are spaced 1 cm apart along the aperture coupling the 2.84-inch by 1.34-inch waveguides. Over the band 2.6–3.1 gc the insertion loss is 0.3 db, recovery time 50 μ sec and maximum power 23 mw peak, 16 kw mean.

The discharge tube in a duplexer protects the receiver from random external pulses only when the keep-alive is working. Under stand-by conditions of the equipment, protection can be afforded by mechanical switches or shutters. These may take the form of a spring-actuated vane which closes the waveguide aperture but which can be pulled out by a solenoid during normal operation. Short-circuiting posts have been built [105] into broadband TR tubes: while giving 40-db protection for one post and 70 db for two, the over-all cost of the tube is increased thereby.

B. Balanced Circuit

The arrangement of a balanced duplexer depends upon the type of gas switch and hybrid junction adopted. Fig. 14(a) shows two hybrid rings or tees and two broadband discharge tubes. The transmitter in arm T feeds the output arms of the hybrid in antiphase and, due to the $\frac{1}{4}\lambda_g$ separation of the gas switches, the reflections arrive back in phase so that the energy proceeds via arm A to the antenna. The leakage powers proceed via arm L to the dummy load while signals from the antenna proceed via arm R to the receiver. Alternative configurations employing 3-db directional couplers, either alone or with other hybrids, are shown in Figs. 14(b) and (c). Balanced duplexers must be followed by a passive-protection tube to safeguard the receiver against random pulses.

Good discrimination in balanced duplexers is obtained only if the phase changes through, and the spike and flat leakages of, the TR tubes are equal throughout the duration of the transmitter pulse. This condition is facilitated by the use of 3-db slot hybrids since, as shown in Fig. 15(a), both switches can then be placed [58] in one gas container. Such dual TR tubes have been made [105] for 3 gc, 5 gc and 9 gc and provide a cancellation of the spike of 4–6 db and of the flat, 6–10 db. Duplexers containing, for example, WF46 or BL-27

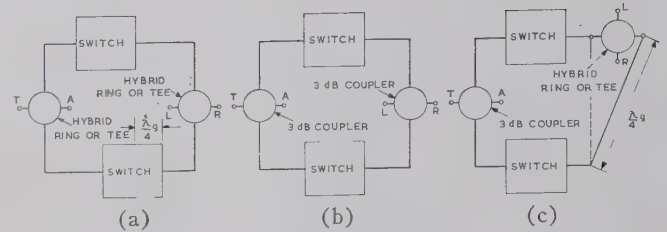


Fig. 14—Types of balanced duplexer configurations. (a) Two hybrid rings or Tees. (b) Two 3-db directional couplers. (c) One 3-db coupler plus one ring or Tee.

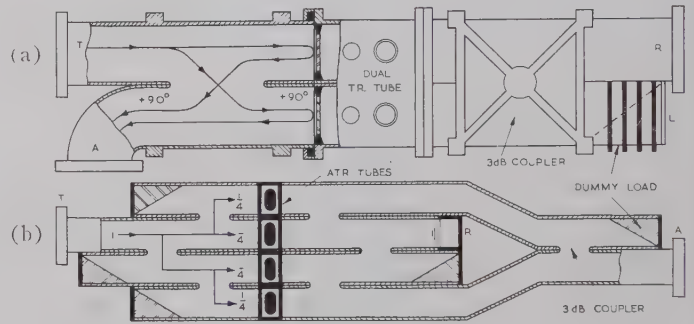


Fig. 15—Balanced duplexers with gas switches. (a) Dual TR type with 3-db couplers. (b) ATR type with power divided by four.

dual TR tubes give an isolation of 20 db, VSWR of 1.2, insertion loss of 0.8 db and an over-all spike of 0.01 erg/pulse in the range 8.5–10.0 gc.

Provided the receiver arm is fitted with a TR tube, balanced duplexers can employ pre-TR tubes with consequent increase in bandwidth and power-handling capacity. Two CV2339 tubes in a balanced circuit can handle [28] 2.5 mw peak, 3.5 kw mean at 3 gc. In a "curtain" arrangement [88] of the slot-hybrid duplexer, a number of quartz switch tubes placed in each of the coupling apertures give a good power and bandwidth performance.

Balanced duplexers may employ ATR tubes and the arrangement with two hybrid tees is rather like that of Fig. 5. For broadband performance, arrays of up to four tubes can be used [67] with advantage. The principle of power division can be extended and Fig. 15(b) shows an ATR duplexer in which the division is by a factor of 4. Such a duplexer for 2.6–3.1 gc, employing 1B44 ATR tubes with a 1B58A TR tube in the receiver arm, has given [88] satisfactory performance with powers up to 5 mw peak, 4 kw mean.

Circularly-polarized waves are employed in the balanced duplexer of Fig. 16. The input at T from the transmitter excites, via the transducer, a plane TE_{11} wave in the circular guide which is converted, by the quarter-wave plate, to circular polarization. The usual two gas switches are here combined into a single non-polarized tube which reflects the incident wave with the opposite hand of circular polarization. After retraversing the quarter-wave plate, the energy emerges from arm A and proceeds to the antenna. Leakage power from the switch proceeds to the output circuit, in this case a turnstile, and thence into the dummy load L .

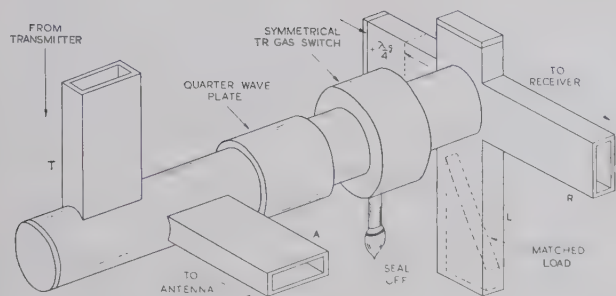


Fig. 16—Balanced duplexer using circular polarization. A quarter-wave plate is at the transmitter end and a turnstile at the receiver end.

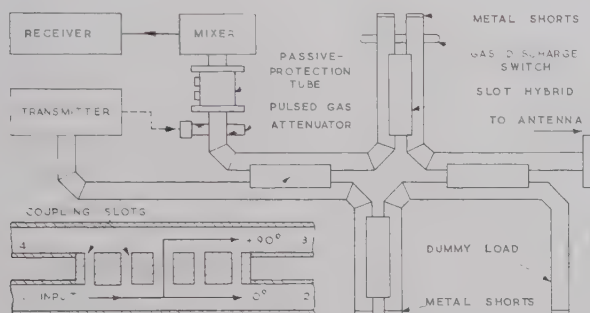


Fig. 17—Phase-change duplexer with slot hybrids. Frequency is 8.5–10.0 gc.

In the low-level condition the gas switch is transparent and signals proceed from the antenna to the receiver via arms *A* and *R*.

The polarization-twist duplexer, as its name implies, consists of a circular guide, supporting a TE_{11} mode, in which an array of, say, 20 discharge tubes provides a mechanism for rotating by 90° the plane of polarization of the transmitted wave. Suitable ports are arranged for connection to the transmitter, antenna, receiver and a dummy load. A simple krypton-filled tube, with quartz chips as the recovery agent, the CV2285, has been so employed by J. R. Thomas in unpublished work. Further protection is given by including [28], in the receiver arm, such TR tubes as the CV2378 and CV2429. The resulting duplexer is very successful as regards life and reliability in operation.

C. Individual Function

A major advance in reliability and performance has been achieved [28], [55] by evolving systems in which each duplexing function is performed by a separate tube designed specifically for that task. The duplexer can be branched or balanced and externally- and/or internally-excited tubes may be employed singly or in any combination. For example, if electrodes are placed [98] in the gas filled auxiliary guide of a full transfer directional coupler, the discharge can be made intense enough to cause cutoff. This means that the power flows uninterrupted along the main guide. Thus if an external prepulse of suitable amplitude is applied, power can be switched, during the period of transmission, from the

auxiliary to the main arm and back again. Other duplexing tubes may be added to give increased protection to the receiver.

In typical arrangements [28] for a branched-guide duplexer, the single TR tube is replaced by any of the following combinations:

- 1) Pre-TR tube, followed by a prepulsed attenuator and a passive-protection tube.
- 2) Pre-TR tube, followed by an unprimed TR and a passive-protection tube.
- 3) Pre-TR tube, followed by an unprimed TR, prepulsed attenuator and a passive-protection tube.

A duplexer [54] for 9.5 gc based on scheme 1) employed a quartz-tube pre-TR switch [94], a prepulsed gas attenuator and a CV2359 passive-protection tube, the resultant leakage being less than 0.01 erg/pulse. An assembly for 3 gc, based on scheme 3), was made up from a CV2339, CV2378, CV2379 and VX3262 in that order: the transmitter power was 2.5 mw peak, 3.5 kw mean. At low levels, the total insertion loss was 0.5 db with a VSWR better than 1.2 over an 8 per cent bandwidth. At high levels, the spike with the CV2379 unpulsed was 0.15 erg and pulsed, 0.01 erg; the over-all recovery time was about 40 μ sec.

Balanced duplexers using any of the configurations of Fig. 14 can be modified [28] by replacing each of the switches by a pre-TR/unprimed TR combination and inserting, in the receiver arm, a prepulsed attenuator followed by a passive-protection tube. The balanced duplexer of Fig. 17 employs [77] two power-sensitive phase-changers: each of these comprises a pair of 3-db directional couplers which, as the inset shows, divides incident power in arm 1 equally between arms 2 and 3 with phase changes of 0° and 90° respectively. One of the phase changers is provided with a CV2482 pre-TR tube placed $\frac{1}{4} \lambda_0$ in front of its short circuit. The electronic length of the phase changer is hence $\frac{1}{2} \lambda_0$ less for high-power signals than for low-power. Thus power proceeds from the transmitter to the antenna and from the antenna to the receiver. The VSWR in either condition is better than 1.2, and the isolation better than 25 db, over the band 8.5–10.0 gc: the power-handling capacity is about 800 kw peak, 400 watts mean. The duplexer is completed by a pulsed attenuator and a CV2359 passive-protection tube placed in the receiver arm. In a life test of such a duplexer, only six receiver diodes failed in a total period of 36,855 h.

VI. METHODS OF MEASUREMENT

A. Attenuation and Impedance

Measurement of the performance of both complete duplexers and the individual parts is required in the process of development and as a control during manufacture. The methods described relate specifically to gaseous-discharge duplexers but they may be applied, with modifications, to passive and solid-state designs.

Typical measurements [6], [109] include insertion loss, input VSWR and frequency bandwidth: they must usually be carried out at both high- and low-power levels. The former usually involve extensive life tests and an economy of power by a factor 2^n may be achieved [127] by using a power-multiplication circuit of n -hybrid junctions. In general, the conventional laboratory instruments must be supplemented by specialized equipment.

The arc loss of, for example, a TR tube can be measured by setting it up in a transmission line and comparing the power entering the load with that when the tube is replaced by a short circuit. In experiments at 35 gc, L. Hodgson, in unpublished work, obtained increased accuracy by a bridge method. The gas tube was placed in one arm and a calibrated attenuator in the other. A subsidiary attenuator and phase-changer were adjusted to balance the bridge with a short circuit in the tube mount. On replacing the tube, the necessary change in the calibrated attenuator to restore balance gave a measure of the arc loss. Increased accuracy, especially at high powers when the fractional arc loss becomes small, is obtained by replacing several tubes in line.

Other properties which require measurement include minimum firing power, keep-alive characteristics and leakage due to direct coupling at the fundamental and harmonic frequencies. Transmission measurements on TR tubes should be made with the keep-alive discharge on: in this way both insertion- and interaction-loss are measured. With ATR and pre-TR tubes the position of the equivalent short circuit is important: this is usually determined by bridge methods, the tube being balanced by a moveable short circuit.

B. Leakage

The spike and flat leakages of a gaseous-discharge duplexer may be separately measured by employing the cancellation principle. As shown in Fig. 18(a), the total leakage energy is first measured. Since this averages only a few microwatts, a thermistor, with suitable bridge, is usually employed. A small fraction of the RF energy is coupled out of the transmission line into the output of the duplexer, the amplitude and phase being adjusted to give cancellation of the flat as observed on a fast sweep oscilloscope: this permits the spike energy alone to be measured. In practice [6] the flat leakage is not constant during the pulse and complete cancellation is not achieved. The measured spike will, therefore, be higher than its true value. With short pulses care must be taken to equalize the path lengths traversed by the leakage and cancellation signals.

Another technique [109] employs a high- Q -factor cavity as a filter to discriminate against the energy in the relatively widely spaced sidebands of the spike. In the arrangement of Fig. 18(b) a suitably positioned rejection cavity causes the flat power to pass through the transmission cavity and be measured by a thermistor.

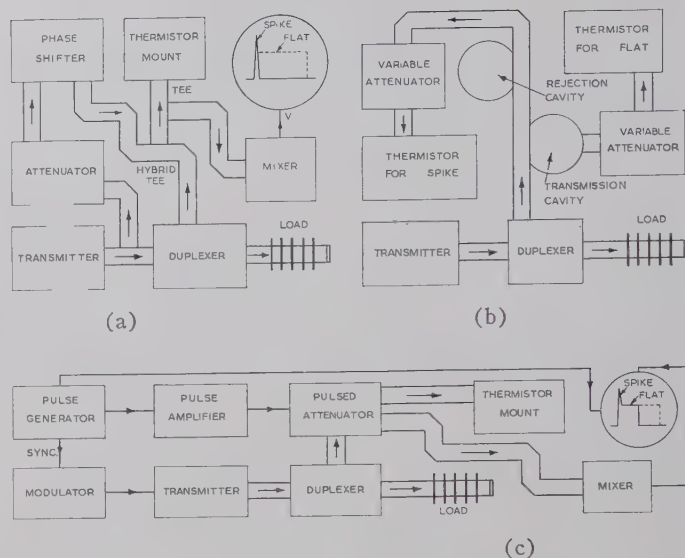


Fig. 18—Methods of measuring duplexer leakage power. (a) Cancellation of flat. (b) Separation of spike and flat by cavities. (c) Variable pulse length.

For Q -factors of, say, 1000 only a negligible portion of the spike energy passes through the cavity: most of it proceeds along the line and enters a second thermistor where it is measured. The cavities must be precisely tuned and corrections made for their small reflection and absorption losses.

Less specialized equipment is required in a further method using transmitter pulses of different durations. Measurement of the total leakage with several pulse durations enables the spike leakage to be determined by extrapolation to zero time. The requirement of a variable pulse-duration modulator is avoided by the use, as shown in Fig. 18(c), of an attenuator to which an excitation pulse can be applied at any chosen time following the spike. The rise in attenuation after pulsing must be rapid and values of 50 db/ μ sec have proved satisfactory. If, for example, the transmitter has a pulse duration of one microsecond, the duration of the measured flat leakage can be varied in 0.1- μ sec intervals by successive reduction in the delay of the pulse generator. Extrapolation then gives, as before, the spike leakage alone.

C. Recovery Time

Measurement of the attenuation of a low-level signal as a function of time after the end of the high-power pulse gives the recovery time of a gaseous-discharge duplexer. In the arrangement shown in Fig. 19 the frequency of the signal generator is set near that of the transmitter and its output fed via a directional coupler into the duplexer. The range of times of occurrence of the probing signal should include an interval preceding the transmitter pulse to provide a reference level. The change in amplitude of the signal displayed on the oscilloscope is determined by a calibrated attenuator.

In a modification of this method, the transmitter is pulsed, for example, only once for every two signal-generator pulses: thus alternate low-level pulses come

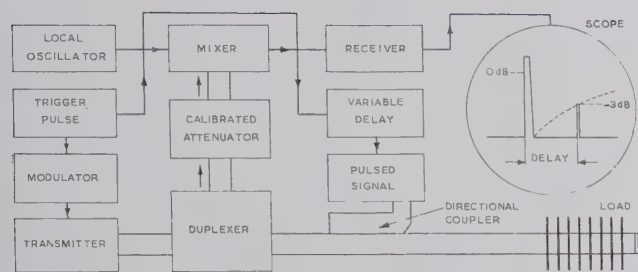


Fig. 19—Arrangement for measuring recovery time. The amplitude of a low-level signal is observed as a function of delay after the transmitter pulse.

through unattenuated. The signal on the oscilloscope shows two superimposed pulses, one unattenuated and the other affected by the recovery time of the tube. The difference in height of the pulses is a measure of the attenuation due to the recovery time. The recovery curve can be made continuously visible on the oscilloscope by arranging for the modulation pulses on the low-level generator to occur at different delay times or, better still, in rapid sequence [102]. Alternatively, by a square-wave modulating the IF amplifier at, say, 2 mc, the display can be made to show [6] a wave of this frequency varying in amplitude according to the recovery law. In all methods transmitter breakthrough must be avoided by using a resonant-cavity or waveguide-bridge filter supplemented by a blanking pulse on the receiver. These techniques are suitable for either low- or high-Q-factor TR tubes and can, with modification, be applied to gas attenuators, pre-TR and other tubes. ATR tubes, for example, can be measured by observing [6] the recovery time of the branching loss or main-line reflection by low-level probing techniques.

VII. ACKNOWLEDGMENT

The author is grateful to T. L. Dutt, F. C. Goddard, P. O. Hawkins, L. Hodgson and D. H. Pringle for helpful comments on the manuscript.

VIII. BIBLIOGRAPHY

- [1] A. J. Ahearn and N. B. Hannay, "The formation of negative ions of sulphur hexafluoride," *J. Chem. Phys.*, vol. 21, p. 119; 1953.
- [2] W. P. Allis and S. C. Brown, "High-frequency electrical breakdown in gases," *Phys. Rev.*, vol. 87, p. 419; 1952.
- [3] W. P. Allis and S. J. Rose, "Transition from free to ambipolar diffusion," *Phys. Rev.*, vol. 93, p. 84; 1954.
- [4] M. A. Armistead, E. G. Spencer, and R. D. Hatcher, "Microwave semiconductor switch," *Proc. IRE*, vol. 44, p. 1875; December, 1956.
- [5] J. N. Barry and W. H. Clarke, "Microwave modulator uses ferrite gyrator," *Electronics*, vol. 28, p. 139; May, 1955.
- [6] R. Belbeoch and M. Bricon, "Measurements on gas-filled (TR and ATR) valves," *Le Vide*, vol. 11, p. 373, 1956; *L'Onde Electrique*, vol. 37, p. 65, 1957.
- [7] M. A. Biondi and S. C. Brown, "Measurements of electron-ion recombination," *Phys. Rev.*, vol. 76, p. 1697; 1949.
- [8] M. A. Biondi, "Concerning the mechanism of electron-ion recombination," *Phys. Rev.*, vol. 83, p. 1078; 1951.
- [9] J. Boissiere and C. Romiguere, "Study of pressures and their evolution in gas-filled tubes," *Le Vide*, vol. 12, p. 117; January, 1957.
- [10] M. Bonnet, M. Matricon and E. Roubine, "Investigation of the Faraday effect in a plasma at 10 kmc/s," *Annales des Telecommunications*, vol. 10, p. 150; 1955.
- [11] S. Boronski, "Some properties and applications of ferrites at 3 cm. wavelength," *Proc. IEE*, vol. 104, pt. B, Suppl. no. 6 p. 331; 1957.
- [12] E. M. Bradley and E. H. Pringle, "The theory and design of gas-discharge microwave attenuators," *J. Brit. IRE*, vol. 15, p. 11; 1955.
- [13] T. J. Bridges, P. O. Hawkins, and D. Walsh, "Keep-alive instabilities in a TR switch," *Proc. IRE*, vol. 44, pp. 535-538; April, 1956.
- [14] A. E. Brown, "The effect of a magnetic force on high-frequency discharge in pure gases," *Phil. Mag.*, vol. 29, p. 302; 1940.
- [15] S. C. Brown, "High-frequency gas-discharge breakdown," *Proc. IRE*, vol. 39, p. 1493; 1951.
- [16] P. N. Butcher, "Theory of three-level paramagnetic masers," *Proc. IEE*, vol. 105, suppl. no. 11, pp. 684, 691, 699 and 705; 1958.
- [17] S. Chapman and T. G. Cowling, "The Mathematical Theory of Non-Uniform Gases," Cambridge University Press, Cambridge, Eng.; 1939.
- [18] F. S. Coale, "A switch-detector circuit," *IRE TRANS. ON MICROWAVE THEORY AND TECHNIQUES*, vol. MTT-3, pp. 59-62; December, 1955.
- [19] J. D. Cobine, "Gaseous Conductors," McGraw-Hill Book Co., Inc., New York, N. Y.; 1941.
- [20] R. S. Cole and W. N. Honeyman, "Two short low-power ferrite duplexers," *Electronic and Radio Engineer*, vol. 35, p. 282; 1958.
- [21] R. Conway, "High-speed magnetic pulsing of ferrites," *J. Appl. Phys.*, vol. 25, p. 678; 1954.
- [22] A. H. Cooke, G. Fertel, and N. L. Harris, "Electronic switches for single-aerial working," *J. IEE*, vol. 93, pt. IIIA, no. 10, p. 1575; 1946.
- [23] F. Diamond, A. Gozzini, and T. Kahan, "Interaction of centimetre waves with a plasma in the presence of a magnetic field," *Comptes Rendus Hebdomadaires des Seances de l'Academie des Sciences (Paris)*, vol. 242, p. 96; 1956.
- [24] A. A. Dougal and L. Goldstein, "The spike in the transmit-receiver (TR) tubes," *IRE TRANS. ON ELECTRONIC DEVICES*, vol. ED-3, pp. 142-148; July, 1956.
- [25] D. W. Downton and R. M. O'Brien, "A method of examining the leakage through duplexing systems," *Services Elec. Res. Lab. Tech. J.*, vol. 7, p. 132; 1957.
- [26] D. W. Downton, "Measurement of clean-up in gas-discharge tubes using radioactive krypton," *Proc. IEE*, vol. 105, pt. B, suppl. no. 10, p. 485; 1958.
- [27] T. L. Dutt and W. I. Moore, "A new type of water-vapour replenisher and its application to a TR switch," *Proc. IEE*, vol. 105, pt. B, suppl. no. 10, p. 492; 1958.
- [28] T. L. Dutt, "Plug-in TR tubes for use in S-band duplexers," *Le Vide*, vol. 12, p. 93; 1957.
- [29] F. B. Fank and G. Wade, "Traveling-wave-tube limiters," *IRE TRANS. ON ELECTRONIC DEVICES*, vol. ED-4, pp. 148-152; April, 1957.
- [30] L. Ferriti and B. Veronèsi, "Influence of a transverse magnetic field on the breakdown voltage of a gas discharge at high frequency," *Il Nuovo Cimento*, vol. 2, p. 639; 1955.
- [31] A. G. Fox, "Notes on microwave ferromagnetics research," *Proc. IEE*, vol. 104, pt. B, suppl. no. 6, p. 371; 1957.
- [32] J. C. French, "Electrode deterioration in transmit-receive tubes," *J. Res. NBS*, vol. 45, pp. 310; 1950.
- [33] R. V. Garver, E. G. Spencer, and R. C. Le Crow, "High-speed microwave switching of semiconductors," *J. Appl. Phys.*, vol. 28, p. 1336; 1957.
- [34] R. V. Garver, E. G. Spencer, and M. A. Harper, "Microwave semiconductor switching techniques," *IRE TRANS. ON MICROWAVE THEORY AND TECHNIQUES*, vol. MTT-6, pp. 378-383; October, 1958.
- [35] R. V. Garver, "High-speed microwave switching of semiconductors—II," *IRE TRANS. ON MICROWAVE THEORY AND TECHNIQUES*, vol. MTT-7, pp. 272-276; April, 1959.
- [36] R. Geballe and M. A. Harrison, "Negative-ion formation in oxygen," *Phys. Rev.*, vol. 85, p. 372; 1952.
- [37] R. H. Geiger and P. E. Dorney, "Coaxial components employing gaseous discharges at microwave frequencies," 1956 IRE NATIONAL CONVENTION RECORD, pt. 5, pp. 193-198.
- [38] R. M. Godfrey, B. L. Humphreys, P. E. V. Allin, and G. Mott, "Application of ferrites at 3.2 cm wavelength," *Proc. IEE*, vol. 104, pt. B, suppl. no. 6, p. 355; 1957.
- [39] L. Goldstein, M. Lampert and J. Heney, "Magnet-optics of an electron gas with guided microwaves," *Phys. Rev.*, vol. 82, p. 956, vol. 83, p. 1255; 1951.
- [40] L. Goldstein and N. L. Cohen, "Behaviour of gas discharge plasma in high-frequency electromagnetic fields," *Electrical Communication*, vol. 28, p. 305; 1951.
- [41] L. Goldstein, "Electrical discharges in gases and modern electronics," in "Advances in Electronics and Electron Physics," Academic Press, New York, N. Y., vol. 7, p. 401; 1955.
- [42] L. Goldstein, "Nonreciprocal electromagnetic wave propagation in ionized gaseous media," *IRE TRANS. ON MICROWAVE THEORY AND TECHNIQUES*, vol. MTT-6, pp. 19-29; January, 1958.

- [43] L. Goldstein and N. L. Cohen, "Radio frequency conductivity of gas-discharge plasmas in the microwave region," *Phys. Rev.*, vol. 73, p. 83; 1948.
- [44] Y. V. Gorokhov, "Observation of gyromagnetic resonance of electrons in a disintegrating plasma," *Radiotekhnika i Elektronika*, vol. 1, p. 794; 1956.
- [45] L. Gould and S. C. Brown, "Microwave determination of the probability of collision of electrons in helium," *Phys. Rev.*, vol. 95, p. 897; 1954.
- [46] L. Gould, E. V. Edwards, and I. Reingold, "A novel approach to microwave duplexer-tube design," *IRE TRANS. ON ELECTRON DEVICES*, vol. ED-4, p. 300; 1957.
- [47] L. Gould, "Improved keep-alive design for T-R tubes," *PROC. IRE*, vol. 45, pp. 530-533; April, 1957.
- [48] A. Gozzini, "Some magneto-optical phenomena connected with the molecular resonance of gases at microwave frequencies," *Journal de Physique et le Radium*, vol. 16, p. 357; 1955.
- [49] H. Gutton, "Dielectric properties of an ionized gas and high-frequency discharge," *Annalen der Physik*, vol. 13, p. 62; 1930.
- [50] H. D. Hagstrum, "Ionization by electron impact in CO, N₂, NO and O₂," *Rev. Mod. Phys.*, vol. 23, p. 185; 1951.
- [51] S. M. Hamburger, "A wide-band multi-way electronic switch," *Proc. I.E.E.*, vol. 105, p. 510; 1958.
- [52] M. A. Harrison and R. Gballe, "Simultaneous measurement of ionization and attachment coefficients," *Phys. Rev.*, vol. 91, p. 1; 1953.
- [53] A. F. Harvey, "Ferrite structures for millimetre wavelengths," *Proc. IEE*, vol. 104, pt. B, suppl. no. 6, p. 346; 1957.
- [54] P. O. Hawkins, "Active microwave duplexing systems," *Proc. IEE*, vol. 105, pt. B, p. 505; 1958.
- [55] P. O. Hawkins, "Recent progress in radar duplexers, with special reference to gas-discharge tubes," *Proc. IEE*, vol. 100, p. 314; 1953.
- [56] P. O. Hawkins and C. C. Costain, "Amplitude modulation of centimetre waves," *Nature*, vol. 164, p. 356; 1949.
- [57] F. E. Haworth, "Electrode reactions in the glow discharge," *J. Appl. Phys.*, vol. 22, p. 606; 1951.
- [58] H. Heins, "Radar duplexer uses dual T.R. tubes," *Electronics*, vol. 27, p. 149; August, 1954.
- [59] M. A. Herlin and S. C. Brown, "Breakdown of a gas at microwave frequencies," *Phys. Rev.*, vol. 74, p. 291; 1948.
- [60] M. A. Herlin and S. C. Brown, "Electrical breakdown of a gas between coaxial cylinder at microwave frequencies," *Phys. Rev.*, vol. 74, p. 910; 1948.
- [61] M. A. Herlin and S. C. Brown, "Microwave breakdown of a gas in a cylindrical cavity of arbitrary length," *Phys. Rev.*, vol. 74, p. 1650; 1948.
- [62] L. G. H. Huxley, "A general formula for the conductivity of a gas containing free electrons," *Proc. Phys. Soc.*, vol. 64, p. 844; 1951.
- [63] R. Jancel and T. Kahan, "Conditions of Discharge in an Electromagnetic Cavity and Progressive Waves in Lorentz-Type Plasmas," *Comptes Rendus Hebdomadaires des Seances de l'Academie des Sciences (Paris)*, vol. 244, p. 2894; 1957.
- [64] R. Jean and D. Reverdin, "The fully-coupled T.R. valve," *Le Vide*, vol. 11, p. 357, 1956; *L'Onde Electrique*, vol. 37, p. 65, 1957; *Annales de Radioelectricite*, vol. 11, p. 165, 1956.
- [65] R. Jean, "Contributions to the study of keep-alive electrodes of TR valves," *Le Vide*, vol. 11, p. 362, 1956; *L'Onde Electrique*, vol. 37, p. 65, 1957.
- [66] R. A. Johnson, B. T. McClure and R. B. Holt, "Electron removal in helium afterglows," *Phys. Rev.*, vol. 80, p. 376; 1950.
- [67] C. W. Jones, "Broad-band balanced duplexers," *IRE TRANS. ON MICROWAVE THEORY AND TECHNIQUES*, vol. MTT-5, pp. 4-12; January, 1957.
- [68] T. Jurriaanse and M. J. Druzvesteyn, "Transition from glow discharge to arc discharge," *Physica*, vol. 3, p. 825; 1935.
- [69] O. Laaff, "Tuneable aerial duplexer," *Fernmelde-technische Zeitschrift*, vol. 7, p. 688; 1954.
- [70] B. Lax, W. P. Allis and S. C. Brown, "The effect of magnetic field on the breakdown of gases at microwave frequencies," *J. Appl. Phys.*, vol. 21, p. 1297; 1950.
- [71] B. Lax and S. C. Brown, "High-frequency breakdown in magnetic fields," *Phys. Rev.*, vol. 76, p. 457; 1949.
- [72] R. C. LeCraw and H. B. Bruns, "Time delay in high-speed ferrite microwave switches," *J. Appl. Phys.*, vol. 26, p. 124; 1955.
- [73] R. C. LeCraw, "High-speed pulsing of ferrites," *J. Appl. Phys.*, vol. 25, p. 678; 1954.
- [74] L. B. Loeb, "Fundamental Processes in Electrical Discharge in Gases," John Wiley and Sons, Inc., New York, N. Y.; 1939.
- [75] P. D. Lomer, "Passive protection cells," *Proc. IEE*, vol. 105, pt. B, suppl. no. 10, p. 508; 1958.
- [76] P. D. Lomer and R. M. O'Brien, "A microwave pulsed attenuator using a R.F. excited discharge," *Proc. IEE*, vol. 105, pt. B, suppl. no. 10, p. 500; 1958.
- [77] P. D. Lomer and R. M. O'Brien, "A new form of high-power microwave duplexer," *IRE TRANS. ON MICROWAVE THEORY AND TECHNIQUES*, vol. MTT-6, pp. 264-267; July, 1958.
- [78] P. D. Lomer, "An experimental study of the reliability of an active duplexing system at X-band," *Services Electronics Res. Lab. Tech. J.*, vol. 7, p. 88; 1957.
- [79] H. A. Lorentz, "The Theory of Electrons," Dover Publications Inc., New York, N. Y.; 1916.
- [80] A. Macleese and J. Ashmead, "The rhumbatron waveguide switch," *J. IEE*, vol. 93, pt. IIIA, no. 4, p. 700; 1946.
- [81] H. Margenau, F. L. McMillan, I. H. Dearnley, C. S. Pearsall, and C. G. Montgomery, "Physical processes in the recovery of TR tubes," *Phys. Rev.*, vol. 70, p. 349; 1946.
- [82] H. Margenau, "Conduction and dispersion of ionized gases at high frequencies," *Phys. Rev.*, vol. 69, p. 508; 1946.
- [83] H. S. Massey, "Recombination of gaseous ions," *Advances in Phys.*, vol. 1, p. 395; 1952.
- [84] H. S. W. Massey, "Negative Ions," Cambridge University Press, Cambridge, Eng.; 1950.
- [85] M. A. Meyer and H. B. Goldberg, "Applications of the turnstile junction," *IRE TRANS. ON MICROWAVE THEORY AND TECHNIQUES*, vol. MTT-3, pp. 40-45; December, 1955.
- [86] A. L. Mikaelyan, "Application of electron plasma in the production of nonreciprocal systems," *Bulletin de l'Academie des Science (U.S.S.R.)*, no. 7, p. 23; 1955.
- [87] M. R. Millet, "Microwave switching by crystal diodes," *IRE TRANS. ON MICROWAVE THEORY AND TECHNIQUES*, vol. MTT-6, pp. 284-290; July, 1958.
- [88] L. Milosevic, "High-power duplexers," *Le Vide*, vol. 12, p. 109; 1957.
- [89] N. Minorsky, "Electronic conduction and ionization in crossed electric and magnetic fields," *J. Franklin Inst.*, vol. 209, p. 757; 1930.
- [90] K. Mitani, "On the radial extent of glow in microwave gas discharge between coaxial cylinders," *J. Phys. Soc. Japan*, vol. 9, p. 299; 1954.
- [91] K. Mitani, "The direct current associated with microwave gas discharge between coaxial cylinders: parts 3 and 4," *J. Phys. Soc. Japan*, vol. 8, p. 642, 1953; vol. 10, p. 391, 1955.
- [92] C. G. Montgomery, R. H. Dicke, and E. M. Purcell, "Principles of Microwave Circuits," McGraw-Hill Book Co., Inc., New York, N. Y.; 1949.
- [93] A. L. Morris, "Microwave ferrite modulators for high signal frequencies," *J. Brit. IRE*, vol. 19, p. 117; 1959.
- [94] A. B. Parker, "A new form of X-band pre-TR cell," *Proc. IEE*, vol. 105, pt. B, suppl. no. 10, p. 488; 1958.
- [95] P. Parzon and L. Goldstein, "Current fluctuations in d.c. gas-discharge plasmas," *Phys. Rev.*, vol. 79, p. 190; 1950.
- [96] D. H. Pringle and W. E. J. Farvis, "Electron groups in the helium negative glow," *Phys. Rev.*, vol. 96, p. 536; 1954.
- [97] D. H. Pringle, "An electronic phase-shift tube for microwave frequencies," *J. Scientific Instruments*, vol. 32, p. 125; 1955.
- [98] D. H. Pringle and E. M. Bradley, "Some new microwave control valves employing the negative glow discharge," *J. Electronics*, vol. 1, p. 389; 1956.
- [99] D. H. Pringle and E. J. Whitmore, "Gas-discharge tubes for control of microwave attenuation," *J. Scientific Instruments*, vol. 30, p. 320; 1953.
- [100] J. F. Ramsay and W. F. Gunn, "A polarized-mirror duplexer for use with a circularly-polarized lens aerial," *Marconi Rev.*, vol. 18, p. 29; 1955.
- [101] F. H. Reder and S. C. Brown, "Energy distribution function of electrons in pure helium," *Phys. Rev.*, vol. 95, p. 885; 1954.
- [102] A. Regeffe, "Measurement of the transmission characteristic of switching valves for millimetre radar," *Le Vide*, vol. 11, p. 377; 1956.
- [103] D. Reverdin, "A wide-band valve incorporating an interdigital line," *Le Vide*, vol. 11, p. 352, 1956; *L'Onde Electrique*, vol. 37, p. 65, 1957.
- [104] R. P. Rizzi, "High-power ferrite circulators," *IRE TRANS. ON MICROWAVE THEORY AND TECHNIQUES*, vol. MTT-5, pp. 230-237; October, 1957.
- [105] M. L. W. Roberts, "Transmit-receive switch tubes," *Le Vide*, vol. 12, p. 83; 1957.
- [106] P. Rosen, "The propagation of e.m. waves in a tube containing a coaxial d.c. discharge," *J. Appl. Phys.*, vol. 20, p. 868; 1949.
- [107] A. L. Samuel, J. W. Clarke and W. W. Mumford, "The gas-discharge transmit-receive switch," *Bell Sys. Tech. J.*, vol. 25, p. 48; 1946.
- [108] W. D. Schumann, "Electric waves along a dielectric cylinder surrounded by a dielectric, one or both of the media being plasma," *Zeitschrift für Naturforschung*, vol. 5A, p. 181; 1950.
- [109] L. D. Smullin and C. G. Montgomery, "Microwave Duplexers," McGraw-Hill Book Co. Inc., New York, N. Y.; 1948.
- [110] R. F. Soohoo, "Power limiting using ferrites," 1958 IRE NATIONAL CONVENTION RECORD, pt. 1, pp. 36-47.

- [111] G. D. Speake, "Problems in protection of radar receivers," *Electronic Engrg.*, vol. 29, p. 313; 1957.
- [112] G. W. Stuart and P. Rosen, "A cylindrical cavity filled with a d.c. discharge," *J. Appl. Phys.*, vol. 22, p. 236; 1951.
- [113] R. F. Sullivan and R. C. LeCraw, "New type of ferrite microwave switch," *J. Appl. Phys.*, vol. 26, p. 1282; 1955.
- [114] J. W. Sutherland, "Waveguide hybrid circuits and their use in radar systems," *Electronic Engrg.*, vol. 28, p. 464; 1956.
- [115] J. W. Sutherland, "Waveguide switches and branching networks," *Electronic Engrg.*, vol. 31, p. 64; 1959.
- [116] S. J. Tetenbaum and R. M. Hill, "High-power broadband, microwave gas discharge switch-tube," 1958 IRE NATIONAL CONVENTION RECORD, pt. 1, p. 83.
- [117] S. J. Tetenbaum and R. M. Hill, "High power, magnetic field controlled microwave gas discharge switches," IRE TRANS. ON MICROWAVE THEORY AND TECHNIQUES, vol. MTT-7, pp. 73-82; January, 1959.
- [118] L. Tourel, P. Tcheditich, M. Lamy, and P. Vincent, "Waveguide switching device using gas-filled tubes," *Annales de Radioelectricite*, vol. 9, p. 163; 1954.
- [119] J. S. Townsend, "Electricity in Gases," Clarendon Press, Oxford, Eng., 1915; Hutchinson and Co., Ltd., London, Eng., 1948.
- [120] J. S. Townsend and E. W. B. Gill, "Generalization of the theory of electrical discharges," *Phil. Mag.*, vol. 26, p. 290; 1938.
- [121] M. A. Treuhaft and L. M. Silber, "Use of microwave ferrite toroids to eliminate external magnets and reduce switching power," *PROC. IRE*, vol. 46, p. 1538; August, 1958.
- [122] E. H. Turner, "A fast ferrite switch for use at 70 kmc," IRE TRANS. ON MICROWAVE THEORY AND TECHNIQUES, vol. MTT-6, pp. 300-303; July, 1958.
- [123] B. J. Udelson, J. E. Creedon and J. C. French, "Microwave measurements of the properties of a d.c. hydrogen discharge," *J. Appl. Phys.*, vol. 28, p. 717; 1957.
- [124] G. S. Uebele, "High-speed, ferrite microwave switch," 1957 IRE NATIONAL CONVENTION RECORD, pt. 1, pp. 227-234.
- [125] D. Walsh, "The electron affinity of hydrogen in a microwave gas discharge," *J. Electronics*, vol. 1, p. 444; 1956.
- [126] D. Walsh, A. W. Bright and T. J. Bridges, "Electrode deterioration in 'keep-alive' discharges in transmit-receive switches," *Brit. J. Appl. Phys.*, vol. 7, p. 31; 1956.
- [127] L. Young, "A hybrid-ring method of simulating higher powers than are available in waveguides," *Proc. IEE*, vol. 101, pt. B, p. 189; 1954.
- [128] Brit. Patent No. 716,372; vol. December 21, 1950.

Impedances of an Elliptic Waveguide (For the eH_1 Mode)*

G. R. VALENZUELA†, MEMBER, IRE

Summary—The power-voltage, power-current and voltage-current impedances for the elliptical waveguide for the fundamental mode (eH_1 mode) are obtained by two different methods.

The first method consists of using the exact fields inside a perfectly conducting elliptical pipe. Numerical results were obtained by numerical integration of the integrals involving Mathieu functions by the Gaussian Quadratures method by a digital computer.

In the second method approximate fields which satisfy the boundary conditions were used. By this approximate method, actual expressions for the impedances are obtained as a function of minor to major diameter ratio with no need of numerical integration.

The actual expressions for the impedance obtained by the approximate method give the impedance for elliptical waveguide within six per cent. On the basis of comparison with the exact numerical solution the expressions for the approximate impedance give the impedance of elliptical waveguide within three per cent if they are scaled by 1.03.

INTRODUCTION

CHU¹ in 1938 obtained numerical results for the exact cutoff wavelength for several modes in elliptical waveguides. He also obtained numerical results for the attenuation in elliptical waveguide.

* Received by the PGMTT, January 15, 1960; revised manuscript received, March 31, 1960. This research was supported by the U. S. Air Force through the Wright Air Dev. Div. of the Air Res. and Dev. Command. The early work reported herein was supported by the Dept. of the Navy, Bureau of Ordnance, at the Applied Physics Lab., The Johns Hopkins University.

† The Johns Hopkins Radiation Lab., Baltimore, Md.

¹ L. J. Chu, "Electromagnetic waves in elliptic hollow pipes of metal," *J. Appl. Phys.*, vol. 9, pp. 583-591; September, 1938.

Kihara² published a paper in 1947 using the variational method to determine the propagation constant of hollow pipes and cavities. Kihara was able to obtain the propagation constant of an elliptical waveguide within one per cent, in the first approximation, using trial fields.

In 1958 Harrowell³ obtained the impedance of elliptical waveguide by using an approximate method. He showed that the magnetic field lines inside a circular waveguide were approximately ellipses. Therefore, he was able to introduce conducting ellipses without disturbing the fields. Harrowell did not mention within what degree of accuracy his impedances would compare with the exact value.

Harrowell's voltage-current impedance agrees perfectly with our exact impedance, but his impedances involving power differ from our exact values; this difference is greater for eccentricities close to unity.⁴

² T. Kihara, "Approximate methods regarding electromagnetic waves in hollow pipes and cavities," *Phys. Soc. Japan*, vol. 2, pp. 65-70; 1947.

³ R. V. Harrowell, "An approximate theory for determining the characteristic impedance of elliptic waveguides," *J. of Electronics and Control*, vol. 5, pp. 289-299; October, 1958.

⁴ In private correspondence we pointed out to R. V. Harrowell that $J_1'(kr)=0$ was not correct inside the circular waveguide. Harrowell acknowledged this. Despite the fact that he modified his impedances, a discrepancy still exists.

In the approximate method used in this paper Kihara's trial fields are used to obtain the expression for the impedances.

THE IMPEDANCE IN WAVEGUIDE

The impedances in a waveguide are arbitrarily defined as,⁵

$$Z_{WV} = \frac{VV^*}{2W}, \quad Z_{WI} = \frac{2W}{II^*}, \quad Z_{VI} = \frac{V}{I}$$

for sinusoidal fields, where * as superscript indicates the complex conjugate. V is the maximum voltage across the waveguide, I is the total axial current and W is the power flowing down the waveguide.

The impedances obtained by these expressions are all different.

THE EXACT IMPEDANCE

The exact impedance is obtained by using the exact fields in the elliptical pipe. The fields components of an H wave in an orthonormal system u_1, u_2, u_3 of coordinates can be expressed as⁶

$$E_1 = \frac{-\mu}{h_2} \frac{\partial^2 \Pi_3^*}{\partial t \partial u_2}, \quad E_2 = \frac{\mu}{h_1} \frac{\partial^2 \Pi_3^*}{\partial t \partial u_1}, \quad E_3 = 0,$$

$$H_1 = \frac{1}{h_1} \frac{\partial^2 \Pi_3^*}{\partial t \partial u_1}, \quad H_2 = \frac{1}{h_2} \frac{\partial^2 \Pi_3^*}{\partial z \partial u_2}, \quad H_3 = (k^2 - \beta^2) \Pi_3^*,$$

where

Π_3^* = the magnetic Hertz vector in the direction u_3 ,
 μ = permeability of the medium,
 k = free space propagation constant,

$$\omega \sqrt{\mu_0 \epsilon_0} = 2\pi/\lambda_0,$$

β = waveguide propagation constant $2\pi/\lambda_g$,

and h_1 and h_2 are the metric coefficients of the respective coordinates.

In elliptical coordinates,

$$x = q \cosh u \cos v,$$

$$y = q \sinh u \sin v, \text{ and}$$

$$z = z$$

where q is the semifocal distance; u and v are the radial and angular variables, respectively.

The magnetic Hertz vector must satisfy the wave equation. In elliptical boundaries the magnetic Hertz vector satisfies the wave equation if it is expressed as a function of Mathieu functions. For the fundamental mode (${}_e H_1$ mode),

$$\Pi_3^* = \frac{B}{(k^2 - \beta^2)} J_{e1}(u) Se_1(v)$$

where

$$Se_1(v) = \sum_{k=0}^{\infty} De_{(2k+1)}^{(1)} \cos(2k+1)v,$$

$$J_{e1}(u) = \sqrt{\frac{\pi}{2}} \sum_{k=0}^{\infty} De_{(2k+1)}^{(1)} J_{2k+1}(h \cosh u)$$

and the coefficients $De_{(2k+1)}^{(1)}$ can be found in National Bureau of Standards' tables.⁷

B is a constant, $Se_1(v)$ is an even Mathieu function, $J_{e1}(u)$ is an even modified Mathieu function of the first kind, and the Mathieu functions have $h = q(k^2 - \beta^2)^{1/2}$ as a parameter.

Assuming an $e^{i(\omega t - \beta z)}$ dependence, the field components in elliptical coordinates are

$$E_u = -B \frac{i\omega\mu}{q_1(k^2 - \beta^2)} J_{e1}(u) Se_1'(v),$$

$$E_v = B \frac{i\omega\mu}{q_1(k^2 - \beta^2)} J_{e1}'(u) Se_1(v),$$

$$E_z = 0,$$

$$H_u = -B \frac{i\beta}{q_1(k^2 - \beta^2)} J_{e1}'(u) Se_1(v),$$

$$H_v = -B \frac{i\beta}{q_1(k^2 - \beta^2)} J_{e1}(u) Se_1'(v),$$

and

$$H_z = B J_{e1}(u) Se_1(v)$$

where

$$q_1 = q(\sinh^2 u + \sin^2 v)^{1/2}$$

and the prime denotes the derivative with respect to u or v .

For readers who desire to know more about Mathieu functions and their derivatives, papers by Wiltse and King^{8,9} are very appropriate.

A. The Voltage

Schelkunoff¹⁰ showed that the maximum voltage across a circular waveguide can be obtained from the longitudinal component of the magnetic field.

⁷ National Bureau of Standards, "Tables Relating to Mathieu Functions," Columbia University Press, New York, N. Y.; 1951.

⁸ J. C. Wiltse and M. J. King, "Values of the Mathieu Functions," The Johns Hopkins Rad. Lab., Baltimore, Md., Tech. Rept. AF-53; August, 1958.

⁹ M. J. King and J. C. Wiltse, "Derivatives, Zeros, and Other Data Pertaining to Mathieu Functions," The Johns Hopkins Rad. Lab., Baltimore, Md., Tech. Rept. AF-57; December, 1958.

¹⁰ S. A. Schelkunoff, "Electromagnetic Waves," D. Van Nostrand Co., Inc., Princeton, N. J., p. 324; 1943.

⁵ S. A. Schelkunoff, "Impedance concept in waveguides," *Quart. of Appl. Math.*, vol. 2, pp. 1-15; April, 1944.

⁶ J. A. Stratton, "Electromagnetic Theory," McGraw-Hill Book Co., Inc., New York, N. Y., p. 351; 1941.

In elliptical coordinates, the maximum voltage across the waveguide can also be obtained from the longitudinal magnetic field:

$$\begin{aligned} i\omega\mu H_z(u, v) &= i\omega\mu(k^2 - \beta^2)\Pi_z^* \\ &= \frac{i\omega\mu}{q_1^2} \left[\frac{\partial}{\partial u} \left(\frac{\partial \Pi_z^*}{\partial u} \right) + \frac{\partial}{\partial v} \left(\frac{\partial \Pi_z^*}{\partial v} \right) \right] \end{aligned}$$

substituting

$$\frac{\partial \Pi_z^*}{\partial v} = \frac{q_1 E_u}{-i\omega\mu} \quad \text{and} \quad \frac{\partial \Pi_z^*}{\partial u} = \frac{q_1 E_v}{i\omega\mu}$$

into H_z , and then integrating, it can be easily shown that

$$V = i\omega\mu \int_0^{u_0} \int_{-\pi/2}^{\pi/2} H_z(u, v) ds_1 ds_2 = 2 \int_0^{u_0} E_u \left(u_1, \frac{\pi}{2} \right) ds_1.$$

Accordingly,

$$\begin{aligned} V &= i\omega\mu \int_0^{u_0} \int_{-\pi/2}^{\pi/2} H_z ds_1 ds_2 \\ &= i\omega\mu B q^2 \int_0^{u_0} \int_{-\pi/2}^{\pi/2} (\sinh^2 u + \sin^2 v) J_{e_1}(u) S_{e_1}(v) du dv ds_1 ds_2 \\ ds_1 ds_2 &= q_1^2 du dv \quad (\text{differential area}). \end{aligned}$$

If we let I_1 represent the integral, then the final expression for the maximum voltage across the waveguide is

$$V = Bi\omega\mu q^2 I_1. \quad (1)$$

B. The Current

If we consider that the elliptical waveguide is in a position such that the major diameter is horizontal, the axial current flow is in one direction on the top face and in the opposite direction in the bottom. Then the total axial current can be obtained by the integral of the transverse tangential magnetic field on the upper half of the elliptical pipe:

$$I = \int_0^\pi H_v(u_0, v) ds_2 = \frac{-Bi\beta}{(k^2 - \beta^2)} J_{e_1}(u_0) \int_0^\pi S_{e_1}'(v) dv$$

and the final expression for the current is

$$I = B \frac{2i\beta}{k_0^2} J_{e_1}(u_0) \quad (2)$$

where $k_0^2 = (k^2 - \beta^2)$.

C. The Power

The power flowing down the waveguide is

$$\begin{aligned} W &= \frac{1}{2} \int_{\text{volume}} E \times H^* d\tau \\ &= \frac{1}{2} \int_0^{u_0} \int_0^{2\pi} (E_u H_v^* - E_v H_u^*) ds_1 ds_2 \cdot 1 \end{aligned}$$

and

$$W = |B|^2 \frac{\omega\mu\beta}{2k_0^4} \int_0^{u_0} \int_0^{2\pi} [J_{e_1}^2(u) S_{e_1}'^2(v) + J_{e_1}'^2(u) S_{e_1}^2(v)] du dv.$$

Although

$$\int_0^{2\pi} S_{e_1}^2(v) dv = \pi \sum_{k=0}^{\infty} [De_{(2k+1)}^{(1)}]^2$$

and

$$\int_0^{2\pi} S_{e_1}'^2(v) dv = \pi \sum_{k=0}^{\infty} (2k+1)^2 [De_{(2k+1)}^{(1)}]^2.$$

In the paper the values of the Mathieu functions were obtained directly by integrating the Mathieu equation, these expressions were not used, and the actual integration was performed.

If we let the integral be represented by I_2 , the power is

$$W = |B|^2 \frac{\omega\mu\beta}{2k_0^4} I_2. \quad (3)$$

Now the impedances can be easily obtained. Let $Z_0 = 120\pi(\lambda_g/\lambda)$ and $h = q(k^2 - \beta^2)^{1/2}$, then

$$Z_{WI} = \frac{h^4 I_1^2}{I_2} \cdot Z_0$$

and

$$Z_{WI} = \frac{I_2}{4J_{e_1}^2(u_0)} \cdot Z_0. \quad (4)$$

At the cut off $\beta=0$

$$h = q \frac{2\pi}{\lambda_c}$$

and the cut off wavelength is

$$\lambda_c = \frac{2\pi q}{h} = \frac{\pi e A}{h}$$

where

e = eccentricity and

A = major diameter of the ellipse.

Numerical Results

The values of the Mathieu functions and their derivatives required for the numerical integrations were obtained directly by integrating the Mathieu differential equations by the Univac-1103A computer.

The characteristic values be_1 were obtained from the expression $be_1 = a + s/2$, where $s = h^2$ and a is a continued fraction expansion of s . a was evaluated by using a routine available for the IBM 650 computer for each s . For more details see a paper by Valenzuela and Bitterli.¹¹

¹¹ G. R. Valenzuela and C. V. Bitterli, "Tables of Even and Even Modified Mathieu Functions of Order One of the First Kind and Their Derivatives," The Johns Hopkins University Appl. Phys. Lab., Silver Spring, Md., Rept. No. APL-CM-966; November, 1959.

TABLE I

B/A	$e = \text{eccentricity}$	$S = b^2$	u_0	I_1	I_2	$J_{e_1}(u_0)$
1.0000	0.0	0.0	∞	∞	2.000	0.7300
0.92367	0.3821	0.50	1.6135400	3.8394620	1.9616937	0.7420
0.8415	0.540	1.00	1.2263444	1.8158124	1.9072496	0.7560
0.7517	0.660	1.50	0.97686012	1.1244031	1.8232323	0.7720
0.6512	0.759	2.00	0.77738676	0.76092589	1.6947832	0.7890
0.5348	0.845	2.50	0.59694283	0.52235541	1.4991724	0.8067
0.3862	0.924	3.00	0.40732370	0.32811390	1.1679826	0.8255
0.1181	0.993	3.50	0.11873645	0.089946928	0.38690746	0.8455
0.0	1.000	∞	0.0	0.0	0.0	∞

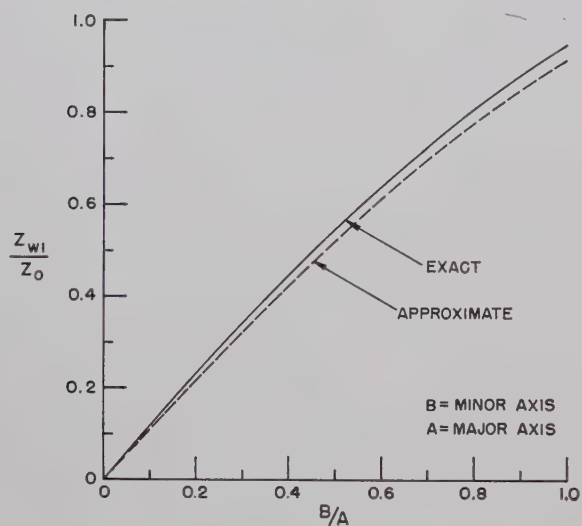


Fig. 1—Power-current impedance vs minor-to-major diameter ratio.

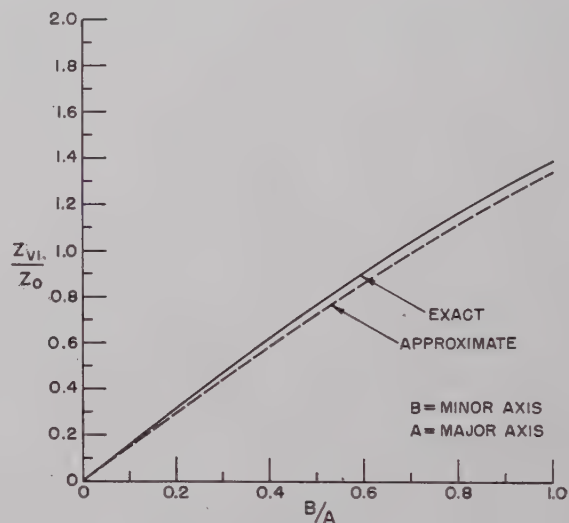


Fig. 3—Voltage-current impedance vs minor-to-major diameter ratio.

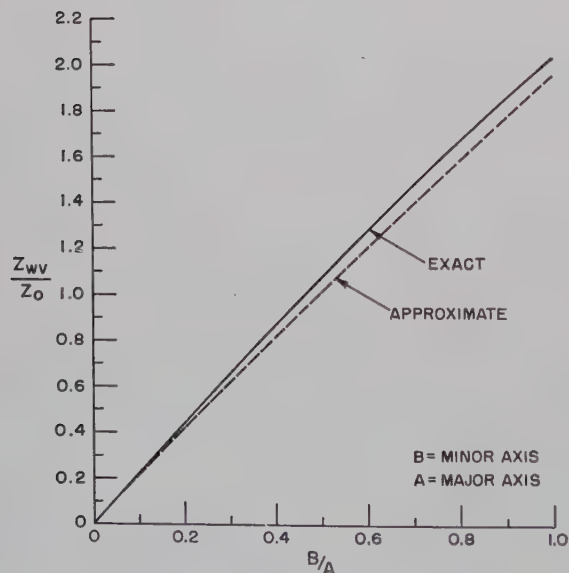


Fig. 2—Power-voltage impedance vs minor-to-major diameter ratio.

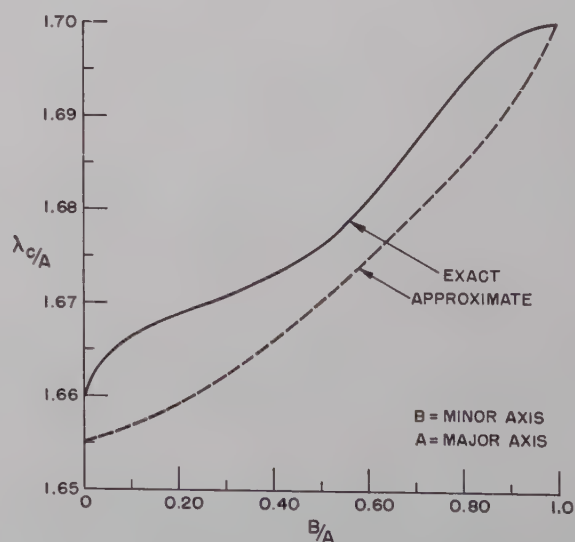


Fig. 4—Cutoff wavelength per major diameter vs minor-to-major axis ratio.

The integration of the Mathieu functions were performed using the Gaussian Quadratures method, sixteen points. The lowest root of the radial Mathieu functions were obtained by using the Univac-1103A.

The axial ratio corresponding to each h can be found from

$$\tanh u_0 = \frac{B}{A} \quad \text{and} \quad e = \sqrt{1 - \tanh^2 u_0}.$$

Note that all the quantities can be obtained from the parameter h . Hence the normalized impedances are only functions of this parameter.

Numerical results obtained by the computer are given in Table I.

THE APPROXIMATE IMPEDANCE

The approximate impedance was obtained using Kihara's approximate field components

$$\begin{aligned} E_x &= 2xy, \\ E_y &= (2a^2 + b^2) \left(1 - \frac{x^2}{a^2} \right) - y^2 \end{aligned}$$

major diameter $A = 2a$ and minor diameter $B = 2b$. These approximate fields do satisfy the boundary conditions.

Now we proceed to calculate the maximum voltage, total axial current and the power flowing in the elliptical waveguide using the approximate fields.

A. The Voltage

The maximum voltage across the waveguide is

$$\begin{aligned} V &= 2 \int_0^b E_y dy \Big|_{x=0} \\ &= 2 \int_0^b \left[(2a^2 + b^2) \left(1 - \frac{x^2}{a^2} \right) - y^2 \right] dy \Big|_{x=0} \end{aligned}$$

performing the integration and the voltage is

$$V = \frac{4}{3} (3a^2b + b^3). \quad (5)$$

B. The Current

The total axial current flowing can be obtained from

$$I = 2 \int_0^b \int_0^{x_0} H_{\tan} dx dy \quad x_0 = a(1 - y^2/b^2)^{1/2},$$

and the expression for the current is

$$I = \frac{4}{3} (2a^3 + ab^2) \frac{1}{Z_0}. \quad (6)$$

C. The Power

The power flowing down the pipe is

$$W = \frac{2}{Z_0} \int_0^b \int_0^{x_0} (E_x^2 + E_y^2) dx dy$$

and the power is

$$W = \frac{\pi}{12Z_0} (15a^5b + 11a^3b^3 + 2ab^5). \quad (7)$$

The expression for the approximate impedances are

$$\begin{aligned} Z_{WV} &= \frac{32}{3\pi} \frac{r(3 + r^2)}{(5 + 2r^2)} Z_0, \\ Z_{WI} &= \frac{3\pi}{32} \frac{r(15 + 11r^2 + 2r^4)}{(2 + r^2)^2} Z_0 \end{aligned} \quad (8)$$

and

$$Z_{VI} = r \frac{(3 + r^2)}{(2 + r^2)} Z_0$$

where

$$r = \frac{b}{a}.$$

In Figs. 1, 2 and 3 the exact and approximate impedances have been plotted for comparison. The exact cutoff wavelength and Kihara's approximate cutoff wavelength have been shown in Fig. 4.

Kihara obtained the propagation constant for the fundamental mode in elliptic waveguide using his trial fields, and his first approximation is correct to within one per cent:

$$\lambda_c = \pi A \sqrt{\frac{1}{6} \frac{(5 + 2r^2)}{(3 + r^2)}}.$$

Although Chu had already presented the cutoff wavelength for this mode, we present it here once more in a form easier to use. Chu in his paper plotted λ_c/s against eccentricities, where s is the circumference of the elliptical waveguide.

CONCLUSION

The exact values of the impedances are presented numerically and graphically. Expressions for the impedance of an elliptical waveguide are given. The impedance is obtained within six per cent of the exact value using the approximate results. Comparison of the curves indicates that expressions (8) can give the impedances of elliptical waveguide within three per cent of the exact values by scaling them by a factor of 1.03.

ACKNOWLEDGMENT

The author would like to thank T. Ap-Rhys for his very helpful suggestions.

Acknowledgment is also due to C. V. Bitterli, Project Supervisor of the Applied Physics Lab. Computing Center, for directing the evaluation of the integrals involving the Mathieu functions.

Analysis of a Transmission Cavity Wavemeter*

LEO YOUNG†, FELLOW, IRE

Summary—A section of transmission line partially closed off at each end constitutes a cavity wavemeter. If fixed in length, it may be used as a reference cavity; or if tunable, it may be used to determine frequency. Such a cavity is here treated systematically as a lossy transmission line, with the two end couplings either lossless or symmetrical. The analysis is by means of the transfer or wave matrix. Various expressions are derived which have previously not been obtained, or for which only approximate expressions have been derived from "equivalent circuits."

I. INTRODUCTION

A "transmission wavemeter" is a wavemeter which normally reflects most of the power incident on the generator side. It transmits appreciable power from the generator to the load only over a narrow frequency band. The load is often a crystal detector which peaks sharply as the wavemeter or generator is tuned through resonance. This transmission line circuit may be represented as shown in Fig. 1, where

a_1 , a_2 , a_2' , and a_3 are wave amplitudes in the direction from generator to load (left to right in Fig. 1) at the reference planes shown,

b_1 , b_2 , b_2' , and b_3 are wave amplitudes in the reverse direction (right to left in Fig. 1) at the same reference planes, and

$$\Gamma_L = \frac{b_3}{a_3} \quad (1)$$

is the reflection coefficient of the load as measured at the last reference plane.

The wave amplitudes a and b will be defined in terms of power flow¹ by

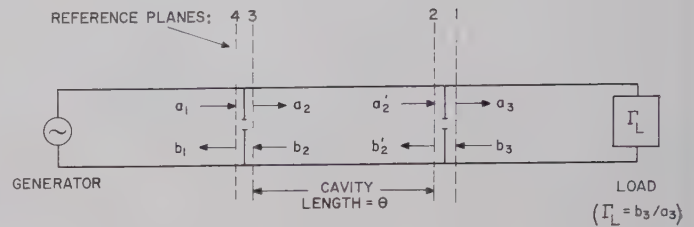
$$\begin{aligned} |a|^2 &= \text{power flow in the forward direction} \\ &\quad (\text{i.e. towards the load}), \\ |b|^2 &= \text{power flow in the reverse direction} \\ &\quad (\text{i.e. back towards the generator}). \end{aligned} \quad (2)$$

The cavity is supposed to be coupled to the outside by two identical couplings (holes or irises, etc.), one at each end of the cavity (Fig. 1). We shall also take each coupling in itself as *either* lossless *or* symmetrical (and possibly lossy), since this simplifies the analysis, and the general case of unsymmetrical lossy couplings is not commonly found. No further restriction is placed on the kind of coupling (e.g. iris thickness, etc.).

* Received by the PGM-TT, February 25, 1960; revised manuscript received, March 11, 1960.

† Electronics Div., Westinghouse Elec. Corp., Friendship International Airport, Baltimore, Md.

¹ L. Young, "Transformation matrices," IRE TRANS. ON CIRCUIT THEORY, vol. CT-5, pp. 147-148; June, 1958.



TRANSFER MATRICES BETWEEN REFERENCE PLANES:
 $T(1 \rightarrow 2) = T, T(2 \rightarrow 3) = \Theta, T(3 \rightarrow 4) = T.$

Fig. 1—Transmission wavemeter cavity.

The electrical length of the cavity, θ radians, is measured between the two reference planes inside the cavity, and is defined by

$$\theta = \frac{2\pi \times \text{cavity length (between inside reference planes)}}{\text{guide wavelength, } \lambda_g}. \quad (3)$$

The treatment presented here is exact to the extent that a) higher-order modes may be neglected, and b) the variable quantity in the definition of θ is cavity length rather than guide wavelength (cavity tuned at fixed frequency), since the coupling parameters at each end of the cavity will generally be frequency sensitive and so vary with guide wavelength. Under certain conditions it is not necessary to stipulate b), and θ can be taken as a frequency variable (fixed cavity and tunable signal generator). This occurs for instance when the couplings are ideal transformers,² which can be realized closely in practice with E -plane waveguide steps.

Resonance

In a simple series L - C - R circuit driven by a constant voltage generator, the current in the circuit, the voltage across L , the charge on C , etc., reach maximum or "resonance" at slightly different frequencies. The "resonant frequency" is usually understood to be the frequency for current resonance, and is independent of the resistance R .

With a cavity too, the reflected wave, the transmitted wave, and the internal fields reach maximum or resonance at slightly different values of θ . However, Q is generally large; it is usually several thousand in microwave wavemeters, so that to speak of a resonant length or frequency is in general substantially correct.

Of all the resonant lengths, the most convenient one is perhaps that length which gives amplitude resonance,

² L. Young, "Design of Microwave Stepped Transformers with Applications to Filters," Ph.D. dissertation, The Johns Hopkins University, Baltimore, Md.; 1959.

that is, maximum wave amplitudes inside the cavity. There are two reasons for this choice. The first is that it is applicable to every cavity wavemeter, regardless of external connections. The second reason is that the pole, which determines the maximum internal cavity fields, also occurs as a pole in the expressions for the reflected and transmitted amplitudes, as will be seen later.

II. ANALYSIS BY TRANSFER MATRICES

Consider a wavemeter symmetrically coupled as shown in Fig. 1 by two separate couplings, into a wave generator on the left and into a load on the right. (The generator and load are only coupled via the cavity.)

The wave or transfer matrix¹⁻⁶ will be used. The cavity length θ is introduced by the line transfer matrix Θ , given by

$$\Theta = \begin{pmatrix} e^{J\theta} & 0 \\ 0 & e^{-J\theta} \end{pmatrix}, \quad (4)$$

where

$$J = j + \frac{A}{2\pi}, \quad (5)$$

A being the attenuation of the cavity transmission line in nepers per guide wavelength. (For a wavemeter with no internal losses, $A=0$, and then J reduces to $j=\sqrt{-1}$.)

Since each coupling hole has been taken to be *either* lossless *or* symmetrical (and possibly lossy), the two reference planes associated with each coupling may be chosen so that the reflection coefficient Γ of a single coupling hole is the same from either side (in amplitude as well as phase), and its transmission coefficient T is the same in both directions. Then the transfer matrix of a single coupling hole may be written⁵

$$T = \frac{1}{T} \begin{pmatrix} 1 & -\Gamma \\ \Gamma & T^2 - \Gamma^2 \end{pmatrix}. \quad (6)$$

From Fig. 1,

$$\begin{pmatrix} a_3 \\ b_3 \end{pmatrix} = T^{-1} \Theta^{-1} T^{-1} \begin{pmatrix} a_1 \\ b_1 \end{pmatrix}. \quad (7)$$

In full,

$$\begin{pmatrix} a_3 \\ b_3 \end{pmatrix} = \frac{1}{T^2} \begin{pmatrix} T^2 - \Gamma^2 & \Gamma \\ -\Gamma & 1 \end{pmatrix} \begin{pmatrix} e^{-J\theta} & 0 \\ 0 & e^{J\theta} \end{pmatrix} \begin{pmatrix} T^2 - \Gamma^2 & \Gamma \\ -\Gamma & 1 \end{pmatrix} \begin{pmatrix} a_1 \\ b_1 \end{pmatrix}. \quad (8)$$

Now b_3/a_3 is the reflection coefficient Γ_L of the load in the reference plane of the cavity, on the load side:

$$\Gamma_L = \frac{b_3}{a_3}. \quad (1)$$

Eq. (8) represents two simultaneous equations. Substituting (1) and eliminating b_1 , yields

$$\frac{a_3}{a_1} = \frac{T^2}{D_1} \quad (9)$$

where

$$D_1 = (1 - \Gamma_L \Gamma) e^{J\theta} - \Gamma \{ \Gamma + \Gamma_L (T^2 - \Gamma^2) \} e^{-J\theta}. \quad (10a)$$

Dividing the two simultaneous equations (8), substituting (1), and solving for b_1/a_1 yields

$$\frac{b_1}{a_1} = \frac{\Gamma(1 - \Gamma_L \Gamma) e^{J\theta} + (T^2 - \Gamma^2) \{ \Gamma + \Gamma_L (T^2 - \Gamma^2) \} e^{-J\theta}}{D_1}. \quad (11)$$

From (11) and from

$$\begin{pmatrix} a_2 \\ b_2 \end{pmatrix} = T^{-1} \begin{pmatrix} a_1 \\ b_1 \end{pmatrix},$$

it follows that

$$\frac{a_2}{a_1} = \frac{T(1 - \Gamma_L \Gamma) e^{J\theta}}{D_1} \quad (12)$$

and

$$\frac{b_2}{a_1} = \frac{T \{ \Gamma + \Gamma_L (T^2 - \Gamma^2) \} e^{-J\theta}}{D_1}. \quad (13)$$

III. ANALYSIS FOR LOSSLESS COUPLINGS

From here to the end of the paper it will be supposed that the couplings themselves introduce no loss. Then from energy considerations

$$|\Gamma|^2 + |T|^2 = 1. \quad (14)$$

The reference planes of the lossless coupling hole may be chosen (without loss in generality) so that Γ is real; then it can be shown^{2,5} that T must be imaginary, and therefore (14) becomes

$$\Gamma^2 - T^2 = 1. \quad (15)$$

Eqs. (10) to (13) then reduce to

$$\frac{a_3}{a_1} = \frac{T^2 e^{-J\theta}}{D_2} \quad (16)$$

$$\frac{b_1}{a_1} = \frac{\Gamma(1 - \Gamma_L \Gamma) - (\Gamma - \Gamma_L) e^{-2J\theta}}{D_2}, \quad (17)$$

$$\frac{a_2}{a_1} = \frac{T(1 - \Gamma_L \Gamma)}{D_2}, \quad (18)$$

$$\frac{b_2}{a_1} = \frac{T(\Gamma - \Gamma_L) e^{-2J\theta}}{D_2} \quad (19)$$

³ G. L. Ragan, "Microwave Transmission Circuits," Mass. Inst. Tech. Rad. Lab. Ser., McGraw-Hill Book Co., Inc., New York, N. Y., vol. 9, pp. 551-554; 1948.

⁴ C. G. Montgomery, R. H. Dicke and E. M. Purcell, "Principles of Microwave Circuits," Mass. Inst. Tech. Rad. Lab. Ser., McGraw-Hill Book Co., Inc., New York, N. Y., vol. 8, pp. 150-151; 1948.

⁵ L. Young, "An Analysis of Resonant Cavities by Matrix Methods," M.S. thesis, The Johns Hopkins University, Baltimore, Md.; 1955.

⁶ L. Young, "Branch guide directional couplers," *Proc. Natl. Electronics Conf.*, Chicago, Ill., vol. 12, pp. 723-732; 1956.

where

$$D_2 = (1 - \Gamma_L \Gamma) - \Gamma(\Gamma - \Gamma_L)e^{-2J\theta}. \quad (10b)$$

Reflectionless Load

If further $\Gamma_L = 0$ (for a reflectionless load), then

$$\frac{a_3}{a_1} = \frac{T^2 e^{-2J\theta}}{D_3}, \quad (20)$$

$$\frac{b_1}{a_1} = \frac{\Gamma(1 - e^{-2J\theta})}{D_3} \quad (21)$$

$$\frac{a_2}{a_1} = \frac{T}{D_3}, \quad (22)$$

$$\frac{b_2}{a_1} = \frac{T\Gamma e^{-2J\theta}}{D_3} \quad (23)$$

where

$$D_3 = 1 - \Gamma^2 e^{-2J\theta}. \quad (10c)$$

Poles and Zeros

The response functions (9) to (13) have the same pole in the complex θ plane, given by

$$e^{2J\theta} = \frac{\Gamma[\Gamma + \Gamma_L(T^2 - \Gamma^2)]}{1 - \Gamma_L \Gamma}. \quad (24)$$

In the special case of lossless coupling (Γ =real, with T =imaginary), reflectionless load ($\Gamma_L=0$), and zero cavity waveguide attenuation ($A=0$), the resonant length is

$$\theta_0 = n\pi, \quad (n = \text{integer}), \quad (25)$$

when it is measured between reference planes defined by Γ =real. The multiplier n will be called the Harmonic Number. If the losses are small, n is still nearly integral. Then

$$n = [n] \pm \epsilon, \quad (26)$$

where $[n]$ is integral and ϵ is small. In this case $[n]$ will be called the Harmonic Number.

The only zero occurs in the expressions for the reflected wave b_1/a_1 . It is given by

$$e^{2J\theta} = \frac{(T^2 - \Gamma^2)\{\Gamma + \Gamma_L(T^2 - \Gamma^2)\}}{\Gamma(1 - \Gamma_L \Gamma)}. \quad (27)$$

This zero will generally be close to the pole. If the cavity line attenuation $A=0$, the transmitted wave and fields inside the cavity reach maximum or minimum values together; the reflected wave will do so in general at a slightly different θ . This value may be found graphically by plotting the locus of the vector b_1/a_1 for various θ near resonance.

Resonant Length or Frequency Pulling by a Mismatched Load

Eqs. (24) and (25) establish the resonant length pulling due to a mismatched load when the cavity coupling is lossless. Then θ has to be increased by

$$\delta\theta = \frac{1}{2} \arg \left[\frac{\Gamma(\Gamma - \Gamma_L)}{1 - \Gamma_L \Gamma} \cdot e^{-A\theta/\pi} \right] \quad (28)$$

$$= \frac{1}{2} \arg \left[\frac{\Gamma(\Gamma - \Gamma_L)}{1 - \Gamma_L \Gamma} \cdot e^{-nA} \right], \quad (29)$$

if it is not too far from the resonant value $\theta = n\pi$.

Note that if both Γ and Γ_L are real in the same reference plane, there will be no pulling.

Maximum Transmitted Amplitude

The maximum values of the internal and transmitted waves are obtained when $\theta = n\pi$ is substituted in (20), (22), and (23), if the load is reflectionless, or θ from (29), if it is not, into (16), (18), and (19).

We thus obtain for a reflectionless load ($\Gamma_L = 0$),

$$\left| \frac{a_3}{a_1} \right|_{\max} = \frac{|T|^2}{1 - |\Gamma|^2 m^2} = \frac{1 - |\Gamma|^2}{1 - |\Gamma|^2 m^2} \quad (30)$$

where

$$m^2 = e^{-A\theta/\pi}, \quad (31)$$

while if the load is not reflectionless

$$\left| \frac{a_3}{a_1} \right|_{\max} = \frac{1 - |\Gamma|^2}{|1 - \Gamma_L \Gamma| - |\Gamma(\Gamma - \Gamma_L)| m^2}. \quad (32)$$

Eq. (30) can be written in terms of Q . Define

$$s = \frac{\lambda_g}{\lambda} \quad (33)$$

where λ_g =guide wavelength, and λ =free space wavelength. The quantity s^2 often occurs in the theory of dispersive transmission lines⁴⁻⁶ and will be called the "dispersion factor."

It can be shown⁷ that Q is given very closely by

$$Q = \frac{\pi s^2}{A} \cdot \frac{1 - e^{-A\theta/\pi}}{1 - |\Gamma|^2 e^{-A\theta/\pi}}. \quad (34)$$

Since

$$1 - |\Gamma|^2 m^2 \doteq \frac{n\pi s^2}{Q}, \quad (35)$$

therefore

$$\left| \frac{a_3}{a_1} \right|_{\max} \doteq \frac{|T|^2 Q}{n\pi s^2}. \quad (36)$$

Resonance Amplification

If Γ_L is not zero, the maximum amplitude inside the cavity is given by $G|T|$, where G is the "resonance amplification,"

$$G|T| \doteq \frac{|a_2| + |b_2|}{|a_1|}_{\max} = \frac{|T| \{ |1 - \Gamma_L \Gamma| + |\Gamma - \Gamma_L| m^2 \}}{|1 - \Gamma_L \Gamma| - |\Gamma(\Gamma - \Gamma_L)| m^2}, \quad (37)$$

⁷ L. Young, "Q-factors of a transmission line cavity," IRE TRANS. ON CIRCUIT THEORY, vol. CT-4, pp. 3-5; March, 1957.

while if $\Gamma_L=0$, this reduces to

$$\frac{|a_2| + |b_2|}{|a_1|} \Big|_{\max} = \frac{|T| (1 + |\Gamma| m^2)}{1 - |\Gamma|^2 m^2} \tag{38}$$

For the rest of this discussion consider only the case of a reflectionless load, $\Gamma_L=0$.

Since $|\Gamma|^2 \doteq 1$ and $m^2 \doteq 1$,

$$\begin{aligned} G|T| &\doteq \frac{|a_2| + |b_2|}{|a_1|} \Big|_{\max} \doteq \frac{2|T|}{1 - |\Gamma|^2 m^2} \\ &\doteq \frac{2Q|T|}{n\pi s^2}, \end{aligned} \tag{39}$$

Thus the resonance amplification G is approximately

$$G \doteq \frac{2Q}{n\pi s^2} \tag{40}$$

In series (or shunt) L - C - R circuits the voltage (or current) resonance amplification is Q . The resonance amplification G here defined is proportional to Q , but if expressed in terms of Q , is also inversely proportional to the harmonic number n , and the dispersion factors s^2 .

Bandwidth

The cavity bandwidth can be obtained from (20) or (22), when $\Gamma_L=0$. The bandwidth is defined in the usual way by $W=2\Delta f$, where $\pm\Delta f$ is the deviation from the resonant frequency, which reduces

$$\left| \frac{a_2}{a_1} \right| \text{ or } \left| \frac{a_3}{a_1} \right| \text{ to } \frac{1}{\sqrt{2}} \text{ of their maximum values.}$$

Now

$$df = -f \frac{d\lambda}{\lambda} = -\frac{f}{s^2} \frac{d\lambda_g}{\lambda_g} \tag{41}$$

Hence

$$W = 2\Delta f \doteq \frac{2f_0}{s^2} \frac{\Delta\theta}{\theta_0} = \frac{2f_0}{s^2} \frac{\Delta\theta}{n\pi} \tag{42}$$

where $\pm\Delta\theta$ is the deviation of θ from its resonant value $\theta_0=n\pi$, which reduces $|a_2/a_1|$ and $|a_3/a_1|$ to $1/\sqrt{2}$ of their maximum values.

For high Q this will be given approximately by

$$1 - |\Gamma|^2 m^2 \doteq 2\Delta\theta. \tag{43}$$

Hence by (35),

$$2\Delta Q \doteq \frac{n\pi s^2}{Q} \tag{44}$$

Therefore

$$W \doteq \frac{f_0}{Q} \tag{45}$$

This result is not surprising since it is the familiar expression for a series or shunt L - C - R circuit, except that there it is exact (whereas for a transmission line cavity it is only a good approximation for high Q).

IV. CONCLUSION

An analysis of a transmission wavemeter has been presented which, given a single-mode in each section of transmission line, is exact. This treatment is based on the transfer matrix, and does not require the use of equivalent L - C - R circuits.⁸

ACKNOWLEDGMENT

This work is based largely on a Master's essay written at The Johns Hopkins University, Baltimore, Md., some years ago, with help and advice from Dr. W. H. Huggins and Dr. D. D. King.

⁸ C. G. Montgomery, "Technique of Microwave Measurements," Mass. Inst. Tech. Rad. Lab. Ser., McGraw-Hill Book Co., Inc., New York, N. Y., vol. 11, ch. 5; 1947.

Scattering of a Plane Wave on a Ferrite Cylinder at Normal Incidence*

W. H. EGGIMANN†

Summary—The scattered field is given as a series of cylinder functions. If the ferrite cylinder is magnetized along its axis the scattering pattern becomes asymmetrical about the direction of incidence. Approximation formulas for the thin cylinder and the far field zone are given. It is shown that in the first approximation the amplitude is an even function and the phase angle of the field is an odd function of the scattering angle. Exact numerical results have been obtained with a Univac digital computer. By a suitable arrangement of the ferrite cylinders, a unidirectional pattern can be obtained which is controlled by the applied magnetic dc field.

INTRODUCTION

THE scattering of a plane wave on a dielectric cylinder has been discussed in a number of papers. The complete solution for arbitrary incidence has been given by Wait.¹ He also discussed approximate solutions for the far field zone and the case of a cylinder whose diameter is small compared with the wavelength.

In this paper the scattering of a plane wave from a homogeneous ferrite cylinder is investigated. The discussion is restricted to the case of normal incidence, for which an exact solution in form of a series of Bessel functions can be found. The ferrite rod is magnetized along its axis. Because of the nonreciprocal properties of the ferrite material, a nonsymmetrical distribution of the scattered field with respect to the direction of incidence is to be expected. The scattered field is a function of the permeability tensor of the ferrite, which in turn depends on the applied magnetic dc field. It is, therefore, possible to control the scattering pattern of the ferrite cylinder by the magnetic field.

THE MATHEMATICAL SOLUTION

An infinitely long ferrite cylinder with its axis along the z direction is considered. A dc magnetic field is applied along its axis. A plane wave is incident in the positive x direction. With these assumptions the problem is reduced to two dimensions in the x - y plane. The polarization of the wave is arbitrary. The field can then be decomposed in two waves, one which is polarized normal to the cylinder axis ($E = E_{\alpha y}$) and one which is polarized parallel to it ($E = E_{\alpha z}$) (see Fig. 1). In the first case the magnetic field of the wave is parallel to the axis and to the applied magnetic dc field and, therefore, no nonreciprocal interaction between the field and the mag-

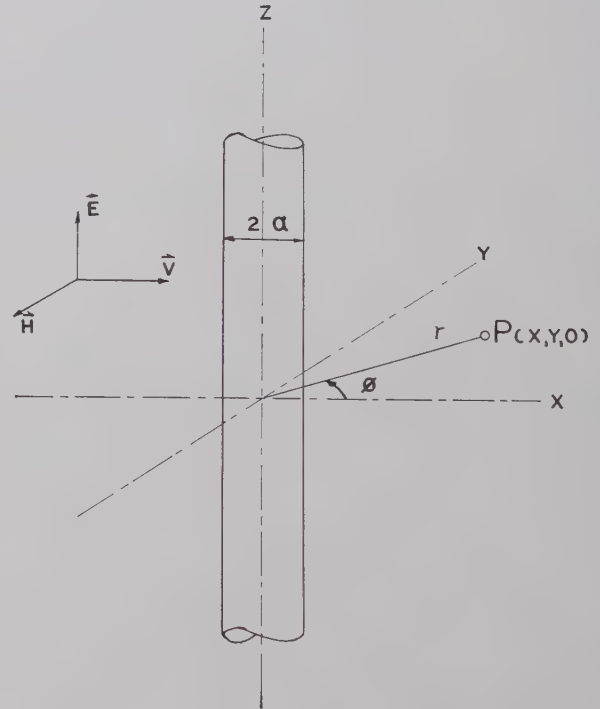


Fig. 1—Plane wave incident normally on a circular ferrite cylinder.

netization of the ferrite takes place. Hence the tensor permeability reduces to a scalar. In other words the problem is the same as the one for a dielectric cylinder.¹ For the wave polarized parallel to the z axis, however, the magnetic dc and ac fields are normal to each other, so that the ac field interacts with the precessing magnetic dipoles of the ferrite. In this case one has to use the tensor permeabilities in Maxwell's equations,

$$\text{curl } \mathbf{H} = \frac{\partial \mathbf{D}}{\partial t} = j\omega \mathbf{D} = j\omega \epsilon \mathbf{E}, \quad (1a)$$

$$\text{curl } \mathbf{E} = -\frac{\partial \mathbf{B}}{\partial t} = -j\omega \mathbf{B} = -j\omega \bar{\mu} \cdot \mathbf{H}. \quad (1b)$$

Because there is no variation in the z direction, (1b) can be replaced by the two-dimensional tensor equation

$$\mathbf{B} = -\frac{1}{j\omega} \begin{pmatrix} 0 & 1 \\ -1 & 0 \end{pmatrix} \cdot \nabla E_z = -\frac{1}{j\omega} \begin{pmatrix} 0 & 1 \\ -1 & 0 \end{pmatrix} \cdot \begin{pmatrix} \frac{\partial}{\partial x} \\ \frac{\partial}{\partial y} \end{pmatrix} E_z, \quad (2)$$

where ∇ is the two-dimensional symbolic gradient. Thus the magnetic field \mathbf{H} is in free space

* Received by the PGMTT, January 4, 1960; revised manuscript received, February 23, 1960.

† Department of Electrical Engineering, Case Institute of Technology, Cleveland, Ohio.

¹ J. R. Wait, "Scattering of a plane wave from a circular dielectric cylinder at oblique incidence," *Can. J. Phys.*, vol. 33, pp. 189-195; 1955.

$$\mathbf{H} = -\frac{1}{j\omega} \mu_0^{-1} \cdot \begin{pmatrix} 0 & 1 \\ -1 & 0 \end{pmatrix} \cdot \nabla E_z, \quad (3)$$

in ferrite

$$\mathbf{H} = -\frac{1}{j\omega} (\mu)^{-1} \cdot \begin{pmatrix} 0 & 1 \\ -1 & 0 \end{pmatrix} \cdot \nabla E_z. \quad (4)$$

The permeability tensor $\bar{\mu}$ can be calculated from the simple model of the precessing magnetic dipole moment of the electron in a magnetic field.² One obtains in two dimensions

$$\bar{\mu} = \begin{pmatrix} \mu & -jk \\ jk & \mu \end{pmatrix}, \quad (5)$$

where the two components μ and k are given by

$$\mu = \mu_0 \frac{\gamma^2 \mu_0 H_0 B_z - \omega^2}{\gamma^2 \mu_0^2 H_0^2 - \omega^2} \quad (6)$$

and

$$k = \mu_0 \frac{\omega \gamma \mu_0 M_z}{\gamma^2 \mu_0^2 H_0^2 - \omega^2}, \quad (7)$$

where $B_z = \mu_0(H_0 + M_z)$ and γ = gyromagnetic ratio of the electron spin. From (5) the reciprocal tensor permeability can be calculated

$$(\bar{\mu})^{-1} = \frac{1}{\mu^2 - k^2} \begin{pmatrix} \mu & jk \\ -jk & \mu \end{pmatrix}. \quad (8)$$

Combining (4) and (8),

$$\mathbf{H} = -\frac{1}{j\omega} \frac{1}{\mu^2 - k^2} \begin{pmatrix} -jk & \mu \\ -\mu & -jk \end{pmatrix} \cdot \nabla E_z. \quad (9)$$

This gives in Cartesian coordinates

$$H_x = \frac{1}{j\omega(\mu^2 - k^2)} \left(jk \frac{\partial E_z}{\partial x} - \mu \frac{\partial E_z}{\partial y} \right) \quad (10a)$$

$$H_y = \frac{1}{j\omega(\mu^2 - k^2)} \left(\mu \frac{\partial E_z}{\partial x} + jk \frac{\partial E_z}{\partial y} \right), \quad (10b)$$

and in cylindrical coordinates

$$H_r = \frac{1}{\omega(\mu^2 - k^2)} \left(k \frac{\partial E_z}{\partial r} + j\mu \frac{1}{r} \frac{\partial E_z}{\partial \phi} \right) \quad (11a)$$

$$H_\phi = \frac{1}{\omega(\mu^2 - k^2)} \left(j\mu \frac{\partial E_z}{\partial r} - k \frac{1}{r} \frac{\partial E_z}{\partial \phi} \right). \quad (11b)$$

INCIDENT FIELD

In order to apply the boundary conditions (continuity of the tangential electric and magnetic field at $r=a$) it is necessary to express the incoming plane wave in cylindrical coordinates. This can be done in terms of a series of Bessel functions³

² C. L. Hogan, "The microwave gyrator," *Bell Sys. Tech. J.*, vol. 31, pp. 1-31; January, 1952.
³ J. H. Stratton, "Electromagnetic Theory," McGraw-Hill Book Co., Inc., New York, N. Y., p. 372; 1941.

$$\begin{aligned} E_z^{\text{inc}} &= E_0 e^{j(\omega t - \beta x)} = E_0 e^{j(\omega t - \beta r \cos \phi)} \\ &= E_0 e^{j\omega t} \sum_{n=-\infty}^{\infty} (j)^n J_n(\beta r) e^{-jn\phi}. \end{aligned} \quad (12)$$

The magnetic field is given by (11) when $\mu = \mu_0$ and $k = 0$.

$$H_r^{\text{inc}} = \frac{1}{\omega \mu_0} \frac{1}{r} \frac{\partial E_z}{\partial \phi} = \frac{E_0}{\omega \mu_0 r} \sum_{n=-\infty}^{\infty} (j)^n J_n(\beta r) n e^{-jn\phi} \quad (13a)$$

$$H_\phi^{\text{inc}} = \frac{j}{\omega \mu_0} \frac{\partial E_z}{\partial r} = \frac{j\beta E_0}{\omega \mu_0} \sum_{n=-\infty}^{\infty} (j)^n J_n'(\beta r) e^{-jn\phi}. \quad (13b)$$

All derivatives are with respect to the argument βr .

SCATTERED FIELD

For the scattered field a similar representation is chosen. Here the Hankel functions of the second kind have to be used, because the asymptotic approximation for large arguments give a decreasing outgoing wave.

$$E_z^{\text{scat}} = \sum_{n=-\infty}^{\infty} a_n^s H_n^{(2)}(\beta r) e^{-jn\phi} \quad (14)$$

$$H_r^{\text{scat}} = \frac{1}{\omega \mu_0} \frac{1}{r} \sum_{n=-\infty}^{\infty} a_n^s H_n^{(2)}(\beta r) n e^{-jn\phi} \quad (15a)$$

$$H_\phi^{\text{scat}} = \frac{j\beta}{\omega \mu_0} \sum_{n=-\infty}^{\infty} a_n^s H_n'^{(2)}(\beta r) e^{-jn\phi}. \quad (15b)$$

INSIDE FIELD

Inside the ferrite the field is represented by Bessel functions of the first kind.

$$E_z = \sum_{n=-\infty}^{\infty} a_n J_n(\beta_2 r) e^{-jn\phi} \quad (16)$$

$$\begin{aligned} H_r &= \frac{1}{\omega(\mu^2 - k^2)} \left[k\beta_2 \sum_{n=-\infty}^{\infty} a_n J_n'(\beta_2 r) e^{-jn\phi} \right. \\ &\quad \left. + \frac{\mu}{r} \sum_{n=-\infty}^{\infty} a_n J_n(\beta_2 r) n e^{-jn\phi} \right] \end{aligned} \quad (17a)$$

$$\begin{aligned} H_\phi &= \frac{j}{\omega(\mu^2 - k^2)} \left[\mu\beta_2 \sum_{n=-\infty}^{\infty} a_n J_n'(\beta_2 r) e^{-jn\phi} \right. \\ &\quad \left. + \frac{k}{r} \sum_{n=-\infty}^{\infty} a_n J_n(\beta_2 r) n e^{-jn\phi} \right]. \end{aligned} \quad (17b)$$

It can be shown that in the ferrite material the wave number is given by

$$\beta_2^2 = \omega^2 \mu_{\text{eff}} \epsilon, \quad (18)$$

where

$$\mu_{\text{eff}} = \frac{\mu^2 - k^2}{\mu}. \quad (19)$$

In (13) to (17) the harmonic time dependence $e^{j\omega t}$ is omitted.

$$E_z^s(r, \phi) = \frac{1}{4} \pi (\beta a)^2 E_0 \left[-j \left(\frac{\epsilon}{\epsilon_0} - 1 \right) H_0^{(2)}(\beta r) + H_1^{(2)}(\beta r) \left(\frac{\frac{\mu_0}{\mu_{\text{eff}}} \left(1 + \frac{k}{\mu} \right) - 1}{\frac{\mu_0}{\mu_{\text{eff}}} \left(1 + \frac{k}{\mu} \right) + 1} e^{-j\phi} - \frac{\frac{\mu_0}{\mu_{\text{eff}}} \left(1 - \frac{k}{\mu} \right) - 1}{\frac{\mu_0}{\mu_{\text{eff}}} \left(1 - \frac{k}{\mu} \right) + 1} e^{j\phi} \right) \right]. \quad (27)$$

BOUNDARY CONDITIONS

Continuity of the tangential electric and magnetic field requires

$$E_z^{\text{inc}} + E_z^{\text{scat}} = E_z \text{ at } r = a \quad (20)$$

$$H_\phi^{\text{inc}} + H_\phi^{\text{scat}} = H_\phi \text{ at } r = a. \quad (21)$$

Substituting (12) to (17) in (20) and (21) and eliminating a_n yields

$$a_n^s = -E_0(j)^n \frac{\frac{D_n(\beta_2 a)}{J_n(\beta_2 a)} - \frac{J_n'(\beta a)}{J_n(\beta a)} \frac{J_n(\beta a)}{H_n^{(2)}(\beta a)}}{\frac{D_n(\beta_2 a)}{J_n(\beta_2 a)} - \frac{H_n'(\beta a)}{H_n^{(2)}(\beta a)}}, \quad (22)$$

where

$$D_n(\beta_2 a) = \frac{\mu_0}{\mu_{\text{eff}}} \frac{\beta_2}{\beta} \left[J_n'(\beta_2 a) + \frac{k}{\mu} \frac{n}{\beta_2 a} J_n(\beta_2 a) \right]. \quad (23)$$

For $k \rightarrow 0$, the permeability tensor $\bar{\mu}$ reduces to a scalar and one obtains the case of the dielectric cylinder.¹

B. Far Field Approximation, $\beta r \gg 1$

Here the asymptotic approximation for the Hankel function with large argument is used

$$H_n^{(2)}(z) \simeq \sqrt{\frac{2}{\pi z}} e^{-jz + j(n\pi/2) + j(\pi/4)} = (j)^n H_0^{(2)}(z), \quad (28)$$

where $H_0^{(2)}(z)$ is given by this equation. Combining (14), (22), and (28) gives

$$E_z^s = j H_0^{(2)}(\beta r) \left[c_0 + \sum_{n=1}^{\infty} (-1)^n (c_{-n} + c_n) \cos n\phi + j(c_{-n} - c_n) \sin n\phi \right], \quad (29)$$

where

$$c_{\pm n} = -(j)^{1-n} a_{\pm n}^s. \quad (30)$$

The coefficients $c_{\pm n}$ can be expressed in terms of cylinder functions of positive order,

$$c_{\pm n} = +j \left\{ \frac{\frac{\epsilon}{\epsilon_0} \frac{\beta}{\beta_2} \left[\frac{n}{\beta_2 a} \left(1 \pm \frac{k}{\mu} \right) - \frac{J_{n+1}(\beta_2 a)}{J_n(\beta_2 a)} \right] - \frac{n}{\beta a} + \frac{J_{n+1}(\beta a)}{J_n(\beta a)}}{\frac{\epsilon}{\epsilon_0} \frac{\beta}{\beta_2} \left[\frac{n}{\beta_2 a} \left(1 \pm \frac{k}{\mu} \right) - \frac{J_{n+1}(\beta_2 a)}{J_n(\beta_2 a)} \right] - \frac{n}{\beta a} + \frac{H_{n+1}^{(2)}(\beta a)}{H_n^{(2)}(\beta a)}} \right\} \frac{J_n(\beta a)}{H_n^{(2)}(\beta a)} E_0. \quad (31)$$

APPROXIMATION FORMULAS

A. Thin Cylinder, $\beta a \ll 1$, $\beta_2 a \ll 1$

It is assumed that the wavelength is much larger than the radius of the cylinder. Then the cylinder functions can be expanded in power series and by keeping only the first terms (22) becomes

$$a_0^s = -\frac{1}{4} \pi (\beta a)^2 \left(\frac{\epsilon}{\epsilon_0} - 1 \right) E_0 j \quad (24)$$

$$a_{\pm n}^s = \pm \frac{n}{2^{2n}(n!)^2} \pi (\beta a)^{2n} \frac{\frac{\mu_0}{\mu_{\text{eff}}} \left(1 \pm \frac{k}{\mu} \right) - 1}{\frac{\mu_0}{\mu_{\text{eff}}} \left(1 \pm \frac{k}{\mu} \right) + 1} E_0 (j)^{n+1}. \quad (25)$$

For the dielectric case ($k=0$),

$$a_n^s = -a_{-n}^s. \quad (26)$$

In the first approximation all terms except the ones with $n=0, \pm 1$ can be neglected,

For the dielectric case one obtains $c_n = c_{-n}$ and the sine term in (29) vanishes. This results in a symmetrical pattern with respect to $\phi=0$. If the approximation for the thin cylinder is used, (25) and (30) yield

$$c_{\pm n} = \pm \frac{n}{2^{2n}(n!)^2} \pi (\beta a)^{2n} \frac{\frac{\mu_0}{\mu_{\text{eff}}} \left(1 \pm \frac{k}{\mu} \right) - 1}{\frac{\mu_0}{\mu_{\text{eff}}} \left(1 \pm \frac{k}{\mu} \right) + 1} E_0 \quad (32)$$

so that the $c_{\pm n}$'s are real. It can be easily shown that the amplitude of $E_z(r, \phi)$ is an even function of ϕ . In order to obtain an asymmetrical pattern the $c_{\pm n}$'s have to be complex, that is, the second-order approximations of the cylinder functions have to be taken in (22). Hence, an almost symmetrical pattern of the field strength for a cylinder for which $a \ll 1/\beta_2 = \lambda^2/2\pi$ is to be expected. In the X-band region the wavelength is about 3 cm in free space and 1 cm in ferrite. That requires $\ll 1.5$ mm.

It is interesting to note, however, that the phase angle θ of the field is an odd function of the scattering angle ϕ in the thin cylinder approximation. From (29) one obtains

$$\tan \theta = \frac{\sum_{n=1}^{\infty} (-)^n (c_{-n} - c_n) \sin \phi}{c_0 + \sum_{n=1}^{\infty} (-1)^n (c_{-n} + c_n) \cos \phi} \cong \frac{\left(\frac{\mu_0}{\mu_{\text{eff}}}\right)^2 \frac{k}{\mu} \sin \phi}{\left[\left(\frac{\mu_0}{\mu_{\text{eff}}}\right)^2 \left(1 + \left(\frac{k}{\mu}\right)^2\right) - 1\right] \cos \phi - \frac{1}{2} \left(\frac{\epsilon}{\epsilon_0} - 1\right) \left[\left(\frac{\mu_0}{\mu_{\text{eff}}} + 1\right)^2 - \left(\frac{k}{\mu} \frac{\mu_0}{\mu_{\text{eff}}}\right)^2\right]} = \frac{a \sin \phi}{b \cos \phi - c}, \quad (33)$$

where a , b , and c are defined by this equation. The maximum phase difference is given by $d/d\phi(\tan \theta) = 0$, which yields a deflection angle

$$\phi_{\text{max}} = \cos^{-1} \frac{b}{c}. \quad (34)$$

NUMERICAL EVALUATION

Eq. (33) shows that the phase angle of the scattered wave does not depend on the wavelength or the cylinder radius in the first approximation for the thin cylinder. To get an idea of the order of magnitude of phaseshift, let us consider some typical values for the parameters μ_0/μ_{eff} and ϵ/ϵ_0 .

$$\frac{\mu_0}{\mu_{\text{eff}}} = 1, \quad \frac{\epsilon}{\epsilon_0} = 11.$$

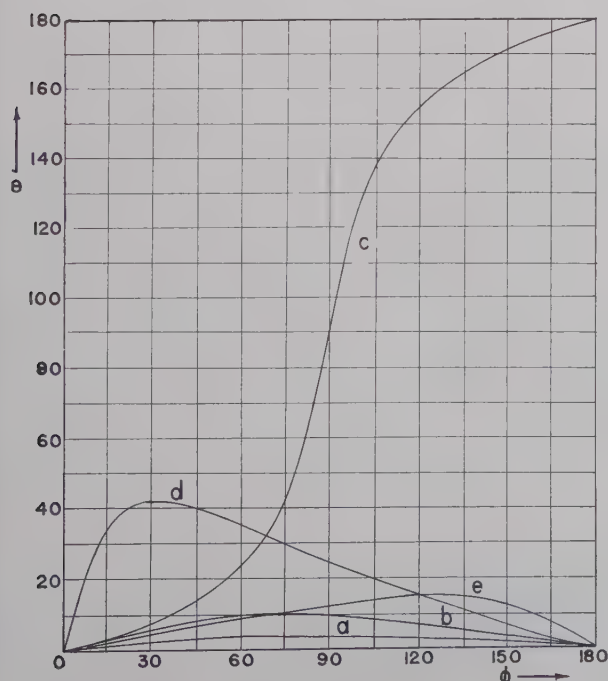


Fig. 2—Phase angle θ of scattered wave as a function of scattering angle ϕ for thin cylinder far field approximation. (a) $k/\mu=1$; (b) $k/\mu=1.5$; (c) $k/\mu=1.8$; (d) $k/\mu=2$; (e) $k/\mu=2.5$.

Then (33) becomes

$$\tan \theta = \frac{\frac{k}{\mu} \sin \phi}{\left(\frac{k}{\mu}\right)^2 \cos \phi + 5 \left(\frac{k}{\mu}\right)^2 - 20}. \quad (35)$$

Fig. 2 gives $\theta(\phi)$ for various values of k/μ . For small and large values of k/μ the largest phaseshift is at a deflection angle $\phi \sim 90^\circ$. For values $1.83 < k/\mu < 2.24$, where $\tan \theta$ becomes infinite at certain deflection angles, the phase angle θ is steadily increasing in the positive direction of ϕ resulting in a spiral wave (Fig. 3). This result can be explained by means of the precessing magnetic dipoles. From (33) it can be seen that for a nondielectric cylinder ($\epsilon/\epsilon_0=1$) the scattered wave is spiral for all values of the magnetic field (e.g. for all values of $k/\mu \neq 0$). For high values of ϵ/ϵ_0 and low values of k/μ , however, the dielectric properties of the ferrite are predominant, and the spiral wave is "covered up" by the wave scattered on a dielectric cylinder.

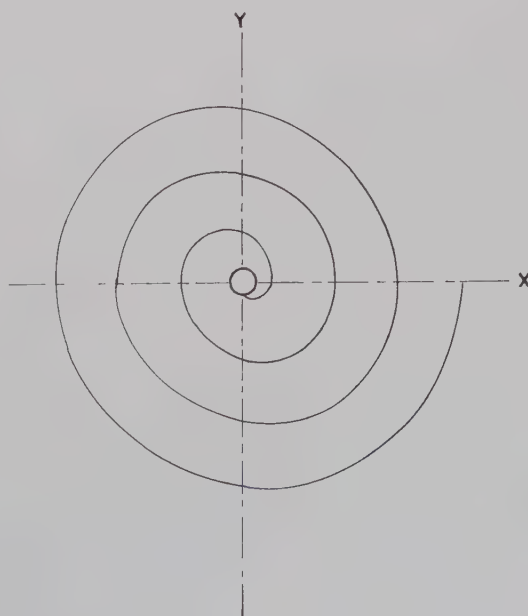


Fig. 3—Spiral wave scattered from thin cylinder. The spiral represents a line of constant phase.

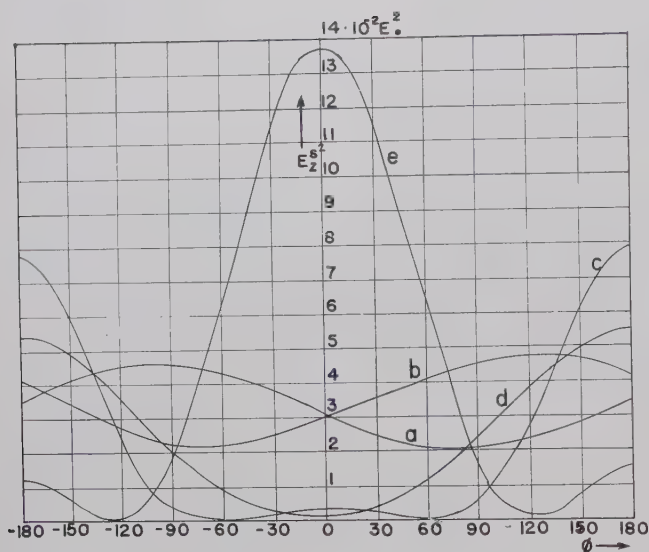


Fig. 4—Amplitude $(E^{\text{scat}})^2$ of scattered electric field as a function of scattering angle ϕ . (a) $\beta a = 0.475$, $\beta_2 a = 1.42$, $a = 2.5 \cdot 10^{-3} m$, $k/\mu = 0.5$, $\beta r = 20$. (b) $\beta a = 0.475$, $\beta_2 a = 1.42$, $a = 2.5 \cdot 10^{-3} m$, $k/\mu = 3$, $\beta r = 20$. (c) $\beta a = 0.475$, $\beta_2 a = 3.80$, $a = 5.0 \cdot 10^{-3} m$, $k/\mu = 3$, $\beta r = 20$. (d) $\beta a = 0.475$, $\beta_2 a = 1.42$, $a = 2.5 \cdot 10^{-3} m$, $k/\mu = 0.25$, $\beta r = 20$. (e) $\beta a = 0.475$, $\beta_2 a = 2.85$, $a = 2.5 \cdot 10^{-3} m$, $k/\mu = 0.25$, $\beta r = 20$.

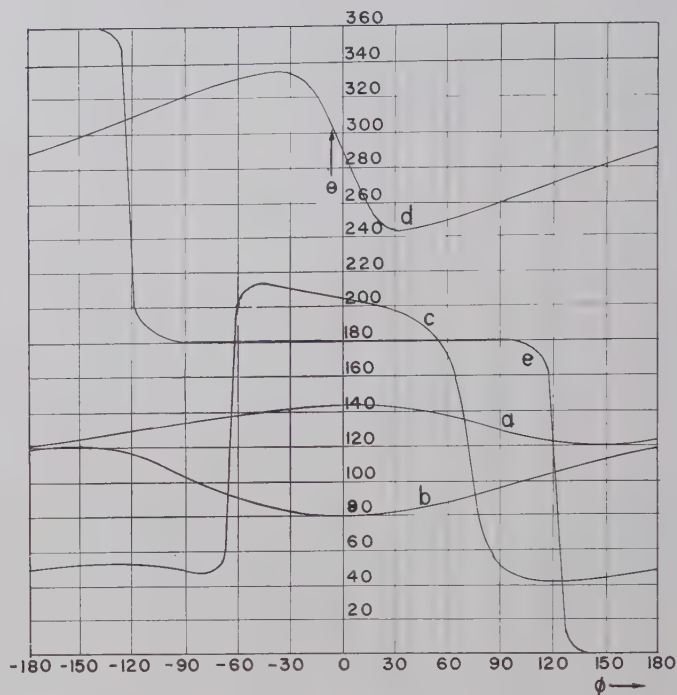


Fig. 5—Phase angle θ of scattered electric field as a function of scattering angle ϕ . (a) $\beta a = 0.475$, $\beta_2 a = 1.42$, $a = 2.5 \cdot 10^{-3} m$, $k/\mu = 0.5$, $\beta r = 20$. (b) $\beta a = 0.475$, $\beta_2 a = 1.42$, $a = 2.5 \cdot 10^{-3} m$, $k/\mu = 3$, $\beta r = 20$. (c) $\beta a = 0.475$, $\beta_2 a = 3.80$, $a = 5.0 \cdot 10^{-3} m$, $k/\mu = 3$, $\beta r = 20$. (d) $\beta a = 0.475$, $\beta_2 a = 1.42$, $a = 2.5 \cdot 10^{-3} m$, $k/\mu = 0.25$, $\beta r = 20$. (e) $\beta a = 0.475$, $\beta_2 a = 2.85$, $a = 2.5 \cdot 10^{-3} m$, $k/\mu = 0.25$, $\beta r = 20$.

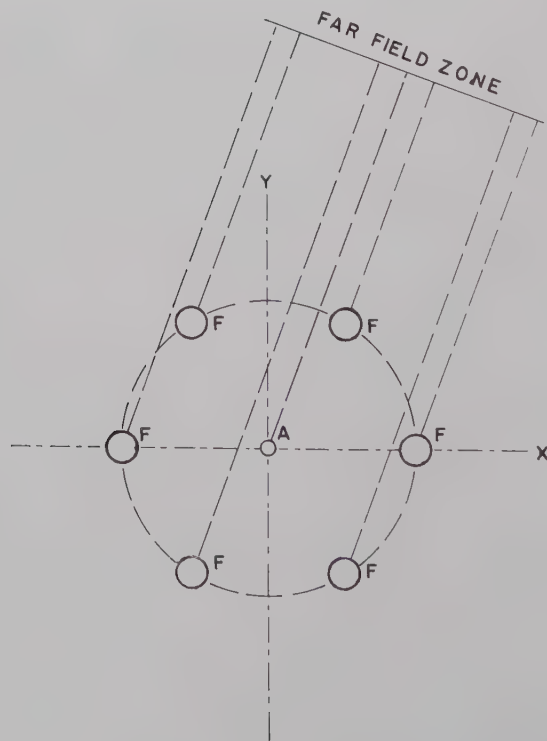


Fig. 6—Circular arrangement of six ferrite cylinders (F) around an antenna (A). The waves scattered from the cylinders are in phase with the incident wave from the antenna in the desired direction and 180° out of phase in the opposite direction.

Numerical calculations of (14) have been carried out on a Univac computer. In order to simplify the programming, the derivatives of cylinder functions and cylinder functions of negative order have been replaced by cylinder functions of positive order [see (31)].

The amplitude and phase of the electric field have been plotted in Figs. 4 and 5. For certain values of the parameters, a , k/μ , β_2 this exact solution yields also a spiral wave. It is interesting to note that except for high values of k/μ either the amplitude or the phase of the electric field is an odd function of the scattering angle ϕ , so that the scattered field is always asymmetrical.

DISCUSSION AND CONCLUSIONS

The foregoing discussion shows that the scattered field from a ferrite cylinder is in most cases asymmetrical about the direction of incidence. The direction of maximum field strength depends on the dc magnetization of the ferrite. By a suitable arrangement of several cylinders, as shown in Fig. 6, the scattered field can be concentrated in one direction. Here the phases of the scattered waves are in phase with the incident wave in the desired direction and 180° out of phase in the opposite direction. With a cyclic application of the magnetic dc field the field pattern is rotated. In order to distort

the field as little as possible under this rotation a large number of scatterers should be used.

Because of the abrupt phase change for certain values of the deflection angle, it seems possible to obtain a narrow beam of a few degrees. The large variations of the amplitude, however, will result in strong sidelobes.

For the design of such an antenna the scattering pattern of the ferrite cylinder has to be measured. Then the time function of the magnetic dc field, which gives the desired antenna pattern, has to be determined.

The advantage of such an electronic scanning antenna is the lack of mechanical parts and the weightless rotation which allows much higher scanning speeds than with a mechanical system.

ACKNOWLEDGMENT

The author wishes to express his sincere appreciation to Prof. B. Davison for suggesting the problem and to A. E. Misek, of the Computing Center of Case Institute of Technology, for obtaining the numerical results of (14). He would, also like to thank Dr. J. R. Wait, National Bureau of Standards, for the information that this problem has also been treated by V. V. Nikol'skii in *Radiotekhnika i Elektronika*, vol. 3, pp. 756-759, 1958 (in Russian).

Phase Adjustment Effects on Cascaded Reflex Klystron Amplifiers*

KORYU ISHII†, MEMBER, IRE

Summary—Reflex klystrons (type 2K25) were used as regenerative amplifiers for the X-band. Two 2K25 reflex klystron amplifiers were cascaded with a coupling circuit which contained a variable phase shifter. The effect of the phase adjustment was investigated in comparison with another coupling scheme which did not contain the phase shifter. The phase adjustment in the coupling circuit gave the amplifier system high gain (more than 50 db max.), and a reasonably low noise figure (8 db-17.5 db). High sensitivity was obtained. Proper phase adjustment of the two stage reflex klystron amplifier could give more than twice the gain in db of the single stage amplifier because of the regenerative feedback between stages. The linearity and dynamic range were considerably improved by the phase adjustment. But the frequency bandwidth became narrow (2 mc), and improvement in stability and directivity was not significant.

* Received by the PGMTT, February 3, 1960; revised manuscript received, April 11, 1960. A part of this original work was done while the author was with the Dept. of Electrical Engineering, University of Wisconsin, Madison, Wis.; supported by the University Research Committee.

† Marquette University, Milwaukee, Wis.

INTRODUCTION

IT has been shown that ordinary reflex klystrons are usable as microwave regenerative amplifiers.¹⁻⁶ In order to obtain high gain, it is natural to think about cascading the reflex klystron amplifiers. This is, however, a rather complicated problem, because a part of the amplified power reflects back and forth between

¹ K. Ishii, "X-band receiving amplifier," *Electronics*, vol. 28, pp. 202-210; April, 1955.

² K. Ishii, "Oneway circuit by the use of a hybrid T for the reflex klystron amplifier," *PROC. IRE*, vol. 45, p. 687; May, 1957.

³ C. F. Quate, R. Kompfner, and D. A. Chisholm, "The reflex klystron as a negative resistance type amplifier," *IRE TRANS. ON ELECTRON DEVICES*, vol. ED-5, pp. 173-179; July, 1958.

⁴ K. Ishii, "Impedance adjustment effects on reflex klystron amplifier noise," *Microwave Journal*, vol. 2, pp. 43-46; December, 1959.

⁵ K. Ishii, "Reflex klystron as receiver amplifiers," *Electronics*, vol. 33, pp. 56-57, January 8, 1960.

⁶ K. Ishii, "Using reflex klystrons as millimeter-wave amplifiers," *Electronics*, vol. 33, pp. 71-73; March 18, 1960.

stages. Phase adjustments of the power fed back between stages have strong influence upon the amplifier performance. In this paper, the phase adjustment effects are described for various kinds of coupling networks of the cascaded 2K25 reflex klystron amplifiers operated in the 9000 mc band.

The reflex klystron amplifier is essentially a one port amplifier. Some types of parametric amplifiers and maser amplifiers are also one port amplifiers. Therefore, the data obtained by investigation of cascading method of the reflex klystron amplifier may suggest an interesting reference to cascading maser or parametric amplifiers.

PHASE ADJUSTMENT EFFECTS ON AMPLIFIER PERFORMANCE

A schematic diagram of the cascaded 2K25 reflex klystron amplifier is shown in Fig. 1. Two reflex klystron amplifiers are coupled by a coupling network which has a variable phase shifter.

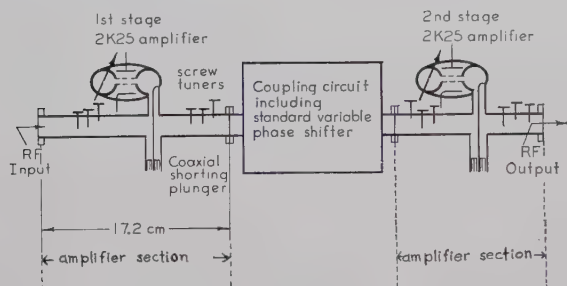


Fig. 1—Cascaded 2K25 reflex klystron amplifier.

In order to have positive feedback, the power fed back must be approximately in phase with the input power or with the electron beam power delivered to the circuit. The phase of the positive feedback can be controlled by the phase shifter.

When the electron beam power is too large, the tube will start oscillating instead of amplifying. The electron beam power can be reduced by the phase shifter, since it controls the phase of the feedback, and hence oscillation can be stopped.

When the tubes are in the amplifying condition, the phase shifter can be used to control the phase of the feedback to obtain optimum gain. Therefore, gain of the amplifier is adjustable by means of the variable phase shifter.

Phase adjustment of the feedback circuit of the cascaded reflex klystron amplifier also affects noise, stability, linearity, and bandwidth as in the case of an ordinary feedback amplifier. If the phase is adjusted so that the amplifier is approaching a near-oscillation condition, generally, the amplifier has high gain, but is noisy, unstable, and has a narrow bandwidth.

Saturation of the cascaded reflex klystron amplifier is mainly caused by both nonlinearity of the electronic

impedances of the amplifier tubes, and external circuit impedance. But these electronic and circuit impedances can be controlled by the phase adjustment of the feedback circuit. Then, the linearity, or dynamic range of the cascaded reflex klystron amplifier is adjustable using a variable phase shifter in the coupling circuit.

Thus, phase adjustment in the coupling network affects the gain, bandwidth, noise figure, stability, sensitivity, and linearity of the cascaded reflex klystron amplifier.

PHASE ADJUSTMENT EFFECTS ON GAIN

When operated at high gain, the gain of a regenerative amplifier of this type is extremely sensitive to very small changes in the impedance presented to its input and output terminals. To obtain reasonable stability and accurate measurement of gain, it was necessary to isolate the input and output of the amplifier system with ferrite isolators. The amplifier system was preceded by a series assembly of a ferrite isolator and several attenuator pads. System stability was achieved by this along with another isolator, and an attenuator pad assembly which was placed before a superheterodyne receiver, which measures gain. This isolator had two effects. The first was the isolation of the amplifier system from load impedance variation, and the second was the prevention of local oscillator disturbance to the amplifier system. The output of the amplifier system was indicated by the output meter of the superheterodyne receiver.

To determine its gain, the amplifier system was replaced by a waveguide section through the use of waveguide switches. The attenuator of the test oscillator was then adjusted to obtain the same output meter reading that was achieved with the amplifier system. The difference between the attenuator readings in the two cases was considered to be the system gain.

Phase characteristics of gains of various kinds of cascaded 2K25 reflex klystron amplifiers are shown in Fig. 2. Curve I shows a phase characteristic of a phase shifter coupled amplifier tested at 9362 mc. Two reflex klystron amplifiers are coupled by a variable phase shifter. As was considered in the previous section, gain was sharply dependent on phase, and regions of oscillation and amplification appear alternately with an increase in phase shift. The oscillation regions are indicated by the shaded areas in Fig. 2. In the case of curve I, the oscillation was critical and it was a near-oscillation condition in the shaded regions. The phase margin, which is the phase shift necessary to keep the gain within 3 db of the optimum gain, was 4° for this amplifier.

Curve II in Fig. 2 shows a phase characteristic of an isolator-phase shifter coupled amplifier tested at 9365 mc. Two 2K25 reflex klystron amplifiers were coupled with an isolator and a phase shifter. In this case, a practical isolator is being considered, that is, the isolation is not perfect. If the isolation were perfect, the phase

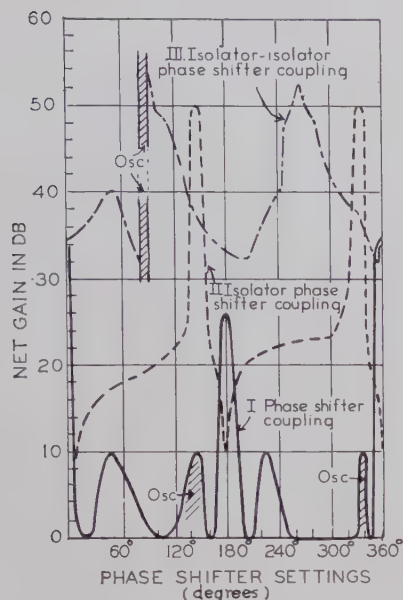


Fig. 2—Phase characteristics of the cascaded reflex klystron amplifiers.

shifter would have no effect on over-all behavior of the amplifier, because no feedback would exist. On the other hand, a practical isolator allows significant feedback to occur because of imperfect isolation. The isolator used in this experiment had 0.5 db forward loss and 30 db backward attenuation at the operating frequency. As a matter of fact, curve II shows that the gain of the amplifier depends upon the phase shifter settings. The phase shifter controls the phase of the power fed back between stages even though there is an isolator. The phase margin was 3° , and was very small, but, because of the isolator, the amplification region extends over a considerable range of the phase shifter setting.

Curve III in Fig. 2 shows a phase characteristic of an isolator-isolator-phase shifter coupled amplifier tested at 9359 mc. This amplifier was formed by coupling two reflex klystron amplifiers with two isolators followed by a variable phase shifter. In this case, the isolation was increased but phase adjustment still had strong influence upon gain. According to curve III, the phase margin was 20° , and the region over which amplification took place was larger than either of the two amplifiers mentioned before. Phase-sensitivity was decreased by increasing the isolation, and the isolation made the realization of higher gain through phase adjustment easier.

EFFECTS OF PHASE SHIFTER ON FREQUENCY CHARACTERISTICS

The use of a phase shifter in a coupling network of a cascaded reflex klystron amplifier usually makes the system frequency sensitive, because the phase shifter itself is one of the most frequency sensitive parts of the system. The frequency sensitivity is caused by the inevitable physical length of the phase shifter. In other words, the phase shifter makes the system narrow band.

For example, when two reflex klystron amplifiers were coupled directly without using the phase shifter, the bandwidth was 6 mc for 30-db gain. On the other hand, bandwidth of the phase shifter coupled amplifier was 2 mc for 43-db gain.

An example of the frequency characteristic of a phase shifter-isolator coupled amplifier is shown in Fig. 3. For comparison, the frequency characteristics of the individual stages are also plotted. The total gain was not equal to the sum of the gains in db of the individual stages because of the feedback. The effect of the negative feedback can be observed at the edges of the selectivity curve where the total gain is less than that of the individual stages. The over-all bandwidth was 2 mc. A somewhat higher gain than that shown in Fig. 3 can be obtained, if the circuit constants are very carefully adjusted.

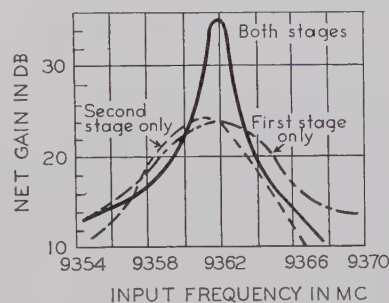


Fig. 3—Frequency characteristics of phase shifter-isolator coupled amplifier.

PHASE ADJUSTMENT EFFECTS ON NOISE FIGURES

Phase adjustment of the feedback circuit of a regenerative amplifier can control the noise of the system. In the case of the cascaded reflex klystron amplifier, similar effects were observed. Noise figures of various kinds of cascaded reflex klystron amplifiers are listed in Table I. The experiment showed that any reflex klystron amplifier system which employed the phase shifter in the coupling network generally had a considerably lower noise figure than the other kinds of amplifiers which did not have the phase shifter in the coupling network. As was considered in the early part of this paper, this result can be explained as follows. Improper phase of feedback may make the amplifier system noisy due to proximity to the near-oscillation condition. This improper phase is corrected by the variable phase shifter.

TABLE I
NOISE FIGURES OF CASCADED REFLEX KLYSTRON AMPLIFIERS

Types of Amplifiers	Noise figures (db)
Direct coupled	28
Isolator coupled	26
Phase shifter coupled	16
Isolator-phase shifter coupled	8
Phase shifter-isolator coupled	17.5

PHASE ADJUSTMENT EFFECTS ON STABILITY

The stability, that is the gain fluctuations with time, of various kinds of cascaded reflex klystron amplifiers were examined using an automatic output recorder for several hours for each kind of amplifier system. In order to keep the ambient temperature constant, the klystron tubes were mounted within $7 \times 8.5 \times 11.5$ cm brass boxes of 2 mm wall thickness. Because of the heat capacity of this scheme, after a one hour warming up period, the environmental temperature of the tube itself remained quite constant. For example, placing a hand on the box or blowing on the box did not affect the gain. In order to avoid instability caused by the power supply, an electronically regulated power supply was used for the anodes of the reflex klystrons, and a battery was used to give stable repeller voltage for each individual tube. The experimental results are listed in Table II. According to this table, when the phase shifter alone

TABLE II
STABILITY OF CASCADED REFLEX
KLYSTRON AMPLIFIERS

Types of Amplifiers	Number of isolators	Stability, average gain fluctuation db/10 minutes
Direct coupled	0	0.08
Phase shifter coupled	0	0.1
Isolator coupled	1	0.066
Isolator-phase shifter coupled	1	0.023
Phase shifter-isolator coupled	1	0.05
Isolator-isolator coupled	2	0.025
Isolator-isolator-phase shifter	2	0.00
Phase shifter-isolator-isolator	2	0.02
Isolator-phase shifter-isolator	2	0.044

was used in the coupling network, the stability improvement was not significant. On the other hand, when the phase shifter was used together with one or more isolators, the stability was somewhat improved in comparison with a case in which an isolator alone was used.

PHASE ADJUSTMENT EFFECTS ON LINEARITY

Linearity of the cascaded 2K25 reflex klystron amplifier was improved with the employment of the phase adjustment in the coupling circuit.

Input power versus output power characteristics of two kinds of cascaded reflex klystron amplifiers, namely, the direct coupled amplifier and the phase shifter coupled amplifier, are shown in Fig. 4. In the case of the direct coupled amplifier, since the two reflex klystron amplifiers were connected directly, no phase adjustment was made between the two amplifier sections. The amplifier sections are shown in Fig. 1. In the case of the phase shifter coupled amplifier, the two amplifier sections were coupled with a variable phase shifter, and this was adjusted to give an optimum gain to the amplifier system. The phase shifter coupled amplifier apparently has wider dynamic range and lower noise output level than the direct coupled amplifier.

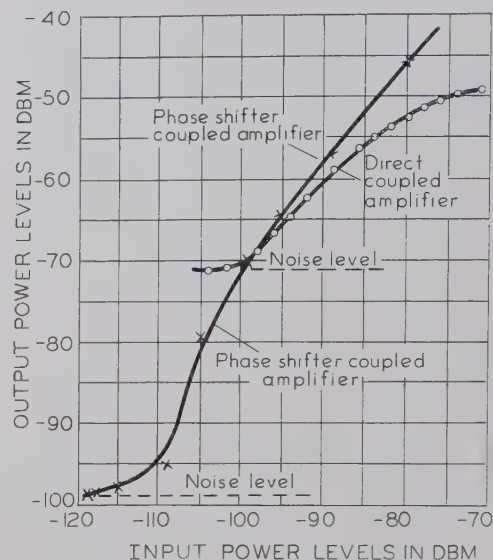


Fig. 4—Linearity of cascaded reflex klystron amplifiers.

PHASE ADJUSTMENT EFFECTS ON SENSITIVITY

It has been experimentally shown that employment of the phase adjustment in the coupling circuit of the cascaded 2K25 reflex klystron amplifier decreases noise and increases gain. Then, the sensitivity must be increased. In this case, the sensitivity was defined as the minimum detectable input power level in dbm of this amplifier-receiver system. Experimental results showed that the sensitivity improvement of the phase shifter coupled amplifier over the sensitivity of the direct coupled amplifier was 15 db. This can be seen from Fig. 4 if the minimum detectable input signal levels of these two curves are compared.

In a similar way, the phase shifter coupled amplifier showed a sensitivity 15 db higher than that of the isolator coupled amplifier, and 7 db higher than that of the isolator-isolator coupled amplifier. When the phase shifter was used together with one isolator in the coupling circuit, the sensitivity improvement over that of the isolator coupled amplifier was 22 db. When the phase shifter was used together with two isolators the sensitivity improvement over the sensitivity of the isolator-isolator coupled amplifier ranged from 14 to 20 db depending upon the position of the phase shifter in the coupling circuit. These results were obtained experimentally. It would be interesting to know if they can be justified theoretically. This problem may, however, not be easy because the two amplifiers are regenerative and another feedback loop is formed between stages. The phase adjustment effect on gain and noise figure must be calculated before obtaining the sensitivity theoretically.

PHASE ADJUSTMENT EFFECTS ON DIRECTIVITY

Because of the very nature of the circuit construction of this kind of amplifier, the amplified power is radiated generally in both directions—one part into the load of the amplifier system, and the other part back in the direction of the signal source.

One might expect that the directivity, which is the ratio of the forward power to the backward power from the amplifier system, would be strongly influenced by the phase adjustment of the coupling circuit. But the experimental results showed that the phase adjustment effect was not significant. For example, the directivity of the direct coupled amplifier was 10 db, and on the other hand, the directivity of the phase shifter coupled amplifier was 11 db. The phase shifter setting for optimizing gain was different from the phase shifter setting for optimizing the directivity.

CONCLUSIONS

Adjusting the phase of the feedback between the amplifier stages of the cascaded 2K25 reflex klystron ampli-

fier is necessary if more than twice the gain in db of a single stage amplifier is to be obtained. The phase adjustment gives high gain and reasonably low noise figure, and, consequently, high sensitivity is obtained. The use of the phase shifter made the system somewhat narrow band but stable. The linearity and dynamic range of the cascaded amplifier were improved considerably using the phase adjustment, but the effect of the phase adjustment on the directivity was not significant.

ACKNOWLEDGMENT

The author wishes to thank Professor E. H. Scheibe, University of Wisconsin, for his valuable discussion, and Dr. J. D. Horgan, S. Krupnik, L. Heiting, and J. Tsui, Marquette University, for their assistance.

TE Modes of the Dielectric Loaded Trough Line*

MARVIN COHN†, MEMBER, IRE

Summary—The properties of TE modes on a dielectric loaded trough waveguide have been investigated. In the case of the dominant mode of this line (TE_{20}), families of design curves giving the field distribution, guide wavelength, power handling capability, wall losses, and dielectric losses as a function of operating wavelength, waveguide dimensions and dielectric constant are presented. For a loosely bound wave, the losses are comparable to those of conventional rectangular waveguide and the power handling capability is an order of magnitude greater. The apparatus and procedure used to measure guide wavelength, rate of field decay in the transverse direction, and attenuation are described. The measured performance is in close agreement with the theoretically predicted characteristics.

INTRODUCTION

THE transmission line to be investigated consists of a rectangular trough structure with a dielectric slab lying on the bottom. A cross section of this line and the coordinate system used in the analysis are shown in Fig. 1. The TE surface wave modes which can propagate in the dielectric loaded trough line have been previously determined in an analysis of the dielectric loaded parallel plane waveguide.¹ A transverse resonance approach has been used by Hatkin² to determine some of the characteristics of these TE modes on an infinite dielectric sheet. The dielectric loaded parallel

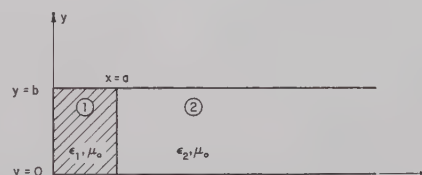


Fig. 1—Cross section of the dielectric loaded trough line. The positive z direction is out of the paper.

plane waveguide consists of two dielectric loaded trough waveguides lying back to back along the $x=0$ plane with the common conducting plate removed. The above mentioned analysis has shown that the dielectric loaded parallel plane waveguide can support a class of TE modes, whose field structure is similar to the TE modes of rectangular waveguide. These TE modes display either even or odd symmetry about the geometrical plane of symmetry ($x=0$). The even symmetry modes correspond to m being an odd integer and vice versa. It was further shown that if a conducting wall is placed at the $x=0$ plane, all of the even TE modes will be suppressed, but the odd modes will be unaffected. The dominant mode of the resulting trough line (half of the original line) will be the TE_{20} mode.

The purpose of this extension to the previous work is to present a series of design curves applicable to the trough line. It is recommended that the reader refer to the earlier work for a derivation of the properties of the odd symmetry TE modes.

A dielectric loaded trough line has been built and measurements have been made of the guide wavelength, rate of field decay in the transverse direction and at-

* Received by the PGM-TT, February 8, 1960, revised manuscript received, April 21, 1960. This research was supported by the U. S. Air Force through the Wright Air Dev. Div., of the Air Res. and Dev. Command.

† Radiation Lab., The Johns Hopkins University, Baltimore, Md.
1 M. Cohn, "Propagation in a dielectric-loaded parallel plane waveguide," IRE TRANS. ON MICROWAVE AND THEORY TECHNIQUES, vol. MTT-7, pp. 202-208; April, 1959.

2 L. Hatkin, "Analysis of propagating modes in dielectric sheets," PROC. IRE, vol. 42, pp. 1565-1568; October, 1954.

tenuation in order to verify the theoretically predicted performance.

FIELD DISTRIBUTION

It has been previously shown,¹ that the fields of the trough line TE modes are sine or cosine functions of x in the dielectric region and decay exponentially in the air space according to $e^{k_{20}(a-x)}$. In the case of the dominant mode, the angle of sinusoidal or cosinusoidal variation is restricted to the second quadrant ($\pi/2 < k_{10}a < \pi$). Fig. 2 is a family of curves of $(k_{10}a)$ as a function of $(2a/\lambda_0)$ and the difference between the inner and outer dielectric constants (ΔK), where $\Delta K = K_1 - K_2 = \epsilon_1/\epsilon_0 - \epsilon_2/\epsilon_0$. A similar family of curves for the outer transverse distribution parameter ($k_{20}a$) is presented in Fig. 3. The field configuration of this mode is identical to that previously published¹ for the TE₂₀ mode of the parallel plane line.

POWER HANDLING CAPABILITY

If the field intensities are the same, the axial power flow of a TE mode on the trough line is equal to half of the axial power flow of the corresponding TE mode of the parallel plane line.

$$P_{zo} = \frac{|A_o|^2 \pi b a}{2} \sqrt{\frac{\mu_0}{\epsilon_0}} \left(\frac{2a}{\lambda_0} \right) \frac{\sqrt{\pi^2 K_1 \left(\frac{2a}{\lambda_0} \right)^2 - (k_{10}a)^2}}{2(k_{10}a)^2} \cdot \left[1 - \frac{\tan k_{10}a}{k_{10}a} \right]. \quad (1)$$

For the TE₂₀ mode, the maximum electric field is located in the dielectric at the transverse position where $k_{10}x = \pi/2$. As a safety factor, the breakdown power level P_{bd} will be calculated assuming that the maximum electric field E_{bd} which can exist is the breakdown field of air (despite the fact that this maximum field occurs in a dielectric loaded region). E_{bd} is taken as 15,000 volts per centimeter (a safety factor of approximately two) to conform to standard waveguide calculations. From the equation for E_{y1} , it is apparent that

$$|A_o| = \frac{k_{10}}{\omega \mu_0} |E_{bd}|. \quad (2)$$

If (2) is substituted into (1), the following equation for the breakdown power level of the TE₂₀ mode in the trough line is obtained:

$$\frac{P_{bd}}{ab} = \frac{4.755 \cdot 10^8}{(2a/\lambda_0)} \left[1 - \frac{\tan k_{10}a}{k_{10}a} \right] \cdot \sqrt{\pi^2 K_1 \left(\frac{2a}{\lambda_0} \right)^2 - (k_{10}a)^2}. \quad (3)$$

For the case where $K_2 = 1$, this function has been calculated for several values of $(2a/\lambda_0)$ and K_1 . The result-

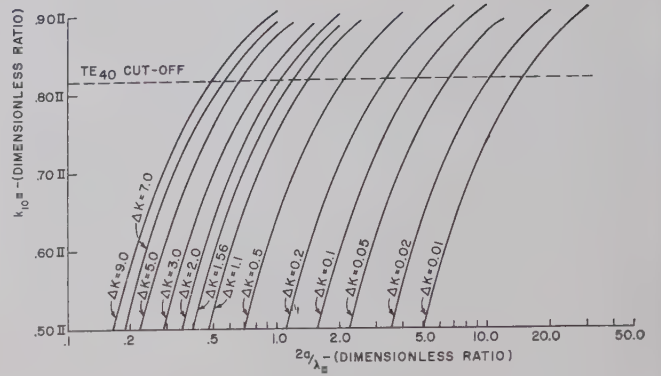


Fig. 2—Curves of the inner transverse distribution parameter ($k_{10}a$) of the TE₂₀ mode as a function of normalized slab width ($2a/\lambda_0$), and the difference of the dielectric constants (ΔK).

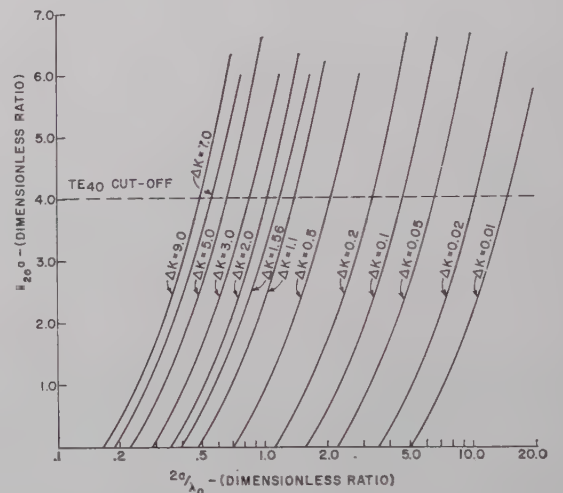


Fig. 3—Curves of the outer transverse distribution parameter ($k_{20}a$) of the TE₂₀ mode as a function of the normalized slab width ($2a/\lambda_0$) and the difference of the dielectric constants (ΔK).

ing family of curves is shown in Fig. 4. These curves show that when $(2a/\lambda_0)$ is only slightly greater than the critical magnitude required to sustain the TE₂₀ mode, P_{bd} becomes very large. This condition corresponds to a very loosely bound wave in which most of the energy is propagated in region 2 and the field extent in the x direction is very large. The TE₂₀ mode of the trough line is thus similar to the TE₁₀ mode of the dielectric loaded parallel plane line in that power levels an order of magnitude greater than those of conventional rectangular waveguide can be propagated if a sufficiently large structure (in the x direction) can be tolerated. The advantage is that single mode operation can be assured even with the larger guiding structure.

TRANSMISSION LOSSES

The attenuation due to losses in the dielectric (α_{do}) and in the parallel side walls (α_{wo}) of the trough guide is identical to that previously derived¹ for the parallel

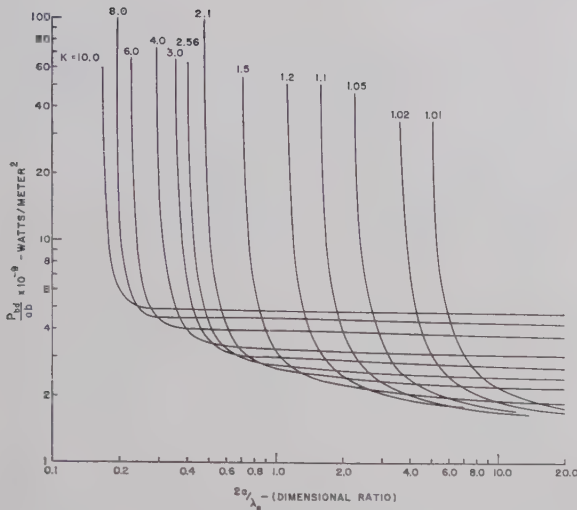


Fig. 4—Curves of the power handling capability (P_{bd}/ab) as a function of the normalized slab width ($2a/\lambda_0$) and dielectric constant (K_1). These curves are for the TE₂₀ mode and the case where the outer region is air or vacuum.

plane waveguide and hence will not be repeated. For the TE₂₀ mode and for $K_2=1$, a family of curves of the attenuation due to losses in the parallel side walls (α_{wo}) is presented in Fig. 5 for a range of ($2a/\lambda_0$) and many values of K_1 . The conductivity of copper ($\sigma_w=5.80 \times 10^7$ mhos per meter) was used in this computation. The curves of Fig. 5 may be used for other wall materials if the values of attenuation obtained from them are multiplied by the square root of the relative resistance of the substituted material. Fig. 6 is a plot of the attenuation due to the dielectric loss ($\alpha_{do}\lambda_0$) as a function of ($2a/\lambda_0$) and many values of K_1 for the TE₂₀ mode. These calculated results were plotted for a value of dielectric loss tangent $\phi_d=0.001$. These curves may be used for other values of ϕ_d if the values of α_{do} obtained are divided by 0.001 and multiplied by the loss tangent of the dielectric used.

In the case of the trough line, there is an additional component of attenuation due to the losses in the bottom plate (α_b) of the trough. The bottom plate wall loss per unit length in the z direction (P_b) is given by

$$P_b = \frac{1}{2} \sqrt{\frac{\omega\mu_0}{2\sigma_w}} \int_0^b |H_{z10}(x=0)|^2 dy$$

$$= \frac{b |A_{10}|^2}{2} \sqrt{\frac{\omega\mu_0}{2\sigma_w}} \quad (4)$$

The attenuation per unit length due to the bottom plate loss is

$$\alpha_b = \frac{P_b}{2P_{zo}} \quad (5)$$

If (1) and (4) are substituted into (5), the following equation for the attenuation due to the bottom plate loss is obtained:

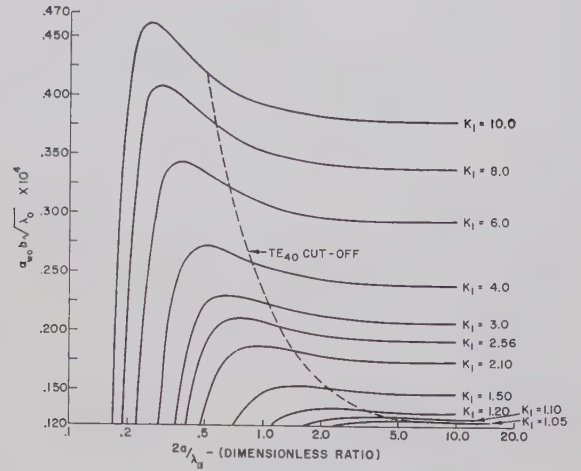


Fig. 5—Attenuation (in nepers per meter) due to the loss in the side walls as a function of the normalized slab width ($2a/\lambda_0$) and dielectric constant (K_1). These curves are for the TE₂₀ mode and the case where the outer region is air or vacuum and the wall material is copper ($\sigma=5.80 \times 10^7$ mhos per meter).

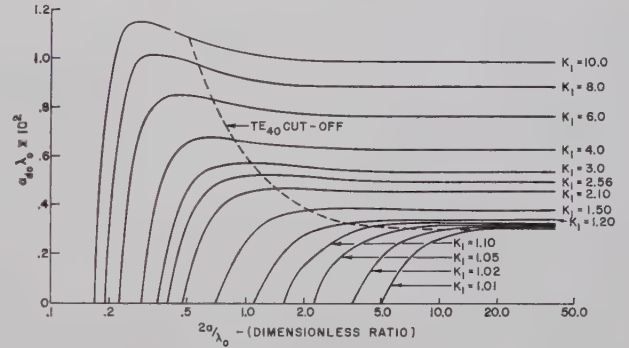


Fig. 6—Attenuation (in nepers per meter) due to the dielectric loss as a function of normalized slab width ($2a/\lambda_0$) and dielectric constant (K_1). These curves are for the TE₂₀ mode and the case where the outer region is air or vacuum. The loss tangent (ϕ_d) equals 0.001.

$$\frac{\alpha_b a^2}{\sqrt{\lambda_0}} = \frac{0.01455}{\sqrt{\sigma_w}} \cdot \frac{(k_{10}a)^3}{\sqrt{\pi^2 K_1 \left(\frac{2a}{\lambda_0}\right)^2 - (k_{10}a)^2 (k_{10}a - \tan k_{10}a)}} \quad (6)$$

Assuming that material of comparable conductivity is used for the bottom plate as is used for the parallel side walls, the bottom plate component of attenuation is negligible compared to the side wall contribution.

MEASUREMENTS

The properties of the TE₂₀ mode of the trough line have been measured in the line shown in Fig. 7. The view shown in Fig. 7 illustrates the method of constructing the line as well as the launching and collecting horns as one integral unit. The two parallel side walls of the trough are bolted firmly in place to make good electric

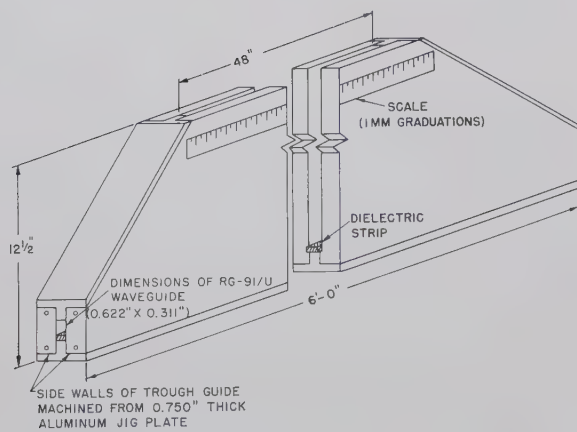


Fig. 7—Perspective view of the trough line.

contact. The spacing between these walls is maintained by the T shaped bars forming the bottom and sloping ends of the trough. Access to the inside of the line, to cement various dielectric strips in place, is easily achieved by removing one of the side walls. Fig. 8 shows a view of the inside of the trough line with one of the side walls removed. Also shown is one of the waveguide sections containing a length of dielectric tapered in the H plane. These sections provide a matched transition from the RG-91/U waveguide to the trough guide. The probe used for sampling the fields is also shown in this view. The probe is held in place by a carriage assembly which in turn slides along the top edges of the side walls of the trough. The vertical position of the probe can be changed by the rack and pinion arrangement shown. In order to insure accurate motion of the probe, the top edges of the side walls were carefully machined to be parallel to each other and to the inside of the bottom of the trough. Scales with one mm graduations and verniers were mounted on the probe and trough line so that the horizontal and vertical positions of the probe could be read to an accuracy of 0.1 mm.

The probe itself consists of Teflon filled RG-53/U waveguide (ID = 0.420 inch \times 0.170 inch) tapering to an inside dimension of 0.420 inch \times 0.006 inch at the tip. For many of the measurements it was desirable to have an even smaller aperture at the tip of the probe. In these cases silver paint was used to coat most of the opening, leaving an aperture of 0.125 inch \times 0.006 inch. A row of tapered resistance cards was mounted in front of the probe so that it appears to the impinging wave to be a matched load.

Two noncontacting short circuits were constructed. These also were held in carriages which slide on the top of the trough and whose horizontal position could be read to an accuracy of 0.1 mm. The shorts could be raised or lowered so that their lower ends were just above the top of the dielectric strip. When the dielectric strip is sufficiently thin relative to λ_0 , the rectangular waveguide formed by the length of dielectric under the short is beyond cutoff and, hence, very little energy leaks under the short.

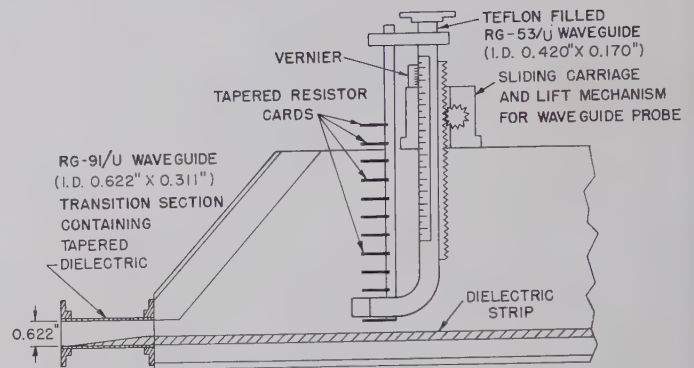


Fig. 8—Interior view of the trough line, with one side wall removed. A transition section, the probe assembly and its sliding carriage are shown.

In order to check the propagation characteristics of the TE_{20} mode of the trough line, it is necessary to determine the electrical properties of the dielectric strip independently of the trough line. The dielectric constant was measured in a rectangular waveguide using a standard short-circuited line method. The dielectric constant (K_1) was determined to be 2.60. The dielectric loss tangent (ϕ_d) was determined from measurements on a short-circuited polystyrene filled slotted line. Account was taken of the wall losses in the dielectric filled line and the dielectric loss and, hence, the dielectric loss tangent were determined from the measured decrease of VSWR with increasing distance from the short-circuited end. The average value of many measurements of loss tangent was 0.00052.

Two polystyrene strips whose thicknesses (a) were 0.399 cm and 0.638 cm were investigated. Their critical frequencies, which must be exceeded for the TE_{20} mode to propagate, were, respectively, 14.86 kmc and 9.30 kmc.

Regions of the trough line were found where the TE_{20} surface wave mode was undisturbed by radiation fields from the launching horn. A phase-sensitive bridge was set up and phase fronts were plotted in these regions and were observed to be parallel vertical planes which were properly spaced.

The waveguide wavelength (λ_g) was measured as a function of frequency in three different ways: 1) the probe and phase bridge were used to determine the spacing between successive phase fronts of equal phase; 2) a short circuit was used to set up a large reflection and the distance between nulls of the standing wave pattern was measured using the probe; and 3) two short circuits were used to set up a transmission cavity whose length could be varied. The cavity technique is described more thoroughly below in the discussion of attenuation measurements. The cavity technique gave the best results, since at resonance the surface wave fields are enhanced relative to the radiation fields. Fig. 9 shows that the measured values of λ_g are in excellent agreement with the theoretically predicted values.

The rate of field decay in a transverse direction away from the dielectric-air interface was measured by a

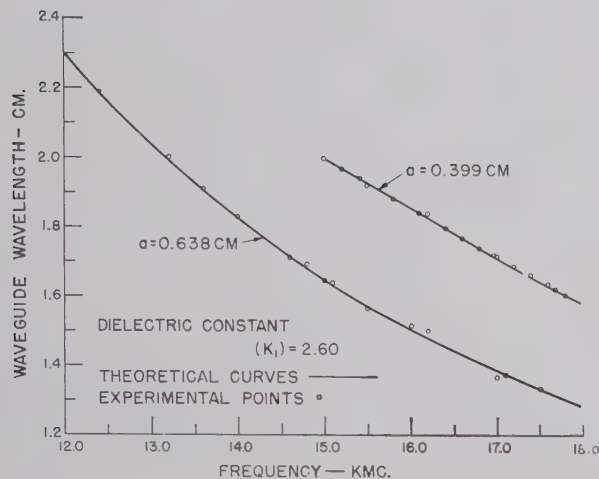


Fig. 9—Comparison of the measured and theoretical waveguide wavelength of the trough line TE_{20} mode as a function of frequency.

standard RF substitution method using the probe and a precision microwave attenuator. The experimental points and theoretical curves are shown in Fig. 10. Although individual points deviate from the theoretical curves, they follow the general direction of these curves very well. This measurement was most difficult to make in the extreme cases where the dielectric strip was either very thin (very loosely bound wave) or very thick (very tightly bound wave) compared to a wavelength. In the loosely bound case, the fields extend a large distance from the dielectric-air interface and as a result the field intensity at any point is low. In the tightly bound case, almost all of the energy propagates within the dielectric strip, but again the field intensity is very low in the air space. In each of these extreme cases, therefore, the stray radiation fields were comparable to the surface wave fields.

Measurements were made of the attenuation of this line using a variable length transmission cavity technique. This method, which has been previously discussed in the literature,³⁻⁵ is well-suited to attenuation measurements on a surface wave line. In the case of the trough line, the cavity was formed by two noncontacting shorts of the type described above. The short on the generator side was maintained in a fixed position, and the short on the detector side was adjusted to a resonant position as manifested by maximum output at the detector. The source klystron was swept in frequency causing the output waveform observed at the detector to be a replica of the cavity band-pass characteristic. The loaded Q of the cavity was determined from the three-db bandwidth of the cavity pass band character-

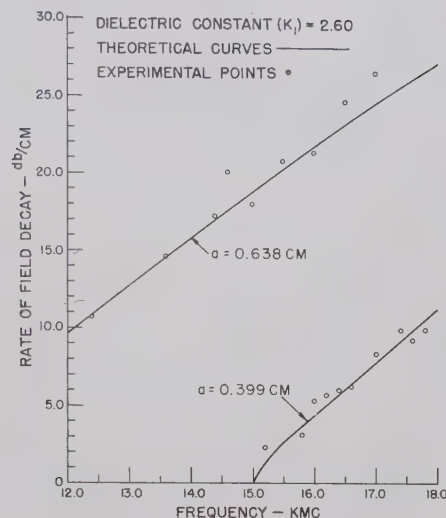


Fig. 10—Comparison of the measured and theoretical rate of field decay in the transverse direction for the trough line TE_{20} mode as a function of frequency.

istic. The short on the detector side was moved to another position where the output was maximized and again the loaded Q of the cavity was measured. The new short position is an integer number of half-waveguide wavelengths from its former position. This procedure was repeated for many short-circuit positions. From the manner in which the cavity Q varied with increasing cavity length, the attenuation per unit length of the trough guide could be determined.

The measured points and the theoretical curves of total attenuation as a function of frequency are shown in Fig. 11. The measured attenuation varies in the prescribed manner as a function of frequency; its magnitude, however, is somewhat higher than predicted. The discrepancy could be due to any or all of the following reasons:

- 1) The actual wall loss may be larger than theoretically predicted (as is invariably the case for rectangular waveguides), due to the roughness of the metal walls being comparable in magnitude to the depth of penetration of the RF currents.
- 2) The vinylite cement used to hold the dielectric strip in place has a considerably higher dielectric loss tangent than polystyrene.
- 3) Any irregularities along the line may cause radiation which would contribute to the total measured attenuation.

CONCLUSION

A number of families of curves have been presented which give the characteristics of the TE_{20} mode on a dielectric loaded trough line. If loosely bound, this mode, like the TE_{10} mode on the dielectric loaded parallel plane waveguide, has losses comparable to those of conventional rectangular waveguide and power handling capabilities an order of magnitude greater. The trough line has the advantages of being closed on three sides

³ E. H. Scheibe, B. G. King, and D. L. Van Zeeland, "Loss measurements of surface wave transmission lines," *J. Appl. Phys.*, vol. 25, pp. 790-797; June, 1954.

⁴ S. P. Schlesinger and D. D. King, "Some Fundamental Properties of Dielectric Image Line," The Johns Hopkins University Radiation Laboratory, Baltimore, Md., Final Rept. AFCRC-TN-56-766, pp. 69-78; December, 1956.

⁵ D. D. King and S. P. Schlesinger, "Losses in dielectric image lines," *IRE TRANS. ON MICROWAVE THEORY AND TECHNIQUES*, vol. MTT-5, pp. 31-35; January, 1957.

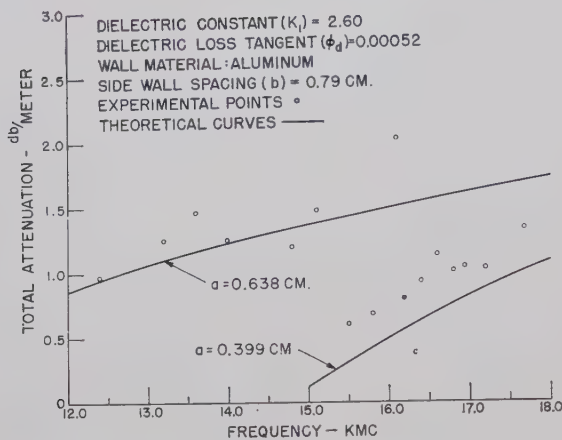


Fig. 11—Comparison of the measured and theoretical total attenuation of the trough line TE_{20} mode as a function of frequency.

and being smaller than the corresponding parallel plate line with comparable attenuation and power handling characteristics. The guide geometry and magnetic field configuration are appropriate for the fabrication of ferrite devices employing transverse magnetization.

The measurements of guide wavelength, rate of field decay and attenuation verify the theoretically predicted properties of this structure.

ACKNOWLEDGMENT

The author would like to thank Dr. E. S. Cassedy for his helpful discussions and criticisms, I. E. Pakulis for his careful carrying out of the measurements, Miss M. D. Velten for the numerical calculations and curve plotting, and J. W. Rodgers and W. Weber for construction of the trough line and associated apparatus.

Coupling of Modes in Uniform, Composite Waveguides*

L. C. BAHIANA† AND L. D. SMULLIN‡

Summary—The principle of coupling of modes is used to compute the phase constant in a uniform waveguide filled with two different dielectric materials. The natural modes of two hypothetical waveguides filled with the different dielectrics are computed. The propagation of the combined system is computed by considering the coupling between the two sets of modes. Comparison is made between the approximate theory and an exact theory.

I. INTRODUCTION

THE expression "uniform, composite waveguide" is used in this paper to describe any hollow metallic cylinder of arbitrary cross section filled with two or more homogeneous isotropic materials. Both the structure and the materials are uniform in the direction of propagation. Familiar examples of uniform, composite waveguides are waveguides partly filled with dielectric or magnetic material. The solution of the boundary value problem in such waveguides invariably leads to transcendental equations. Numerical solutions for a few particular cases have been published.¹

* Received by the PGMTT, January 20, 1960; revised manuscript received, April 14, 1960. This work was supported in part by the U. S. Army (Signal Corps), the U. S. Air Force (Office of Scientific Research, Air Research and Development Command), and the U. S. Navy (Office of Naval Research).

† Diretoria de Eletrônica da Marinha, Ministerio da Marinha, Rio de Janeiro, Brazil. Formerly with Mass. Inst. Tech., Cambridge, Mass.

‡ Dept of Electrical Engrg. and Res. Lab. of Electronics, Mass. Inst. Tech., Cambridge, Mass.

¹ T. Moreno, "Microwave Transmission Design Data," Dover Publications, Inc., New York, N. Y.; 1958.

A different formulation of the problem is presented here and applied to the case of lossless waveguides containing two media. The fields are expressed in terms of the natural modes of two hypothetical waveguides, found by imposing short-circuit ($\vec{n} \times \vec{E} = 0$) or open-circuit ($\vec{n} \times \vec{H} = 0$) constraints at the boundary between the two media. Maxwell's equations are then transformed, by the use of conventional techniques, into an infinite set of coupled transmission-line equations. Although this formulation is completely general, its practical usefulness stems from the possibility of obtaining approximate solutions without cumbersome numerical computation.

II. FORMULATION OF THE PROBLEM

A. Equivalent Current Sheets

Fig. 1 shows the cross section of a composite waveguide. Surface S_1 is the metallic envelope. Surface S_2 is the boundary between the two media. The solution of Maxwell's equations in medium 1 is unique if either $\vec{n} \times \vec{E}$ or $\vec{n} \times \vec{H}$ is specified over the boundary. The same is true of medium 2. Let $\vec{n} \times \vec{E}_2(S_2)$, where \vec{E}_2 is the unknown field in region 2, be specified over S_2 . Then we can solve Maxwell's equations in medium 1. In order to do this, surface S_2 is replaced by a metallic wall S (short circuit, with $\vec{n} \times \vec{E} = 0$) and a magnetic current sheet $\vec{K}_m = \vec{n} \times \vec{E}_2(S_2)$. Mathematically, this is equivalent to

transforming a homogeneous differential equation with inhomogeneous boundary conditions into an inhomogeneous differential equation with homogeneous boundary conditions. The solution of Maxwell's equations in medium 1 gives us the tangential magnetic field, $\bar{n} \times \bar{H}_1(S_2)$, at the boundary S_2 . Next, we solve Maxwell's equations in medium 2, with $\bar{n} \times \bar{H}_1(S_2)$ specified over S_2 . This time, we replace the surface S_2 by a magnetic wall S (open-circuit, with $\bar{n} \times \bar{H} = 0$) and an electric current sheet $\bar{K}_e = \bar{n} \times \bar{H}_1(S_2)$. By this procedure, we have split the original boundary value problem into one of two conventional waveguides, driven by electric or magnetic surface currents (Fig. 2). The two hypothetical waveguides will be called subwaveguides 1 and 2.

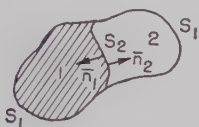


Fig. 1—Composite waveguide of arbitrary cross section.

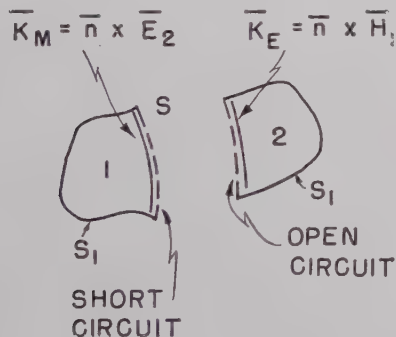


Fig. 2—Equivalent driving currents and boundary constraints.

B. Short-Circuit and Open-Circuit Expansions

The fields in the subwaveguides can be expanded in terms of E -modes and H -modes that satisfy either short-circuit or open-circuit conditions at the common boundary. If the fictitious wall S is short-circuited, the modes will be short-circuit modes; if S is open-circuited, the modes will be open-circuit modes. In either case, the modes are solutions of the scalar Helmholtz equation. These modes form a complete set.

The E -modes are given by the following:

$$\begin{aligned}\bar{e}_t^e &= -\nabla_t \phi, \\ \bar{h}_t^e &= \bar{k} \times \bar{e}_t^e, \text{ and} \\ e_z &= \frac{p_e^2}{\Gamma} \phi,\end{aligned}\quad (1)$$

where Γ is the propagation constant, \bar{k} is the unit vector in the z -direction, ϕ satisfies the equation $\nabla_t^2 \phi + p_e^2 \phi = 0$, and the boundary conditions are:

$$\left. \begin{aligned}\phi &= 0 \text{ over } S \text{ and } S_1 \\ \phi &= 0 \text{ over } S_1 \\ \bar{n} \cdot \nabla_t \phi &= 0 \text{ over } S\end{aligned} \right\} \begin{array}{l} \text{for short-circuit modes,} \\ \text{for open-circuit modes.} \end{array}$$

The H -modes are given by the following:

$$\begin{aligned}\bar{h}_t^h &= -\nabla_t \psi, \\ \bar{e}_t^h &= \bar{h}_t^h \times \bar{k}, \text{ and} \\ h_z &= \frac{p_h^2}{\Gamma} \psi,\end{aligned}\quad (2)$$

where Γ is the propagation constant, ψ satisfies the equation $\nabla_t^2 \psi + p_h^2 \psi = 0$, and the boundary conditions are:

$$\left. \begin{aligned}\bar{n} \cdot \nabla_t \psi &= 0 \text{ over } S \text{ and } S_1 \\ \psi &= 0 \text{ over } S \\ \bar{n} \cdot \nabla_t \psi &= 0 \text{ over } S_1\end{aligned} \right\} \begin{array}{l} \text{for short-circuit modes,} \\ \text{for open-circuit modes.} \end{array}$$

In terms of these modes, the transverse fields in either subwaveguide can be expressed² as

$$\begin{aligned}\bar{E}_t &= \sum_{j=1}^{\infty} V_j(z) \bar{e}_{tj}(x, y) \\ \bar{H}_t &= \sum_{j=1}^{\infty} I_j(z) \bar{h}_{tj}(x, y).\end{aligned}\quad (3)$$

This expansion includes both \bar{E} and \bar{H} modes, but the choice of the imaginary wall determines whether they are short-circuit or open-circuit modes.

If we use the orthogonality condition,

$$\int (\bar{e}_{ti} \times \bar{h}_{tj} \cdot \bar{k}) da = \delta_{ij}, \quad (4)$$

then the amplitudes V_j and I_j for the j th mode are

$$\begin{aligned}V_j(z) &= \int (\bar{E}_t \cdot \bar{h}_{tj} \times \bar{k}) da \\ I_j(z) &= \int (\bar{H}_t \cdot \bar{k} \times \bar{e}_{tj}) da,\end{aligned}\quad (5)$$

and the integration is extended over the cross section of the subwaveguide.

C. Solution of Maxwell's Equations in the Subwaveguides

Maxwell's equations for harmonic time-dependence in a loss-free region containing electric and magnetic currents are

$$\begin{aligned}\nabla \times \bar{E} &= -j\omega\mu\bar{H} - \bar{J}_m \text{ and} \\ \nabla \times \bar{H} &= j\omega\epsilon\bar{E} + \bar{J}_e.\end{aligned}$$

After separating the fields into longitudinal and transverse components, the use of (3) yields, for the longitudinal components,

² H. A. Haus, "Microwave Circuits," Course 6.621 Class Notes, Mass. Inst. of Tech., Cambridge, Mass.; 1959. (Unpublished.)

$$E_z = \frac{1}{j\omega\epsilon} \sum_{j=1}^{\infty} I_j [\nabla_t \cdot \bar{h}_{tj} \times \bar{k}] - \frac{J_{ez}}{j\omega\epsilon} \text{ and}$$

$$H_z = \frac{1}{j\omega\mu} \sum_{j=1}^{\infty} V_j [\nabla_t \bar{k} \times \bar{e}_{tj}] - \frac{J_{mz}}{j\omega\mu}. \quad (6)$$

By using (3)–(6), the transverse part of Maxwell's equations for the j th mode can be transformed into the following:

$$-\frac{dV_j}{dz} = j\omega\mu_j I_j + \frac{p_{ej}^2}{j\omega\epsilon} I_j + \int (\bar{J}_m \cdot \bar{h}_{tj}) da$$

$$+ \frac{\Gamma_{ej}}{j\omega\epsilon} \int (\bar{J}_e \cdot \bar{e}_{zj}) da$$

$$-\frac{dI_j}{dz} = j\omega\epsilon V_j + \frac{p_{hj}^2}{j\omega\mu} V_j + \int (\bar{J}_e \cdot \bar{e}_{tj}) da$$

$$+ \frac{\Gamma_{hj}}{j\omega\mu_j} \int (\bar{J}_m \cdot \bar{h}_{zj}) da. \quad (7)$$

Equations of this form have been derived, for metallic waveguides, by Marcuvitz.³ They are extended here for open-circuit modes. Detailed proofs are omitted.

D. Coupled Transmission-Line Equations

The coupling equations for a composite waveguide containing two media will now be derived. The subscript j has been retained for the subwaveguide with the short circuit imposed at the wall, and the subscript k has been used for the subwaveguide with the open circuit imposed at the boundary.

For the short-circuited subwaveguide,

$$\bar{J}_m = \bar{K}_m(S) = \bar{n} \times \bar{E}^0(S),$$

$$\bar{J}_e = 0, \quad (8)$$

where $\bar{E}^0(S)$ is the electric field in the open-circuited subwaveguide at the boundary S .

Similarly, for the open-circuited subwaveguide,

$$\bar{J}_e = \bar{K}_e(S) = \bar{n} \times \bar{H}^0(S),$$

$$\bar{J}_m = 0. \quad (9)$$

Use of (7)–(9) yields the coupling equations:

$$-\frac{dV_j}{dz} = M_{jj}I_j + \sum_k M_{jk}I_k \quad \left. \begin{array}{l} \\ \\ \end{array} \right\} \text{and} \quad (10a)$$

$$-\frac{dI_j}{dz} = N_{jj}V_j + \sum_k N_{jk}V_k$$

$$-\frac{dV_k}{dz} = M_{kk}I_k + \sum_j M_{kj}I_j$$

$$-\frac{dI_k}{dz} = N_{kk}V_k + \sum_j N_{kj}V_j \quad \left. \begin{array}{l} \\ \\ \end{array} \right\}, \quad (10b)$$

where the sums are over all the modes of the opposite subwaveguide, and the coupling terms M and N are given by

$$M_{jj} \equiv j\omega\mu_j + \frac{p_{ej}^2}{j\omega\epsilon_j} + \frac{1}{j\omega\epsilon_k} \int (\bar{h}_{tj} \cdot \bar{h}_{tj}) ds$$

$$M_{jk} \equiv \frac{\Gamma_{ek}}{j\omega\epsilon_k} \int (\bar{n} \cdot \bar{e}_{zk} \times \bar{h}_{tj}) ds$$

$$N_{jj} \equiv j\omega\epsilon_j + \frac{p_{hj}^2}{j\omega\mu_j}$$

$$N_{jk} \equiv \frac{\Gamma_{hj}}{j\omega\mu_j} \int (\bar{n} \cdot \bar{e}_{tk} \times \bar{h}_{zj}) ds \quad (11)$$

and

$$M_{kk} \equiv j\omega\mu_k + \frac{p_{ek}^2}{j\omega\epsilon_k}$$

$$M_{kj} \equiv \frac{\Gamma_{ek}}{j\omega\epsilon_k} \int (\bar{n} \cdot \bar{e}_{zk} \times \bar{h}_{tj}) ds$$

$$N_{kk} \equiv j\omega\epsilon_k + \frac{p_{hk}^2}{j\omega\mu_k} + \frac{1}{j\omega\mu_j} \int (\bar{e}_{tk} \cdot \bar{e}_{tk}) ds$$

$$N_{kj} \equiv \frac{\Gamma_{hj}}{j\omega\mu_j} \int (\bar{n} \cdot \bar{e}_{tk} \times \bar{h}_{zj}) ds \quad (12)$$

The integrals are taken along the boundary, in the transverse plane. The subscripts j and k have been used on μ and ϵ , to avoid inserting a second subscript. They are necessary because μ and ϵ of each subwaveguide appear in the equations for the other. They do not imply that ϵ and μ are different for each mode.

In the following discussion we shall consider only the case of coupling between two modes, one in each subwaveguide.

If we assume propagation of the form $e^{-\Gamma z}$ for the composite system, we obtain

$$\frac{dV_j}{dz} = -\Gamma V_j, \quad \frac{dI_j}{dz} = -\Gamma I_j,$$

$$\frac{dV_k}{dz} = -\Gamma V_k, \quad \frac{dI_k}{dz} = -\Gamma I_k. \quad (13)$$

Then the coupling equations (10a) and (10b) can be reduced to

$$[\Gamma^2 - (M_{jj}N_{jj} + M_{jk}N_{kj})]V_j$$

$$- [M_{jj}N_{jk} + M_{jk}N_{kk}]V_k = 0;$$

$$- [(M_{kk}N_{kj} + M_{kj}N_{jj})V_j$$

$$+ [\Gamma^2 - (M_{kk}N_{kk} + M_{kj}N_{jk})]V_k = 0. \quad (14)$$

Hence Γ^2 is given by

$$\Gamma^2 = \frac{1}{2}[(T_{jj} + T_{kk}) \pm \sqrt{(T_{jj} - T_{kk})^2 + 4T_{jk}T_{kj}}], \quad (15)$$

³ N. Marcuvitz, "Representation of electric and magnetic fields," *J. Appl. Phys.*, vol. 22, pp. 806–819; June, 1951.

where

$$\begin{aligned} T_{jj} &\equiv M_{jj}N_{jj} + M_{jk}N_{kj}, \\ T_{kk} &\equiv M_{kk}N_{kk} + M_{kj}N_{jk}, \\ T_{jk} &\equiv M_{jj}N_{jk} + M_{jk}N_{kk}, \text{ and} \\ T_{kj} &\equiv M_{kk}N_{kj} + M_{kj}N_{jj}. \end{aligned} \tag{16}$$

III. APPLICATIONS

In order to obtain good approximations with a few modes (preferably two), care must be taken in the choice of modes. For instance, inspection of (11) and (12) will show that M_{jk} and M_{kj} tend to be small when the dielectric constant of the open-circuit waveguide (ϵ_k) is large. Therefore, if one of the regions has a large dielectric constant, the use of open-circuit modes in this region, and of short-circuit modes in the second region, will insure small coupling between E -modes in the subwaveguides. For dielectric constants larger than 10, the subwaveguides are practically decoupled from each other, and the propagation constants can be found easily. For H -modes, the same advantage is gained if short-circuit modes are used for regions of high μ . In either case, for sufficiently high frequencies, (11) and (12) show that the modes tend to decouple, so that the propagation constants are those of each subwaveguide, taken by itself.

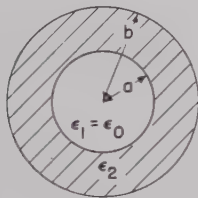


Fig. 3—Circular waveguide half-filled with dielectric material.

A. Weak Coupling (ϵ_2 large compared with ϵ_1)

As an example of how these approximations can be found, we shall take the case of a circular waveguide, half-filled with dielectric material (Fig. 3). We are looking for the dispersion characteristics of the circular symmetric TM_{01} (or E_{01}) mode.

Assuming that the two systems are completely decoupled, we solve for the open-circuit modes in the dielectric region. The boundary conditions are:

$$\begin{aligned} r = b, \quad E_z &= 0; \\ r = a, \quad H_\psi &= 0. \end{aligned}$$

The solution for the dielectric subwaveguide is found by solving:

$$\Gamma^2 = p^2 - k_2^2 = p^2 - \omega^2 \mu_0 \epsilon_2;$$

and

$$\frac{J_1(pa)}{N_1(pa)} = \frac{J_0(pb)}{N_0(pb)}.$$

When $b=2a$, for example, we find that $p=1.14\pi/b$.⁴ It follows that

$$\begin{aligned} \Gamma^2 &= -\beta^2 = -\frac{(2\pi)^2}{\lambda_0^2} = \frac{(1.14\pi)^2}{b^2} - k_2^2 \\ \beta^2 &= \omega \mu_0 \epsilon_0 \left[\frac{\epsilon_2}{\epsilon_0} \right] - \left[\frac{1.14\pi}{b} \right]^2 \end{aligned}$$

or

$$\left[\frac{2\pi}{\lambda_g} \right]^2 = \left[\frac{2\pi}{\lambda} \right]^2 \epsilon_\gamma - \left[\frac{1.14\pi}{b} \right]^2,$$

where $\epsilon_\gamma \equiv \epsilon_2/\epsilon_0$.

Finally, we obtain the approximate relationship

$$\left[\frac{\lambda}{\lambda_g} \right]^2 = \epsilon_\gamma - 1.3 \left[\frac{\lambda}{2b} \right]^2. \tag{17}$$

The exact boundary-value problem has been solved for this case, and the propagation characteristics have been plotted by Marcuvitz.⁵ The reader will see that the curves (except for $\epsilon=2.54$) shown there are described very accurately by (17).

B. Synchronous Coupling

For low values of μ and ϵ , the coupling terms cannot be ignored. In order to obtain good approximations in these cases, we take advantage of the fact that when the propagation constants of two modes are approximately equal, the contribution from all other modes may be neglected. If two modes are so chosen that their β - ω characteristics cross each other within the frequency range that is of interest, we can expect good approximations. To illustrate the method, we have calculated the propagation constants of the fundamental mode of a rectangular waveguide half-filled with dielectric of dielectric constant $\epsilon_1=2.45 \epsilon_0$. (See inset, Fig. 4.)

The fundamental mode can be found by coupling the TE_{10} modes of each subwaveguide. The approximation is good if we choose short-circuit modes in the dielectric (subwaveguide 1) and open-circuit modes in the air (subwaveguide 2) because the ω - β curves of these TE_{10} modes cross. Each of these modes is the dominant mode in its respective subwaveguide, and the crossing point is near the cutoff of each. For this simple case, (15) reduces to

$$\Gamma^2 = \frac{1}{2}[(\Gamma_1^2 + \Gamma_2^2) \pm \sqrt{(\Gamma_1^2 - \Gamma_2^2)^2 + 4K^2}],$$

⁴ E. Jahnke and F. Emde, "Tables of Functions with Formulae and Curves," Dover Publications, Inc., New York, N. Y., 4th edition, pp. 207-208; 1945.

⁵ N. Marcuvitz, "Waveguide Handbook, Radiation Laboratory Series," Vol. 10, McGraw-Hill Publishing Company, Inc., New York, N. Y., p. 395; 1951.

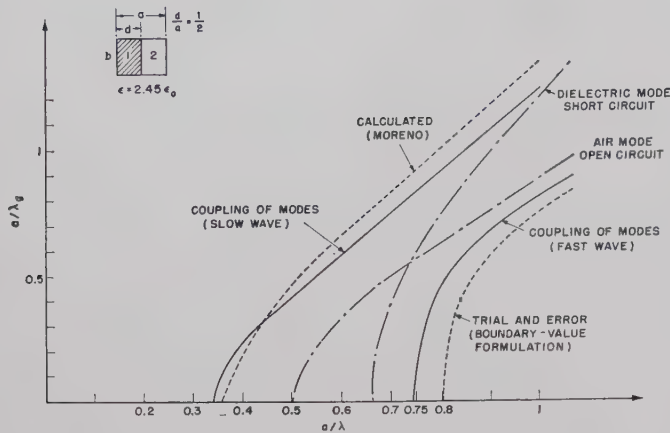


Fig. 4—Propagation in rectangular waveguide half-filled with dielectric material.

where

$$\Gamma_1^2 = p_1^2 - k_1^2 = \left[\frac{\pi}{d} \right]^2 - \left[\frac{\epsilon_1}{\epsilon_0} \right] k_0^2$$

$$k_0^2 = \omega^2 \mu_0 \epsilon_0,$$

$$\Gamma_2^2 = p_2^2 - k_0^2 = \left[\frac{\pi}{2d} \right]^2 - k_0^2$$

$$K = \frac{\pi}{d\sqrt{d(a-d)}} = \frac{4\pi}{a^2}.$$

A few algebraic transformations lead to

$$\left(\frac{a}{\lambda_g} \right)^2 = -\frac{1}{8} \left\{ 5 - 13.8 \left[\frac{a}{\lambda} \right]^2 \right. \\ \left. \pm \sqrt{3 - 5.8 \left[\frac{a}{\lambda} \right]^2 + 6.5} \right\}.$$

If we solve for the cut-off wavelength, we find that $a/\lambda_c = 0.34$ or $a/\lambda_c = 0.74$. Here we see that we obtain two solutions for $\lambda_g(\lambda)$ as a result of the coupling between the modes in the two subwaveguides. One is a slow wave, and the other a fast wave.

The results of our calculation are plotted in Fig. 4 and compared with the results of an exact computation based on the boundary-value formulation.⁶

ACKNOWLEDGMENT

The authors wish to express their appreciation to Professor H. A. Haus, and to Professor R. L. Kyhl for their many suggestions and stimulating discussions, and to Paul Chorney who read the manuscript and provided helpful criticism.

⁶ Moreno, *op. cit.*, p. 192.

CORRECTION

R. C. Johnson, author of "Design of Linear Double Tapers in Rectangular Waveguides," which appeared on pp. 374-378 of the July 1959 issue of these TRANSACTIONS has brought the following corrections to the attention of the Editor.

The first line under (2) should read "where γ_m is the propagation constant in the m th segment."

The expression for b above (7) should be

$$b = b(x) = b_0 + \frac{b_1 - b_0}{L} x.$$

The integral in (14) can be evaluated in closed form; therefore, instead of determining l through the use of (15), it is preferable to use

$$= \frac{L}{2(a_1 - a_0)} \left[\frac{2a_1}{\lambda_{g1}} - \frac{2a_0}{\lambda_{g0}} + \arctan \frac{2a_0}{\lambda_{g0}} - \arctan \frac{2a_1}{\lambda_{g1}} \right],$$

where

$$\lambda_{g0} = \frac{\lambda}{\sqrt{1 - (\lambda/2a_0)^2}} \\ \lambda_{g1} = \frac{\lambda}{\sqrt{1 - (\lambda/2a_1)^2}}.$$

The imaginary operator was left out of the exponent term of (19); it should be

$$\Gamma = \frac{i}{8\pi L/\lambda_g} \left[\frac{b_1 - b_0}{b_1} \exp(-i4\pi L/\lambda_g) - \frac{b_1 - b_0}{b_0} \right]. \quad (19)$$

The close parenthesis symbol was left out of the cosine term in (20); it should be

$$|\Gamma| = \frac{1}{8\pi L/\lambda_g} \left| 1 - \frac{b_0}{b_1} \left[1 + \left(\frac{b_1}{b_0} \right)^2 \right. \right. \\ \left. \left. - 2 \left(\frac{b_1}{b_0} \right) \cos(4\pi L/\lambda_g) \right]^{1/2} \right|. \quad (20)$$

Correspondence

The Extended Theory of the Manley-Rowe's Energy Relations in Nonlinear Elements and Nonlinear Lossless Medium*

Energy relations for a lumped nonlinear reactance excited by two different fundamental frequencies were derived by J. M. Manley and H. E. Rowe [1]. R. H. Pantell [10] developed the energy relations in a nonlinear resistive element. Furthermore, H. A. Haus extended the Manley-Rowe's energy relations to a nonlinear lossless medium excited by two fundamental frequencies [2]. This paper extends the Manley-Rowe relations in the case of a lumped nonlinear element (lossless reactance and resistive element) and nonlinear lossless reciprocal medium excited by k numbers of fundamental frequencies, wherein the extended relations consist of k independent equations.

I. IN THE CASE OF NONLINEAR LOSSLESS REACTANCE

In this case, generalized energy relations have been independently derived by this author [6] in Japan, and Yeh in America [9].

The author derived the extended relations by using the multiple Fourier Series [6], [9].

The energy relations obtained in both papers have the same results and consist of k independent equations. This relation is also obtained by using the energy conservation theory directly [8]. This extended energy relation can be applied to the multi-pumping parametric amplifier. If there are $(k-1)$ pumping frequencies, $f_{p1}, f_{p2}, \dots, f_{p(k-1)}$, and if we choose the idling frequency according to

$$f_i = \sum_{j=1}^{k-1} f_{pj} - f_s$$

(f_s : signal frequency), the general energy relations in the multi-pumping parametric amplifier are derived as

$$\frac{W_s}{f_s} = \frac{W_i}{f_i},$$

$$\frac{W_{p1}}{f_{p1}} = \frac{W_{p2}}{f_{p2}} = \dots = \frac{W_{p(k-1)}}{f_{p(k-1)}} = -\frac{W_i}{f_i}, \quad (1)$$

where

$$\sum_{j=1}^{k-1} f_{pj} > f_s.$$

II. IN THE CASE OF A NONLINEAR RESISTIVE ELEMENT

The energy relations in a nonlinear resistive element excited by two fundamental frequencies were derived by R. H. Pantell [10].

We can extend this relation to the multi-exciting system by using multiple Fourier Series. Assume that,

- 1) The relations between the voltage v and the current i in a nonlinear resistor can be expressed by single valued function,

$$v = f(i): \text{single valued function}, \quad (2)$$

- 2) There are k numbers of fundamental frequencies $f_1, f_2, f_3, \dots, f_k$ (k : positive integer). Higher harmonics and sidebands

$$\sum_{i=1}^k n_i f_i,$$

are generated by the nonlinearity.

Then, the voltage v and the current i may be expressed by the multiple Fourier Series as follows:

$$\left. \begin{aligned} \sum_{n_k=-\infty}^{\infty} \sum_{n_{k-1}=-\infty}^{\infty} \dots \sum_{n_2=-\infty}^{\infty} \sum_{n_1=0}^{\infty} n_1 X_{n_1 n_2 \dots n_k} &= 0 \\ \sum_{n_k=-\infty}^{\infty} \sum_{n_{k-1}=-\infty}^{\infty} \dots \sum_{n_2=0}^{\infty} \sum_{n_1=-\infty}^{\infty} n_2 X_{n_1 n_2 \dots n_k} &= 0 \\ &\vdots \\ \sum_{n_k=0}^{\infty} \sum_{n_{k-1}=-\infty}^{\infty} \dots \sum_{n_2=-\infty}^{\infty} \sum_{n_1=-\infty}^{\infty} n_k X_{n_1 n_2 \dots n_k} &= 0 \end{aligned} \right\} \quad (8)$$

For the real power,

$$\left. \begin{aligned} \sum_{n_k=-\infty}^{\infty} \sum_{n_{k-1}=-\infty}^{\infty} \dots \sum_{n_2=-\infty}^{\infty} \sum_{n_1=0}^{\infty} n_1^2 W_{n_1 n_2 \dots n_k} &= h_{n1} \\ \sum_{n_k=-\infty}^{\infty} \sum_{n_{k-1}=-\infty}^{\infty} \dots \sum_{n_2=0}^{\infty} \sum_{n_1=-\infty}^{\infty} n_2^2 W_{n_1 n_2 \dots n_k} &= h_{n2} \\ &\vdots \\ \sum_{n_k=0}^{\infty} \sum_{n_{k-1}=-\infty}^{\infty} \dots \sum_{n_2=-\infty}^{\infty} \sum_{n_1=-\infty}^{\infty} n_k^2 W_{n_1 n_2 \dots n_k} &= h_{nk} \end{aligned} \right\} \quad (9)$$

where

$$h_{ni} = \frac{1}{(2\pi)^k} \int_0^{2\pi} dx_k \int_0^{2\pi} dx_{k-1} \dots \int_0^{2\pi} dx_1 \int_0^{2\pi} dx_i \frac{\partial i}{\partial v} \left(\frac{\partial v}{\partial x_i} \right)^2.$$

III. ENERGY RELATIONS IN NONLINEAR LOSSLESS MEDIUM WITH MULTI-EXCITATIONS

Energy relations in nonlinear lossless medium have been published by H. A. Haus [2], whereby the number of excitations is confined to the case of two. The extended theory in nonlinear lossless medium which contains k excitations, and whose frequencies are f_1, f_2, \dots, f_k , will be considered.

Assumed that,

- 1) the medium is nonlinear,
- 2) the medium is lossless, the conductivity $\sigma = 0$,
- 3) the medium is reciprocal, but is not necessary if required to be isotropic, and

* Received by the PGMTT, January 4, 1960; revised manuscript received, March 7, 1960.

4) there are no free charges, $\rho = 0$,

Maxwell's equations are satisfied at any point in the medium

$$\nabla \times H = -\frac{\partial B}{\partial t} \quad (a)$$

$$\nabla \times E = \frac{\partial D}{\partial t} \quad (b)$$

$$B = \mu_0(H + M) \quad (c)$$

$$D = \epsilon_0 E + P \quad (d)$$

$$\text{div } D = 0, \quad \text{div } B = 0 \quad (e).$$

Let the medium be excited sinusoidally with respect to time, the excitation angular frequencies being $\omega_1, \omega_2, \omega_k$. Their sideband and higher harmonics

$$\sum_{i=1}^k n_i \omega_i,$$

are generated by the nonlinearity.

At any point in the medium, the electric field E , whose frequency is $n_1\omega_1 + n_2\omega_2 + \dots + n_k\omega_k$, can be expanded by the multiple Fourier Series

$$E(r) = \sum_{n_k=-\infty}^{\infty} \dots \sum_{n_1=-\infty}^{\infty} E_{n_1 n_2 \dots n_k}(r) \cdot e^{j(n_1\omega_1 + n_2\omega_2 + \dots + n_k\omega_k)t}, \quad (11)$$

where r is the vector representing the position of observation from the origin.

Since E is real, it follows that

$$E_{n_1 n_2 \dots n_k} = E_{-n_1 -n_2 \dots -n_k}^* \quad (12)$$

These results are also valid for magnetic field H , electric polarization P , current density J , and magnetization M .

From (10a) and (10b),

$$\nabla \times E_{n_1 n_2 \dots n_k} = -j\mu_0(n_1\omega_1 + n_2\omega_2 + \dots + n_k\omega_k) \cdot (H_{n_1 n_2 \dots n_k} + M_{n_1 n_2 \dots n_k}) \quad (13)$$

$$\nabla \times H_{n_1 n_2 \dots n_k} = j(n_1\omega_1 + n_2\omega_2 + \dots + n_k\omega_k) \cdot (\epsilon_0 E_{n_1 n_2 \dots n_k} + P_{n_1 n_2 \dots n_k}). \quad (14)$$

Making the vector product $E_{n_1 n_2 \dots n_k} \times H_{n_1 n_2 \dots n_k}$ by (13) and (14) and applying the vector formula

$$\nabla \cdot (A \times B) = B \cdot \nabla \times A - A \cdot \nabla \times B;$$

and summing up with the frequencies, from $-\infty$ to $+\infty$, k independent relations are obtained as follows,

$$\nabla \cdot \sum_{n_k=-\infty}^{\infty} \dots \sum_{n_1=-\infty}^{\infty} \frac{n_i E_{n_1 n_2 \dots n_k} \times H_{n_1 n_2 \dots n_k}^*}{n_1\omega_1 + n_2\omega_2 + \dots + n_k\omega_k} = -j \sum_{n_k=-\infty}^{\infty} \dots \sum_{n_1=-\infty}^{\infty} n_i M_{n_1 n_2 \dots n_k} \cdot H_{n_1 n_2 \dots n_k}^* \quad (15)$$

$$\begin{aligned} \nabla \cdot \sum_{n_k=-\infty}^{\infty} \sum_{n_{k-1}=-\infty}^{\infty} \dots \sum_{n_1=-\infty}^{\infty} \frac{n_i E_{n_1 n_2 \dots n_k} \times H_{n_1 n_2 \dots n_k}^*}{n_1\omega_1 + n_2\omega_2 + \dots + n_k\omega_k} &= 0 \\ \nabla \cdot \sum_{n_k=-\infty}^{\infty} \sum_{n_{k-1}=-\infty}^{\infty} \dots \sum_{n_1=-\infty}^{\infty} \frac{n_i E_{n_1 n_2 \dots n_k} \times H_{n_1 n_2 \dots n_k}^*}{n_1\omega_1 + n_2\omega_2 + \dots + n_k\omega_k} &= 0 \\ \vdots \\ \nabla \cdot \sum_{n_k=-\infty}^{\infty} \sum_{n_{k-1}=-\infty}^{\infty} \dots \sum_{n_1=-\infty}^{\infty} \frac{n_i E_{n_1 n_2 \dots n_k} \times H_{n_1 n_2 \dots n_k}^*}{n_1\omega_1 + n_2\omega_2 + \dots + n_k\omega_k} &= 0. \end{aligned} \quad (23)$$

$$+j \sum_{n_k=-\infty}^{\infty} \dots \sum_{n_1=-\infty}^{\infty} n_i E_{n_1 n_2 \dots n_k}^* \cdot E_{n_1 n_2 \dots n_k} \quad (15)$$

From assumption (2), $\sigma=0$, and (3), the functions describing the relations between H and M and between E and P are single valued, i.e.,

$$H = H(M), \quad E = E(P) \dots \text{Single Valued.} \quad (16)$$

The energy supplied to the material of unit volume so as to cause magnetic polarization M , is given by the integral (16), H being a function of M ,

$$\int_0^M H(M) dM. \quad (17)$$

Since H is single valued, integral (17) is independent of the integrating path. The integral along the closed path vanishes, since the medium is lossless. The magnetic polarization M is expanded in the multiple Fourier Series at any point in the medium as,

$$M = \sum_{n_k=-\infty}^{\infty} \dots \sum_{n_1=-\infty}^{\infty} M_{n_1 n_2 \dots n_k} e^{j(n_1 x_1 + n_2 x_2 + \dots + n_k x_k)} \quad (18)$$

The coefficient $M_{n_1 n_2 \dots n_k}$ in (18) is expressed by,

$$M_{n_1 n_2 \dots n_k} = \frac{1}{(2\pi)^k} \int_0^{2\pi} dx_k \int_0^{2\pi} dx_{k-1} \dots \int_0^{2\pi} dx_i M(x_1 x_2 \dots x_k) e^{-j(n_1 x_1 + n_2 x_2 + \dots + n_k x_k)} \quad (19)$$

$$M_{n_1 n_2 \dots n_k} = M_{-n_1 -n_2 \dots -n_k}^* \quad (19)$$

which may be rewritten as

$$H = H[M(x_1, x_2, \dots, x_k)] = H(x_1, x_2, \dots, x_k). \quad (20)$$

Likewise, H may be expressed by multiple Fourier Series.

By using the condition that $H(M)$ is single valued, the following equations are obtained.

$$\sum_{n_k=-\infty}^{\infty} \dots \sum_{n_1=-\infty}^{\infty} j n_i E_{n_1 n_2 \dots n_k}^* \cdot M_{n_1 n_2 \dots n_k} = 0 \quad (i = 1, 2, \dots, k). \quad (21)$$

For P and E

$$\sum_{n_k=-\infty}^{\infty} \dots \sum_{n_1=-\infty}^{\infty} j n_i P_{n_1 n_2 \dots n_k}^* \cdot E_{n_1 n_2 \dots n_k} = 0 \quad (i = 1, 2, \dots, k). \quad (22)$$

Putting (21), (22) and $\sigma=0$, into (15), k independent equations are obtained in the lossless reciprocal medium excited by k fundamental frequencies. Thus

The author wishes to thank Prof. S. Sonoda and Prof. S. Mito for their guidance and valuable suggestions.

H. IWASAWA

Dept. of Wireless Engrg.
Okubo Works, Kobe Kogyo Corp.
Okubo, Akashi, Japan

BIBLIOGRAPHY

- [1] J. M. Manley and H. E. Rowe, "Some general properties of nonlinear elements—part I, general energy relations," *PROC. IRE*, vol. 44, pp. 904-914; July, 1956.
- [2] H. A. Haus, "Power-flow relations in lossless nonlinear media," *IRE TRANS ON MICROWAVE THEORY AND TECHNIQUES*, vol. MTT-6 pp. 317-324; July, 1958.
- [3] S. Bloom and K.K.N. Chang, "Parametric amplifier using low frequency pumping," *J. Appl. Phys.*, vol. 29, p. 594; March, 1958.
- [4] A private letter to the author from Prof. S. Sonoda, February 15, 1959.
- [5] C. Page, "Frequency conversion with nonlinear reactance," *J. Res. NBS*, vol. 58, pp. 227-236; May, 1957.
- [6] H. Iwasawa, "The extended theory of the Manley-Rowe's energy relations in a nonlinear element," *Inst. Elec. Comm. Engrg. Japan Natl. Convention Record*, pt. I, no. 18; 1959.
- [7] A private letter to the author from Prof. S. Sonoda, July 31, 1959.
- [8] J. M. Manley and H. E. Rowe, "General energy relations in nonlinear reactances," *PROC. IRE*, vol. 47, pp. 2115-2116; December, 1959.
- [9] C. Yeh, "Generalized energy relations of nonlinear reactive elements," *PROC. IRE*, vol. 48, p. 253; February, 1960.
- [10] R. H. Pantell, "General power relations for positive and negative resistive elements," *PROC. IRE*, vol. 46, pp. 1910-1913; December, 1958.

A Method of Improving Isolation in Multi-Channel Waveguide Systems*

In microwave measurements, frequent use is made of "two channel" or multiple channel systems, in order to obtain isolation from amplitude fluctuations in the generator output and/or various other benefits. In such systems it is generally required that the signal delivered to one channel be independent of changes in loading, etc., in the second channel, and a common problem is that of achieving or determining that an adequate degree of isolation exists between the different channels. It is the purpose of this letter to describe briefly procedures for obtaining and recognizing this condition.

Consider first the three arm junction of Fig. 1, where the generator feeds arm 1. The required condition for isolation is that

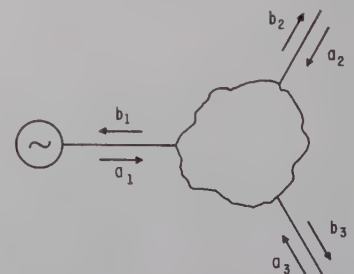


Fig. 1—Three arm waveguide junction

* Received by the PGMTT, March 10, 1960.

the ratio of the complex amplitudes of the emergent waves from arms 2 and 3 (b_2 , and b_3), be constant:

$$\frac{b_2}{b_3} = K$$

(1)

where K is a complex constant of finite magnitude and different from zero.

It may be noted that this condition does not actually insure that b_2 , for example, will be independent of changes in the loading on arm 3. However, it does require, if a change in b_2 occurs, a simultaneous change in b_3 such that the net result is equivalent to an amplitude variation and/or phase shift in the generator to which the system is presumably insensitive.

In terms of the incident wave amplitudes (a_1, a_2, a_3), b_2 and b_3 are given by:

$$\begin{aligned} b_2 &= S_{21}a_1 + S_{22}a_2 + S_{23}a_3 \\ b_3 &= S_{31}a_1 + S_{32}a_2 + S_{33}a_3, \end{aligned}$$

(2)

where the $S_{m,n}$ are the scattering coefficients of the junction.

Substituting (2) in (1) yields

$$(S_{21} - KS_{31})a_1 + (S_{22} - KS_{32})a_2 + (S_{23} - KS_{33})a_3 = 0.$$

(3)

In practice a_1 will not vanish since this is the emergent wave from the generator, and in the general case both a_2 and a_3 will assume arbitrary and independent values. The criterion for isolation, therefore, requires that each of the coefficients of the a 's vanish.

With reference to the coefficient of a_1 , if S_{21} vanishes, so must S_{31} and conversely. But this would mean that no transmission would be possible between arm 1 and either of the other two arms, and consequently represents a trivial solution. Therefore,

$$\frac{S_{21}}{S_{31}} = K.$$

Substituting this result in the coefficients of a_2 and a_3 yields

$$S_{22} - \frac{S_{21}S_{32}}{S_{31}} = 0$$

(4)

$$S_{33} - \frac{S_{31}S_{23}}{S_{21}} = 0.$$

(5)

Eqs. (4) and (5) give the necessary and sufficient conditions that the junction satisfy (1).

In practice these conditions are approximately satisfied by a "Magic T" whose shunt or series arm has been terminated in a matched load, or by a directional coupler. In such junctions, each of the terms S_{22} , S_{23} , S_{32} , and S_{33} ideally vanish. The degree of isolation achieved when using a non-ideal hybrid junction or directional coupler can generally be improved in the following manner.

Let tuning transformers be added to each of the arms of the junction as shown in Fig. 2. The generator is removed from arm 1 and replaced by a passive load (not necessarily matched). If transformer T_1 is now adjusted so that a null¹ obtains in arm

3 with the generator connected to arm 2, it can be shown that the reflection coefficient "looking into" arm 2 is just the left hand member of (4). Transformer T_2 is now adjusted so that this reflection coefficient vanishes, and (4) is satisfied. It may be intuitively recognized that this adjustment is independent of the subsequent adjustment of transformer T_3 since if a null exists in arm 3, the reflection coefficient observed at arm 2 will evidently be independent of the manner of terminating arm 3. The interchange of arms 2 and 3 in the above procedure satisfies (5). (If, as is frequently the case, the load terminating one of the arms, arm 3 for example, is constant or not subject to variations in impedance, then it can be shown that this second step or the adjustment of the transformer in the arm terminated by the fixed load is not required.) Once the proper adjustment of T_2 and T_3 has been realized, the adjustment of T_1 is no longer important since the conditions expressed by (4) and (5) are invariant to the adjustment of T_1 . If, as an additional condition, T_1 is terminated by a load equal to the generator impedance during the tuning procedure, then b_2 and b_3 individually, as well as their ratio, will remain constant. In many applications this is of at least nominal interest.

The extension of this procedure to three or more channels is straightforward. In the four arm junction of Fig. 3, for example, let the arm which will ultimately be connected to the generator (arm 1) be connected to an arbitrary load as previously. If now by means of tuner T_1 and other "internal" tuning adjustments (which will in general be required), it is possible to achieve the condition where no coupling exists between the remaining arms (no output is observed at arms 3 and 4 with arm 2 connected to the

generator, etc.) and if tuners T_2, T_3, T_4 , have been adjusted so that the reflection coefficients at the respective arms vanish, then it can be shown that the desired condition obtains. The considerations involving tuner T_1 , as outlined above, also continue to apply.

One possible method of obtaining such a junction is shown in Fig. 4, where tuner T_a provides the "internal" adjustment as required above.

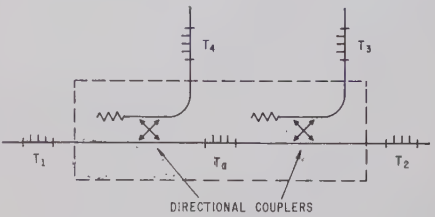


Fig. 4—Four arm junction with internal tuning.

G. F. ENGEN
U. S. Dept. of Commerce
Nat'l. Bur. of Standards
Boulder Labs.
Boulder, Col.

A Microwave Impedance Meter Capable of High Accuracy*

Recent applications of directional couplers with auxiliary tuners for accurate VSWR and phase shift measurements have made possible a microwave impedance meter capable of high accuracy. It is similar to some bridges in that one obtains an initial detector null and a final null, before and after connecting the unknown. Both the magnitude and phase angle of the reflection coefficient of the unknown are determined in this operation, and these can be made direct reading if desired. The principle of operation is as follows.

The use of directional couplers with auxiliary tuners permits adjustment for the conditions $S_{31} = \Gamma_{2c} = 0$, whereupon

$$b_3 = C\Gamma_L.$$

(1)

The symbols have the following meanings, which become clearer upon reference to Fig. 1.

- S_{31} = transmission (scattering) coefficient for waves going from arm 1 to arm 3,
- Γ_{2c} = reflection coefficient which would be measured "looking into" arm 2 if the generator were replaced by a passive impedance having the same impedance as the generator,
- b_3 = amplitude of wave emerging from arm 3,
- C = a constant which depends upon the parameters of the adjusted directional coupler-tuner combination,

¹ If transformer T_1 is assumed to be dissipationless, this adjustment may be realized provided that the junction satisfies the condition

$$\left| \frac{S_{11} - \frac{S_{12}S_{21}}{S_{22}}}{S_{22}} \right| > 1.$$

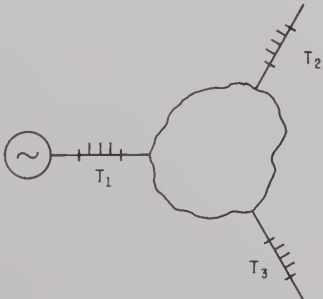


Fig. 2—Three arm junction with tuners.

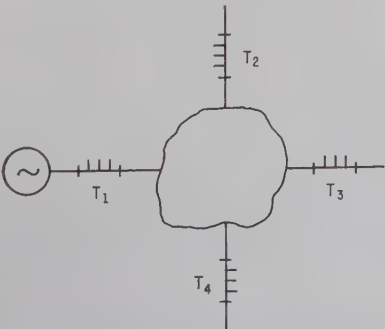


Fig. 3—Four arm junction and tuners.

* Received by the PGMTT, April 1, 1960.

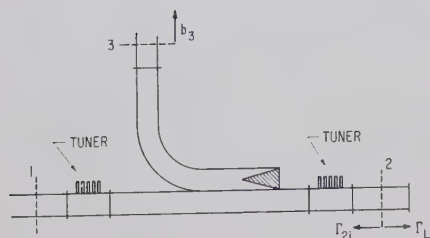


Fig. 1.

The phase ψ_u of Γ_u , the reflection coefficient of the unknown, equals the phase shift produced by the sliding short circuit plus the phase ψ_s of Γ_s ,

$$\psi_u = 2\beta l + \psi_s. \quad (3)$$

In this equation, it is apparent that l is the displacement toward T_{X1} of the short-circuit and β the phase constant of the waveguide containing the sliding short circuit. If the phase shifter ϕ is varied instead of the short circuit, one substitutes its phase change for $2\beta l$ in (3).

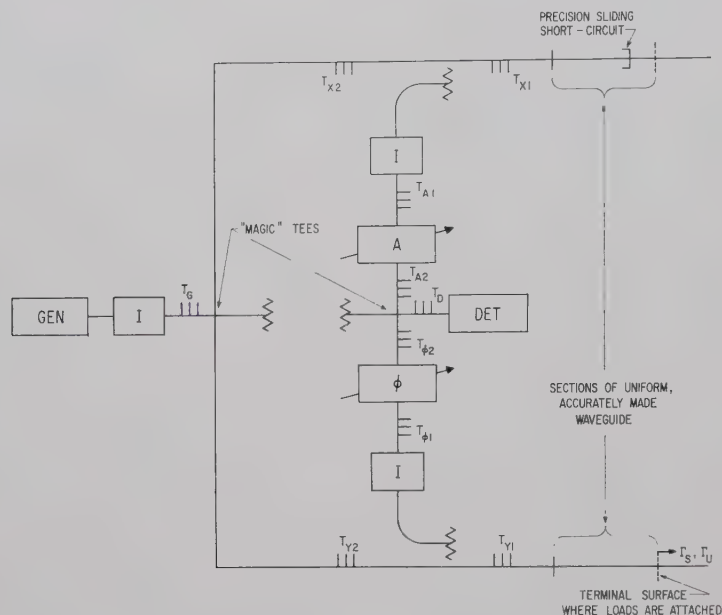


Fig. 2.

Γ_L = reflection coefficient of load terminating arm 2.

The tuning of a junction to obtain the performance indicated by (1) is the basis for a reflectometer¹ to determine $|\Gamma_L|$ and for a phase shift standard² which makes use of the fact that the phase of b_3 tracks the phase of Γ_L .

A microwave impedance meter can be constructed by a combination of the two ideas. A way in which this can be assembled is shown in Fig. 2.

After proper adjustment of the tuners, one adjusts the calibrated attenuator and sliding short circuit to obtain detector nulls with a standard known (Γ_s) termination and the unknown (Γ_u) alternately connected to the place indicated in Fig. 2. The variable phase shifter shown in the lower arm is not essential but may be used for convenience in zero-setting the short circuit or in making rapid, direct-reading phase measurements.

One calculates the magnitude of Γ_u from the increase in attenuation ΔA required to restore the null when Γ_s is replaced by Γ_u ,

$$\Delta A = 20 \log_{10} \left| \frac{\Gamma_s}{\Gamma_u} \right|. \quad (2)$$

¹ G. F. Engen and R. W. Beatty, "Microwave reflectometer techniques," IRE TRANS. ON MICROWAVE THEORY AND TECHNIQUES, vol. 7, pp. 351-355; July, 1959.

² M. Magid, "Precision microwave phase shift measurements," IRE TRANS. ON INSTRUMENTATION, vol. 7, pp. 321-331; December, 1958.

The following assumptions implicit in the above procedure are noted:

- 1) Adjustment of the attenuator does not produce any change in phase. (Attenuators are commercially available which come close to meeting this requirement, and in principle, one could measure their phase shift and deduct it.)
- 2) Adjustments of the attenuator and phase shifter in the side arms of the couplers do not disturb the adjustments of the tuners to make $\Gamma_{2i} = 0$. (The isolators labeled I in the diagram are suggested to reduce trouble from this possibility.)
- 3) The complex ratio of the amplitudes of the waves entering the two channels is not affected by changes of loading occurring during a measurement. (The decoupling offered by the hybrid tees or 3-db directional couplers may be augmented by the auxiliary tuners T_{X2} and T_{Y2} shown in Fig. 2; the isolation can be made arbitrarily high at any particular operating frequency.)

Suitable standards of reflection are a) quarter-wavelength short circuits,³ in which case $\Gamma_s = 1$, (2) yields the return loss $\Delta A = 20 \log_{10} 1/|\Gamma_u|$, and (3) yields the phase

$\psi_u = 2\beta l$ directly, and b) half-round inductive obstacle impedance standards,⁴ i.e., obstacles having accurately calculable magnitude and phase of reflection, in which Γ_s may be chosen close to Γ_u , thereby reducing the error in the measurement.

The adjustments of the tuners to obtain the best accuracy with the components and instrumentation available are adaptations of known techniques¹ with the exception of steps 1) and 5) which were originated by G. F. Engen as a modification of a more general tuning procedure.⁵ The steps in the tuning procedure are as follows:

- 1) With generator connected to the uniform waveguide section which normally contains the sliding short circuit, and a detector connected to the other uniform waveguide section, adjust T_G and T_D separately for a detector null, blocking in turn the paths from T_D , then T_G , to the detector. (Switches may be permanently installed in the waveguide system for this purpose, if desired.)
- 2) Temporarily remove the attenuator A and adjust T_{A1} and T_{A2} for no reflection. (This condition may be recognized with an auxiliary reflectometer.)
- 3) Temporarily remove the phase shifter ϕ , and adjust $T_{\phi 1}$ and $T_{\phi 2}$ for no reflection.
- 4) Adjust T_{X1} and T_{Y1} for infinite directivity of the directional couplers and associated tuners. Two ways will be described for doing this. a) Introduce a nonreflecting termination into the waveguide section connected to the tuner and adjust the tuner until a null is obtained in the sidearm output. b) Introduce a weakly reflecting (VSWR < 1.01) termination into the waveguide section connected to the tuner, and while sliding it back and forth in the waveguide, adjust the tuner until there are no cyclical variations in the sidearm output. This procedure will not in itself give infinite directivity but in practice will usually result in a very high value.¹
- 5) With the generator connected as shown in Fig. 2, a) adjust T_{X2} so that sliding a short circuit in the uniform waveguide section in channel X produces no cyclical variation in the detector output, and b) adjust T_{Y2} so that sliding a short circuit in the uniform waveguide section in channel Y produces no cyclical variation in the detector output.

When the above adjustments have been completed, the two channels are well isolated, the two directional coupler and tuner combinations have approximately infinite directivity, and a nonreflecting equivalent generator at their outputs in the uniform waveguide sections; and the calibrated attenuator and phase shifter are connected to

⁴ D. M. Kerns, "Half-round inductive obstacles in rectangular waveguide," to be published in *J. Res. NBS*, Section B, Mathematics and Mathematical Phys.

⁵ G. F. Engen, "A method of improving isolation in multi-channel waveguide systems," this issue, p. 460.

³ R. W. Beatty and D. M. Kerns, "Recently developed microwave impedance standards and methods of measurement," IRE TRANS. ON INSTRUMENTATION, vol. 7, pp. 319-231; December, 1958.

nonreflecting waveguides, preventing mismatch errors.

Standards of phase shift and impedance may be made to high precision by careful machining techniques. With refined instrumentation, the system should prove capable of impedance measurements of the highest accuracy and therefore useful in calibration work.

R. W. BEATTY
Radio Standards Lab.
Natl. Bur. of Standards
Boulder, Colo.

On the Noise Temperature of Coupling Networks*

When a passive coupling network, such as a waveguide, transmission line, matching filter, etc., is used to connect a source to a receiver, it is apparent that it will contribute noise to the output because of its lossiness. If the noise temperature of the source is T_s and the temperature of the coupling network is T_n , then the noise temperature, T_o , at the output (under matched conditions) is given by¹

$$T_o = \frac{T_s}{L} + T_n \left(1 - \frac{1}{L}\right), \tag{1}$$

where L is the coupling-network power loss ratio. This relationship was derived by constructing a transmission line analog to the coupling network and treating the source and loss noises as propagating signals. An alternative derivation based on a more physical representation is presented in this note.

Consider the coupling network as a generalized two-port with matched input and output. Its noise power output, P , can be written

$$P = \frac{kT_s B}{L} + kT_n B f, \tag{2}$$

where the first term is simply the attenuated source noise power and the other is some fraction, f , of the noise power available from the coupling network. Since (2) is true for all values of the parameters, it is true, in particular, when the coupling network is at the same temperature as the source, yielding

$$P_{T_n=T_s} = kT_s B \left(\frac{1}{L} + f\right). \tag{3}$$

However, the noise contributions to the output from the source and from the coupling network become indistinguishable when both are at the same temperature. That is, the output from the coupling network then looks exactly like that from the source itself, so

$$P_{T_n=T_s} = kT_s B, \tag{4}$$

* Received by the PGMTT, April 1, 1960.
¹ P. D. Strum, "A note on noise temperature," IRE TRANS. ON MICROWAVE THEORY AND TECHNIQUES, vol. MTT-4, pp. 145-151; July, 1956.

and combining (3) and (4) yields

$$f = 1 - \frac{1}{L}. \tag{5}$$

Writing the general noise power output, P , as $kT_o B$ then gives

$$T_o = \frac{T_s}{L} + T_n \left(1 - \frac{1}{L}\right), \tag{6}$$

Q.E.D.

E. BEDROSIAN
Engrg. Div.
RAND Corp.
Santa Monica, Calif.

A Logarithmic Transmission Line Chart*

In his article above,¹ Hudson raises the question: "What length of line of what impedance will match a given impedance?" He states, "Conventional charts do not answer this question explicitly."

This problem can be solved on the "conventional" Smith Chart (Fig. 1) explicitly without trial-and-error, by the following method. If A and B are two quite general impedances, the matched condition requires that A be transformed into B^* , the complex conjugate of B .

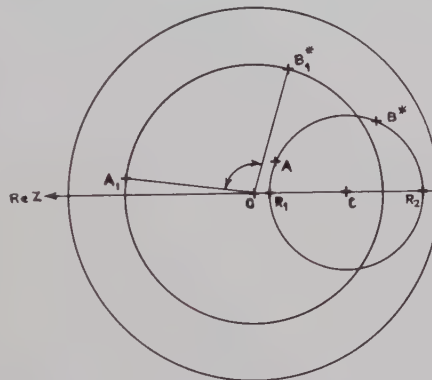


Fig. 1—Smith Chart.

- 1) Plot A and B^* on the Smith Chart and draw the circle through these two points which has its center (C) on the real axis. If this circle lies fully within the Smith Chart, the question has a solution, otherwise not.
- 2) Read off the values at the intersections of the real axis and the circle (R_1, R_2), and determine their geometric mean $\sqrt{R_1 \times R_2}$, which will be the characteristic impedance of the matching line.
- 3) On the Smith Chart normalized to

To find the length of this line,

3) On the Smith Chart normalized to

* Received by the PGMTT, April 1, 1960.
¹ A. C. Hudson, IRE TRANS. ON MICROWAVE THEORY AND TECHNIQUES, vol. MTT-7, pp. 277-281; April, 1959.

- $\sqrt{R_1 \times R_2}$, represent A and B^* by A_1 and B_1^* .
- 4) The electrical length of the matching line will be given by half of the angle $A_1 \odot B_1^*$.

This method is based upon the following two properties of loss-free transmission lines:

- 1) The locus of the impedance along a line is always a circle on the Smith Chart (having its centre on the real axis) irrespective of the value of the normalizing resistance.
- 2) The characteristic impedance of the line is given by $Z_0 = \sqrt{(\text{Re } Z)_{\text{max}} \times (\text{Re } Z)_{\text{min}}}$, where Z is the impedance along the line.

PETER I. SOMLO
Commonwealth Sci. and
Ind. Res. Org.
Div. of Electrotechnology
Natl. Standards Lab.
Chippendale, New South Wales

Velocity Sorting Detection in Backward Wave Autodyne Reception*

An electronically tunable microwave receiver which uses an oscillating backward wave amplifier driving a crystal detector has been described previously.¹ This receiver has the advantages of large dynamic range and good rejection of unwanted signals, but has the disadvantage that its frequency response can be no better than that of its crystal detector. Since a variation in sensitivity of greater than 3 db over the tuning range of 8 to 12 kmc would seriously lower its usefulness as a spectrum display device, the restrictions on the crystal detector performance are quite severe.

In the paper describing the operation of the device, the author made the suggestion that it might be possible to detect the video output by means of a suitable collector. This letter describes the results of an experimental velocity sorting detector used with the backward wave autodyne receiver.

The first tube used was a Varian VAD-161-2. The collector in this tube was not designed for depressed operation, and, as a result, when the collector voltage was lowered to within a few volts of the cathode potential a virtual cathode was formed near the collector.

A three-dimensional plot of collector current vs collector voltage and beam current is presented in Fig. 1. The current is a multivalued function of collector potential which resulted in the production of oscillations when a load resistance was connected to the collector. Because the oscillations occurred at the setting of collector voltage

* Received by the PGMTT, December 28, 1959; revised manuscript received, April 4, 1960.
¹ J. K. Puffer, "Application of a backward wave amplifier to microwave autodyne reception," IRE TRANS. ON MICROWAVE THEORY AND TECHNIQUES, vol. MTT-7, pp. 356-359; July, 1959.

which produced maximum sensitivity, detection in this tube was not satisfactory.

A new tube designated type VAD-161-4 was developed which had a collector redesigned for depressed operation. With this tube no instability was observed at any value of collector voltage, beam current or beam velocity.

Fig. 2 is a three-dimensional model of collector current for the VAD-161-4. The collector current below the oscillation starting current increases with both beam current and collector voltage, indicating that no virtual cathode exists.

At the start of oscillations (a beam current of about 3.5 ma), there is an abrupt change in collector current. At a low collector voltage the collector current rises at the oscillation starting point, but at a higher collector voltage the beam current drops steeply when oscillations begin. This steep drop may be used to detect small changes in beam velocity distribution.

Fig. 3 is a plot of detected output signal level for a constant input vs collector voltage. Beam current was optimized for maximum output.

An important characteristic of the autodyne detector is the rate at which the output signal is reduced as the beam current is increased beyond starting current. In Fig. 4, normalized output from the two types of detector is plotted against normalized beam current. One hundred on the abscissa represents starting current. The crystal detector is much less sensitive to variations in beam current. Note that in contrast to the crystal detector the collector detection efficiency falls off almost as rapidly above starting current as it does below.

The mechanism of detection by a nega-

tively biased collector is such that it is the beat frequency between the oscillation and the signal which is actually detected. When either of these becomes large relative to the other, the change in collector current due to the beat becomes small and detection efficiency drops off.

When the beam current is increased above starting current, the amplitude of the oscillation increases extremely rapidly, so that detection efficiency decreases rapidly for beam currents above starting current.

Because of this effect, a velocity sorting detector has not proved superior to a crystal detector in the electronically tunable receiver application, although sensitivity equivalent to a good crystal detector can be easily obtained.

The backward wave oscillator tubes used in these experiments were developed by Varian of Canada, Ltd., under the auspices of the Defence Research Board, Canada, (Electronic Components Research and Development Committee).

J. K. PULFER
Rad. Elec. Engrg. Div.
Natl. Res. Council
Ottawa, Canada

A Broad-Band Crystal Mount 10.5 kmc to 20 kmc*

Laboratory measurements at microwave frequencies very often require the use of a sensitive detector with broad-band characteristics.

A crystal mount has been developed with a nearly uniform response from 10.5 kmc to 20.0 kmc using coaxial crystals type 1N26 or 1N78A. The best over-all sensitivity is obtained with 1N78A crystals, although the 1N26 crystals are more sensitive from 17 to 20 kmc.

Basically, the mount consists of a section of type RG-91/U waveguide containing a tapered ridge guide-to-coaxial-line junction [1]. The first design matched the waveguide to a 65-ohm coaxial line, but as the crystal impedance was not 65 ohms the dimensions had to be modified considerably to obtain the maximum sensitivity across the frequency band. Dimensional details of the crystal mount are shown in Fig. 1. A low impedance between the crystal body and the mount is obtained by means of an insulated sleeve which forms a capacity of 50 μf . With a bias current of 75 μamp the video impedance is about 700 ohms, which results in a rise time of less than 0.1 μsec .

The narrow dimension of the waveguide was reduced from the standard 0.311 inch to 0.281 inch to eliminate a sharp dip in sensitivity at 19.2 kmc. In the final version of this mount, the tapered ridge and the insert which reduces the narrow dimension of the guide were machined from one piece of metal, and then placed in the standard waveguide. This method of construction places the junction of the insert and the waveguide at the walls of the guide instead of at the base of the ridge. The results of electrical tests indicated that the performance of the mount does not depend on a good electrical contact at this junction. With this method of fabrication, the assembly of the mount will be greatly simplified.

During all measurements, crystals were biased with 75 μamp of forward current to improve both the detection efficiency and the RF impedance of the complete mount. The video amplifier following the crystal detector had an input impedance of 50 ohms and a bandwidth of 0.5 mc. A pulse-modulated signal was used, with a pulse width of 1 to 2 μsec . The measurements were limited to a few crystals of each type, as the effort

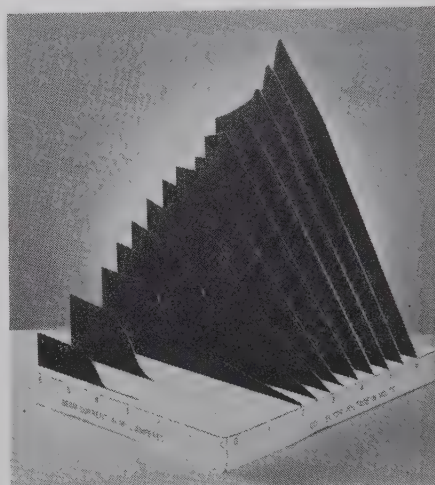


Fig. 2—Three-dimensional graph of measured collector current for type VAD-161-4 tube.

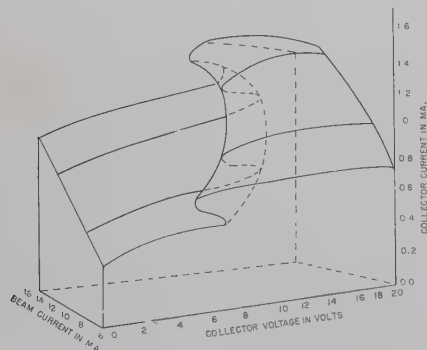


Fig. 1—Three-dimensional graph of measured collector current for type VAD-161-2 tube.

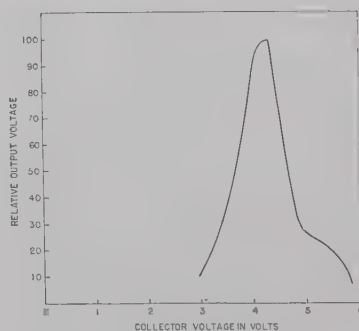


Fig. 3—Detected output level vs collector voltage.

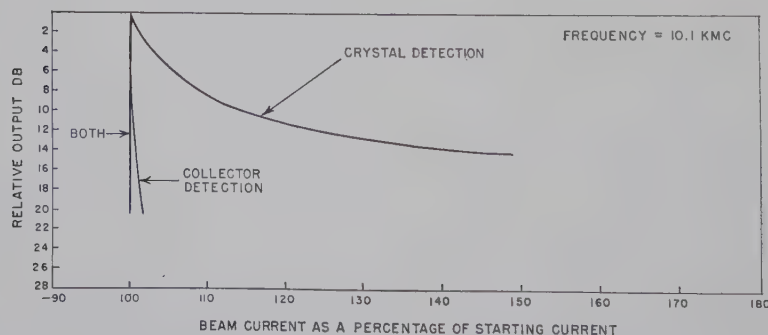


Fig. 4—Normalized output for two types of detector vs beam current.

* Received by the PGMTT, December 22, 1959; revised manuscript received, February 23, 1960.

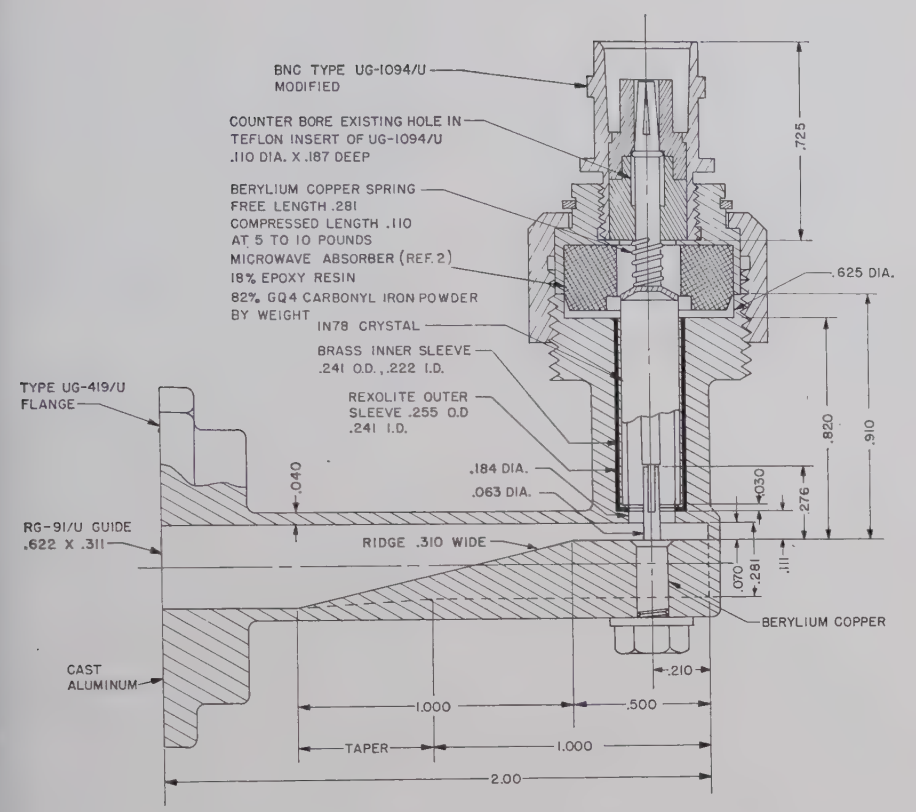


Fig. 1—KU band crystal mount (all dimensions in inches).

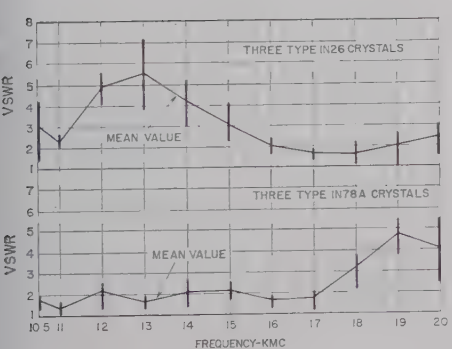


Fig. 2—VSWR at -36 dbm.

available did not permit a more extensive investigation.

The VSWR's of the mount, with two types of crystals, are shown in Fig. 2. The type 1N78A is a better match below 17 kmc, whereas the 1N26 crystal is better between 17 and 20 kmc. The mean tangential sensitivity vs frequency is plotted in Fig. 3, with two types of crystals. The short vertical lines indicate the spread in sensitivity of the group of crystals at each frequency. The arithmetic average sensitivity of the 1N78A crystals was -46.5 dbm, and that of the 1N26 crystals was -44.5 dbm.

In certain applications, such as in ratimeters, it is desirable that the sensitivity curves be parallel. The departure from this condition, known as "tracking error," was estimated from the data and is shown in Table I.

The choice of crystal type depends upon which frequencies are the most important in the particular application. The 1N78A crystals, designed for 16 kmc, have a higher

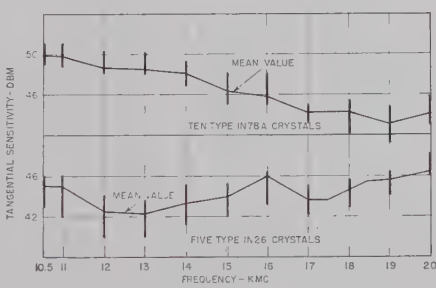


Fig. 3—Tangential sensitivity; video bandwidth 0.5 mc.

TABLE I
TRACKING OF SENSITIVITY OF CRYSTALS AND MOUNTS

Crystal			Tracking Error	
Num-ber	Type	Number of Mounts	10.5-15 kmc	15-20 kmc
Ten	1N78A	One	2 db	2.7 db
Five	1N26	One	1.5 db	1.1 db
One	1N78A	Eight	1.5 db	2.5 db

sensitivity and a lower VSWR from 10.5 to 17.0 kmc, whereas the 1N26 crystals designed for 24 kmc are better from 17 to 20 kmc.

A. STANFORTH
Radio and Electrical Engrg. Div.
Natl. Res. Council
Ottawa, Canada

BIBLIOGRAPHY

[1] S. B. Cohn, "Design of simple broad-band waveguide-to-coaxial-line junctions," *Proc. IRE*, vol. 35, pp. 920-926; September, 1947.
[2] A. Staniforth and K. A. Steele, "Casting lossy microwave parts in resin aids design work," *Canad. Electronics Engrg.*, vol. 2, pp. 16-20; May, 1958.

Proposed Parametric Amplifier Utilizing Ferroelectric Substance*

Ferroelectric substance has been utilized as nonlinear substance in parametric amplifiers.¹⁻⁴ However, all of these have been done at low-frequency regions. A surface-wave parametric amplifier employing ferroelectric substance in the microwave region has been proposed.⁵

The character of ferroelectric substance is not so clear at microwave frequencies as at lower frequencies. The nonlinearity caused by the domain wall motion cannot be utilized in the microwave region, because of the slow response of the wall motion.⁶ However, the nonlinearity of (BaSr)TiO₃ has been measured in the microwave region (3000 mc).⁷ This nonlinearity may be caused by the potential of the ionic atom (Ti atom or O atom). Therefore, we may consider the frequency limitation to depend upon the response of the motion of ionic atom. Infrared spectrum studies⁸ show that the resonant wavelength of the Ti atom is in the order of 50 μ . From these results it seems feasible that some ferroelectric substance can be utilized in parametric amplifiers at microwave frequencies.

There are several problems to be considered in using ferroelectric substance for a parametric amplifier. First, three different frequencies (signal, idling, and pumping) should be supplied into the substance with minimum reflection. Second, the amplifier is desired to be operated with a low pumping power, especially at high frequencies.

Now, when microwave is applied to an isotropic, homogeneous material whose length is equal to an integer multiple of the half wavelength in the material, the wave reflected at the first surface is cancelled by the wave reflected at the other surface, and there is no reflected wave, provided that the material is lossless. When a TEM wave is used, e.g., when the ferroelectric substance is set between two parallel plates or between the conductors of a strip line or coaxial line, the wave length in the material is expressed as follows:

$$\lambda = \frac{\lambda_{air}}{\sqrt{\epsilon}} \propto \frac{1}{\omega} \quad (1)$$

Therefore, when

$$\omega_{pumping} = \omega_{signal} + \omega_{idling} \quad (2)$$

* Received by the PGM-TT, February 1, 1960; revised manuscript received, April 19, 1960. The work described in this paper was carried out under the sponsorship of the Wright Air Development Center under Contract No. AF 33(616)-6139.
¹ W. H. Higa, "Theory of non-linear coupling in a novel ferroelectric device," *J. Appl. Phys.*, vol. 27, pp. 775-777; July, 1956.
² W. P. Mason and R. F. Wick, "Ferroelectrics and the dielectric amplifier," *Proc. IRE*, vol. 42, pp. 1606-1620; November, 1954.
³ S. Kumagai, private communication.
⁴ T. Tanaka, A. Kwabata, and Y. Shimabara, paper presented at the Joint Meeting of the Electrical Society of Japan, October, 1955.
⁵ E. S. Cassedy, Jr., "A surface wave parametric amplifier," *Proc. IRE*, vol. 47, pp. 1374-1375; August, 1959.
⁶ W. J. Meltz, "Domain formation and domain wall motions in ferroelectric BaTiO₃ single crystals," *Phys. Rev.*, vol. 95, pp. 690-689; August 1, 1954.
⁷ L. Davis, Jr. and L. G. Rubin, "Some dielectric properties of barium strontium-titanate ceramics at 3000 mc," *J. Appl. Phys.*, vol. 24, pp. 1194-1197; September, 1953.
⁸ R. T. Mara, G. B. B. M. Sutherland, and H. V. Typpell, "Infrared spectrum of barium titanate," *Phys. Rev.*, vol. 96, pp. 801-802; November 1, 1954.

it is possible to make the length of the material equal to integer multiples of each half wavelength of the three waves, if the dielectric constant does not vary with the frequency. (Since the dielectric constant can be changed by dc bias voltage, the wavelength can be adjusted by dc bias. Consequently, the length of the material can be made equal to the multiples of the half wavelengths of all three frequencies.)

Suppose that a TEM wave is applied into a ferroelectric substance both of whose surfaces facing each other are parallel and are perpendicular to the propagating direction of the wave. The ratio, t , of the amplitude of the wave which passes through the substance and of the incidental wave is easily obtained.

$$|t| = 4\xi e^{-\alpha D} / \sqrt{(1+\xi)^4 - 2(1-\xi)^2 e^{-2\alpha D} \cos \theta + (1-\xi)^4 e^{-4\alpha D}}, \quad (3)$$

where $\xi = \sqrt{\epsilon_{\text{air}}/\epsilon_{\text{substance}}}$, D is the length of the substance, α is the attenuation constant of the substance, and $\theta = 4\pi D/\lambda$. λ is a wavelength in the substance.

On the other hand, the gain of the parametric amplification with respect to the signal wave in the substance is obtained from a modified theory of Tien and Suhl.⁹ As for the attenuation constant of the signal wave, α , in (3) should be expressed by

$$\alpha = \alpha_1 - \alpha_g, \quad (4)$$

where α_1 is the true attenuation constant of the substance, and α_g is the gain and is expressed as follows:

$$\alpha_g = \frac{1}{4} \sqrt{\beta_s \beta_i} \frac{|\epsilon_p^0|}{\epsilon_0}, \quad (5)$$

where β_s and β_i are phase constants of signal wave and idling wave, respectively, ϵ_0 is the constant part of the dielectric constant, and ϵ_p^0 is the amplitude of the alternating part of the dielectric constant caused by pumping wave. When $D = n\lambda/2$, (3) is simplified, and

$$|t| = 4\xi e^{-\alpha D} / \{(1+\xi)^2 - (1-\xi)^2 e^{-2\alpha D}\}. \quad (6)$$

These results show that amplification can be obtained when $\alpha_1 < \alpha_g$, where $|t|$ is the amplification of the amplifier. The maximum amplification is obtained when

$$e^{-\alpha D} = \frac{1+\xi}{1-\xi}. \quad (7)$$

In the practical design of the amplifier, the following must be considered:

1) *Roughness of the surface of the ferroelectric substance.* In order to make the length of the ferroelectric substance equal to multiples of the half wavelength, opposite faces perpendicular to the wave must be exactly parallel to each other. The roughness of these surfaces decreases the amplification. There are two possible effects. One of the effects is such that the roughness affects $|t|$ directly. The other is that the roughness decreases the amplitude of the pump wave in the substance and consequently decreases the gain α_g .

2) *Change of the dielectric constant with the microwave frequency.* Amplification was calculated with the assumption that the dielectric constant was independent of frequency. When the dielectric constant varies with the frequency, two undesirable effects take place. One is that the wavelength in the substance depends on the dielectric constant, so that similar effects as that of roughness occur. The other is that the gain α_g is decreased by the change of the dielectric constant with frequency. These were analytically calculated, but only numerical results will be shown.

Finally, some practical examples will be presented. First, let us consider the case when the nonlinear material is barium (73 per cent)-strontium (27 per cent)-titanate

ceramics, which was measured by Davis, and Rubin at 3000 mc.⁷

Material (BaTiO₃, 73 per cent; SrTiO₃, 27 per cent) at 23°C with 5 kv/cm bias

Dielectric constant	about 3600
Dielectric loss	$\tan \delta = 0.1$
	$\lambda_0 \alpha_1 = 18.8$ nepers
Nonlinearity	ϵ_p^0/ϵ_0 per field strength = 7 per cent/(kv/cm)

Amplifier

Frequency	3000 mc	
signal		
idling	{ 3000 mc or	{ 6000 mc
pumping	{ 6000 mc	{ 9000 mc
Dimension		
thickness	0.1 mm	
length	0.83 mm (= $\lambda_s/2$)	
width	5 mm	

Results

Pumping voltage	
at minimum gain	2 kv/cm
at 20-db gain	2.4 kv/cm
at maximum gain	2.5 kv/cm
Pumping power	
at 20-db gain	4.7 kw at peak power
The roughness of surface must be within	± 0.01 mm. ¹⁰
The change of the dielectric constant at the pumping frequency and at the signal frequency must be within	2.2 per cent. ¹⁰

These results show that

- 1) material must be extremely small;
- 2) very precise work is necessary to fabricate the material;
- 3) rather high pumping power is necessary.

These undesirable facts are caused by the high dielectric constant and high dielectric loss of the material.

Next, let us consider the case when a new material, whose characteristic is shown in the following table, is used as a nonlinear substance. This material was originally proposed by Cassedy.⁵ It is believed, however, that the material could not be easily pre-

pared by suspending (BaSr)TiO₃ in a nonpolar binder as Cassedy proposed, because of the difference in the dielectric constant of (BaSr)TiO₃ and the nonpolar binder. It may be possible to obtain the desired material by mixing certain materials with BaTiO₃.

Material

Dielectric constant	about 100
Dielectric loss	$\tan \delta = 0.01$
	$\lambda_0 \alpha_1 = 0.31$ neper
Nonlinearity	ϵ_p^0/ϵ_0 per field strength = 7/(kv/cm)

Amplifier

Frequency same as that for (BaSr)TiO ₃	
Dimension of material	
thickness	0.1 mm
length	5 mm ($=\lambda_s/2$)
width	5 mm

Results

Pumping voltage	
at minimum gain	330 volts/cm
at 20-db gain	420 volts/cm
at maximum gain	460 volts/cm
Pumping power	
at 20-db gain	1.5 watts at peak power
The roughness of surface must be within	± 0.3 mm. ¹⁰
The change in the dielectric constant at the pumping frequency and the signal frequency must be within	13 per cent. ¹⁰

It is concluded that the new material would be suitable for an amplifier. The physical size of such material would not be too small for fabrication, and precise work will not be required. The pumping power would be only perhaps one to two watts.

The author would like to thank Profs. S. Silver and T. E. Everhart and Dr. N. Kumagai for their useful suggestions and helpful discussions.

YOSHIMASA AOKI
Osaka City University
Osaka, Japan

A Broad-Band Ferrite Reflective Switch*

Several types of reflective ferrite switches have recently been described in the literature.^{1,2} These have typically made use either of the Faraday rotation effect or of a waveguide cutoff induced by a transversely-magnetized ferrite slab. A different and very simple type of switch, which exhibits similar reflective behavior, may also be obtained by the use of a short section of heavily-loaded (or filled) coax, stripline, or waveguide. Application of an axial magnetic field

⁹ P. K. Tien and H. Suhl, "A traveling-wave ferromagnetic amplifier," *Proc. IRE*, vol. 46, pp. 700-706; April, 1958.

¹⁰ In this case, the amplification coefficient $|t|$ does not decrease below half of that of the ideal case.

* Received by the PGM-TT, May 5, 1960.
¹ R. F. Soohoo, "A ferrite cutoff switch," *IRE TRANS. ON MICROWAVE THEORY AND TECHNIQUES*, vol. MTT-7, pp. 332-336; July, 1959.

² G. S. Uebele, "High-speed, ferrite microwave switch," 1957 IRE NATIONAL CONVENTION RECORD, pt. 1, pp. 227-234.

of sufficient magnitude can cause the effective permeability of the ferrite to approach zero and under this condition electromagnetic waves are strongly reflected by the ferrite, producing a cutoff effect that is relatively independent of the type of propagating structure. This type of device possesses the advantages of being small in size and broad-band. It requires only a moderate magnetic field, whose magnitude can vary over a wide range. Furthermore, it may be used over much of the UHF and SHF frequency regions by choosing a ferrite with the proper saturation magnetization ($4\pi M_s$).

Some typical measured data are shown in Figs. 1 and 2 for a short section of shielded stripline filled with Trans-Tech TT 414 ($4\pi M_s = 600$ gauss). This structure does not represent an optimized design; rather, it is the simplest arrangement. The ferrite pieces are rectangular in shape with blunt ends (*i.e.*, no tapering or chamfering). The ends of the stripline section contain conventional ("straight-through") transitions to type *N* coaxial connectors. From Figs. 1 and 2 it may be seen that an attenuation greater than 45 db and a VSWR greater than 18 may be obtained over the frequency region from 2000 to 2800 mc if a magnetic field of 400 oersteds is applied during the OFF state. If only narrow-band operation near 2000 mc is desired, an insertion loss of 40 db and a VSWR of 23 may be achieved with a field of less than 150 oersteds. The axial magnetic field is provided by passing a current through a coil wrapped directly on the stripline. Since the structure is extremely short and also very small in cross section, relatively rapid switching is possible, particularly if narrow-band operation is permissible. Switching times of the order of ten microseconds can be achieved for moderate switching powers.

By using materials with higher saturation magnetizations, similar characteristics may be obtained at higher frequencies. The same stripline (2½ inches long) filled with a ferrite whose $4\pi M_s$ value was 1500 gauss gave results at *C* band comparable to those in Figs. 1 and 2. Waveguide heavily loaded

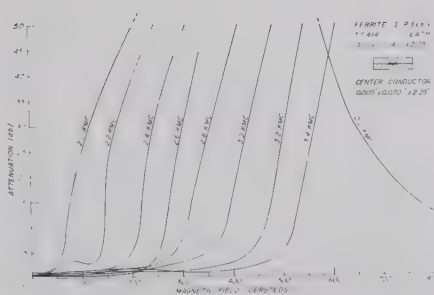


Fig. 1—Attenuation characteristics of stripline ferrite switch at S band.

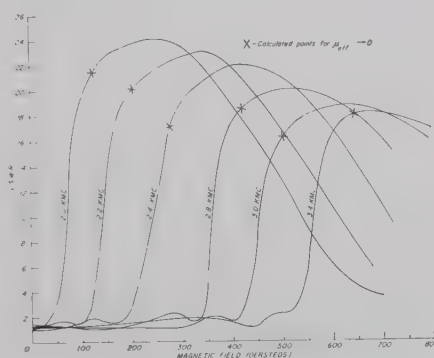


Fig. 2—VSWR characteristics of stripline ferrite switch at S band.

with this same ferrite was investigated as a possible configuration for a *C*-band switch. The waveguide was of reduced size (0.17 inch by 0.9 inch I.D.) and was filled with polystyrene to reduce the waveguide cutoff frequency well below the operating range of 5 to 6 kmc. A centrally-located piece of ferrite 0.16 inch high and about half as wide as the guide gave switching action that was nearly comparable to that obtained with the stripline; however, about 50 per cent more length of ferrite was needed in the waveguide configuration.

It has been shown³ that the effective permeability of axially-magnetized ferrite slabs loading a stripline as shown in Fig. 1

is given by

$$\mu_{\text{eff}} = \frac{\mu^2 - \kappa^2}{\mu} \quad (1)$$

where μ and κ are the diagonal and off-diagonal terms of the well-known permeability tensor. If the μ and κ are evaluated in terms of the magnetization, $4\pi M$, the applied field H , the frequency ν , and the gyro-magnetic ratio γ , (1) becomes

$$\mu_{\text{eff}} = \frac{\nu^2 - \gamma^2(H^2 + 8\pi MH + 16\pi^2 M^2)}{\nu^2 - \gamma^2 H(H + 4\pi M)} \quad (2)$$

At $H=0$, M is also zero and $\mu_{\text{eff}} \approx 1$. As H increases, $4\pi M \rightarrow 4\pi M_s$ and both the numerator and denominator of (2) decrease. The numerator, however, decreases faster and $\mu_{\text{eff}} \rightarrow 0$ at some higher value of H . These $\mu_{\text{eff}} = 0$ points as calculated from (2) (with $4\pi M_s = 600$ gauss and $\gamma = 2.74$ mc/gauss) are shown on the experimental curves of Fig. 2.

At present, a range of values of $4\pi M_s$ from 400 to 5000 gauss and of γ from 1.5 to 3.7 mc/gauss can be obtained from commercially available ferrites. With an arbitrary limitation of 800 oersteds on the maximum switching field, available ferrites limit the usefulness of this type of switch to the range from 500 to 11,000 mc. Use of fields as high as 1000 oersteds extends the upper frequency limit to 12,300 mc.

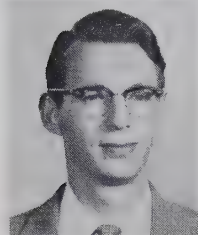
The authors are indebted to D. A. Youngberg and W. F. Janyska for making the necessary measurements.

C. M. JOHNSON
Emerson Res. Labs.
Silver Spring, Md.
Formerly at Electronic
Communications, Inc.
Timonium, Md.
J. C. WILTSE
Electronic Communications, Inc.
Timonium, Md.

³ C. M. Johnson and G. V. Buehler, "Ferrite Phase Shifter for the UHF Region, Part II," AF Cambridge Res. Center, Bedford, Mass., Electronic Communications Sci. Rept. No. 2 on Contract AF 19(604)-2407; October 31, 1959.

Contributors

Carl F. Augustine was born in Shiawassee County, Mich., on April 19, 1925. He received the B.S. and M.S. degrees in physics from Michigan State University, East Lansing, in 1950 and 1952, respectively.

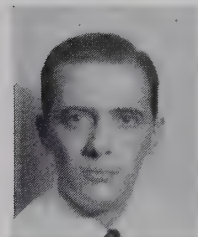


C. F. AUGUSTINE

From 1952 to 1957, he was employed by Bell Telephone Laboratories, N. Y. He was concerned with developments of computer equipment, communication relay links, and equipment capable of precision measurements at microwave frequencies. In 1957, he joined Bendix Research Laboratories, Detroit, Mich., where he has since been active in the development of broad-band microwave components. He has devised new techniques and designed new equipment for precise, rapid measurement of microwave component characteristics.



Luiz C. Bahiana was born in Rio de Janeiro, Brazil, on February 18, 1928. He attended the Naval Academy from 1945 to 1951, and served in the Navy, as a career officer from 1951 to 1956. During this time, he worked primarily with fire control systems. He entered Massachusetts Institute of Technology, Cambridge, as a graduate student in 1956, and received the M.S. and E.E. degrees in 1958 and 1959, respectively.



L. C. BAHIANA

In 1959, he returned to the Brazilian Navy (Diretoria de Eletronica da Marinha), working as a systems engineer in the field of communication.

Mr. Bahiana is a member of Sigma Xi and the Acoustical Society of America.



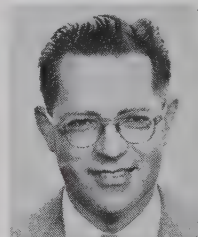
John Brown (SM'57) was born on July 17, 1923, in Auchterderran, Scotland. He received the M.A. degree in mathematics and natural philosophy from the University of Edinburgh, Scotland, in 1944, and the Ph.D. and D.Sc. (Eng.) degrees from the University of London, England, in 1954 and 1960, respectively.

From 1944 to 1951, he was on the staff of the Radar Research and Development Establishment, Malvern, Eng., and was mainly concerned with theoretical studies of microwave antennas. In 1951, he became a lecturer in electrical engineering at the Imperial College of Science and Technology and in 1955 moved to University College, London, where he is now reader in electrical engineering.

Dr. Brown is an associate member of the IEE.



James Cheal (M'57) was born in Sunfield, Mich., on March 3, 1924. He received the B.S.E.E. degree from Michigan State University, East Lansing, in 1950.



J. CHEAL

From 1950 to 1952, he was employed by International Business Machines Corporation, Lansing, Mich., as field engineer. He joined Bendix Research Laboratories, Detroit, Mich., in 1952, and was responsible for the development of a new K-band feed for a paraboloidal reflector and for the design of UHF antennas and duplexers. From 1953 to 1956, he was employed by the Burroughs Corporation, Detroit, where he was assigned to the development effort which resulted in the prototype Sage computer. He rejoined Bendix Research Laboratories in 1956, and has since been responsible for the development of a wide range of microwave components using new materials and new techniques.



Marvin Cohn (S'49-A'51-M'57) was born in Chicago, Ill., on September 25, 1928. He received the B.S.E.E. degree in 1950 and the M.S.E.E. degree in 1953, both from the Illinois Institute of Technology, Chicago.



M. COHN

From 1951 to 1952, he was employed by the Glenn L. Martin Company, Baltimore, Md.; he was with the Radiation Laboratory of The Johns Hopkins University, Baltimore, from 1952 until he entered the U. S. Army Signal Corps in 1953. He was sta-

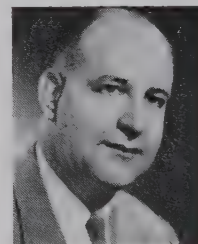
tioned at White Sands Proving Grounds, where he worked on the analysis of missile tracking systems. In 1955, he returned to the Radiation Laboratory, where he has done research and development work on broad-band and superheterodyne receivers and surface-wave transmission lines. He was head of the Millimeter Wave Techniques Group of the Radiation Laboratory.

In June, 1960, he completed the requirements for the Doctor of Engineering degree at The Johns Hopkins University. He is presently a research scientist with the research division of Electronic Communications, Inc., Timonium, Md.

Mr. Cohn is a member of Eta Kappa Nu, Tau Beta Pi and Sigma Xi.



Paul D. Coleman (A'46-M'56) was born in Stoystown, Pa., on June 4, 1918. He received the B.A. degree from Susquehanna University, Selinsgrove, Pa., in 1940, the M.S. degree in physics from Pennsylvania State University, University Park, in 1942, and the Ph.D. degree in physics from the Massachusetts Institute of Technology, Cambridge, in 1951.



P. D. COLEMAN

He was employed as a physicist with the U. S. Signal Corps and subsequently the U. S. Air Force at Wright Air Development Center, Dayton, Ohio, from 1942 to 1946. During this period, he was engaged in work on electromagnetic theory, and received the AAF Meritorious Civilian Award in 1946 for his contribution to aircraft antenna theory.

From 1946 to 1951, he was a physicist with the U. S. Air Force at the Cambridge Air Research Center and later a research associate in physics in the Research Laboratory of Electronics at M.I.T., where he was concerned with the generation of submillimeter waves.

In 1951, he became an associate professor in electrical engineering at the University of Illinois, Urbana, where he established the Ultramicrowave Group in the Electrical Engineering Research Laboratory. He is presently a professor on the graduate electrical engineering staff, directing research on submillimeter wave generation.

In 1959, Dr. Coleman became a member of the Board of Technological Counselors of FXR, Inc., Woodside, N. Y., and was later elected chairman. He is a member of Sigma Xi, the American Physical Society, and Pi Mu Epsilon.

Wilhelm H. Eggmann was born on April, 1929, in Zürich, Switzerland. He received the diploma in electrical engineering in 1954 from the Swiss Federal Institute of Technology, Zürich. From 1954-1956, he worked as an instructor and research assistant at the same institute. In 1956, he entered Case Institute of Technology, Cleveland, Ohio, working as an instructor. He received the M.S.E.E.

degree in 1959 from Case Institute, where he is now studying towards the Ph.D. degree. He is presently engaged in research work on ferrites in microwave applications and artificial dielectrics.

Mr. Eggmann is an associate member of Sigma Xi.

Georges Goudet (SM'50-F'60) was born in Dijon, France, in 1912. He received several scholarships at the Ecole Normale Supérieure, Dijon. In 1936, he became an Agrégé (fellow) of physical science at the University. After serving as an artillery officer during World War II, he completed his work for the Ph.D. degree in physics in 1942, at Paris University.

During 1943 and 1944, he worked on microwave tubes at the Laboratoire Centrale de Télécommunications, in Paris. He then became the head of the ultra-high-frequency laboratory of the French Posts, Telegraphs and Telephones Administration. In 1951, he joined the staff of Nancy University, Nancy, as a professor and director of the special school of electricity and mechanics. He has served as a consultant to Laboratoire Centrale de Télécommunications, and in 1955 became its director.

Dr. Goudet is a member of the Société Française de Physique, the Société Française des Electriciens and a Vice-President of the Société des Radioélectriciens.

Basil W. Hakki (S'58) was born in Damascus, Syria (U.A.R.) on November 10, 1935. He received the B.E.E. degree from the American University of Beirut, Beirut, Lebanon, in 1957, and the M.S. degree in communication engineering from the University of Illinois, Urbana, in 1958.

In 1956, he worked for Philips Telecommunication Industry in Hilversum, The Netherlands, on the analysis of transients in

filter networks. Since 1958, he has been associated with the Ultramicrowave Section of the Electrical Engineering Department of the University of Illinois, where he is working for the Ph.D. degree. He is now involved in the analysis and design of a submillimeter primary source of electromagnetic radiation.

Mr. Hakki is a member of Pi Mu Epsilon, the Society for Industrial and Applied Mathematics, and the American Physical Society.

A. F. Harvey, for a photograph and biography please see page 482 of the October, 1959 issue of these TRANSACTIONS.

Robert D. Haun, Jr. (S'56-M'57) was born in Lexington, Ky., on April 3, 1930. He received the B.S. degree in physics from the University of Kentucky in 1952. After one semester at the graduate school of Columbia University, New York, N. Y., he entered the Massachusetts Institute of Technology, in Cambridge, where he worked under J. H. Zacharias as a research assistant on the development of

the cesium atomic beam frequency standard. He received the Ph.D. degree in physics from M.I.T. in 1957.

Since then he has been engaged in ferromagnetic resonance, parametric amplifier, and tunnel diode studies at the Westinghouse Research Laboratories, Pittsburgh, Pa.

Dr. Haun is a member of the American Physical Society, Sigma Xi, and Phi Beta Kappa.

Koryu Ishii (M'55) was born in Tokyo, Japan, on March 18, 1927. He received the B.S.E.E. degree from Nihon University, Tokyo, in 1950, and the M.S. and Ph.D. degrees in electrical engineering in 1957 and 1959, respectively, from the University of Wisconsin, Madison.

From 1949 to 1956, he did research on microwave circuits and amplifiers, and instructed students at Nihon Uni-

versity. From 1956 to 1959, he worked particularly on research of the noise figure of the reflex klystron amplifiers and cascaded reflex klystron amplifiers at the University of Wisconsin.

Since July, 1959, he has been engaged in establishing a millimeter-wave laboratory at Marquette University, Milwaukee, Wis. At present, he is an Assistant Professor at Marquette.

Dr. Ishii is a member of Sigma Xi, the ASEE, and the Institute of Electrical Communication Engineers of Japan.

Kiyoshi Morita (SM'54) was born in Tokyo, Japan, on March 18, 1901. He was graduated in 1921 from Tokyo Higher Technical School, which was chartered later at the Tokyo Institute of Technology, and won the Tejima honor prize the same year. In 1933 he received the Doctorate degree in electrical engineering from the Tokyo Imperial University.

He was appointed professor at the Tokyo Institute of Technology in 1941, and was primarily concerned with the development of measuring apparatus for dielectric loss, paraboloidal reflectors, and triple-line feeders. Since then he has given lectures on high-frequency and electronic engineering.

He won an honor prize for his contribution on UHF techniques from the Nippon Radio Kyokai in 1946. The same year he became chief of the Special Committee for UHF Measurement, sponsored by the Ministry of Education, and was active in the development of the wattmeter for UHF. Since 1949 he has headed the Committee for the Development of Vacuum Tubes for Microwaves.

In 1950, he was sent to the United States by the Galioa Fund. He visited Cornell University, Polytechnic Institute of Brooklyn, the University of Michigan, and other universities to observe the American electrical engineering educational system, and later contributed to the improvement of teaching methods in Japanese universities. He has also worked, in collaboration with American professors visiting Japan, in the engineering section of the Institute for Educational Leadership.

Dr. Morita is an official member of Commission VI of URSI (International Scientific Radio Union).

Louis D. Smullin (S'39-A'40-SM'51-F'57) was born on February 5, 1916, in Detroit, Mich. He received the B.S.E.E. degree from the University of Michigan, Ann Arbor, in 1936, and the M.S. degree from the Massachusetts Institute of Technology, Cambridge, in 1939.

Prior to World War II, he was active in industrial research. From 1941 to 1946, he served on the staff of M.I.T.'s Radiation Laboratory, where he was responsible for the development of TR tubes and duplexers. From 1946 to 1947, he headed the Microwave Tube Group at the Federal Telecommunications Laboratory in Nutley, New Jersey. He was on the staff of the M.I.T. Research Laboratory of Electronics from



L. D. SMULLIN

1947 to 1950. Prior to joining the faculty of M.I.T. in 1955, where he is now Professor of Electrical Engineering and Head of the Microwave Laboratory in the Research Laboratory of Electronics, he served as Head of the Radar and Weapons Division of the Lincoln Laboratory, M.I.T.

In that capacity he was responsible for the development of new, high-power, ground and air-borne radars, and an anti-aircraft weapon system. Since 1955, his research has been in the microwave tube field, and more recently it has been concerned with the interaction phenomena between electron beams and plasmas.

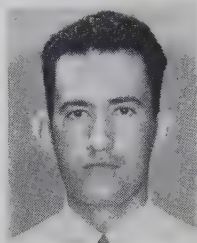
Prof. Smullin is a member of the American Physical Society and a Fellow of the American Academy of Arts and Sciences.

Gaspar R. Valenzuela (S'54-M'56) was born on January 6, 1933, in Coelemu, Chile. He received the B.S.E.E. and M.S.E.E. degrees from the University of Florida, Gainesville, in 1954 and 1955, respectively.

After graduation, he joined the electronics division of the Westinghouse Electric Corporation, Baltimore, Md., as an associate engineer, where he was engaged in microwave components development until 1957.

From 1957 to 1959, he worked at the Applied Physics Laboratory of The Johns Hopkins University, Baltimore, as an associate staff member. In 1959, he became a senior staff member. During his stay at APL, he worked in research and development of printed microwave transmission lines, radar techniques, general microwave design and development.

Presently he is at The Johns Hopkins Radiation Laboratory where, since 1956, he has been engaged in part-time graduate work.



G. R. VALENZUELA

❖

Leo Young (M'54-SM'57) was born in Vienna, Austria, on August 18, 1926. After winning a scholarship from St. Johns College, Cambridge, England, he obtained the B.A. degree with honors in mathematics in 1945 and the B.A. degree with honors in physics in 1947.



L. YOUNG

He received the M.A. degree from Cambridge University in 1950.

He was an engineer with A. C. Cossor, Ltd., London, from 1948 to 1951. From then until 1953, he was associated with Decca

Radar Ltd., as head of the Microwave and Antenna Laboratory.

He came to the United States in 1953 to join the Westinghouse Electric Corporation, Baltimore, Md. where he is presently an advisory engineer in the Electronics Division.

He was awarded the M.S.E.E. degree by The Johns Hopkins University, Baltimore, in 1956, held the Westinghouse Electric Corporation's B. G. Lamme Scholarship during 1958-1959, and obtained the Dr.Eng. degree from Johns Hopkins in 1959.

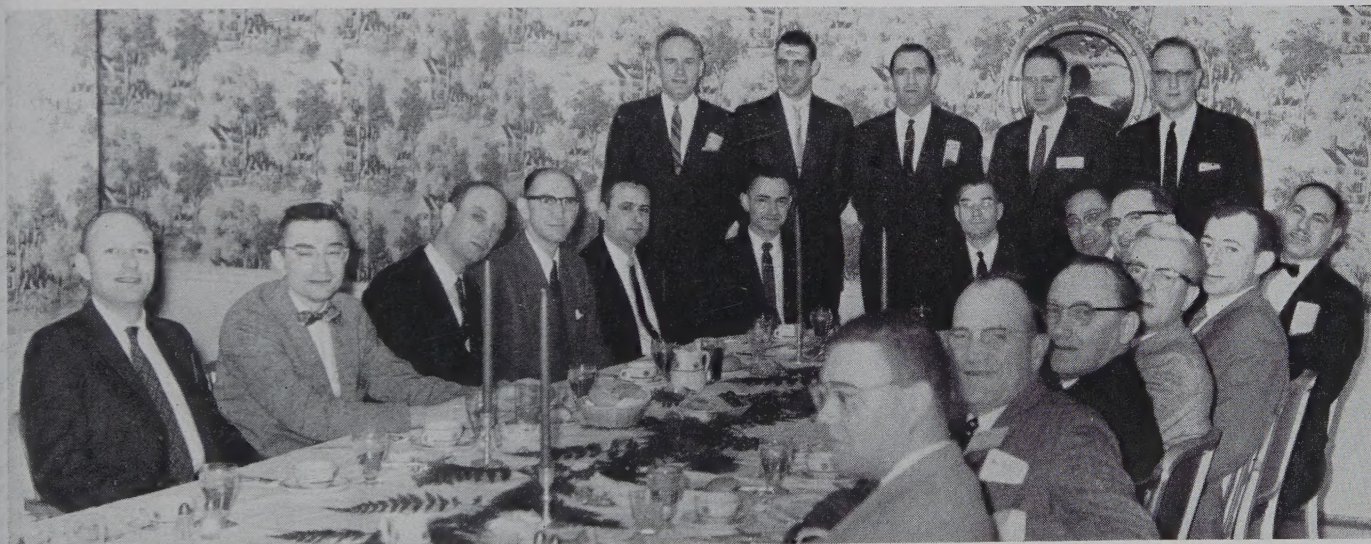
Dr. Young, a registered professional engineer in Maryland, is a member of Sigma Xi, the AIEE and the IEE.

PGMTT News

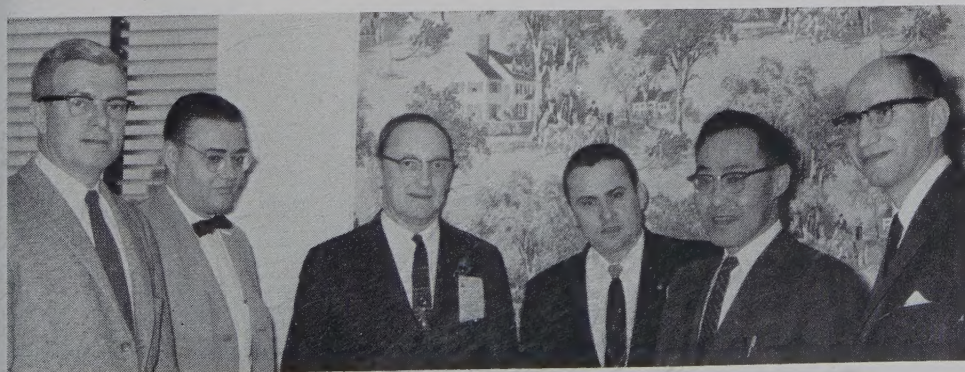
1960 IRE INTERNATIONAL CONVENTION

PHOTOGRAPHS OF THE PGMTT ADMINISTRATIVE COMMITTEE MEETING

H. M. Altschuler, *Secretary-Treasurer*; R. F. Schwartz; W. W. Mumford; G. Shapiro; R. E. Beam; D. D. King, *TRANSACTIONS Editor*; T. S. Saad; H. L. Bachman, *Long Island Chapter Chairman*; G. Sinclair; A. A. Oliner, *Chairman*.



Left to right seated: R. C. Hansen; R. F. Schwartz; W. L. Pritchard; S. W. Rosenthal; R. D. Wengenroth; H. M. Altschuler; A. A. Oliner; K. Tomiyasu; D. D. King; G. Shapiro; R. O. Stone, *Washington Chapter Chairman*; H. F. Engelmann; A. C. Beck; W. W. Mumford; D. J. Stock. Standing: G. Sinclair, H. L. Bachman, T. S. Saad, R. A. Rivers, R. E. Beam.

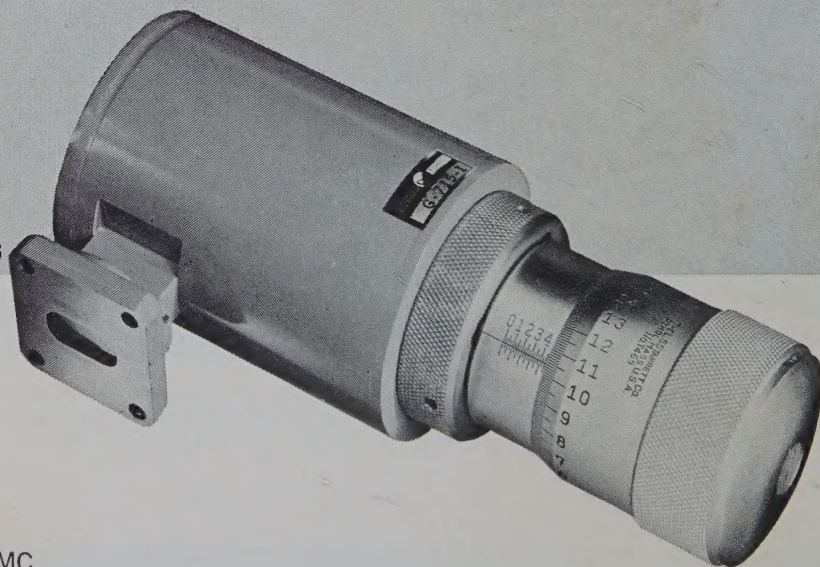


H. Englemann, *Ex-Officio*; D. J. Stock, *New York Chapter Chairman*; A. C. Beck; R. D. Wengenroth, K. Yomiyasu, *Vice Chairman*; S. W. Rosenthal.

THERE'S MORE TO A D-B BROADBAND WAVEMETER THAN JUST THE DIAL!



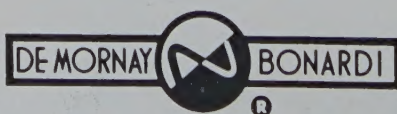
Here is the D-B calibration chart showing the high resolution and accuracy you get with any D-B wavemeter. The X-Band curve, for example, is over 22 feet long!



Fail-Safe Design—

loss of gas pressure makes unit immediately inoperative.

Twelve models cover from 2.6 KMC to 140 KMC. Write for complete data in Bulletin D-B 715.



DE MORNAY-BONARDI
780 SOUTH ARROYO PARKWAY • PASADENA, CALIF.

INSTITUTIONAL LISTINGS

The IRE Professional Group on Microwave Theory and Techniques is grateful for the assistance given by the firms listed below, and invites application for Institutional Listing from other firms interested in the Microwave field.

AIRTRON, INC., A Division of Litton Industries, 200 East Hanover Ave., Morris Plains, N.J.
Designers and Producers of Complete Line of Microwave Electronic and Aircraft Components

HUGHES AIRCRAFT CO., Florence and Teale Sts., Culver City, Calif.
Res., Dev., Mfg.: Radar Systems and Components, Microwave Devices and Components, Antennas, Tubes

ITT LABORATORIES, 500 Washington Ave., Nutley 10, N.J.
Line-of-Sight and Over-the-Horizon Microwave Systems; Test Equipment and Components

LITTON INDUSTRIES, Electron Tube Div., 960 Industrial Rd., San Carlos, Calif.
Magnetron, Klystrons, Carcinotrons, TWT's, Backward Wave Oscillators, Gas Discharge Tubes, Noise Sources

MICROWAVE DEVELOPMENT LABS., INC., 92 Broad St., Babson Park 57, Mass.
Designers, Developers and Producers of Microwave Components and Assemblies, 400 mc to 70 kmc

WHEELER LABORATORIES, INC., Great Neck, N.Y.; Antenna Lab., Smithtown, N.Y.
Consulting Services, Research & Development, Microwave Antennas & Waveguide Components

The charge for an Institutional Listing is \$50.00 per issue or \$210.00 for six consecutive issues. Applications for Institutional Listings and checks (made out to the Institute of Radio Engineers) should be sent to Robert A. Rivers, PGMTT Advertising Editor, Aircom Inc., 354 Main St., Winthrop 52, Mass.

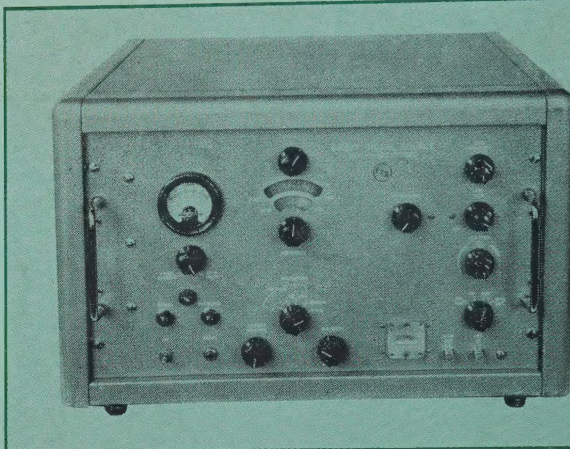
NOTICE TO ADVERTISERS

Effective immediately the IRE TRANSACTIONS ON MICROWAVE THEORY AND TECHNIQUES will accept display advertising. For full details contact Robert A. Rivers, Advertising Editor, PGMTT TRANSACTIONS, Aircom Inc., 354 Main St., Winthrop 52, Mass.



X-BAND SWEEP SIGNAL SOURCE

8,200mc to 12,400mc Frequency Range



Advanced Features
Include:

- ☒ ELECTRONIC SWEEP
- ☒ AUTOMATIC GAIN CONTROL
- ☒ DIRECT READING
FREQUENCY DIALS

"If a man's work be true and good...challenging comparison will be his strength."

David Charles

The FXR Model X775A X-Band Sweep Signal Source, challenging comparison, is unsurpassed for the measurement of VSWR and reflection coefficient. The Model X775A utilizes a permanent magnet BWO as the rf source. A unique built-in AGC amplifier produces a flat rf level, with respect to a bolometer detector, over the entire swept frequency range. Both ends of the swept frequency range can be accurately preset on separate direct reading frequency dials.

Specifications for the FXR Model X775A:

- **FREQUENCY RANGE:** 8,200mc to 12,400mc.
- **SWEEP RATE (RESOLUTION):** 300mc/sec to 300kmc/sec, linear with time.
- **SWEEP WIDTH:** to 4,200mc, direct reading, continuously adjustable.
- **OUTPUT TYPES:** cw, square wave modulation (internal 800cps to 1,200cps).
- **OUTPUT POWER:** 0 to 20mw minimum cw into matched load, continuously adjustable. With AGC-detected output flat to ± 0.5 db (when used with matched bolometers and directional couplers).
- **FREQUENCY DIAL ACCURACY:** $\pm 1\%$ — fixed frequency operation (at specified grid voltage).
 $\pm 2\%$ — sweep frequency operation.
- **OUTPUT CONNECTOR:** 1 X $\frac{1}{2}$ waveguide.
- **POWER REQUIREMENTS:** 115/230V, 50/60cps, 200 watt.
- **DIMENSIONS:** 12 $\frac{7}{8}$ " high X 21 $\frac{3}{4}$ " wide X 18" deep.
- **WEIGHT:** 78 lbs.

*For more details,
contact your FXR representative.*



FXR, Inc.

Design • Manufacture • Development

25-26 50th STREET
WOODSIDE 77, N.Y.